Technical University of Catalonia
BarcelonaTech

Doctorate Program in Civil Engineering

Doctoral Thesis

Model Predictive Control of Resonance Sensitive Irrigation Canals

Author:
Klaudia Horváth

Supervisors:
Dr. Manuel Gómez Valentín
Dr. José Rodellar Benedé

A thesis submitted in fulfilment of the requirements for the degree of Doctor of Philosophy

in the

FLUMEN INSTITUTE
Department of Hydraulic, Maritime and Environmental Engineering

April 2013, Barcelona

"Mi dolgunk a világon? küzdeni
Erőnk szerint a legnemesbekért.
Előttünk egy nemzetnek sorsa áll.
Ha azt kivíttuk a mély sülyedésből
S a szellemharcok tiszta sugaránál
Olyan magasra tettük, mint lehet,
Mondhatjuk, térvén őseink porához:
Kösznjük élet! áldomásidat,
Ez jó mulatság, férfi munka volt!"

"What, in this world, is our task? To struggle,
according to our strength, for noble goals.
Before us stands the fate of a nation -
when we, from the irrevocable fall
have preserved it and restored it to its heights,
fighting under the clear beam of the spirit,
we can say, returning to our ancestors
in the dust:Thank you, life, for thy blessings -
this has been great joy, yea, the Work of Men!"

Vörösmarty Mihály (Translated by Hart, H.H.)

Abstract

Saving water is an economic and ecological need. One way to save water is to reduce losses in irrigation networks by canal automation. The goal of canal automation is to make the right amount of water to arrive in the right time. In order to achieve this goal, one of the ways is controlling the gates in the irrigation network by some control algorithm. In this work the control of a specific type of canal pools is studied: short and flat pools that are prone to resonance.

The downstream water level control of this type of canals is investigated using the example of the 3-reach laboratory canal of the Technical University of Catalonia. Numerical and experimental studies are carried out to investigate the following: the choice of models for predictive control, the possibility to achieve offset-free control while using gravity offtakes and the best choice of control action variables.

The objective of this work is to develop a well performing centralized model predictive controller (MPC) for the laboratory canal that is able to handle known and unknown setpoint changes and disturbances, and also to draw further conclusions about controller design for this type of canals.

A recently developed model for resonant canals, the Integrator Resonance, is implemented and successfully tested experimentally for the first time. A new method to achieve offset free control for model predictive control is developed and tested numerically and experimentally. A choice of control variables are tested: As opposed to the discharge which is generally used as the control action variable, a state space model is formulated by using the gate opening as control variable without the need of water level measurement downstream of the gates. The results are summarized and conclusions are presented for control of short and flat canals that are prone to resonance.

Preface

Water is essential for life. The need for freshwater is increasing and its distribution is uneven in space and in time. One of the biggest and most important water users is agriculture, which is highly inefficient. Irrigated crop yields are about 2.7 times those of rain-fed farming. Automatic control is one of the ways of improving the efficiency of irrigation.

Automatic control of irrigation canals is a research line in the research group FLUMEN in cooperation with CoDaLab group from the beginning of the 90s when the first articles were published [Rodellar et al., 1989], [Rodellar et al., 1993] about using predictive control for irrigation canals with the help of simplified models. The research continued in the direction of predictive [Cardona et al., 1997], [Gómez et al., 2002] and also feedforward control [Soler et al., 2008].

To follow this line of investigation, a simulation tool was developed [Mantecón et al., 2002] and in 2005 the laboratory canal of the Technical University of Catalonia was built. The instrumentation and building of the SCADA system is described in the first doctoral thesis made using this canal [Sepúlveda, 2008].

This work continues this research line by investigating the properties of the laboratory canal, its modelling and control. The canal can be classified as short and flat canals (that is a common canal type in real canal operation). The control of these type of canals is challenging due to the resonance phenomena they show. Therefore this work investigates the modelling and control of this type of canals in general, using the laboratory canal as an example. Different models and control architectures are tested using the framework of model predictive control.

Acknowledgements

First of all I would like to thank for the opportunity to do this research work to my supervisors, Professor Manuel Gómez and Professor José Rodellar. Their constant guidance, patience and help and the freedom that they gave me during my work was essential.

I would like to thank for the advices, help, encouragement of all my colleagues whose discussions helped me to develop my ideas, especially for Dr Juan Mantecón, Dr Carlos Ocampo Martinez and Pedro Langarita.

Also for the people of FLUMEN, for the good working environment, for all the nice times, birthdays, Chicas Flumen events that we had.

For the laboratory work, Eduard Galvis showed me all the secrets of the laboratory canal, and constantly supported me, thanks for all those happy hours of fighting with the controller in the lab.

I would like to thank to Dr Pierre-Olivier Malaterre, for the possibility of using the SIC software and for always being ready to answer for all my questions.

I would like to thank to Dr Peter-Jules van Overloop for showing me the beauty of MPC and the joy of modelling.

I have to thank for all those artists, musicians, whose work make me happy in these days, without them I could not have carried on.

Finally I owe thanks to my parents who were always in my heart. To my mother, for teaching my creativity, and to my father for teaching me reason.

Last but not least for my husband, José Miguel, who stood next to me during all these times, and supported me with all his love.

Thanks all of you for these marvellous years!

Contents

List of Figures

List of Tables

Abbreviations

ARX	**A**uto-**R**egressive with e**X**ogenous Input
ASCE	**A**merican **S**ociety of **C**ivil **E**ngineers
ATV	**A**uto **T**une **V**ariation
FO	**F**irst **O**rder model
ID	**I**ntegrator **D**elay
IDZ	**I**ntegrator **D**elay **Z**ero
IR	**I**ntegrator **R**esonance
GPC	**G**eneralized **P**redictive **C**ontrol
LPV	**L**inear **P**arameter **V**arying control
LQG	**L**inear **Q**uadratic **G**aussian
MAVE	**M**aximum **A**lloved **V**alue **E**stimate
MAPE	**M**ean **A**verage **P**ercentage **E**rror
MIMO	**M**ultiple **I**nput **M**ultiple **O**utput
MUS	**M**uskingum model
MPC	**M**odel **P**redicitve **C**ontrol
PI	**P**roportional **I**netgral
SCADA	**S**upervisory **C**ontrol **A**nd **D**ata **A**cquisition **S**ystem
SIC	**S**imulation of **I**rrigation **C**anals
SISO	**S**ingle **I**nput **S**ingle **O**utput
SV	**S**ant **V**enant equations
UPC-PAC	**U**niversitat **P**olitècnica de **C**atalunya
	Canal de **P**rueba de **A**lgoritmos de **C**ontrol

Nomenclature

Latin Letters

Δq_i	discharge increment in the i^{th} reach	m^3/s
A_s	backwater surface	m^2
A_{eIDZ}	backwater area for the IDZ model	m^2
A_{eID}	backwater area for the ID model	m^2
A_e	storage surface	m^2
C_L	dimensionless coefficient characterizing a canal reach	-
d	delay steps	-
D_0	diffusion coefficient	m^2/s
e_i	relative water level error in the i^{th} reach	m
G_{ID}	ID model transfer function between the upstream discharge and the downstream water level	-
G_M	Muskingum transfer function between the upstream discharge and the downstream water level	-
h_i	relative water level in the i^{th} reach	
h_{spi}	downstream water level setpoint in the i^{th} reach	m
K_1	time constant of the first order model	s

K_p	proportional gain (feedback)	-
k_{hw}	gain of the water level of the linearized weir equation	m^2/s
K_{IDZ1}	parameter for the IDZ model	-
K_{IDZ2}	parameter for the IDZ model	-
m	side slope	m/m
$M_R(\omega_R)$	magnitude of the resonance peak	s/m^2
q_{in}	relative input discharge	m^3/s
T_R	travel time	s
u_{gen}	general input vector	
x_{gen}	general state vector	
A_{cr}	cross sectional area	m^2
Q_{in}	absolute input discharge	m^3/s
g	acceleration fo gravity	m/s^2
Q_{in0}	steady state (reference) input discharge	m^3/s
T	top width of a cross section	m
v_{sto}	relative storage volume	m^3
K	storage time constant	s
S_b	bottom slope	m/m
S_f	friction slope	m/m
n	Manning's roughness coefficient	$sm^{1/3}$
P_w	wetted perimeter	m
Q	discharge	m^3/s
R_h	hydraulic radius	m
C_{KW}	kinematic wave celerity	m/s
C_{z0}	Chézy coefficient	$m^{1/2}/s$
C_{DW0}	dynamic wave celerity	m/s
C_{df}	Discharge coefficient of the sluice gate for free flow	-
X	canal (pool) length	m
X	channel length	m

C_d	Discharge coefficient of the sluice gate for submerged flow	-
C_{dw}	Weir discharge coefficient	-
L	Gate opening	m
B_w	Width of the weir opening	m
B	Width of the weir (and the canal)	m
W	Weir height	m
B_{we}	effective weir width	m
C_{dwa}	parameter of the Kindsvater-Carter equation	-
C_{dwb}	parameter of the Kindsvater-Carter equation	-
H_e	head over the weir	m
K_b	Kindsvater-Carter width correction coefficient	m
K_h	Kindsvater-Carter head correction coefficient	m

Greek Letters

α_1	root of the characteristic equation	-
χ	weighing coefficient in the Muskingum model	-
$\omega_p(k)$	Frequency of the resonance peaks	rad/s
τ_{IDZ}	time delay for the IDZ model	s
τ_{id}	time delay of the ID model	s
ζ	damping	-
α_2	root of the characteristic equation	-
ω_R	resonance frequency of the first harmonic	rad/s

τ_{DW}	dynamic wave travel time	s
τ_{KW}	kinematic wave travel time	s

To the memory of my father

Chapter 1

Introduction and objectives

1.1 Irrigation canals

Agriculture is the biggest water consumer in the world; it is responsible for 70% of freshwater withdrawals from rivers, lakes and aquifers – up to more than 90% in some developing countries. On average only an estimated 37% of the water withdrawn for agriculture is effectively consumed by plants while the remaining portion is lost due to evaporation, ineffective structures, leakage and insufficient management [World Water Assessment Programme and Unesco, 2009]. The Food and Agriculture Organization of the United Nations (FAO) estimates an 11% increase in irrigation water consumption from 2008 to 2050 [World Water Assessment Programme and Unesco, 2012].

1.1.1 Canal operation types

Irrigation is the artificial application of water to the soil for assisting in growing crops. It is performed in large scale by irrigation canals. These canals are distributing the water to each farmer and need to be controlled in order to ensure the supply for all users. There are different types of existing control techniques. This introduction of control is based on the information about control from CANARI, the web Database on Irrigation Canals [Malaterre, 2011] and [Malaterre, 1998a].

Manual canal operation

Irrigation canals are traditionally operated manually. In most of the cases operators handle gates based on prescribed orders, local information and working experience. In the modern manual operation, the canal is equipped with sensors and the operators receive the signals and act locally. However, the manual operation has several disadvantages. It is a rigid system hence it cannot react against unforeseen changes (one farmer starting to take water, rain). In order to fulfill the demand, the supply is provided in excess: increasing the discharge or providing water after the irrigation time. Therefore an optimal balance between the water supply and demand is not achieved. The water conveyance is not controlled, the delay of the supply and the demand is not calculated, nor the effect of the hydraulic structures.

Canal automation

Canal automation offers a more likely alternative. With the real time operation of gates, using the feedback information of the demand and the real time sensors, a better supply-demand balance and more efficient of water management can be achieved. The efficiency is the ratio of volume of water used by crops to volume of water extracted from the available source. The goal of canal automation is to manipulate gate openings in real time, by using feedback of the measured state of the canal and information on known demand schedules, in order to achieve a desired performance in the water supply. There are several advantages of canal automation. The water conveyance efficiency can be improved considerably (estimated 30% to 60%) and it also provides more flexibility to users. In case of on demand operation it is possible to convey only the amount of water that is demanded at the time. It leads to better use of the canal dynamics and the storage capacity of the canal can be used without the need for constructing new reservoirs. The adaptation to smaller and bigger discharges is easier, without bank overflows. With the automatic control, less but more skilled people are needed. The state of art in canal automation is summarized in several works [Rogers and Goussard, 1998], [Malaterre, 1998a], [Mareels et al., 2005], [Lopez-Antens et al., 2007] and [Bastin et al., 2009].

1.1.2 Open channel flow

Irrigation canals are mainly open channels, their behaviour is governed by the non-linear hyperbolic partial differential Saint-Venant equations. This set of equations contains a mass and momentum conservation equation and they have no analytical solutions for all cases.

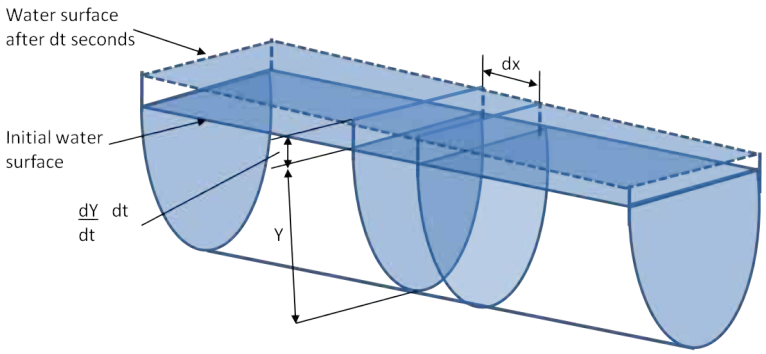

FIGURE 1.1: A scheme of an open channel showing the variables for the Saint-Venant equations

The continuity equation is

$$\frac{\partial Q}{\partial x} + \frac{\partial A_{cr}}{\partial t} = q_L \tag{1.1}$$

where $A_{cr}(x,t)$ is the wetted cross sectional area (m^2), $Q(x,t)$ is the discharge (m^3/s) at cross a cross-section A_{cr} and q_L is the lateral inflow or outflow (m^2/s).

The momentum equation is

$$\frac{\partial Q(x,t)}{\partial t} + \frac{\partial}{\partial x}\left(\frac{Q^2(x,t)}{A_{cr}(x,t)}\right) + gA_{cr}(x,t)\left(\frac{\partial H(x,t)}{\partial x} - S_b(x) - S_f(x,t)\right) = 0 \tag{1.2}$$

where $H(x,t)$ is the water depth (m), S_f (x,t) is the friction slope (m/m), $S_b(x)$ is the bed slope (m/m), and g the gravitational acceleration (m/s^2). The first term of the equation is the local and the second term is the convective inertia. The third term accounts for the hydrostatic pressure effect. The last two terms account for the gravity and the friction.

The friction slope can be calculated using Equation 1.4:

$$S_f = \frac{Q^2 n^2}{A_{cr}^2 R_h^{4/3}} \tag{1.3}$$

where n the Manning's roughness coefficient ($\mathrm{sm}^{-1/3}$) and R_h the hydraulic radius (m) defined by

$$R_h = A_{cr}/P_w \tag{1.4}$$

where P_w is the wetted perimeter (m).

Generally they are solved by different numerical methods, like the method of characteristics, finite volumes or finite differences. In this work a 1D hydrodynamic software is used based on the Preissmann Scheme [Cunge et al., 1980] that belongs to the category of implicit finite differences.

1.1.3 Analysis of the waves in open channels

The behaviour of the linearized Saint-Venant equations is analyzed in [Schuurmans et al., 1995] and [Schuurmans, 1997]. By assuming flow boundary conditions, Figure 1.2 summarizes the main processes.

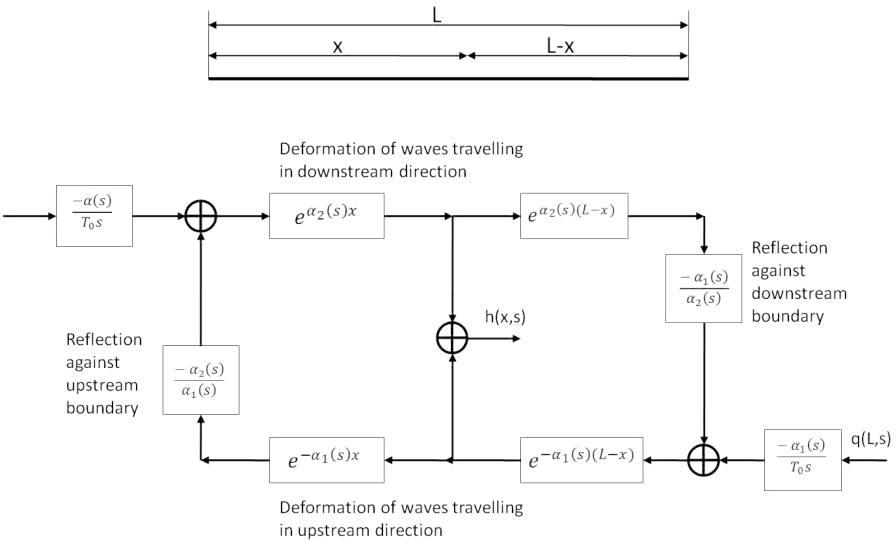

FIGURE 1.2: Block diagram of open channel flow, from [Schuurmans et al., 1995]

At the boundaries the relation between the flow rate and the water level is described with the terms $-\alpha_1/T_0/s$ and $-\alpha_2/T_0/s$, where s is the Laplace variable, T_0 is the top width of the channel and α_1 and α_2 are parameters obtained through the linearization of the Saint-Venat equations. They are the eigenvalues of the ordinary differential equations that are the Laplace transformed forms of the linearized Saint-Venant equations. The terms $-\alpha_1/\alpha_2$ and the reciprocal of this term $-\alpha_2/\alpha_1$ describe the reflection of the waves that depend on the structures on each side of the canal pool. The water level is the multiple of the discharge and the corresponding terms $-\alpha_1/T_0/s$ or $-\alpha_2/T_0/s$, in other words the change water level is the integral value of the flow change. $e^{\alpha_1(s)x}$ and $e^{\alpha_2(s)x}$ describe the wave attenuation in the downstream and upstream direction. It was shown that by substituting s=0 to both expressions, a wave travelling downstream always arrives to the downstream end, while a wave travelling upstream dampens exponentially. It is also shown that a wave head travels with a velocity $C_0 + V_0$ downstream and $C_0 - V_0$ upstream, assuming subcritical conditions, where C_0 is the steady state celerity and V_0 is the steady state velocity.

After a perturbation upstream, a wave is created that travels with the dynamic wave speed downstream $C_0 + V_0$, where V_0 is the initial velocity and C_0 is the initial celerity of the gravity wave. However, this wave is too fast for the inflow to create a new steady state. The bulk of the wave arrives with another celerity, called kinematic wave speed C_{KW}, to transform the system to a new steady state [Clemmens et al., 2012]. The kinematic wave theory assumes a unique relationship between the discharge and the water level, that is, a disturbance that travels with no attenuation. The minimum travel time can be estimated by the dynamic wave delay with the following equation:

$$\Delta\tau_{DW} = \frac{X}{C_{DW0}} = \frac{X}{V_0 + C_0} \tag{1.5}$$

where zero denotes the conditions at the beginning of the transient.

The denominator C_{DW0} gives the initial speed, therefore $\Delta\tau_{DW}$ estimates the minimum travel time (Equation 1.5). The kinematic wave delay is

$$\Delta\tau_{KW} = \frac{X}{C_{KW0}} = \frac{X}{\frac{dQ}{dA_{cr}}} \tag{1.6}$$

where X is the length of the reach. In contrast, C_{KW} estimates the ultimate speed attained by the bulk of wave so that $\Delta\tau_{KW}$ estimates the maximum travel time (Equation 1.6) [Bautista and Clemmens, 2005]. The actual wave celerity is between the two. In case of control, the goal is that neither the leading edge nor the bulk of the flow to arrive but the substantial fraction. Therefore a delay value that minimizes the water level deviations should be within the range $\Delta\tau_{DW} < \Delta\tau < \Delta\tau_{KW}$.

An analysis of the shape and propagation about kinematic, gravity and dynamic waves can be found in [Chung and Kang, 2006]. The effects of the upstream perturbations in a pool entirely under backwater are shown in Figure 1.3.

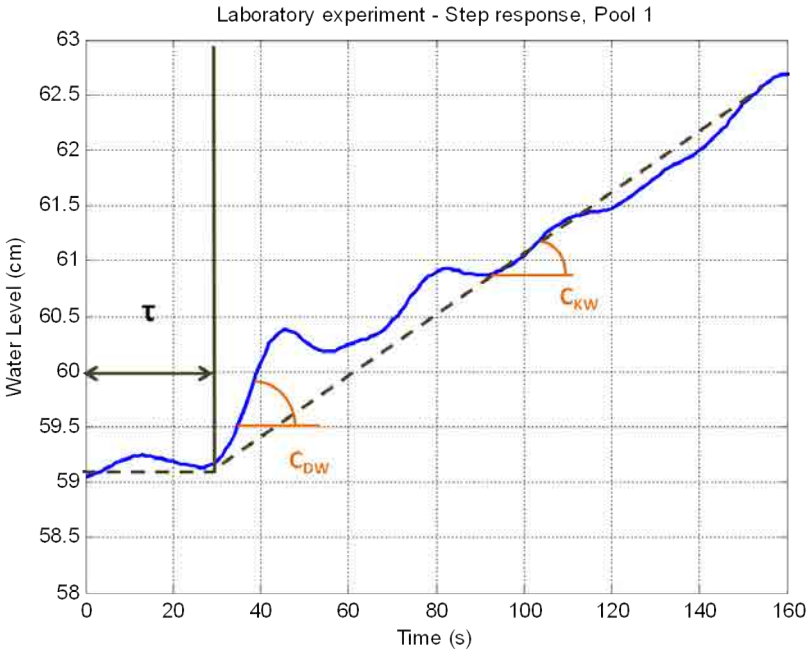

FIGURE 1.3: Step response of the laboratory canal with resonance waves

There is an initial fast increase due to the arrival of the dynamic wave, and it is followed by oscillations and a rise with a constant rate, that is the equivalent to the kinematic wave. In other words first the wavefront travels with dynamic wave speed, it reaches the backwater part. This acts as water level boundary and it makes the wavefront travel fast downstream. Then the uniform depth stays more or less constant acting as a flow boundary (slow increase). The slope

of this rise is the flow divided by the surface area (see Equation 1.6). In case of trapezoidal cross sections as the depth increases the surface also increases just as the slope of the step. After the fast increase in each oscillation, the slope of the wave is decreasing finally approaching the the straight (dashed) line with the constant slope (Figure 1.3).

In reaches that are completely affected by backwater (short reaches), the wave hardly deforms, and it is reflected and travels several times back and forth, producing high water levels locally and risk of overflow. This can be considered as resonance. The categorization of canals with respect to resonance can be found in [van Overloop, 2006b].

The control of these kind of canal pools is very challenging since due to the presence of the resonance wave the downstream end of the canal is in counter-phase with the upstream end. For example if the downstream water level is under setpoint, the controller tries to open the upstream gate more. However, the upstream water level is just in the other (high) phase and opening the gate will increase this level and excites the resonance phenomenon. This behaviour leads to oscillations and eventual overflow and should be avoided. There are several on-going studies about resonance in irrigation canals.

The problem of resonance is explained in [Schuurmans, 1997] and studied qualitatively in [Litrico and Fromion, 2004a], [van Overloop, 2006b] and quantitatively in [Miltenburg, 2008], [Clemmens et al., 2012] and [van Overloop and Bombois, 2012]. The detection of unwanted oscialltions is described in [Ooi and Weyer, 2011] and a model for this kind of canal pools developed in [van Overloop et al., 2010b].

The problem with the resonance can be observed using numerical simulation on the laboratory canal of the Technical University of Catalonia. In Figure 1.4 control techniques are used without taking the resonance into account and it can be seen that it lead to oscillations in the gate movements.

In Figure 1.5 a controller is developed for the canal taking into account the resonance during the controller development. There water level is controlled without problems. The control techniques and the controller development will be detailed later in this document.

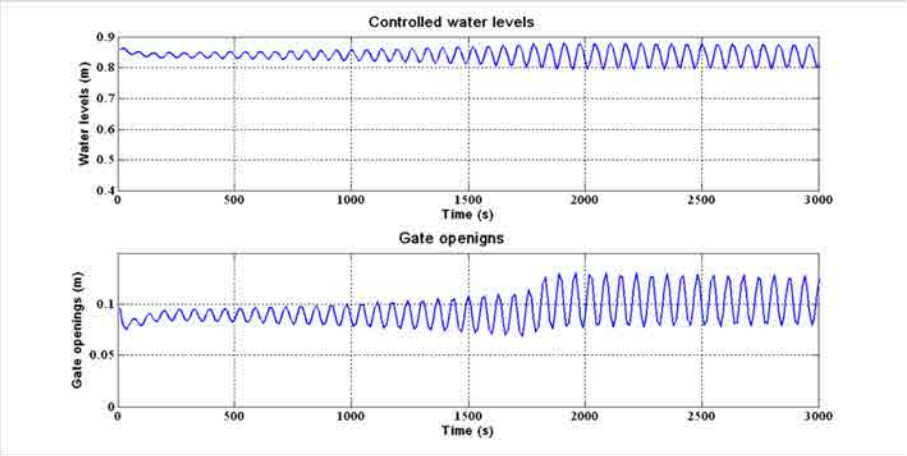

FIGURE 1.4: Numerical result of the laboratory canal controlled by a predictive controller without considering the resonance

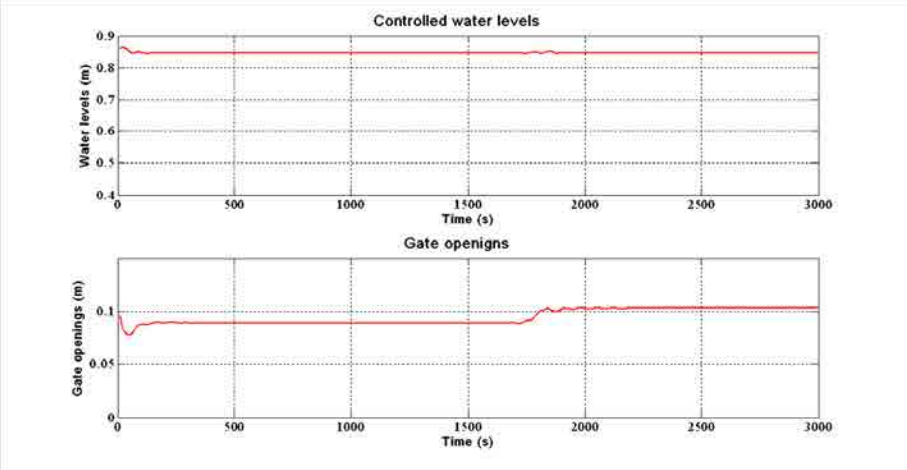

FIGURE 1.5: Numerical result of a predictive controller based on a model especially developed for resonant canals

1.1.4 Automatic control of irrigation canals

- **Types of canal control**

  There are two main control types: feedforward (open loop) and feedback (closed loop).

– **Feedforward control**

In the open-loop, the control action variable (input) is calculated from the dynamics of the system, the targeted output and the estimation of perturbations (Figure 1.6a). The open-loop can compensate time delays, but the system needs information that has to be approximated from climatic, agronomic, sociological data and past water consumption. An open-loop is insufficient due to the model errors, unknown perturbations. It can be applied to all types of variables.

– **Feedback control**

In case of closed-loop control (Figure 1.6b) the control action variable is calculated from the error measured between the real controlled variable and the corresponding target. Perturbations are taken indirectly, since they affect the output of the system. Closed loops can be applied to all controlled variables. There are two types of closed-loops in water level control depending on the relative location of the control action and controlled variable: water level can be controlled by modification of the upstream discharge (Feedback downstream control, FBdn) or the modification of the downstream water level (Feedback upstream control, FBup). The feedback control directly relies on measurements. It can be improved by introducing feed forward control or constructing storage volumes. However, it is a costly solution. A single closed-loop can only function correctly if storage volumes are available. Since both open-loop and closed-loop control have its limitations often the combination of the two is used. For a multivariable system with several variables, the different control actions can be combined (Figure 1.6c). Usually the discharge is controlled by open-loop and the water level is controlled by closed-loop, since open-loop does not need measurements just estimates and the water level is easier to measure. This work focuses on the closed-loop (feedback) control.

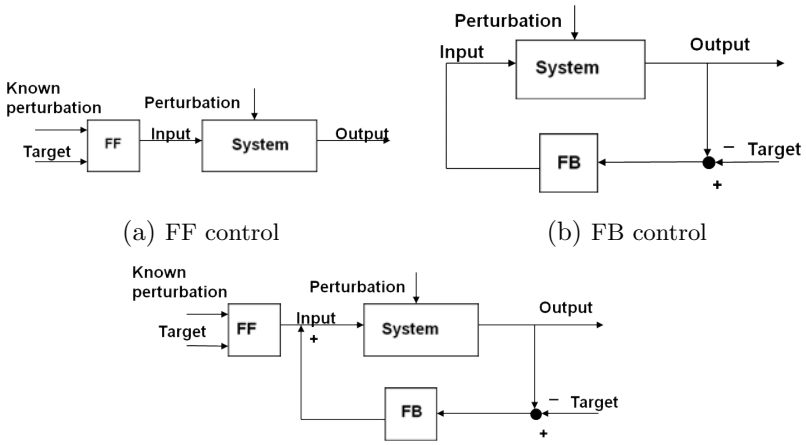

(a) FF control

(b) FB control

(c) Combined FB and FF control

FIGURE 1.6: Directions of control (from [Malaterre, 1998a])

- Direction of the control

  - **Downstream control**

    In case of downstream control the controlled variables are located downstream of the control action variables: for example the upstream the water level in a canal pool is controlled by a sluice gate at the upstream end of the pool. The check structure adjustments are based on information from downstream (Figure 1.7a). Downstream control generates indirectly discharge closed-loop control, since it is obtained from modification of upstream discharge. There is no need of supplementary discharge control loop.

  - **Distant Downstream control**

    In case of distant downstream control, the controlled variables are located downstream of the control action variables and the measured water depth is at the downstream end of the pool. In this case the time delay between the change in the control action variable and its effect on the target water level should be taken

into account. This type of control is very common, and it will be used in this work.

– **Upstream control**

In case of upstream control, the controlled variables are located upstream of the control action variables (Figure 1.7a), therefore the check structure adjustments are based on information from upstream. This control has to be completed by an explicit discharge control loop, since it does not generate any discharge control, it is appropriate for supply oriented systems. Without this, in case of on-demand operation it can leave the canal completely dry.

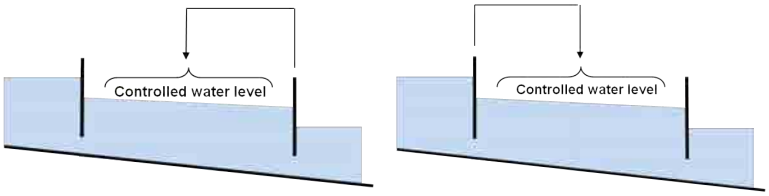

(a) Downstream control logic (b) Upstream control logic

FIGURE 1.7: Directions of the control

- Design techniques

Several design techniques are listed and briefly described, and examples from control of water systems are given.

– **Heuristic control methods**. These methods do not base on physical laws, the system is for them a black box. Examples for heuristic control are the following:

* **Control based on rules-of-thumb**

These methods are control rules derived from traditional operation. They can even be used if there is not much data available.

* **Neural network**

This control method can be used when large amount of measurements is available and the system is too complex to model: [Durdu, 2004] and [Damas et al., 2000].

  - **Fuzzy logic**

    This control method can be used when multiple operators are working on the same control task: [Stringam, 1998], [Begovich et al., 2005] and [Begovich et al., 2007b].

  - **Genetic algorithm**

    These algorithms are faster to find optimal solutions, however, optimality is not guaranteed in case of large systems: [Nixon et al., 2001] and [Ines et al., 2006].

- **Proportional Integral Derivative (PID)** control is one of the most common control methods, it is based on the use of the proportional/derivative/integral of the measured error to correct the control action in a feedback loop: [Ratinho et al., 2002], [Rijo, 2003] and [Montazar et al., 2005].

- **Control by model inversion** includes control schemes that are based on the inversion of the equations describing the movement of the water. This inversion can also be dynamic: [Benayache et al., 2008].

- **Predictive control** is based on the optimization of a given criterion for the present and a given length of future. This optimization is repeated at every time step and the data is updated by measurements: [Rodellar et al., 1989], [Lemos et al., 2009], [Malaterre and Rodellar, 1997] and [van Overloop et al., 2010a].

- **Optimal control** is based on finding a control law to a system in order to achieve to optimality of a given criterion (e.g. minimum of the error): [Sawadogo et al., 1995] and [Malaterre, 1998b].

- **Linear Parameter Varying Control (LPV)** consideres controlling a linear system whose parameters can change in time. In case of canals this parameter is often the time delay: [Bolea et al., 2009] and [Duviella et al., 2010].

- **H∞** is an optimization technique that is able to achieve optimal control, considering robustness, dealing with model uncertainity by minimizing the $H\infty$ norm: [Li et al., 2004] and [Litrico and Fromion, 2006a].

- Structure of the control

  - **Centralized control**

    Centralized control strategy takes into account all the objectives that have to be fulfilled at different control sections and a unique controller is designed using global information of canal state. The best control performance can be obtained with this strategy, however, in order to implement centralized control it is necessary to build communication links between the control structures and a central control unit: [Montazar et al., 2005] and [van Overloop et al., 2010a].

  - **Decentralized control**

    The decentralized control strategy is normally based on simpler control methods. There are separate controllers designed for each pool, taking into consideration the interaction between the pools. In some cases a higher level controller supervises the independent controllers. With this strategy, suboptimal control is achievable: [Sawadogo et al., 2000] and [Gómez et al., 2002].

  - **Distributed control**

    Distributed control is defined by [Maestre Torreblanca, 2010] as each controller of the subsystems communicate an order to find a cooperative solution for the overall control problem. An example for its implementation for irrigation canals is in [Negenborn et al., 2009c].

- Canal modelling

  Some control techniques can use lumped, distributed, high order or non-linear models to describe the canal dynamics. However most methods require simple linear models. Most of the control methods are formulated based on internal models describing the system dynamics. There are three main categories of internal models: black box and white box models and in between these two categories the grey box models, having characteristics of both of the previously mentioned groups (Figure 1.8).

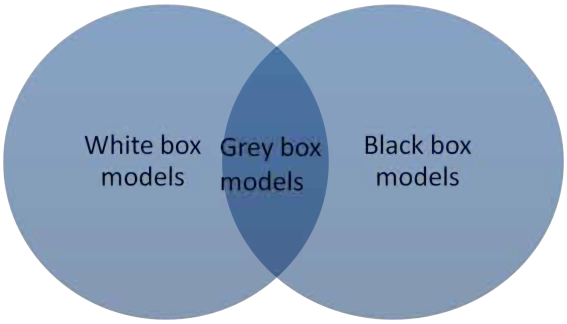

FIGURE 1.8: The three type of models

– **Black box models**

In the case of black box models, measured data are used and a model of any structure is fit to the measured data. The advantage of this method is its simplicity: only experimental data is taken and a model can be fit without any knowledge of the dynamics of the system. The disadvantage of this method is that sometimes the model structure does not take into account the whole real dynamics. It can be very different from the real process, especially in operation points further from the point where the data for the identification was collected, or even in some cases it may not be possible to collect data or the process could be very expensive.

This methodology is often used in control problems. In [Sepúlveda, 2008] ARX (AutoRegresive model with eXternal input) models were identified with orders between 5 and 10. Second and third order models were identified for a laboratory irrigation canal at the Mexican Institute of Water Technology [Begovich et al., 2007c]. Linear parameter varying first order models were applied for the Lunax dam-gallery at Gascogne by [Puig et al., 2005]. In [van Overloop and Bombois, 2012] the authors identify 9th order model from experimental data using an existing canal at the Central Arizona Irrigation and Drainage District.

– **White box models**

The white box models are based on the mathematical description (conservation laws) of the system. The model is calculated from

known/measured parameters and the measured data might be used only for verification [Malaterre, 1998b], [Gómez et al., 2002], [van Overloop et al., 2008] and [Xu et al., 2010b]. The advantages of this approach are that the model contains the real dynamics of the system, it might have a wider range of validity and it does not require measurements. However, these models may not be simple to establish, and the dynamics of the complete system may not be known in all the cases. Or even sometimes the whole system is so complicated that there is a need for simplification of the original model.

There are several works considering the whole linearized set of Saint-Venant equations. There are methods to simplify the computational burden in order to make the real time implementation possible [Xu et al., 2010b].

Simplified versions of these equations have been proposed, for example the diffusive wave equations, which with the help of the moment matching method can be approximated as second order model with delay [Malaterre, 1994] and [Litrico and Georges, 1999].

Simplified hydraulic models like the Muskingum model have been used by some authors: [Rodellar et al., 1989], [Gómez et al., 1998] and [Alvarez Brotons, 2004]. Another simplified hydraulic model, the Hayami model is also used for control purposes by [Chentouf, 2001] and [Charbonnaud et al., 2011].

The most common simplified model used in practice is the Integrator Delay model: [van Overloop et al., 2005], [Wahlin and Clemmens, 2006], [van Overloop et al., 2010a] and [Zafra-Cabeza et al., 2011].

– **Grey box models**

Between the two previous approaches there is the gray box model concept. In this case the model dynamics is a priori given, but the parameters are identified using experiments and . There are examples of models of different structures: in [Weyer, 2001] a third order, in [Aguilar et al., 2009] a first order with delay and in [Aguilar

et al., 2011] and [Aguilar et al., 2012] an Integrator Delay Zero model is identified.

- Control action variables

  The most common choice for control action variable is discharge or gate opening.

  - **Discharge**

    If discharge is used as control action variable there is a need for a method to calculate the gate openings. This method can either be an equation (for example the inversed gate equation) or an inner control cycle with a higher sampling time that controls the position of the gate in order to achieve the required discharge.

  - **Gate opening**

    If gate openings are used as control action variable the values can be directly sent to the structure. The advantage is that the controller directly gives a value for a physical variable, there is no need for further conversion. It is also possible to include constraints on the gate opening directly in the controller. However, for decentralized control the coupling effects should be taken into account, decouplers should be used.

- Controlled variables

  Controlled variables can be discharges, water levels or water volumes.

  - **Discharges**

    The needs of the irrigation canals are usually defined as discharges, therefore it is a natural choice to use discharges as controlled variables. To maintain sufficient discharge is necessary to fulfill the demand of the different needs:

    * agricultural: irrigation flow, supply to secondary canal
    * urban: flows to treatment plants or residential areas, maximum flows in storm water conditions
    * industrial: flows to facilities
    * environmental: ecological flows.

If natural or artificial reservoirs are available, the demand can be defined as volume distributed over a time, and the controlled variable is no longer the discharge but the volume. However, construction of reservoirs is costly.

– **Water levels**

The main advantage of using water level as controlled variable is that it is easy to measure. Moreover, several demands are expressed in terms of water levels:

* constraints of feeding gravity turnouts
* stability of canal banks
* efforts to reduce weed growth
* constitution of intermediate water storage volumes
* risks of overflow.

Controlled water levels can be upstream, downstream or intermediate inside the pool as seen in Figure 1.9.

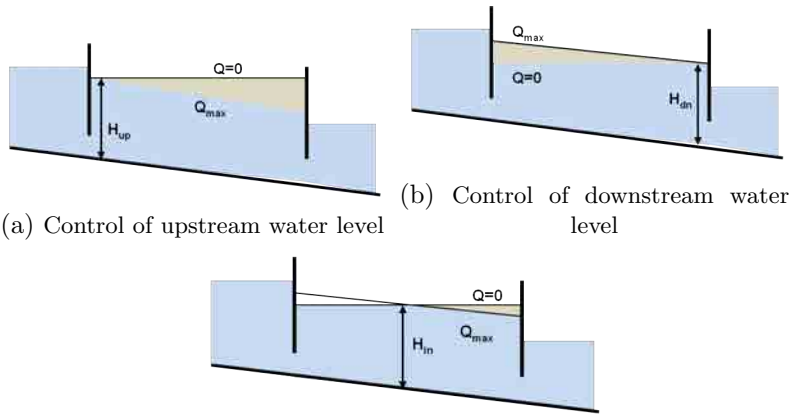

(a) Control of upstream water level

(b) Control of downstream water level

(c) Intermediate water level

FIGURE 1.9: Location of controlled water levels within a canal pool

Controlled water level is upstream of the pool

The controller maintains at setpoint the water level upstream in the pool (Figure 1.9a). Storage volume is available between the

null discharge volume and the maximum discharge volume. It allows rapid response to the unforeseen demands of turnouts, and it can store water. However, the canal banks have to be horizontal, which is expensive. Also an upstream control can lead to scarcity in downstream pools, since it retains water in order to ensure the upstream water level.

Controlled water level is downstream of the pool

In case of downstream control the controller maintains at setpoint the water level downstream in the pool (Figure 1.9b). The canal banks can follow the field natural slope, which reduces construction costs. However, no storage volumes are available therefore the system cannot respond quickly to unforeseen downstream demands. This logic of control is appropriate for demand-oriented systems. The storage wedge responds to the outflows variations rapidly and efficiently [Buyalski et al., 1991] and [Goussard, 1993]. However, the canal bench has to be horizontal to accommodate the null flow surface profile, and canal building becomes much more expensive and difficult.

Controlled water level in the middle of the pool

In case of intermediate water level control, the controlled water level is close to the middle of the pool, hence it controls the volume stored in the pool (Figure 1.9c). It is a compromise between upstream and downstream control, considering construction costs and availability of storage volume. However, one or several distant water levels have to be measured which implies the installation of a measurement network. Controlling the intermediate water level is not so common, one example can be the BIVAL controller [Chevereau and Schwartz-Benezeth, 1987].

– **Volumes**

Controlled variables can be also be water volumes, that is the integral of flows. It is applicable to canals with large storage volumes equipped with lateral offtakes whose discharges do not depend on the canal level, such as pumps. These controllers are less sensitive to perturbations, but have longer response times.

1.2 Model predictive control on water systems

Model predictive control (MPC) is one of the most commonly used advanced control method in industry. Its development started in the 1970s [Martín Sánchez, 1974] and since then several applications are implemented in industry. Predictive control refers to a group of controllers that have the following main characteristics in common:

- explicit use of a model to predict the process output at future time instants
- minimizing an objective function by calculating a control sequence
- receding strategy: at each instant only the first calculated control action is applied, and the ones for the future instants are updated at every control step.

The definition of the predictive control is outlined as follows: using a simple model of a system to be controlled, the predictive control makes the calculated (predicted) output of the process equal to the desired one, while giving the input conditions for this calculated output. Figure 1.10 from [Martín Sánchez, 1974] illustrates the main blocks defining the predictive control. Predictive control is based on a linearised model (predictive model) that can approximate the output of the system. Using this model and approximating the output in every time step, the desired result can be given, and from this the desired input can be calculated in a reverse way. This time length, the prediction horizon can be chosen according to the constraints of the process. A key advantage of MPC is that it can accommodate hard constraints on the inputs, states and output of the controlled system.

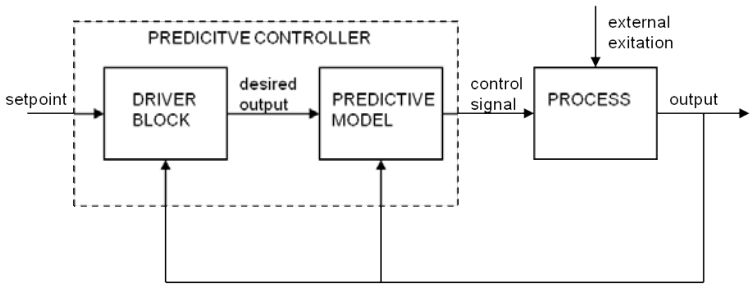

FIGURE 1.10: Model predictive control from [Martín Sánchez, 1974]

The application of predictive control for water systems has been investigated for a long time. It was applied as decentralized [Sawadogo et al., 1998] and centralized [Akouz et al., 1998] control of irrigation canals. Different types of predictive control have been implemented to water systems: predictive functional control was also tested for canal operation by Pages [Pages et al., 1998].

Adaptive predictive control has been applied to canals [Cardona et al., 1997], rivers [Foss et al., 1989], and laboratory experiments have been published with this type of control, too [Lemos et al., 2007]. Optimal predictive control is implemented on a 100 km long canal in order to maintain the ecological flow [Puig et al., 2009].

Nonlinear predictive control can also be applied to water systems: [Georges, 2009], [Igreja and Lemos, 2009] and [Schwanenberg et al., 2010].

For control of water systems, often the input variables are uncertain, and there are different points of operation depending on the weather conditions. The solution of using multiple models is developed in [van Overloop et al., 2005] and incorporate the stochastic behaviour of the variables to the predictive controller [Raso et al., 2012].

Model predictive control is used to control water levels [Wahlin, 2004] or discharges [Rodellar et al., 1989] or even to control water quality [Xu et al., 2010a], or for risk mitigation [Zafra-Cabeza et al., 2011].

There are several decentralized and centralized operation examples, and recently there has been a great interest for distributed model predictive control on irrigation canals [Negenborn et al., 2009b]. There are many ways to implement the communication between agents: non-iterative [Negenborn et al., 2009a], or iterative approaches [Doan et al., 2009]. For the latter a good example is when the negotiation between agents is based on game theory [Maestre Torreblanca, 2010].

Model predictive control due to its flexible nature and possible application of constraints can be used to achieve special goals in canal control, for example store water in certain canal pools [Hashemy Shahdany et al., 2012]. MPC can be applied to irrigation canals [Puig et al., 2009], rivers [Compas et al., 1997],

hydropower plants [Setz et al., 2008] or to drainage canals [van Overloop, 2006a] and [van Overloop et al., 2008].

Apart from the investigations, predictive control proved to be applicable and has been implemented and tested on real cases. One of the milestones of model predictive control practical implementations is its application on the West-Maricopa canal, that is considered to be a benchmark for numerical tests [Clemmens et al., 1998]. First a numerical test for two reaches [Akouz et al., 1998] and later for the whole canal has been published [Ruiz and Ramirez, 1998]. The first actual demonstration was in 2010 by van Overloop [van Overloop et al., 2010a]. It is shown that the water is efficiently delivered to the users and the water level deviations are small.

Several applications of controllers on real systems are now implemented. In Spain adaptive-predictive expert control is tested on the Canal Imperial de Aragón by [Aguilar et al., 2012]. A general predictive control is implemented on 12 basins for the Rhone river [Compas et al., 1997]. Also adaptive predictive control is implemented on a river with hydroelectric power plants, Ulla-Forre power production system on the South-west coast of Norway by Foss [Foss et al., 1989]. Also there are several practical applications of MPC can be found in the Netherlands for drainage purposes: [van Overloop, 2006b], [van Overloop et al., 2008] and [van Overloop et al., 2010c].

1.3 Problem statement and objectives of the thesis

1.3.1 Problem statement

To develop and test experimentally well-performing water level controllers for canals affected by resonance.

1.3.2 Main objective

The main objective of this thesis is the development of a centralized predictive controller in order to control resonant canals. The study includes different options for canal modelling, including the choice of the control variables.

All controllers are to be implemented numerically and experimentally on the laboratory canal of the Technical University of Catalonia. In order to achieve this objective the followings are proposed.

1.3.3 Detailed objectives

- Calibration of the hydraulic structures used for discharge and level measurement in the laboratory canal.
- Analysis of the hydraulic behaviour of the laboratory canal, and finding a model for control purposes in order to develop MPC for the laboratory canal.
- Tackling the problem of modelling and controlling the gravity offtakes that produce and unknown disturbance for the controller.
- Analyzing the choice of control variables, using the example of the laboratory canal.
- Implementing a centralized model predictive controller, testing it numerically and experimentally.

1.3.4 Contributions

- A deep analysis of model predictive control techniques for irrigation canals in presence of resonance.
- Application of offset free model predictive control.
- Experimental verification of all the results.

1.4 Thesis outline

This thesis is a description of a process of finding well performing controllers to the UPC-PAC. Each chapter is analyzing one aspect of the controller building. The process is summarized in Figure 1.11. There are three mains parts are summarized: first obtaining the model for the canal. This consists of the choice of the model then the identification. Secondly, having the model chosen control algorithms are developed. Finally the chosen control algorithms are tested numerically and experimentally.

- The work starts with a brief introduction in Chapter 1.
- In Chapter 2 the laboratory canal is described in detail, with focus on the flow measurement techniques and their calibration.
- In Chapter 3 identification procedures are used to obtain a model for control purposes, while Chapter 4 is analyzing the performance of white box models. In the same chapter all models are compared and tested, and the final model is chosen.
- In Chapter 5 the offset free MPC is discussed, and a new methodology is suggested to achieve offset free control.
- In Chapter 6 the choice of control variables is analyzed.
- By arriving to Chapter 7 an offset free MPC have been developed for the laboratory canal, based on a model, and chosen the best control variables. In this last chapter the whole work is concluded.

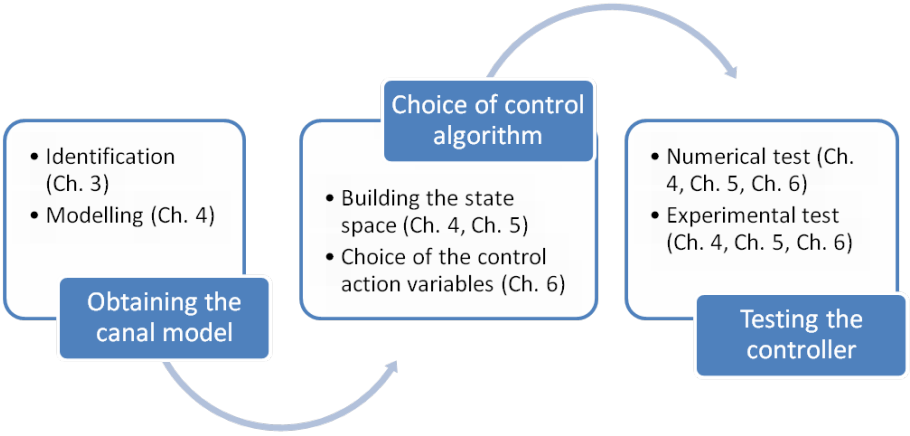

FIGURE 1.11: The controller development through this work

Chapter 2

The laboratory canal UPC-PAC

2.1 Introduction

In this chapter the laboratory canal of the Technical University of Catalonia is introduced. After the physical description of canal, some ways to obtain flow measurements are discussed. On one hand it is not closely related to automatic control, on the other hand the correct measurement of discharge is crucial for control of irrigation canals. In the laboratory canal the flow measurement is carried out by means of hydraulic structures, like in most of the real canals. They are very often used in practice and their accuracy and calibration is an important issue in case of real canals just like in the laboratory. Therefore some general and specific aspects of their calibration are discussed. For the gates a short description is presented, since a calibration study about this canal was already published [Sepúlveda et al., 2009]. For the weirs, the calibration and the flow measurement are discussed more in detail.

2.2 Laboratory canals

A short revision is given about similar installations in the world and their developments. There are few hydraulic laboratories that have a scale model of an irrigation canal with control facilities. These are located in Évora (Portugal), Mexico city (Mexico), Denver (USA) and in Barcelona, at the Technical University of Catalonia (Spain).

2.2.1 The Hydraulics and Canal Control Centre (NuHCC)

The Hydraulics and Canal Control Centre belongs to the University of Évora (Portugal). The experimental canal has U-shape with a length of 141 m, containing 4 pools, each of them is approximately 40 m long. The cross section is trapezoidal and the maximum flow is 0.09 m^3/s, the uniform water depth is 0.7 m. The channel is equipped with 3 motorized sluice gates, while in the downstream end there is an overshot gate. The offtakes are orifice types, the flow is controlled by servo motorized valves [Ratinho et al., 2002].

Several control strategies have been implemented and tested, starting from the simple ones until the most sophisticated ones. Local PI control was developed in [Ratinho et al., 2002] and [Rijo, 2003], and adaptive and non-adaptive predictive control in [Lemos et al., 2007] and [Lemos et al., 2009]. Model predictive control based on the whole set of linearized Saint-Venant equations was implemented in [Silva et al., 2007]. Distributed model predictive control is implemented numerically in [Igreja et al., 2011] and later experimentally in [Lemos et al., 2012b]. Distributed linear-quadratic-Gaussian (LQG) control [Lemos et al., 2012a] was the latest development.

2.2.2 Laboratory canal of the Mexican Institute of Water Technology (IMTA)

In Mexico, the experimental canal is situated at the Mexican Institute of Water Technology (IMTA). The laboratory canal has four pools (13 m, 12 m, 12 m

and 13 m), the whole canal is 50 m long, 0.6 m wide and 1 m deep. The nominal inflow is 80 l/s. The controlled variables are the downstream water levels of the first three pools and the control variables are the openings of the sluice gates. There are no lateral outlets [Begovich et al., 2007c].

Different control strategies have been implemented: predictive control [Begovich et al., 2007c], decentralized LQG (Linear-quadratic-Gaussian) control [Begovich et al., 2007a] and also fuzzy gain scheduling control [Begovich et al., 2005].

2.2.3 Laboratory canal of the Bureau of Reclamation, Denver

A model canal facility is located in Reclamation's Hydraulics Laboratory. It is 91 m long and it is made from clear acrylic and aluminum. It has five motorized control gates, four turnouts, a long-throated flow measurement flume and an inverted siphon. It is fully instrumented to remotely monitor and control water levels, gate positions, and flows with both manual and automatic control features. The canal was designed for demonstration and education purposes, and has many of the modern control features used on actual canals [U.S. Department of the Interior, Bureau of Reclamation, 2013].

2.3 Laboratory canal of the Technical University of Catalonia

2.3.1 History

The construction of the laboratory canal of the Technical University of Catalonia started in 2003 and was finished in 2005. The design and instrumentation of the canal was under the responsibility of Carlos Sepúlveda, whose doctoral thesis is the result of this work [Sepúlveda, 2008]. Also the first control operation tests can be found in this document. He carried out the first calibration of the sluice gates for flow measurement [Sepúlveda et al., 2009].

2.3.2 Physical description

The UPC-PAC canal (Canal de Prueba de Algoritmos de Control – Universitat Politècnica de Catalunya) is specially designed to develop basic and applied research in the irrigation canals control area. The canal is designed with a serpentine shape in order to achieve the greatest length using small surface area. The geometrical data of the canal is the following: it is 220 m long, 0.44 m wide and 1 m deep. The canal has zero slope in order to achieve the largest possible time delay. The geometrical data is summarized in Table 2.1, where n is the Manning's roughness coefficient, B is the channel width (m), S_b is the bottom slope (m/m) and X is the length (m) of the canal pool. In the upstream end there is a constant level reservoir, that is connected with a sluice gate to the canal. Photographs of the UPC-PAC are shown in Figure 2.1.

(a) Top view (b) Reservoir

(c) Weirs (d) Sluice gates

FIGURE 2.1: Pictures of the UPC-PAC

n (-)	B (m)	S_b (m/m)	X (m)
0.016	0.44	0	220

TABLE 2.1: The geometric parameters of the UPC-PAC

The canal contains 3 operative motorized sluice gates, therefore it is possible to divide it into 3 reaches. At the downstream end there is a sharp crested weir with variable height. The same structures are found at the downstream end of every reach to model the gravity offtakes for irrigation (with minimum height of 34.3 cm). The maximum discharge that can circulate is 150 l/s. The schematics of the canal is shown in Figure 2.2. The UPC-PAC can be configured from 1 to 3 pools. It is possible to simulate water level or discharge control, and to produce known or unknown disturbances.

2.3.3 Instrumentation

The water levels are measured by 9 pressure sensors, and the data from the water level and gate opening measurement is connected to a supervisory control and data acquisition system (SCADA). The canal can be configured from one pool up to three pools, hence both SISO (Single Input/Single Output) or MIMO (Multiple Input/Multiple Output) controllers can be tested. The SCADA system was developed in Matlab/Simulink environment, which makes straightforward the test of any control algorithm developed in Embedded Matlab language [Mathworks, 2008].

The water levels are measured by sensors, and the measured signals, after an analog-digital conversion, arrive to the data acquisition card of the central computer. The controller programmed in Embedded Matlab calculates the control action, and the signal after digital-analog conversion is sent to the actuators (the motors of the gates).

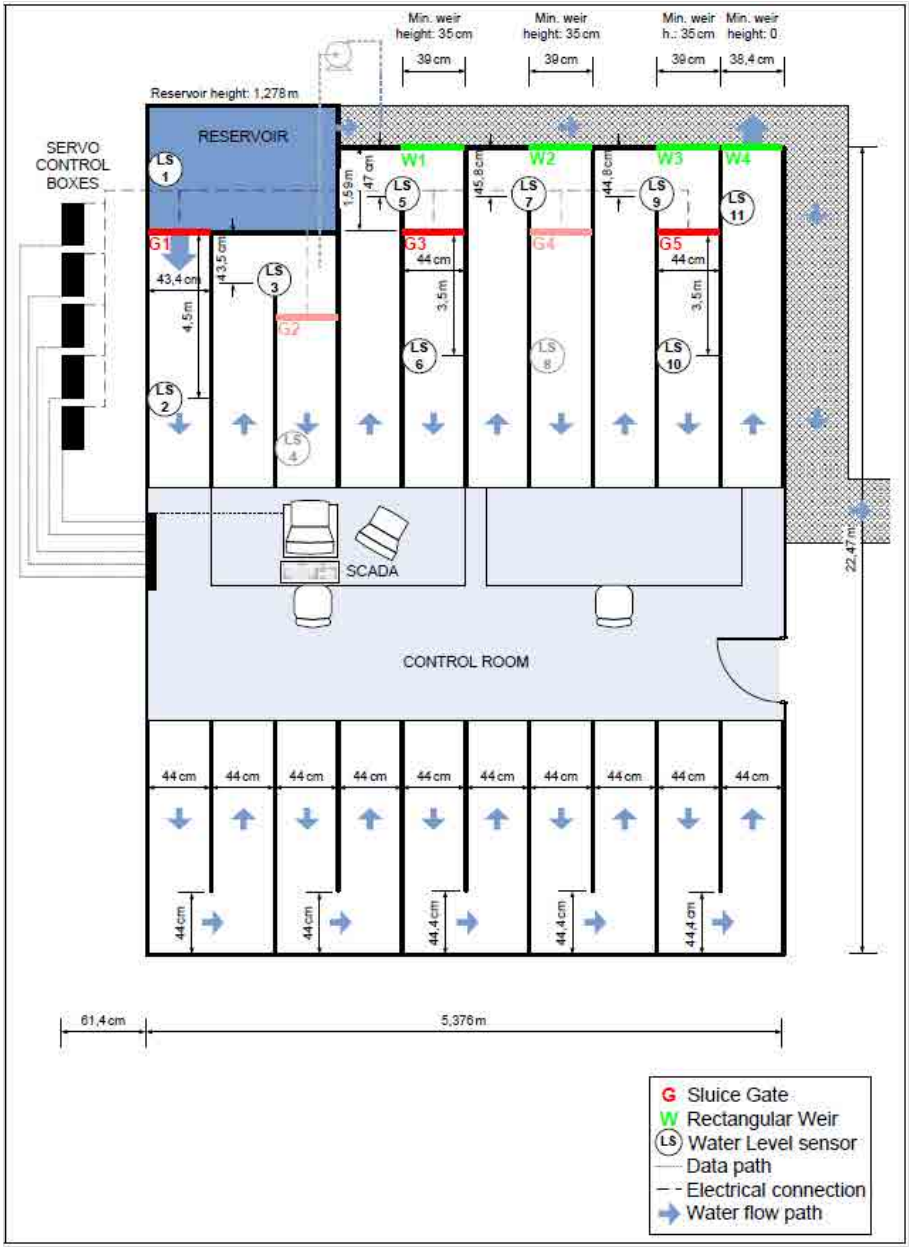

FIGURE 2.2: Schematic layout of the UPC laboratory canal, from [Sepúlveda, 2008]

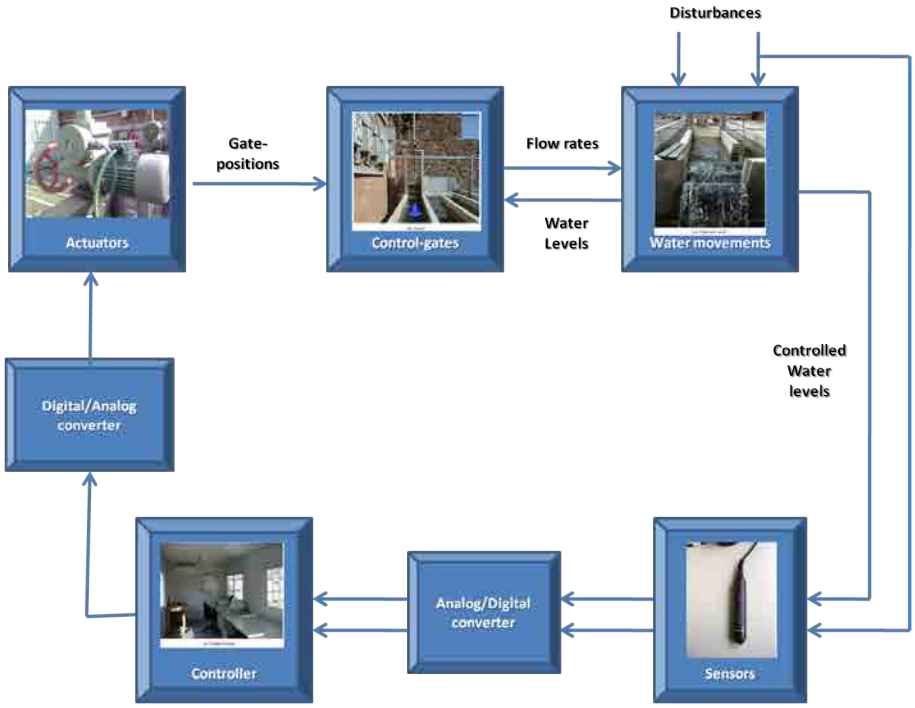

FIGURE 2.3: Schematics of the instrumentation of the UPC laboratory canal

2.3.4 The numerical model of the UPC-PAC

The SIC software (Simulation of Irrigation Canals) is a hydraulic simulation software adapted to the calculation of flows in irrigation canals developed by IRSTEA [Malaterre and Baume, 1997]. The Saint-Venant equations are solved numerically using Preissmann Scheme, an implicit finite difference scheme. The development of SIC started in the early 1970s and it is still going on. The software was especially developed for simulation of automatic control of irrigation canals, and there are several possibilities to model different hydraulic structures. Some of the most common control algorithms (e.g. PID, BIVAL) are already incorporated and it is possible to evaluate any algorithm written using the computational software Matlab [Mathworks, 2008].

The UPC-PAC is modelled using 6 nodes and 4 reaches (a reach is a part of the canal bounded by nodes). This configuration is shown in Figure 2.4. The

reaches are separated by the inner nodes, which are the places of the offtakes (Weir 1, Weir 2 and Weir 3). The last node is in the place of Weir 4. The gates are placed downstream to weir 1 (node 3) and weir 3 (node 5). Weir 4 is included as boundary condition. All reaches belong to one branch.

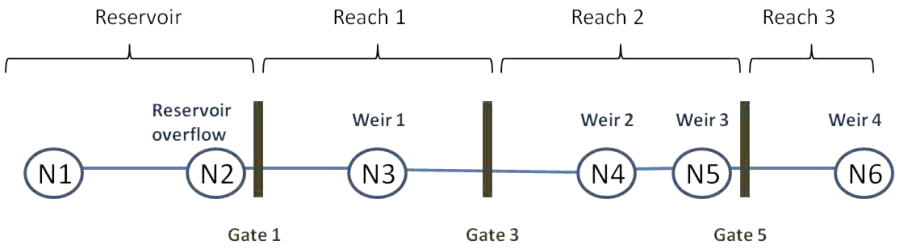

FIGURE 2.4: Model of the UPC-PAC in SIC

The schematic view of the head reservoir can be seen in (Figure 2.5). The height of the overflow weir is 1.28 m. The surface area of the reservoir is 3.08 m^2. The overflow of the reservoir was implemented as a weir type offtake, as open flume with the following data. The reservoir is modelled by using the first and part of the second reach. The first reach is 0.2 m long, and an offtake is inserted (at the first node). At that location the width of the flume was given to be 4.44 m. Gate 1 is placed 0.1 m downstream.

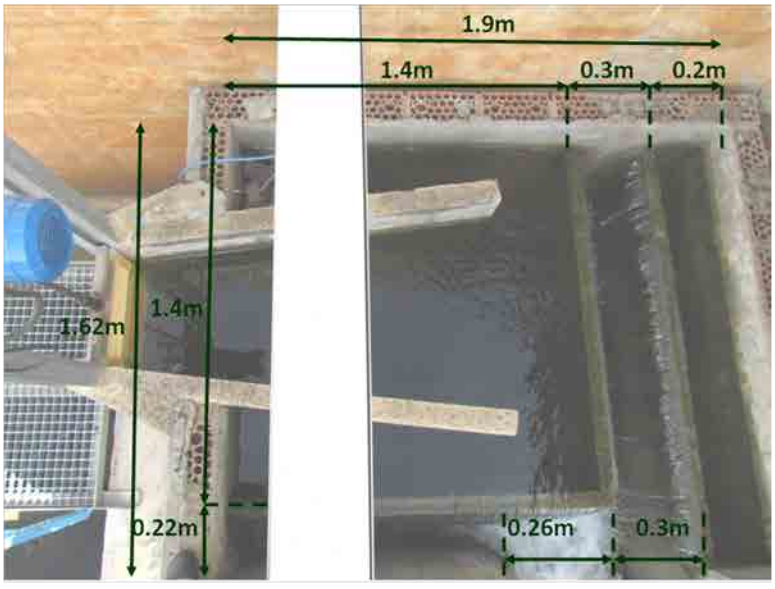

FIGURE 2.5: The upstream reservoir of the UPC-PAC

The sections are rectangular are 0.44 m wide. The canal has zero slope. Every reach has one cross section at the beginning and one cross section at the end. The reaches containing gates (reach 2 and 4) have altogether 4 cross sections, with two additional ones. The first one is a "singular" cross section: it is a cross section that shows the location of the gate and the second one directly downstream of the singular cross section.

Validation of the SIC model

The numerical model was validated by using measurement data. The calibration parameters were the gate discharge coefficients and the Manning's roughness coefficient. The value of the roughness coefficient is 0.016 and the resulting values of the gate discharge coefficients are shown in Table 2.2. The same roughness coefficient was assumed for the whole canal.

	Gate discharge coefficient (-)
Gate 1	0.67
Gate 3	0.64
Gate 5	0.69

TABLE 2.2: Calibrated discharge coefficients for the Kindsvater-Carter equation and measured error

The measured gate openings of a real experiment were fed to SIC and the resulting water levels were compared in Figure 2.6. A change of water level in the first canal pool is simulated: at 30 min the water level was reduced and at 60 min the water level setpoint was changed back to 85 cm. The differences between the numerical simulation and the experiment are due to the physical constraints of the installation. Similar constraints are present in case of real irrigation canals. They are the followings:

- Minimal gate movement: 8 mm
- Measurement errors
  - Gate position measurement error: 2 mm
  - Water level measurement error: 8 mm

- Modelling of the hydraulic structures

  There was a study carried out about modelling the hydraulic structures, whose behaviour still cannot be exactly described by the equations.

- Unmodelled processes

  - Small flows on the side of the gates
  - Local energy losses and 2D effects due to the curvature of the canal
  - The unmodelled dynamics of the gates, transitional flows between submerged and free flow

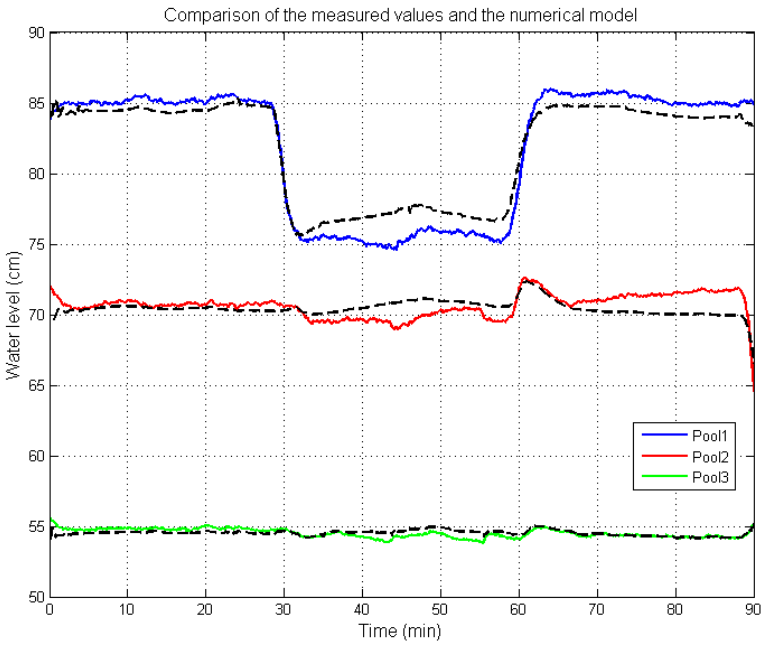

FIGURE 2.6: Comparison of the measured (blue, green and red) and the simulated (dashed black lines) water levels

2.4 The calibration of the gates of the UPC-PAC

2.4.1 General description of sluice gates

The canal check gate structure has become the dominant tool for implementing canal system operations [Buyalski et al., 1991]. The sluice gate can be defined as a wooden or metal plate, vertical or curve, which slides in grooves in the sides of the canal [Sepúlveda, 2008]. It is often used as a control structure in canals.

2.4.1.1 Flow types of the sluice gate

Free flow

If the flow is free flow through the opening gap, the flow smoothly accelerates from subcritical (upstream) to critical (near the gap) to supercritical (downstream) [White, 1999]. For the sudden obstruction, as the jet is coming from the gate, the flow is contracted to a minimum height, called the vena contracta (H_2). See Figure 2.7.

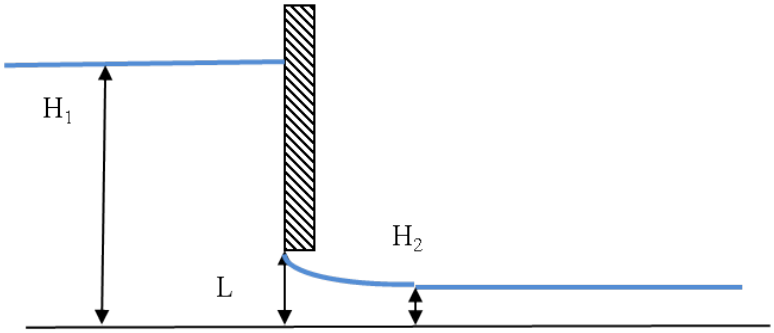

FIGURE 2.7: Sluice gate - free flow

In case of a sluice gate the flow upstream the gate is subcritical, downstream the gate is supercritical. In this way the downstream water level is determined by the gate. In order to have subcritical flow condition further downstream hydraulic jump develops to perform the transition in energy [Henderson, 1966].

The shape of the hydraulic jump depends on the relationship between the downstream water depth and the conjugate water depth H_3'.

If the downstream water depth is equal to the conjugate water depth, the hydraulic jump occurs exactly downstream the gate ($H_3 = H_3'$). See Figure 2.8.

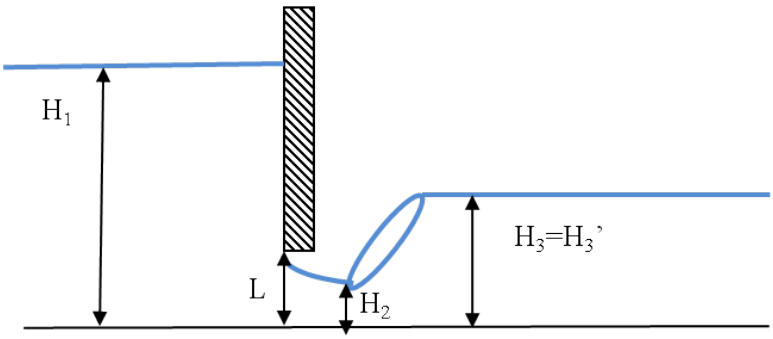

FIGURE 2.8: Sluice gate - hydraulic jump

If the downstream water depth is smaller than the conjugate water depth the hydraulic jump is located downstream the gate, until it can satisfy the energy equation (conjugate depths) ($H_3 < H_3'$). See Figure 2.9.

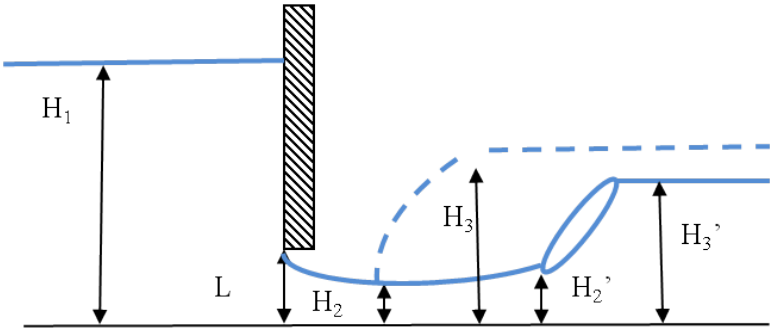

FIGURE 2.9: Sluice gate - hydraulic jump further downstream

Submerged flow

If the downstream water depth is higher than the conjugate water depth (high tailwater) the hydraulic jump is forced to move upstream and may eventually drown in the source and become a submerged hydraulic jump ($H_3 > H_3'$). The sluice gate is said to be drowned or partially drowned. See Figure 2.10. The

energy will dissipate in the exit flow in the form of a drowned hydraulic jump, and the downstream flow will return to subcritical. Most of the gates working as discharge control structures are under submerged flow condition. Therefore it is crucial to ensure that the gates in the canal are operating submerged. It is also important for the flow calculations: different relationships apply to submerged and to free flow [White, 1999].

The canal system should be designed either for submerged or for free flow. The sudden changes in flow conditions can cause operational problems [Buyalski et al., 1991]. In case the sluice gates have discharge control function it is crucial that the gates operate in a submerged condition. In the UPC-PAC canal the upstream gate always operates with small gate openings, therefore the flow is always submerged.

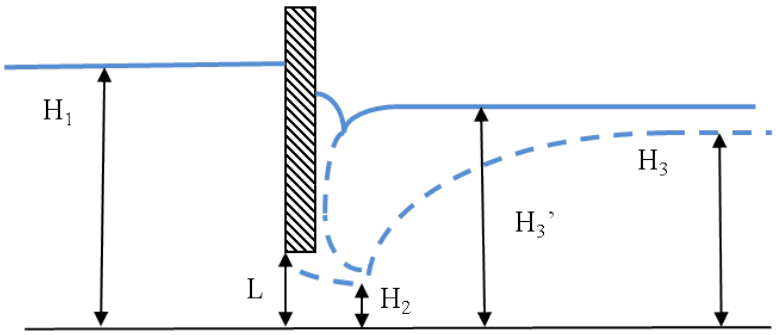

FIGURE 2.10: Sluice gate - submerged hydraulic jump

The limit between free and submerged flow

According to the manual of the HEC-RAS hydrodynamic model [Brunner, 1995] submergence occurs when tailwater depth/headwater energy is bigger than 0.67. It completely changes when the ratio increases to 0.8.

The condition from [Swamee, 1992] is used to make a difference between free and submerged flow: where H_1 upstream depth, H_3 downstream depth and L is the gate opening. If Equation 2.1 holds, it is free flow condition, while if Equation 2.2 holds the flow is submerged:

$$H_1 \geq 0.81 H_3 \left(\frac{H_3}{L}\right)^{0.72}, \tag{2.1}$$

$$H_3 < H_1 < 0.81 H_3 \left(\frac{H_3}{L} \right)^{0.72}. \tag{2.2}$$

2.4.2 Flow measurement with sluice gate

From the energy equation the flow under a sluice gate in free flow conditions is

$$Q = C_{df} B L \sqrt{2g \left(H_1 + \alpha \frac{V_1^2}{2g} \right)} \tag{2.3}$$

where C_{df} is the discharge coefficient for free flow, B is the width of the gate, L is the opening, H_1 is the upstream water depth, $\alpha V_1^2/(2g)$ is the velocity head of the approaching flow. For submerged flow, the effective height should be used in addition to the upstream water level or the difference between the upstream and the downstream water level. For the experiments, the velocity head can be included in the discharge coefficient [Chow, 1959]

$$Q = C_{df} B L \sqrt{2g H_1} \tag{2.4}$$

and for submerged flow:

$$Q = C_d L B \sqrt{2g \left(H_1 - H_3 \right)}. \tag{2.5}$$

The discharge coefficient is different for submerged C_d and for free flow C_{df} conditions. In case of submerged flow it depends on the contraction coefficient, the gate width, the upstream water level, and the downstream water level.

The contraction coefficient shows the proportion of the water depth at the vena contracta and the gate opening: H_2/L (see Figure 2.8). The contraction coefficient depends on the amount of gate opening, shape of the gate lip, upstream water depth and the gate type [Lin et al., 2002]. The analysis of Lin shows that contraction coefficient affects not only the discharges for both free flow and submerged flow, but also the distinguishing condition.

The gates often serve not only as control structures but also as discharge measurement tools. Clemmens [Clemmens, 2003] claimed only 5% error of discharge measurement in submerged state for radial gates. Using the Ferro method [Ferro, 2000] for the laboratory canal the Mean Absolute Percentage

Error (MAPE) was reported to be of MAPE<3% and for the constant coefficient 0.611 MAPE<6% in [Sepúlveda, 2008].

The equations are compared in the article of Sepúlveda [Sepúlveda et al., 2009]. The Ferro equations were chosen after sufficient calibration. The parameters to calibrate were the discharge coefficient including the effects of the velocity head in the approach canal, the viscous effects, turbulence, and nonuniform velocity distribution [Ferro, 2000].

Lozano [Lozano, 2009] calibrated sluice gates in irrigation canals. In case of small gate openings and greater water level difference the main contributor is the discharge coefficient. In case of very small gate openings this value has a crucial role. They obtained the best results when the discharge coefficient is a parabolic function of the gate opening. They also reported changes in the discharge coefficient by time due to the physical defections of the gates from the use.

2.4.3 Flow measurement with the gates in UPC-PAC

FIGURE 2.11: Sluice gate in the UPC-PAC

Due to the zero slope canal, the gates work most of the time in submerged flow conditions. Gate 1 separates the upstream reservoir and the canal. The the upstream water level can be considered constant. Gate 1 is 44.3 cm wide and it is made of methacrylate reinforced with a metal skeleton. It is moved by a constant speed servomotor of about 0.3 cm/s speed.

Numerous measuring campaigns have been made on the UPC-PAC canal in order to calibrate the gates. Several methods have been considered, and finally the classical gate equation showed good results. The measured dataset was divided into two parts: half of it was used for calibration and the other half was used for verification. The following calibration curves have been obtained (Figures 2.13, 2.14 and 2.15).

The three-pool configuration is shown in Figure 2.12. The naming of the gates corresponds to the names shown in the schematic view (Figure 2.2): they are not consecutive numbers, because at the time of this work was carried out only these gates were operative from the 5 possible gates.

Taking into account the errors in the devices and the measurement error propagation, the current accuracy of the discharge measurement is about 2 l/s. The resulting calibrated constant discharge coefficients are summarized in Table 2.3 that are used with Equation 2.5.

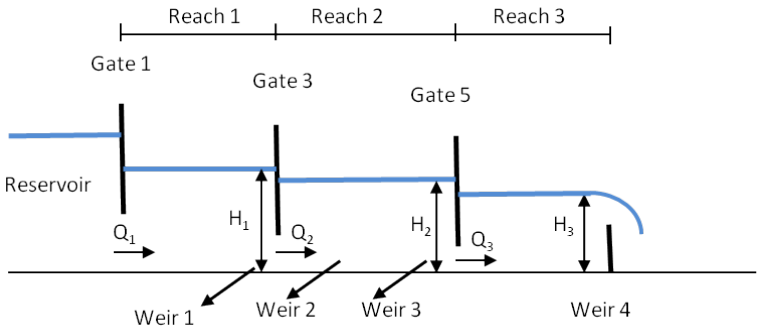

FIGURE 2.12: The three-pool configuration of the UPC-PAC

Gate	**Discharge coefficient (-)**
Gate1	0.628
Gate3	0.645
Gate5	0.686

TABLE 2.3: The discharge coefficients of the gates of the UPC-PAC

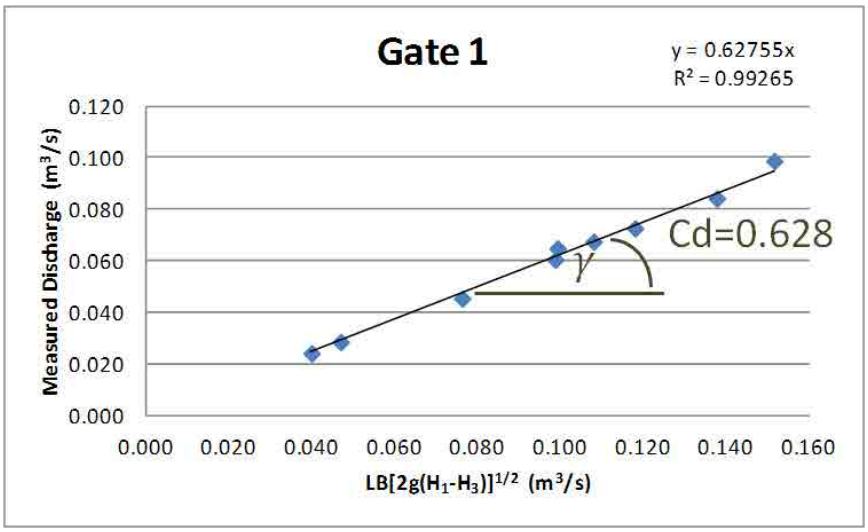

FIGURE 2.13: Calibration of Gate 1

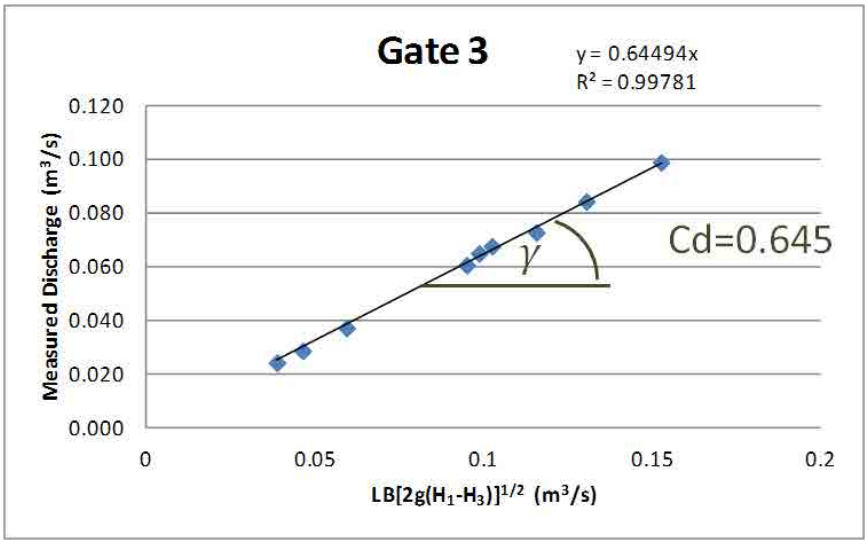

FIGURE 2.14: Calibration of Gate 3

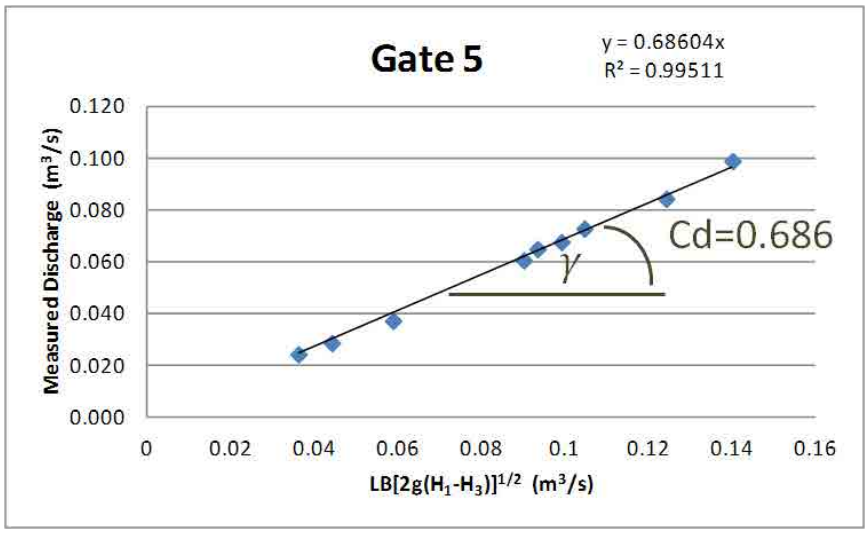

FIGURE 2.15: Calibration of Gate 5

2.5 Flow measurement with the weirs

2.5.1 Introduction

Weirs are used in irrigation canals as control structures. They can be placed at turnouts when the discharge in the lateral canal depends on the water level in the main canal or used as side-channel spillways. Weirs are also simple and reliable flow measurement tools consisting of an overflow crest or notch [Buyalski et al., 1991].

A measuring weir is defined as an overflow structure built perpendicular to an open channel axis to measure the flow rate of water [Kulin and Compton, 1975]. The flow measurement with weirs is one of the oldest flow measurement methods. Its accuracy can be ±3% [Sepúlveda, 2008].

2.5.2 Nomenclature of weirs

Weirs can be categorized according to their shape, width and position (e.g. lateral weirs). A weir in the form of a relatively long raised channel control crest section is a **broad-crested** weir (Figure 2.16). If the water springs clear

downstream, does not cling to the downstream face of the weir plate it is called **sharp-crested weir or thin plate weir** (Figure 2.17).

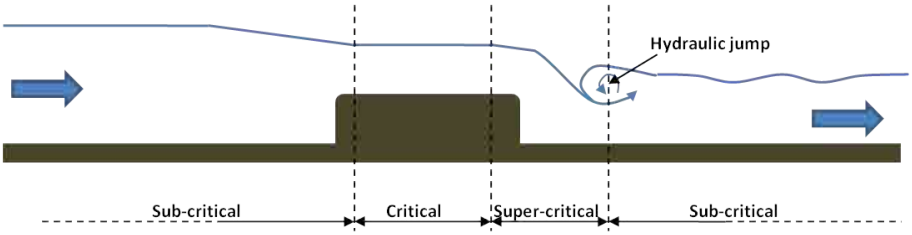

FIGURE 2.16: Broad crested weir

(a) Weir in the laboratory

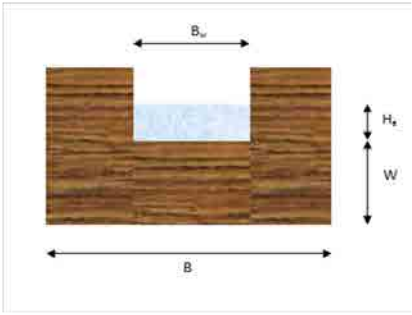

(b) Sharp crested weir

FIGURE 2.17: Photo and schematics of a sharp crested weir

Weirs are commonly named by the shape of their blade overflow opening shape for sharp-crested weirs or the flow control section shape for broad-crested weirs. Therefore, weirs can be classified as rectangular, trapezoidal and triangular.

The cut into the section of the thin plate of the weir is called the **notch**. Weirs with a triangular shape cutting are called V-notch weirs and are often used for the measurement of low flows (Figure 2.18).

When the width of the notch is equal to the width of the canal there is no contraction, it is called **suppressed weir**.

FIGURE 2.18: V-notch weir

In case the opening is smaller than the width of the weir, the water flows with small velocity and then when it reaches the plate it turns to the opening. This turn cannot be instantaneous - it continues downstream the opening - and therefore the width of the flume is smaller than the opening. This process is called side contraction. It is **fully contracted** if the distance between the opening and the canal side is at least equal to two heads. Otherwise the weir is **partially contracted**.

The falling sheet of water is called the **nappe**.

The water surface starts to drop more or less two heads distance upstream from the weir - this is called drawdown. This is also the location of the head measurement. This results from the acceleration as the water approaches the weir, the hydrostatic head is converted into velocity head.

The term **vertical contraction** includes both crest contraction and drawdown at the weir plate. When there are full contractions at the ends and at the bottom, the weir is called **contracted weir**.

For good measurements it is required to have full air ventilation under the nappe and the proper crest elevation. **Free flow** occurs when the air can go freely under the falling jet sheet or **nappe**.

If the downstream water rises above the crest elevation the weir is called **submerged**. For this case formulas are developed in [Villemonte, 1947] for discharge measurement, however, only for rectangular canals.

In the following section the focus is on sharp crested weirs, and the notation is introduced: B as width of the weir (also the canal width), B_w as opening of the weir, H_e as head over the weir and W as weir height.

2.5.3 The general sharp crested weir equation

The calculation of discharge over a weir can be deduced from the Bernoulli equation [Sánchez-Juny et al., 2005]. The velocity head at any point 2 above the weir crest is assumed to equal the total head upstream.

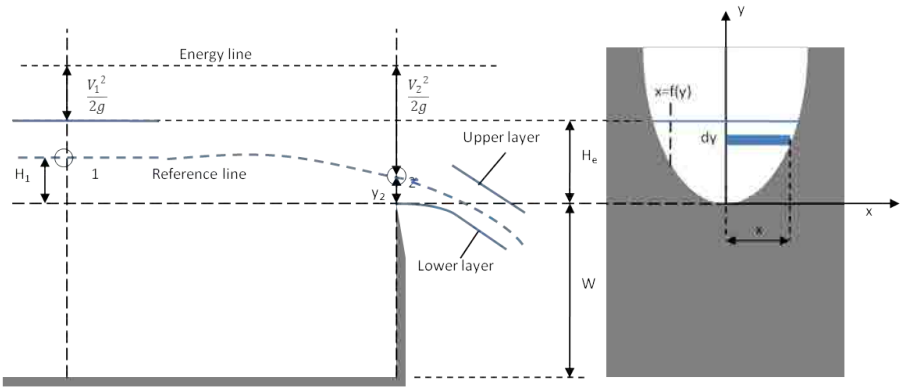

FIGURE 2.19: Flow over the weir

The energy balance on the streamline between point 1 and 2:

$$H_1 + \frac{V_1^2}{2g} = Y_2 + \frac{V_2^2}{2g} \tag{2.6}$$

where V_1 is the velocity at point 1, V_2 is the velocity at point 2 and the other notation are shown in Figure 2.19. Equation 2.6 can be generalized to any point of the streamline:

$$H_e + \frac{V_1^2}{2g} = y + \frac{V_2^2}{2g} \tag{2.7}$$

The higher the weir the more negligible is the $V_1^2/2g$ and can be approximated by H_e. Hence the velocity at any two points over the weir crest is

$$V = \sqrt{2g(H_e - y)}. \tag{2.8}$$

The flow is expressed as:

$$Q = VA. \tag{2.9}$$

A small increase in the flow is the following:

$$dQ = VdA = V2xdy. \tag{2.10}$$

Equation 2.8 and Equation 2.10 can be combined and for the effect of the contraction of the flow the weir discharge coefficient C_{dw} is introduced:

$$dQ = C_{dw}2x\sqrt{2g}\sqrt{H_e - y}dy \tag{2.11}$$

where C_{dw} accounts for the effect of contraction of the water layer over the weir, and it is called the discharge coefficient. Data about the value of C_{dw} can be found in literature, it can be calculated from the weir crest height and the head, or also it can be calibrated. Experiments show that if the flume leaving the weir is on atmospheric pressure (aired) the coefficient C_{dw} can be considered constant for sharp crested weirs [Chow, 1959].

Integrating Equation 2.11 in the vertical direction the following expression can be obtained:

$$Q = 2\sqrt{2g}C_{dw}\int_0^h x\sqrt{H_e - y}dy. \tag{2.12}$$

In case of no lateral contraction the horizontal distance along the x axis can be expressed as the half of the width of the cross section

$$x = \frac{B}{2}. \tag{2.13}$$

Therefore Equation 2.12 together with Equation 2.13 can be written as

$$Q = 2\sqrt{2g}C_{dw}\int_0^h \frac{B}{2}\sqrt{H_e - y}dy. \tag{2.14}$$

Carrying out the integration the following expression is obtained:

$$Q = -\frac{2}{3}\sqrt{2g}C_{dw}B[\sqrt{H_e - y}(H_e - y)]_0^{H_e}. \tag{2.15}$$

The final equation for the discharge over a sharp crested weir is:

$$Q = \frac{2}{3}\sqrt{2g}C_{dw}BH_e^{3/2}. \tag{2.16}$$

There are different methods of approximating the discharge coefficient. In some books, a general discharge coefficient is defined by collecting some terms in the weir discharge equation (Equation 2.16), C_w is the following:

$$C_w = C_{dw}\frac{2}{3}\sqrt{2g} \tag{2.17}$$

and the discharge is calculated as

$$Q = C_w BH_e^{3/2}. \tag{2.18}$$

2.5.4 Constant discharge coefficient

There are different authors using constant approximation for the discharge coefficient. In [White, 1999] 0.81 is used as a coefficient and the author indicates that is should be decreased. In SIC 0.6 is suggested [Malaterre, 2012]. In the manual of Hec-Ras hydrodynamic model [Brunner, 1995] a range of coefficients is suggested. From Dias a calculated value is used [Dias et al., 1988].

Using the Equation 2.17 general values both for C_w and C_{dw} are presented in Table 2.4.

	C_w (-)	C_{dw} (-)
Sic	1.77	0.60
Hec_min	1.69	0.57
Hec_max	1.80	0.61
Dias	1.83	0.62
Ferro	1.86	0.63

TABLE 2.4: Constant discharge coefficients for the weirs

2.5.5 Discharge coefficient depending on the head and the weir height

Some authors do not consider the discharge coefficient constant, but dependent on the head (H_e) and the weir height (W).

Rehbock

The discharge coefficient for a rectangular weir without contraction can be determined by the Rehbock formula [Henderson, 1966]:

$$C_{dw} = 0.611 + 0.08\frac{H_e}{W}. \tag{2.19}$$

White

The following discharge coefficient approximation is given in [White, 1999]

$$C_w = 0.564 + 0.0846\frac{H_e}{W} \tag{2.20}$$

if H_e/W is less than 2.

Rouse

Rouse proposed an equation for cases when $H_e/W > 15$ [Swamee, 1988]

$$C_{dw} = 1.06\left(1 + \frac{W}{H_e}\right)^{1.5}. \tag{2.21}$$

Swammee

In [Swamee, 1988] the equations of Rouse and Rehbock are combined and obtained the following full range equation:

$$C_{dw} = 1.06\left(\left(\frac{14.14W}{8.15W + H_e}\right)^{10} + \left(\frac{H_e}{H_e + W}\right)^{1.5}\right)^{-0.1}. \tag{2.22}$$

The same author provides approximation for the discharge coefficient for contracted weirs:

$$C_{dw} = \frac{0.611 + 2.23\left(\frac{B}{B_w} - 1\right)^{0.7}}{1 + 3.8\left(\frac{B}{B_w} - 1\right)^{0.7}} + \frac{0.075 + 0.011\left(\frac{B}{B_w} - 1\right)^{1.46}}{1 + 4.8\left(\frac{B}{B_w} - 1\right)^{1.46}} \frac{H_e}{W} \tag{2.23}$$

where B is the width of the weir and B_w is the weir width and H_e is the head over the weir.

Bagheri and Heidarpour

In [Bagheri and Heidarpour, 2012] experimental upper and lower nappe profiles were used and fitted them by quadratic and cubic equations and in addition free vortex theorem was used to determine the discharge coefficient:

$$C_{dw} = 0.324 \exp\left(0.94 \frac{B_w}{B}\right) \ln\left(1 + \frac{0.73\left(\frac{H_e}{W} + 3.64\right)}{\exp\left(1.18 \frac{B_w}{B}\right)}\right). \tag{2.24}$$

Afzalimehr and Bagheri

In [Afzalimehr and Bagheri, 2009] a calibrated coefficient was used, there is a correction factor that should be determined as a function (power) of H_e/W:

$$C_{dw} = 0.409 \left(\frac{W}{H_e}\right)^{0.459} \left[\left(1 + \frac{H_e}{W}\right)^2 - 1\right]^{1/2}. \tag{2.25}$$

2.5.6 Kindsvater-Carter equation

To calculate the discharge, one of the most recommended methods is the Kindsvater-Carter method [Dodge, 2001]. The method is suitable for submerged and free flow, and the improved version also for V-notch weirs. The advantage of this method is that it accounts for the dependence of the weir coefficient on the effective length of the weir and on the head. The method applies to both fully and partially contracted weirs, and also for suppressed weirs. This makes it very useful, because most of the methods are only applicable for fully contracted or suppressed cases [Dodge, 2001].

The Kindsvater-Carter equation for rectangular weir is also recommended by several authors:

$$Q = C_{dw}\frac{2}{3}\sqrt{2g}\,(B_w + K_b)\,(H_e + K_h)^{\frac{3}{2}} \tag{2.26}$$

where Q is the discharge, C_{dw} is the discharge coefficient, g is the acceleration of gravity, B_w is the width of the notch and H_e is the head. The sum $B_w + K_b$ is called "effective width" and the sum $H_e + K_h$ is called "effective head". K_b and K_h account for the combined effects of several phenomena including viscosity and surface tension.

In [Herschy, 1995] the Kindsvater-Carter equation is presented with the following constant numbers: K_h was estimated to be 0.001 m just like later in [Sepúlveda, 2008] and K_b was taken to be K_b=0.003 m. Therefore,

$$Q = C_{dw}\frac{2}{3}\sqrt{2g}\,(B_w + 0.003)\,(H_e + 0.001)^{3/2} \tag{2.27}$$

where

$$C_{dw} = 0.587\left(1 - 0.003\frac{W}{H_e}\right). \tag{2.28}$$

The discharge coefficient Kindsvater-Carter equation can be calibrated. The dependence of the discharge coefficient on the ration of the head and the weir height can be expressed in the following way:

$$C_{dw} = C_{dwa}\frac{W}{H_e} + C_{dwb} \tag{2.29}$$

where C_{dwa} and C_{dwb} are calibrated values.

2.6 Calibration of the weirs of the UPC-PAC

The laboratory canal has four weirs: one at the end of the canal, that is completely orthogonal to the flow (Figure 2.20) and three weirs that are located at the curvature of the flow (Figure 2.21). All the weirs are sharp crested weirs with a height that is possible to change. During the construction of the canal these weirs were calibrated using the Kindsvater-Carter method [Dodge, 2001], but with the original calibration they had a considerable measurement error. Therefore it was decided to carry out a study and a new calibration campaign.

FIGURE 2.20: Top view of Weir 4

During this campaign, the upstream discharge was measured using a triangular weir and a limnimeter and the water level 0.5 m upstream of the weirs was measured with a metallic ruler (0.5 mm accuracy). Every measurement was conducted in steady state that was reached in 30 min of waiting after setting the conditions. The number of measured points are 12, 9, 12, 55 for Weir 1, Weir 2, Weir 3 and Weir 4, respectively. The reason for measuring more points for Weir 4 is its role: while the other weirs are used occasionally as offtakes, Weir 4 is always in use and its discharge-stage relationship determines the water level in the last pool. There is a small contraction (the opening is 0.395 m and the width of the section us 0.44 m), therefore equations both with and without taking the contraction into account are tested.

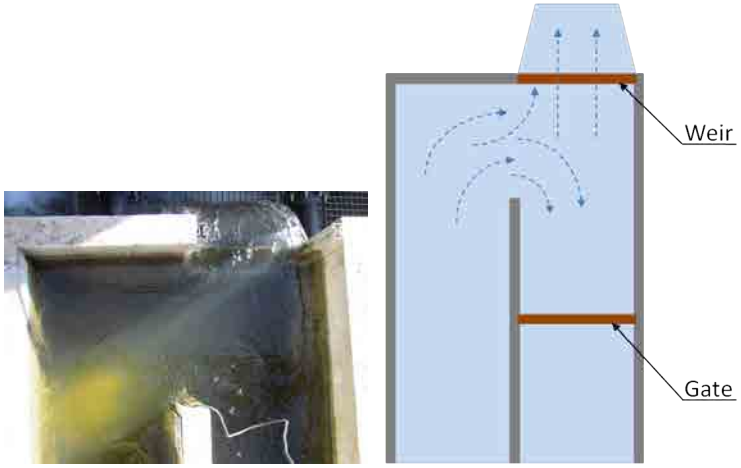

(a) Photograph of weir (b) Weir schematics

FIGURE 2.21: The position of the offtake weirs in the UPC-PAC

The test of the discharge coefficients

Some constant approaches were tested. The average error in discharge was calculated using the measured points. Discharge coefficients as functions of the head or the head-weir height ratio have been tested. The equations were tested with and without using the effective width. The effective width (B_{we}) can be computed using the Francis equation [Chow, 1959]:

$$B_{we} = B_w - 0.2H_e. \tag{2.30}$$

In [Bagheri and Heidarpour, 2010] it was found that the effective width varies with the water depth. The minimum effective width was measured not at the vicinity of the weir. They use an average value between the minimum effective width and the effective width measured at the vicinity of the weir. The following formula is suggested:

$$B_{we} = B_w - 0.19H_e. \tag{2.31}$$

The two formulas were tested and the latter (Equation 2.31) proved to be better describing the conditions in the laboratory canal. In order to measure the discharge a known flow was set and all the outflow was directed to the weir to be calibrated by closing the gate just downstream of the given weir. In some cases small leakages were observed, especially in case of the calibration of Weir 3: the gate downstream of Weir 3 was not possible to be closed completely. This leakage was estimated and the date were corrected with this leakage. This explains the poorer quality of the calibration results for Weir 3.

2.6.1 Results with constant coefficient

Constant weir discharge coefficients suggested by different authors have been tested. The average discharge error is presented in Table 2.5 and 2.6. The same values are shown for each weir in Figures 2.22, 2.23, 2.24 and 2.25.

	HEC-RAS	**SIC**	**Dias**	**Ferro**	**0.61**
Weir 1	2.4	3.1	4.4	5.1	3.8
Weir 2	2.7	3.4	4.9	5.7	4.2
Weir 3	3.8	4.7	6.7	7.7	5.7
Weir 4	1.2	1.3	2.3	3.0	1.7

TABLE 2.5: Average discharge error (l/s) using the constant coefficients

	HEC-RAS	**SIC**	**Dias**	**Ferro**	**0.61**
Weir 1	1.5	1.3	1.5	1.9	1.4
Weir 2	2.5	1.9	1.3	1.5	1.4
Weir 3	3.8	3.5	3.0	2.9	3.2
Weir 4	4.5	3.9	2.8	2.3	3.3

TABLE 2.6: Average discharge error (l/s) using the constant coefficients

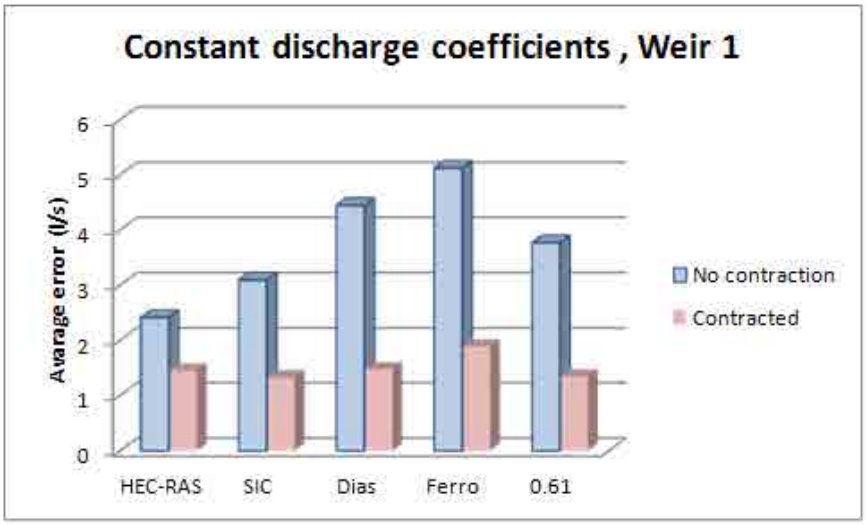

FIGURE 2.22: Calibration of Weir 1

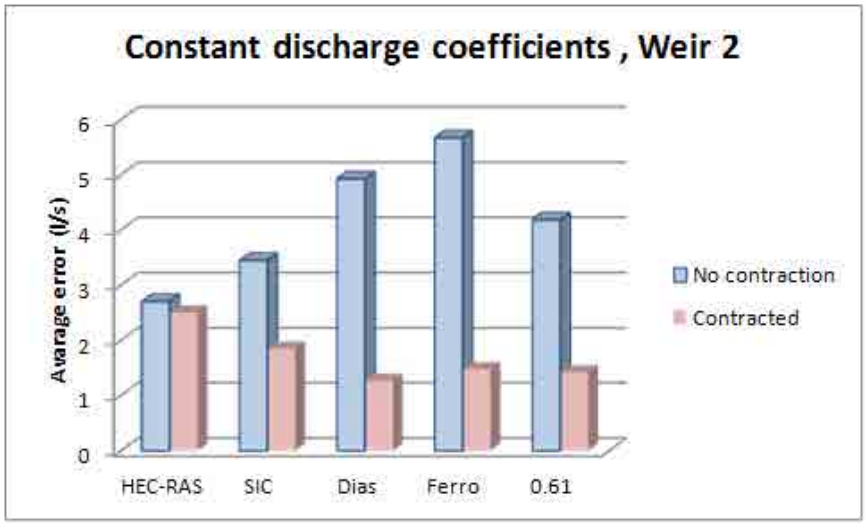

FIGURE 2.23: Calibration of Weir 2

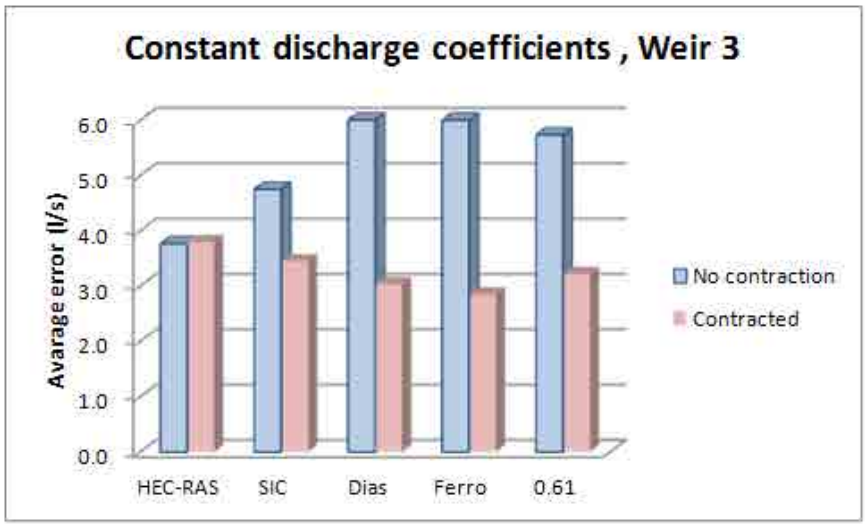

FIGURE 2.24: Calibration of Weir 3

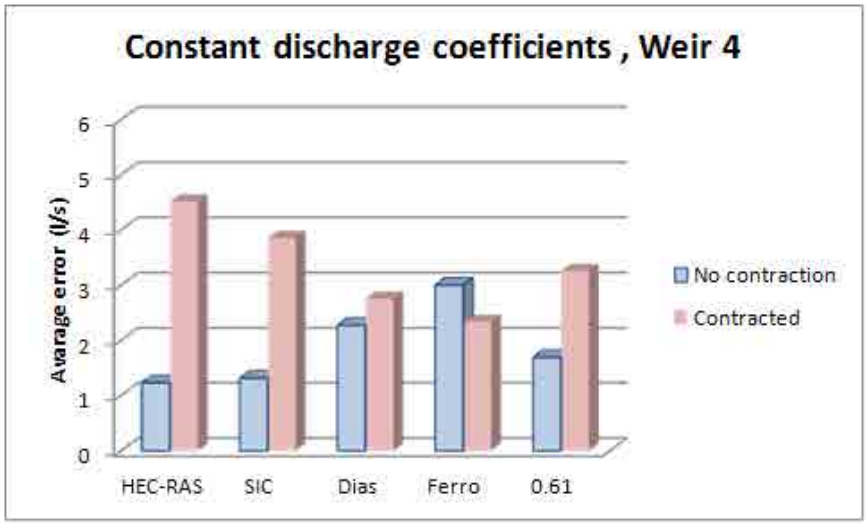

FIGURE 2.25: Calibration of Weir 4

In case of the weirs where the flow is not completely orthogonal (all except Weir 4) the graphs show the same pattern: the HEC-RAS and SIC method show the best results and the constant 0.61 if contraction is not taken into account. However, if contraction is assumed, the results are much better and for all the methods the error is less than 2 l/s (except for Weir 3, Figure 2.24). In this case there is no considerable difference between the methods, and generally 0.61 works well. For Weir 4, the use of formulas without contraction shows better results, given the flow approaching Weir 4 is completely orthogonal.

2.6.2 Results with non-constant coefficients

The different methods introduced in subsection 2.5.5 to obtain the discharge coefficient are evaluated. From the measured data the discharge coefficient is calculated and the error between the measured (reference) and the calculated discharge is compared.

The results with non-constant coefficients are shown in Table 2.7 and for the non-contracted and for the contracted case in Table 2.8. For the latter the contraction was included by using the approach of Equation 2.31. The same values are shown for each weir in Figures 2.26, 2.27, 2.28 and 2.29.

	Rehbock	**White**	**Swammee**	**Bagheri**	**Afzalimehr**
Weir 1	5.3	4.7	5.1	5.6	6.3
Weir 2	6.6	5.9	6.4	7.0	7.7
Weir 3	8.9	8.1	8.7	9.6	10.4
Weir 4	5.1	4.5	4.9	5.7	6.3

TABLE 2.7: Average discharge error (l/s) using the calculated coefficients, no contraction is assumed

	Rehbock	**White**	**Swammee**	**Bagheri**	**Afzalimehr**	**K-C**
Weir 1	2.2	1.7	2.1	2.5	3.1	2.4
Weir 2	2.1	1.6	2.0	2.6	3.1	2.9
Weir 3	2.9	2.5	2.8	3.2	4.0	4.0
Weir 4	1.4	1.4	1.4	1.6	1.9	1.2

TABLE 2.8: Average discharge error (l/s) using the calculated coefficients, including contraction

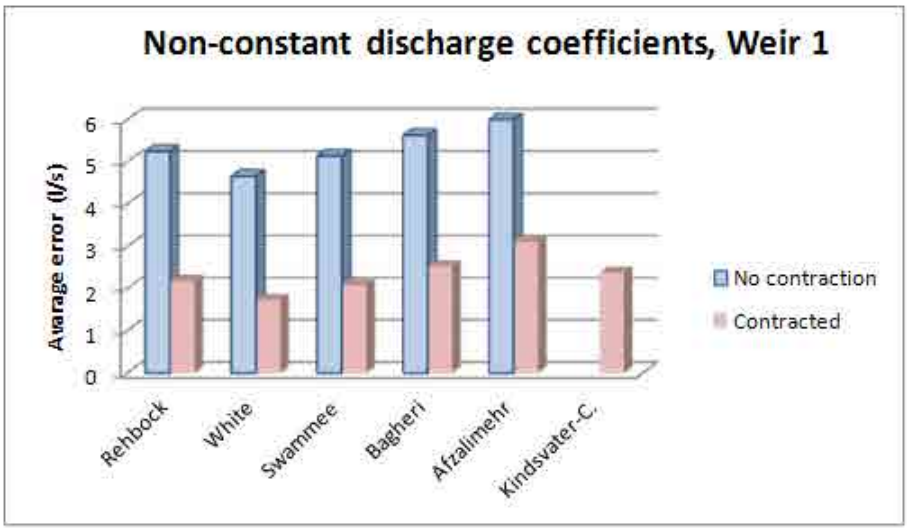

FIGURE 2.26: Calibration of Weir 1 - Non-constant discharge coefficient

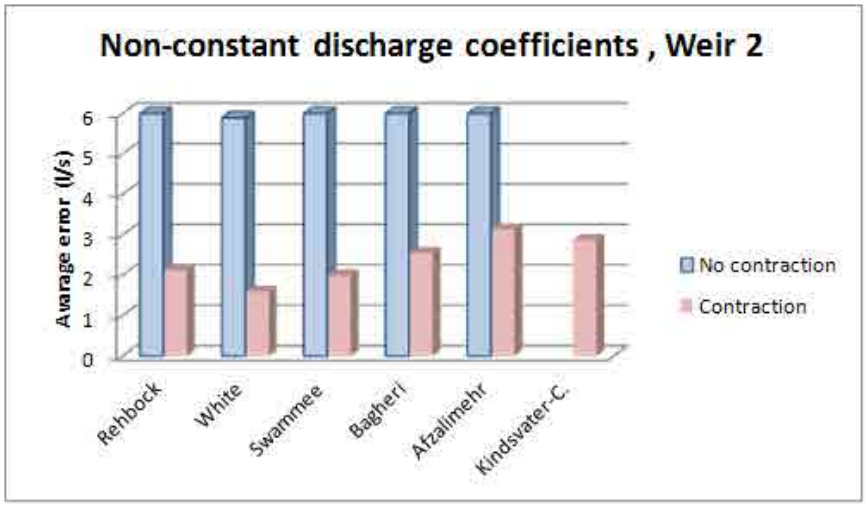

FIGURE 2.27: Calibration of Weir 2 - Non-constant discharge coefficient

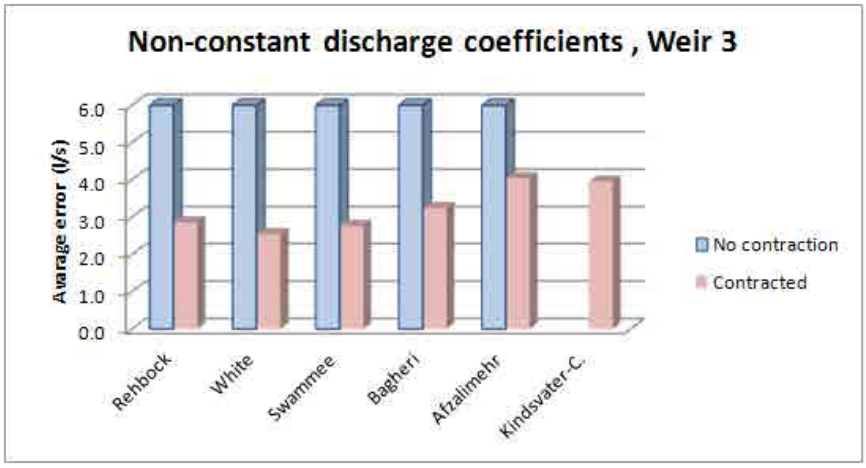

FIGURE 2.28: Calibration of Weir 3 - Non-constant discharge coefficient

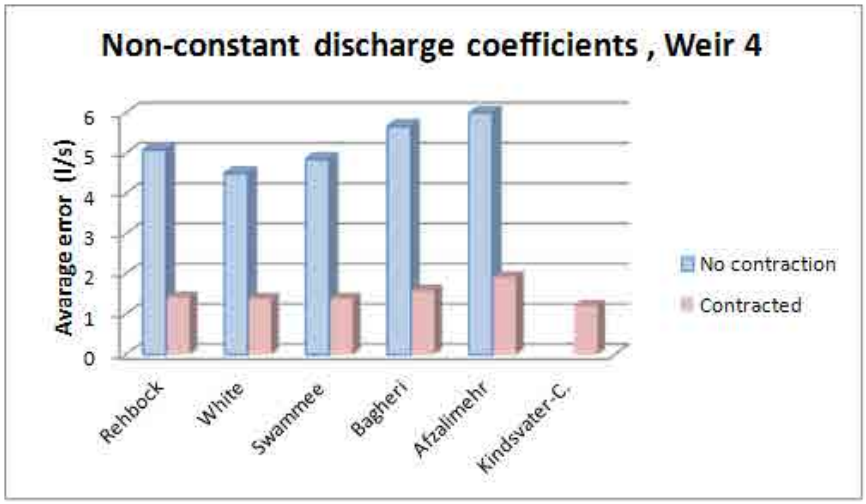

FIGURE 2.29: Calibration of Weir 4 - Non-constant discharge coefficient

The results in general are slightly worse than with constant coefficients. This result is quite unexpected. One reason can be the propagation of the measurement errors: once the head is wrongly measured this error is multiplied when the discharge coefficient is calculated. Also for the calibration of the gates, Sepúlveda [Sepúlveda et al., 2009] obtained similar results: the constant coefficient had very good performance compared to other methods.

Here in all cases including the contraction to the equation gives better results, even for Weir 4 (Figure 2.29). The error is generally less than 3 l/s, and White contracted method gives the best results.

2.6.3 Calibration of the discharge coefficient

The advantage of the calibration is that some phenomena that cannot be accounted directly can be included. In order to calibrate the Kindsvater-Carter equation, the data was split into calibration data and validation data. The calibration is shown in Figures 2.30, 2.31, 2.32 and 2.33. The results with the calibrated coefficients using the Kindsvater-Carter method are shown in Table 2.9 and Figure 2.34. As expected the calibrated results are better than the constant or the calculated ones. The error was around 1.5 l/s except in case of Weir 3.

	Error (l/s)	C_{dwa}(-)	C_{dwb} (-)
Weir 1	1.4	0.123	0.586
Weir 2	1.4	0.012	0.639
Weir 3	2.3	0.334	0.486
Weir 4	1.5	0.178	0.591

TABLE 2.9: Calibrated discharge coefficients for the Kindsvater-Carter equation and measured error

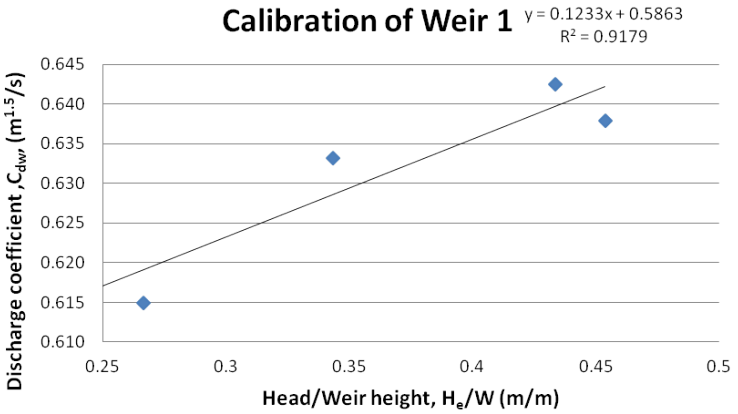

FIGURE 2.30: Calibration curve for the Kindsvater-Carter formula, Weir 1

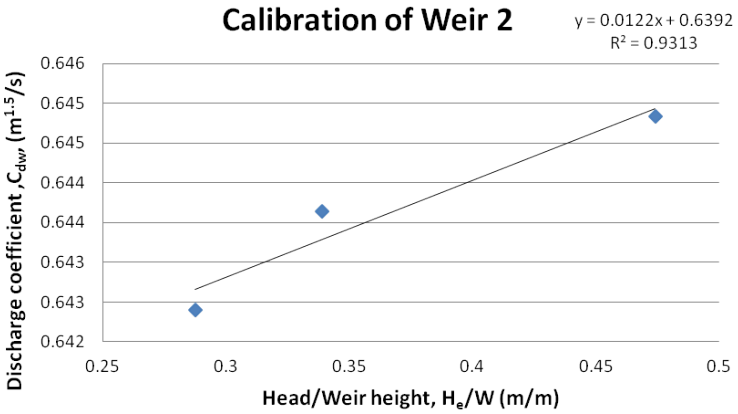

FIGURE 2.31: Calibration curve for the Kindsvater-Carter formula, Weir 2

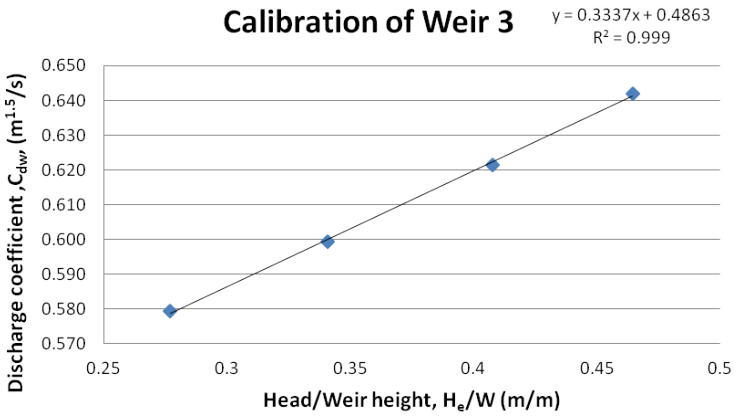

FIGURE 2.32: Calibration curve for the Kindsvater-Carter formula, Weir 3

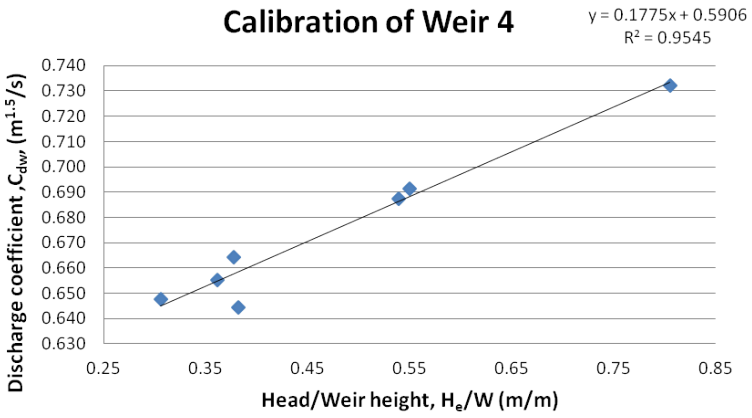

FIGURE 2.33: Calibration curve for the Kindsvater-Carter formula, Weir 4

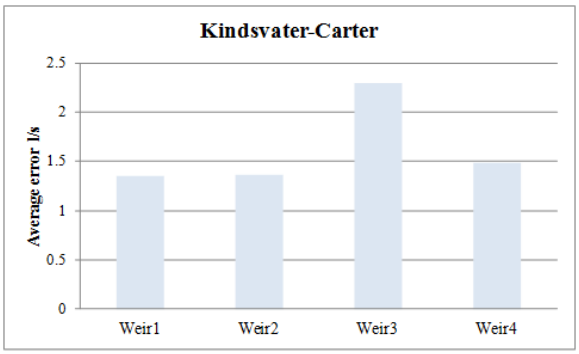

FIGURE 2.34: Kindswater-Carter

2.7 Conclusion

- The hydraulic structures can be used as effective discharge measurement equipments in open channels in front of other measurement methods.
- In the UPC-PAC the gates and the weirs have been calibrated. For the weirs several calibration methods have been used and compared: constant, non-constant and calibrated discharge coefficient both supposing and not supposing contraction. The best results were obtained with the calibrated coefficients, as it was expected.
- The contraction is a very important factor, even in cases when it is very small (the canal is 44 cm wide and the weir is 39.5 cm). It influences the flow considerably and its effects should be taken into account.
- In most of the cases Weir 4 (completely orthogonal to the flow) showed different characteristics than the other weirs whose position is not completely orthogonal. For these weirs the formulas with contraction showed better results. This contraction can also be observed on the pictures taken of the flow pattern.
- The average error in discharge measurement for the UPC-PAC is less than 2.5 l/s, that is less than 4% for normal operation conditions (70 l/s discharge).
- The best performance was obtained with the calibrated discharge coefficient (Kindsvater-Carter method). However, with constant

discharge coefficient also acceptable results were obtained. Therefore in case of possibility, calibration can be suggested. However, also without calibration the weirs can be used to measure discharge by using constant or calculated coefficients. In this case the constant coefficients performed better than the variable ones.

Chapter 3

Properties of canal pools and identification

3.1 Introduction

In order to make robust and well performing controllers it is crucial to know very well the characteristics of the canal. In this chapter the dynamics of the canal pools are analyzed. Then an identification method, the Auto Tune Variation (ATV) method, is described and used in the UPC-PAC. The results are analyzed and the canal properties are summarized quantitatively.

3.2 General description of the hydraulic behaviour of the canal pools

3.2.1 Type of canal pools

The canal pools can be classified into two types based on their dynamic behaviour: (1) long and shallow pools with considerable delay time and (2) short and deep pools. A short description of the categories is given in the following.

3.2.2 Long and flat canal pools

Long and flat canal pools can mainly be characterized by the time delay: the time it takes for a disturbance (change in discharge or water level) to travel from the upstream to the downstream end. A wave attenuates by the time it reaches the downstream end of the canal reach due to the loss of energy caused by the friction [Schuurmans, 1995]. An example for a long canal pool is the first pool of one of the ASCE test canals [Clemmens et al., 1998], the Corning canal (Figure 3.1a).

The canal pool can be divided in two parts: backwater and uniform flow portion. In the uniform flow portion the friction loss is balanced by the bottom slope and the canal reach has constant depth, called normal depth. In the backwater portion the water depth exceeds normal depth and the water surface is nearly horizontal. In canals that have both backwater and uniform flow portion, the waves developed in the backwater part dampen fast as they interact with the normal depth part, therefore they show few resonance.

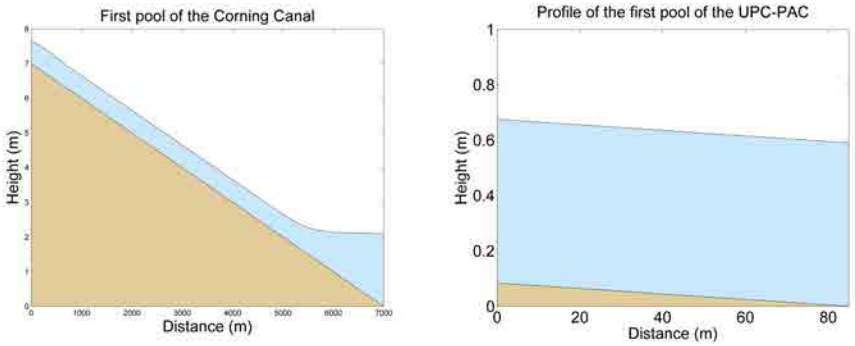

(a) (b)

FIGURE 3.1: Examples of profiles of a long (a) and a short (b) canal pools

The Bode diagram of an example for this type is shown for the transfer function between the upstream discharge and the downstream water level in Figure 3.2a and the transfer function between the downstream discharge and the downstream water level in Figure 3.2b. The Bode diagram shows the response of a function to sinusoidal excitation: the magnitude plot shows the change of the amplitude and the phase plot shows the phase shift of the

output compared to the input. The low frequency gains show the integrator behaviour, a straight line, whose gain can be determined from the slope of the straight line. There are no resonant peaks. This shows the fact that a wave coming from upstream attenuates and does not have enough energy to reflect and go back again upstream. The phase starts at $-90°$ showing the presence of the integrator, while it decreases towards high frequencies showing the time delay. The Bode plot for a pure integrator would be a straight line with a slope of -20dB. However, this line bends at high frequencies representing the zero shown by [Litrico and Fromion, 2004b].

This type of pools is very common and their control has been analyzed. Research has been conducted to develop stable controller tuning rules: [Schuurmans et al., 1999] and [Litrico and Fromion, 2006b].

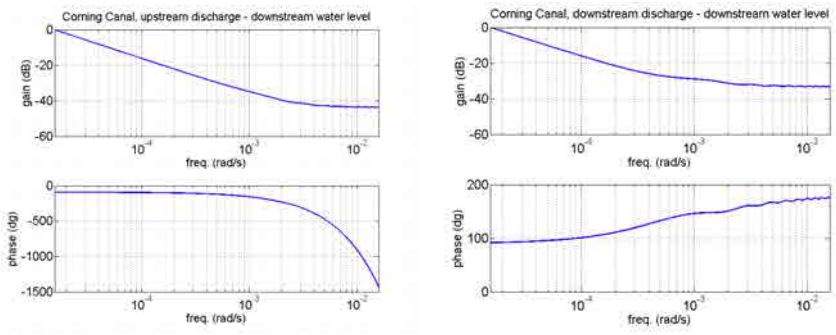

(a) (b)

FIGURE 3.2: Transfer function between the upstream discharge-downstream water level (a) and between the downstream discharge-downstream water level (b)

3.2.3 Short and flat canal pools

Short and flat canal pools are almost entirely under backwater and the water surface is nearly horizontal (see Figure 3.1b).

As the water level exceeds normal depth, the depth of a disturbance wave is also bigger and it does not dissipate so fast. A disturbance occurring at the upstream end reaches the downstream end and is able to reflect and travel back upstream and then downstream again before it attenuates. The presence of these waves are influenced positively by several factors: short canal pool,

low friction, high water levels. The detailed description can be found in [van Overloop, 2006b]. Figure 3.3 from [van Overloop, 2006b] summarizes the pool characteristics influencing the resonant behaviour.

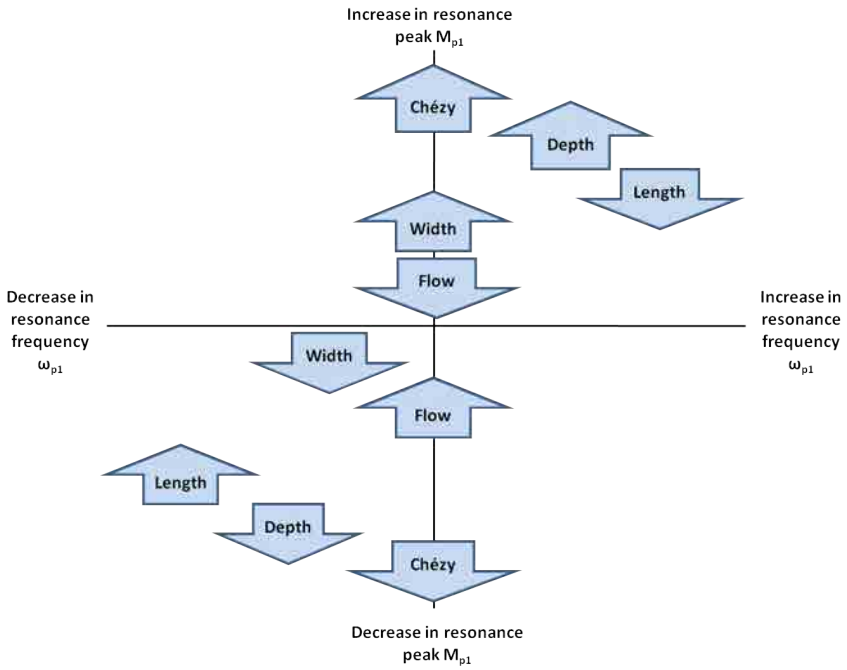

FIGURE 3.3: Canal pool properties influencing the resonance behaviour, from [van Overloop, 2006b]

The UPC-PAC belongs to this type of canals. The Bode plot of the transfer function between the upstream discharge and the downstream water level is shown in Figure 3.4. At low frequencies the integrator behaviour can be seen just as in case of the long pools, however at high frequencies peaks in the amplitudes appear. These peaks show the resonance behaviour of the system, if it is excited with its own frequency it behaves as an oscillator: the amplitude (gain) increases. The first peak corresponds to the wave that starts upstream, reflects downstream then travels upstream, reflects at the upstream end and arrives downstream again. The subsequent peaks represent the higher order harmonics.

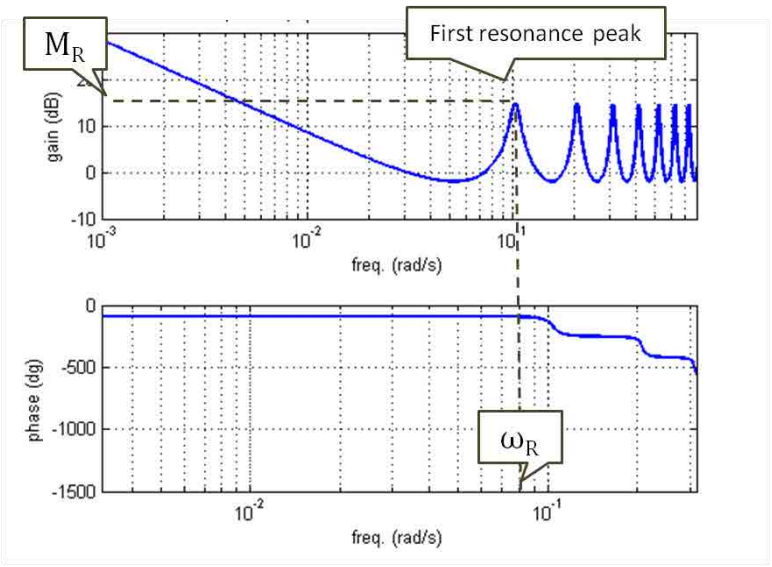

FIGURE 3.4: Bode plot of a canal pool with resonance

The control of this type of canal pools is much less studied and it is challenging since the controlled and the control action variable are in counter-phase. In case the wave is present at the downstream end, the controller will decrease the discharge in the upstream end. However, the upstream wave is already decreased, therefore in this way it just generates more resonant waves (Figure 3.5). Some references about the study of this lind of canal pools are already presented in subsection 1.1.3.

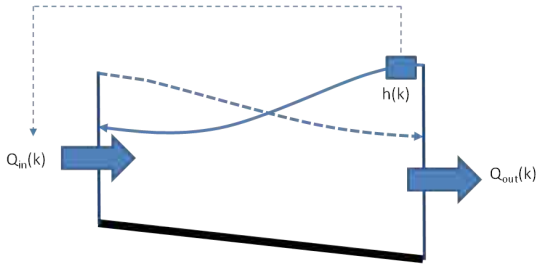

FIGURE 3.5: Illustration of resonance waves, from [van Overloop, 2006b]

The control of these canal pools raises difficulties, because the resonance peaks can cause instability in the controller. The controller will be unstable in closed loop according to the Nyquist stability criterion. According this criterion the

number of unstable closed-loop poles is equal to the number of unstable open-loop poles plus the encirclements of the point (-1,0) on the Nyquist plot of the transfer function multiplied by the feedback gain. If the magnitude of the resonance peak in open loop is larger than 1, the transfer function will be unstable according to this criterion. To avoid this problem, in most of the cases, low pass filters are used to filter out this resonance peak to avoid the controller acting on it.

3.2.4 Resonance

As it was mentioned above, for short and flat canal-pool resonance is a common phenomenon. An illustration of the waves traveling back and forth in the first pool of the UPC-PAC is shown in Figure 3.6.

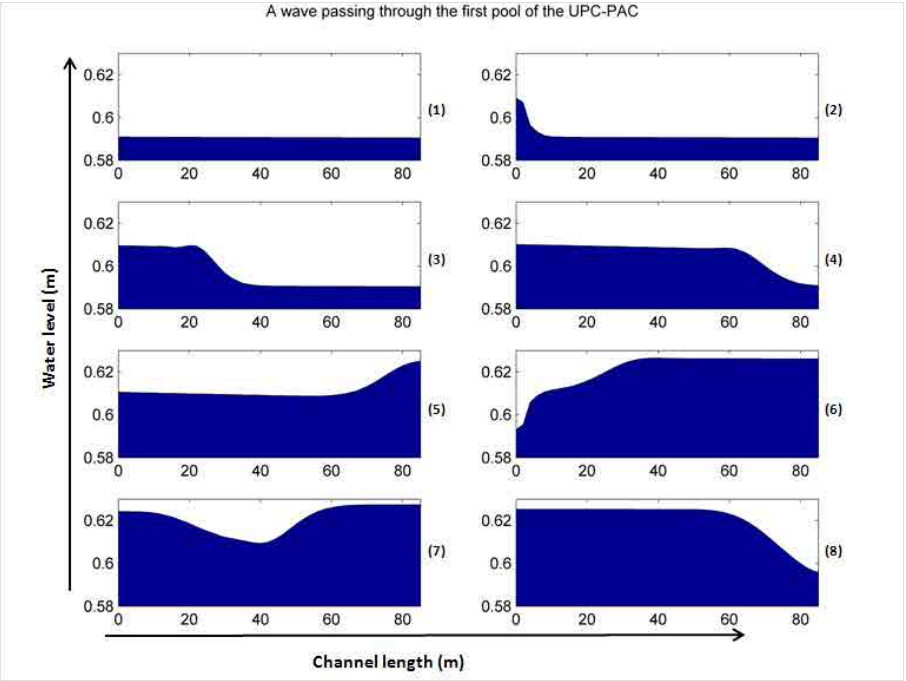

FIGURE 3.6: Illustration of resonance waves, numerical simulation of the first pool of the UPC-PAC

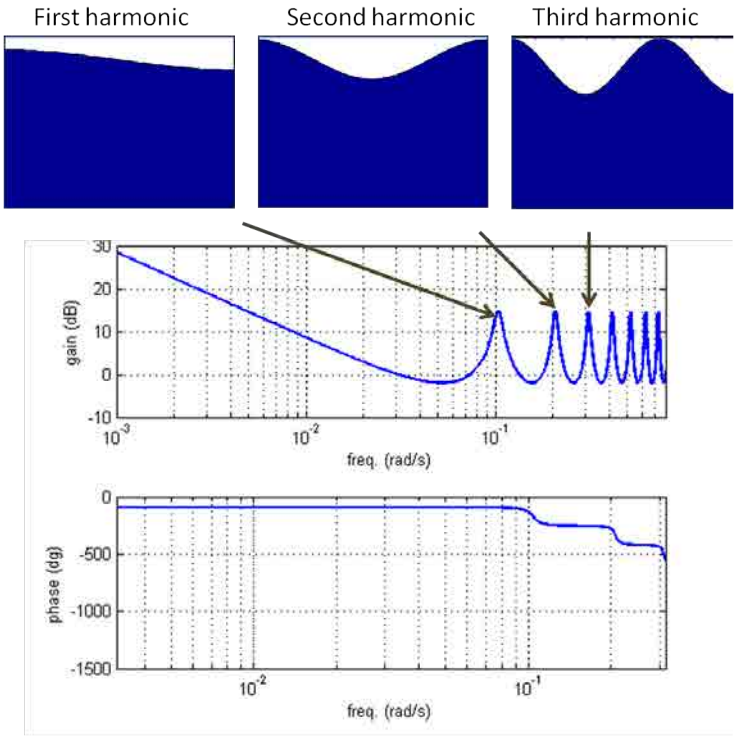

FIGURE 3.7: The first harmonics in the third pool of the UPC-PAC

The plot is obtained by with 1D hydrodynamic simulator SIC. In the first subfigure the surface is completely flat. Then the upstream gate in the pool is opened (second subfigure) in order to send perturbation (additional discharge) downstream. The wave travels downstream (3) reaches the downstream end (4) and bounces back (5). The same process continues (6-8), the wave keeps on travelling and bouncing back.

The peaks of the Bode plot are related to these resonance waves. This is illustrated in Figure 3.7. The first peak corresponds to the first harmonic, the second peak shows the second harmonic. The small figures show the standing wave pattern that corresponds to that harmonic. There are infinite number of harmonics that can be calculated using the following equation:

$$\omega_p(k) = \frac{2\pi k}{T_R} \tag{3.1}$$

where $k = 1, 2, ..., \infty$, $\omega_p(k)$ is the frequency of the resonance peaks and T_R is the travel time: the time it takes for a wave to travel back and forth in the canal pool and its calculation is given later by Equation 3.4. The first harmonic is specially important for controller design (see the small figure related to the first peak). When the downstream water level is under setpoint, the controller would try to increase the upstream discharge. However, by the time this increase arrives to the downstream end, the water level will be in counter-phase and a larger peak level is produced. This is also shown in Figure 3.5. In other words, due to the Nyquist stability criterion, the feedback control system becomes unstable if the total gain of the canal pool and the controller exceeds 1. Hence, systems with high resonance peaks are more difficult to control since the controller gain cannot be too high. According to the gain margin criterion, the proportional gain limitation is expressed in the form:

$$K_p < \frac{1}{2M_R} \tag{3.2}$$

where K_p is the proportional gain of the feedback control system and M_R is the magnitude of the resonance peak.

There are three basic ways to deal with the resonance phenomenon:

1. Make a controller design that is always on the safe side, using the biggest possible peaks for the design. This would result in a stable, but slowly responding controller. In most of the cases, especially when the resonance properties are unknown, this option is chosen.

2. Filter out the resonance. By adding a low pass filter to the incoming water level signals, a controller can be designed as if resonance was not present. Filtering would also slow down the controller reaction. In this case the resonance will be present, but the controller will not act on it. There are filter designs given in [Schuurmans, 1997] based on the resonance properties of a canal pool.

3. The option of including the resonance in the model of the canal for the controller is first treated in [van Overloop et al., 2010b].

In this work the first and the third option is treated in Chapter 4. The second option was examined in [Horváth et al., 2013b], and in this work is not treated due to the observed delay introduced by the filter.

3.3 Identification of canal properties including resonance characteristics

In this work the focus is on the control of short and flat canals, just as the laboratory canal presented above. In order to develop or tune well performing controllers, the main properties of the behaviour of the canal pool need to be known. In [Schuurmans, 1997] tuning rules are developed for filters in order to control these type of canal pools by filtering out the resonance peaks. In [Litrico et al., 2007] tuning rules are developed for PI controllers based on the same properties: backwater area, resonance frequency, resonance peak. Also for more advanced control techniques these properties are crucial to develop simple models, as it is described in [van Overloop et al., 2010b].

In the following some ways of obtaining these parameters are discussed.

3.3.1 Method 1: Equations

From the geometry of the canal some properties can be well approximated, like the backwater surface (A_s) as the multiple of the canal top width (T) and the length (X) in case of regular channels:

$$A_s = XT. \tag{3.3}$$

The resonance frequency can also be very well approximated from the travel time (T_R): the time it takes for a wave travel back (T_{RD}) and forth (T_{RU}) in the canal:

$$T_R = T_{RD} + T_{RU} = \frac{X}{C+V} + \frac{X}{C-V} \tag{3.4}$$

where C is the celerity and V is the velocity. And the frequency (ω_R) of the first resonance peak can be calculated as the following:

$$\omega_R = \frac{2\pi}{T_R}. \tag{3.5}$$

The resonance peak is more difficult to approximate. One approximation based on second order model from [van Overloop et al., 2010b] is the following:

$$M_R(\omega_R) = \frac{R_h^{4/3} H}{2gQXn^2} \tag{3.6}$$

where M_R is the magnitude of the resonance peak, R_h is the hydraulic radius, H is the water level, Q is the discharge and n is the Manning's coefficient. In the above mentioned work, the results of a high-order model and the approximations are compared: the resonance frequency is well approximated by Equation 3.5, but the magnitude approximation is not so good by Equation 3.6. Therefore there is a need for other methods to obtain the value of the resonance peak.

3.3.2 Method 2: Bode plots

Using the frequency response of the pool, the canal properties can be calculated. The frequency response can be obtained by approximating the Saint-Venant equations with a high order linear model using Preissmann scheme or other numerical schemes. A simple approximation is detailed in [Litrico and Fromion, 2004a], which is used in this work. The location of the first peak and its height can be read from the graph, like in Figure 3.4. The backwater area (A_s) can be calculated from the low frequency domain where the graph is a straight line using:

$$A_s = \frac{1}{M(\omega_L)\omega_L} \tag{3.7}$$

where ω_L is the frequency and $M(\omega_L)$ is the magnitude read from the low frequency part (where the graph is a straight line) of the Bode plot.

The canal pools are modelled with constant discharge boundary condition, that is, not taking into account the damping effect of the structures.

3.3.3 Method 3: System identification

Using system identification procedures and field/simulated data, a model containing the resonance properties can be identified. This procedure is detailed in [Miltenburg, 2008], [van Overloop et al., 2010b] and later some improvements are given in [van Overloop and Bombois, 2012].

3.3.4 Method 4: Auto Tune Variation

A simple experimental method to find the canal pool properties is the Auto Tune Variation method (ATV), first described in [Litrico et al., 2007] and later successfully applied in [Clemmens et al., 2012].

The basic idea of the ATV test is that a positive wave is sent downstream (opening the upstream gate, increasing the upstream discharge), and when the wave reflects from the downstream end the gate is closed again, and when the wave arrives upstream, another positive change (opening the gate again) is added in order to provide a maximum effect on the water level. The downstream measurement location is in counter-phase with the upstream perturbations.

In terms of system identification it can be seen as a simple relay experiment that is used to find the ultimate values (gain and period where the phase lag is $-180°$) for monovariable processes. The amplitude of the relay should be chosen large enough to achieve good signal-noise ratio, but not too large to avoid overflow. It is suggested to have an opening change that causes 10-20% of discharge variation.

The resonance frequency can be calculated using Equation 3.5, where the travel time is determined as the difference between two peaks of the measured downstream water level. The calculation of the resonance peak is the following from [Litrico and Fromion, 2004b]:

$$M_R(\omega_R) = \frac{\pi \Delta y}{4 \Delta Q} \tag{3.8}$$

where Δy is the change in water depth and ΔQ is the change in flow rate.

In order to calculate the backwater surface, low frequency data is needed: it can be achieved by using delayed ATV tests. Adding a delay to the ATV loop, the response of the system can be estimated in frequencies lower than the resonance frequencies. In practice the delayed ATV test is similar to the ATV test: a perturbation is generated by the upstream gate, and the perturbation in the counter direction is made some time, later instead of the time when the downstream water level crosses the setpoint. Depending on this time delay the output signal (water level) will have different frequency, it will give a point at different part of the Bode plot. From the test using the obtained frequency and magnitude, the backwater area can be calculated according to Equation 3.7.

3.4 The effect of downstream structures on the resonance properties

A hydraulic structure at the downstream end of the canal can change the behaviour to a considerable extent. The effect of the downstream structure depends on the relationship that it imposes between the discharge and the water level. This can be expressed by linearizing the equation of the structure and using the factor (gain) between the discharge and the water level.

In case of a sluice gate, this gain is low. This is a typical example of the canal pools separated by a sluice gate, for example Pool 1 and Pool 2 of the UPC-PAC.

In contrast, in case of a thin plate weir, the gain of transfer function between the water level and the outflow is not negligible, since the structure determines the water level. It depends on the weir and the flow regime, but in some cases it can be around one half. This means that the canal pool no longer acts as an integrator. The transfer functions between the input discharge and the downstream water level (p_{21}) and between the downstream discharge and the downstream water level (p_{22}) can be calculated by using the the Saint-Venant model. The downstream water level an be expressed by combining the Saint-Venant model with the linearized equation of the weir:

$$h(s) = \frac{p_{21}(s)}{1 - k_{hw} p_{22}(s)} q_{in}(s) \tag{3.9}$$

where h is the relative downstream water level, q_{in} is the relative upstream discharge, k_{hw} is the gain of the downstream weir, p_{21} is the transfer function between the upstream discharge and the downstream water level and p_{22} is the transfer function between the downstream discharge and the downstream water level [Litrico and Fromion, 2004a]. The variables and the transfer functions are illustrated in Figure 3.8. The Bode plot of this transfer function calculated for the third pool of the UPC-PAC is shown in Figure 3.9. The magnitude plot has not longer a slope, it is almost horizontal, and the phase plot is not -90 degrees.

The downstream structure influences the response time, hence the resonance frequency. Its influence was investigated in [Munier et al., 2010]. It deepens

on the discharge equation of the structure and the gain of the transfer function between the water level at the downstream end of the pool and the discharge of the structure.

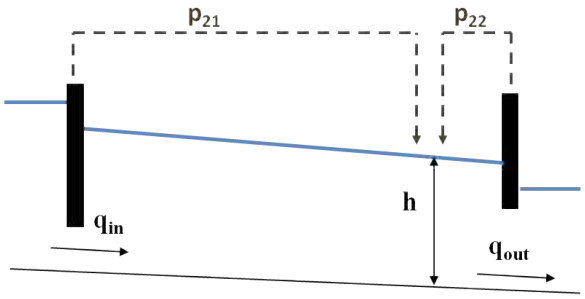

FIGURE 3.8: Illustration of the transfer functions

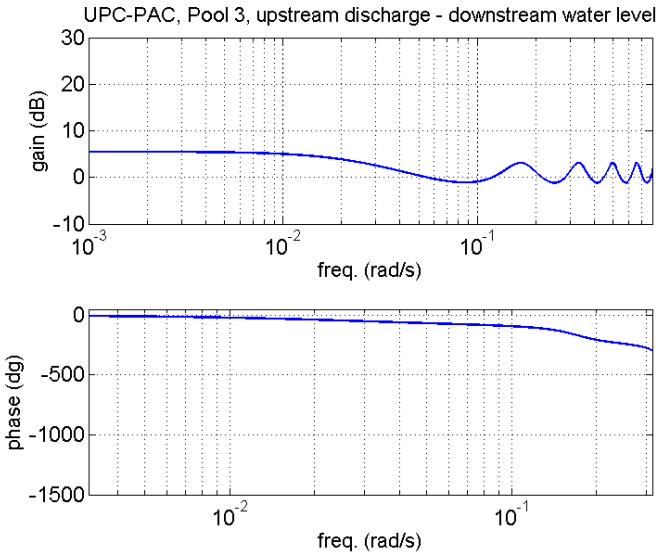

FIGURE 3.9: Bode plot of Pool 3 of UPC-PAC with a downstream weir

3.4.1 Numerical test on the third pool of UPC-PAC

A numerical study was conducted by taking as example the third reach of the UPC-PAC to analyze the effect of the downstream structure on the resonance frequency and the magnitude of the resonance peak height. ATV test was carried out with different downstream conditions: constant discharge (for

example a pump), weirs with different height and sluice gates with different opening (Figure 3.10). An example for the numerical ATV test is shown in Figure 3.11. The resonance frequency and the resonance peak was calculated in all cases, and the results are shown in Table 3.1.

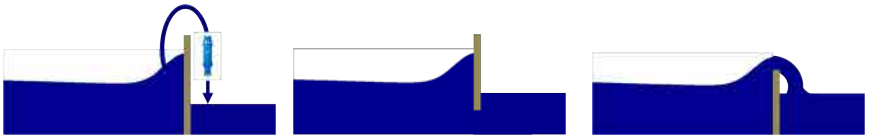

(a) Constant discharge (b) Sluice gate (c) Weir

FIGURE 3.10: A canal reach with different boundary conditions

	Resonance Frequency ω_R (rad/s)	**Resonance peak M_R (s/m^2)**
Pump	0.179	3.85
Weir 30cm	0.169	1.17
Weir 35cm	0.174	1.18
Weir 40cm	0.179	1.23
Gate opening 8.5cm	0.185	3.15
Gate opening 11.5cm	0.170	2.35
Gate opening 14.5cm	0.161	1.73

TABLE 3.1: The effect of the hydraulic structures to the resonance frequency and peak height

The resonance peak is the highest in the constant discharge case. Using a sluice gate the bigger the gate opening, the smaller the resonance peak height. This is explained by the fact that as the gate opening increases, the gain on the water level also increases, that is the discharge depends more on the water level: as a peak level is produced, the output discharge also increases and lowers the peak level. A similar effect occurs in case of the weirs: as the weir height decreases the gain on the discharge decreases as well, and the resonant peak increases. The peak decreased more in case of the weir due to its bigger gain on the water level. The frequency increases with the weir height but decreases with the gate opening.

While the resonance peak was influenced to a great extend by the structure (the peak height can change 50%), the resonance frequency changed only in a range of 10%.

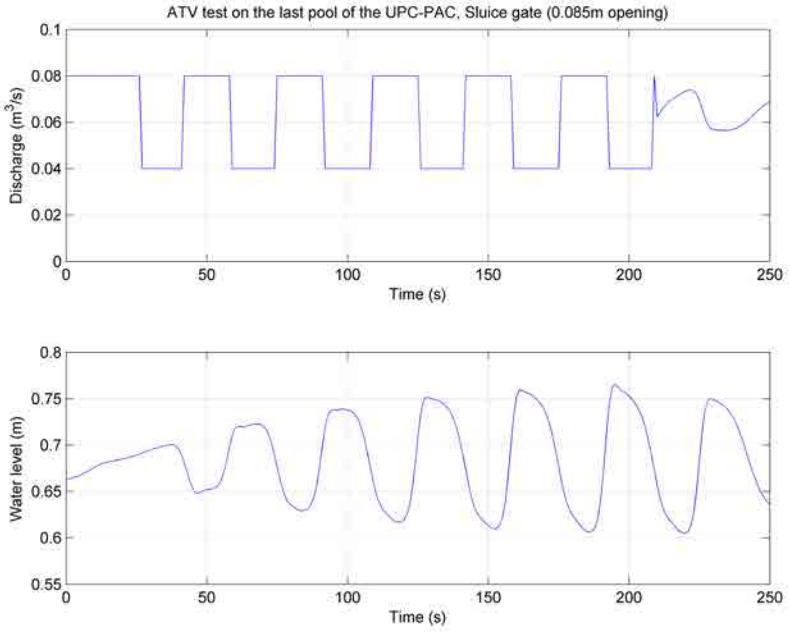

FIGURE 3.11: Numerical ATV test on a canal pool, with sluice gate downstream boundary condition

3.5 ATV experiments on the laboratory canal

The ATV tests are used to get the resonance properties of the pools and the delayed ATV test is used to get the backwater area. For all the experiments the same base discharge, 60 l/s was used, just as for the calculations.

3.5.1 ATV test

The ATV tests were carried out in the following way at each pool: first a steady state was set. After achieving the steady state (20 min) the upstream gate was moved in order to produce a positive disturbance that is equivalent to about 5 l/s discharge. When the wave arrived downstream and the water level started to change, the change in discharge was reversed by the discharge controller. Every time the downstream water level crossed the setpoint the gate movement was reversed. The resulting amplitude of the gate movement was

about 3 cm. A bigger amplitude could not be chosen due to the constraint of the gate opening speed. This signal already produced a measurable disturbance that was possible to be distinguished from the noise.

The water levels (Figure 3.12a, Figure 3.13a and Figure 3.14a) and the discharges (Figure 3.12b, Figure 3.13b and Figure 3.14b) are recorded for each pool.

The obtained water level signals are shown in Figure 3.12a, Figure 3.13a and Figure 3.14a. Using these figures the period and the amplitude of the waves can be read.

As Figure 3.12b, Figure 3.13b and Figure 3.14b shows the discharge signals were not exactly step signals as it is needed for the test. The reason is that it took time for the gates to open and close in order to maintain the required discharge: in other words, the gate speed is slow compared to the travel time of the waves.

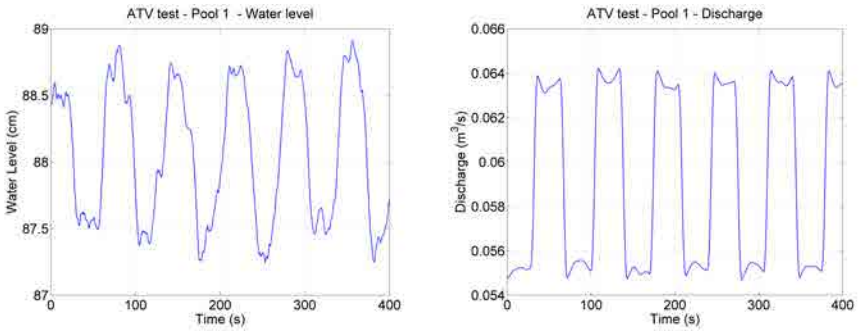

(a) Water level (b) Discharge

FIGURE 3.12: The ATV test on Pool 1

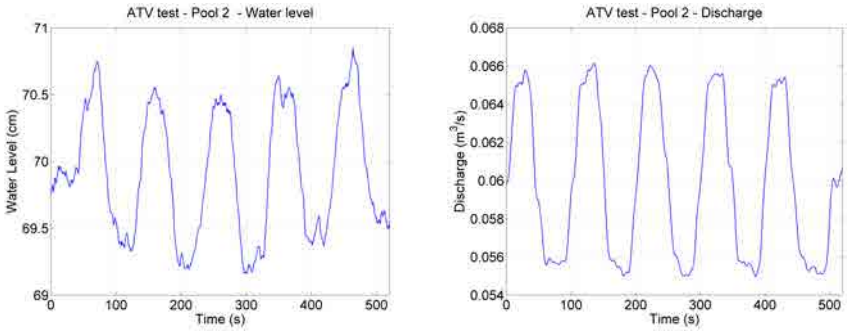

(a) Water level (b) Discharge

FIGURE 3.13: The ATV test on Pool 2

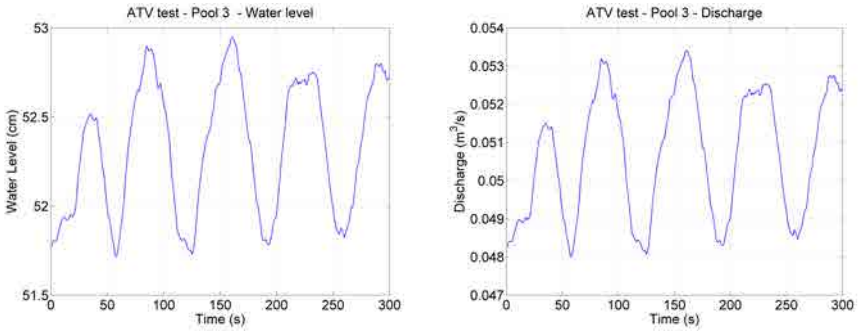

(a) Water level (b) Discharge

FIGURE 3.14: The ATV test on Pool 3

3.5.2 Delayed ATV test

In order to find the backwater area, delayed ATV tests were carried out in a similar manner as the ATV test. The upstream discharge of every pool was increased and then decreased by 10 l/s. In these tests the period was set as the combination of the original ATV test plus 1, 4 and 8 times the cycle time. The corresponding frequencies and the actual frequencies achieved can be seen in Table 3.2.

In case of Pool 3 the lowest actual frequency does not correspond to the planned one due to the constraint of the gate speed. Since Pool 3 is half as short as Pool 1 and 2, its resonance frequency is about the double of that of the other pools. To excite this system according to the test fast gate movements

are required. (Smaller gate movements would have resulted in unacceptable signal-noise ratio.)

While establishing these frequencies, several factors need to be considered: the frequency needs to be low enough to avoid the effect of the first resonance peak. In some cases the discharge controller had difficulties to maintain the same discharge for a long time. This occurred in case of the third experiment (longest period) for the second pool (that is why only two tests are included in Figure 3.16). As the water level at the downstream end of the gate increased the gate opened to give more discharge. However, after certain time, the water level increased more in the downstream pool due to the extra water volume and the water level downstream of the gate increased. This suggested to the discharge controller even bigger gate openings, and in case of the third experiment for the second pool, these openings were too big and the gate was not any more under submerged conditions. It did not happen for the first or the third pool. In case of the first pool, due to the high water level of the reservoir, the gate never opened so much to leave the submerged flow regime and for the third pool the cycle times were shorter and the same discharge did not have to be maintained for such long time.

		Cycle time T_R (s)	**Actual frequency ω (rad/s)**	**Planned frequency $\omega_{planned}$ (rad/s)**	**Backwater area A_s (m^2)**
Pool 1	Test 1	112	0.056	0.054	22.2
	Test 2	464	0.014	0.014	35.5
	Test 3	927	0.007	0.007	41.7
Pool 2	Test 1	130	0.048	0.049	20.0
	Test 2	507	0.012	0.012	34.0
Pool 3	Test 1	238	0.026	0.105	21.5
	Test 2	361	0.017	0.026	29.3
	Test 3	584	0.011	0.013	43.4

TABLE 3.2: Results of the delayed ATV test

The upstream discharge signal and the downstream water depth are shown in Figure 3.15a and Figure 3.15b, respectively.

The discharge signal was not an exact step signal (Figure 3.15b) due to the physical constraints of the system (speed of the gate motors). As a result

of this input signal, the downstream water level (Figure 3.15a) oscillates in different frequencies. Also the amplitude was changing, but not monotonically, as it was observed in [Clemmens et al., 2012]. We remark that the long peak in Figure 3.16b was due to an accidental gate movement.

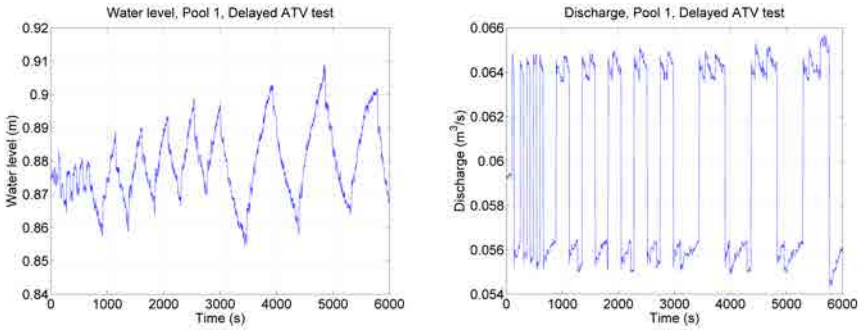

(a) Water level (b) Discharge

FIGURE 3.15: The delayed ATV test on Pool 1

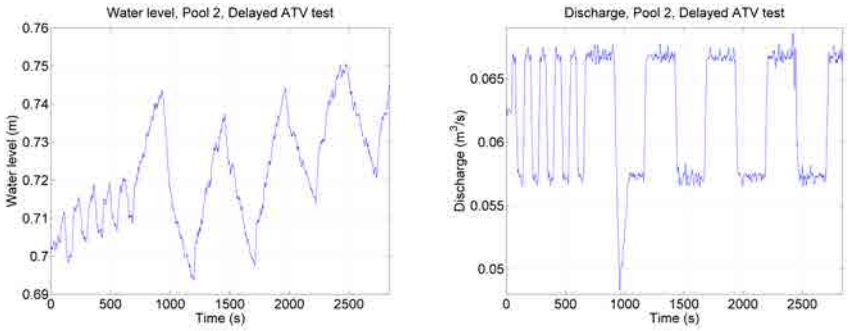

(a) Water level (b) Discharge

FIGURE 3.16: The delayed ATV test on Pool 2

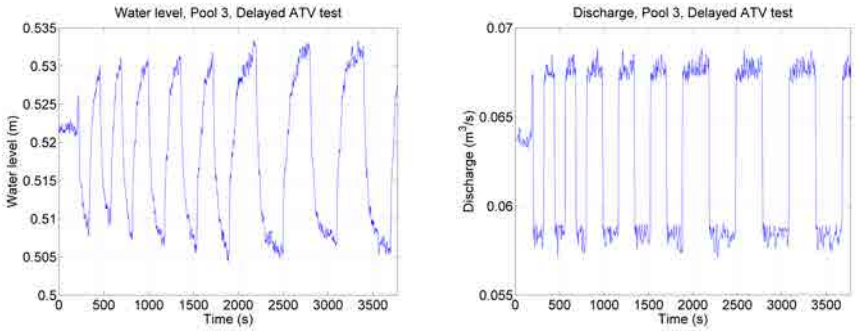

(a) Water level (b) Discharge

FIGURE 3.17: The delayed ATV test on Pool 3

The ATV with the smallest delay is very close to the resonance frequency, and in the third test there were problems with establishing the discharge signal, so the results (backwater area) are taken from the second ATV test (8 times the cycle time).

3.6 Results: resonance properties obtained by different methods

3.6.1 Method 1: Equations

The characteristics obtained by the above described Method 1 (using equations) is shown in Table 3.3. This way of calculating the backwater area can be used when the canal pool completely under backwater and the surface is close to horizontal. In case of the UPC-PAC due to the zero slope the use of this method is completely justified and the calculated backwater area is expected to be good.

	Backwater area A_s (m²)	**Travel time T_R (s)**	**Resonance Frequency ω_R (rad/s)**	**Resonance peak M_R (s/m²)**
Pool 1	38.3	60	0.104	3.17
Pool 2	39.7	76	0.083	2.38
Pool 3	19.1	38	0.166	3.55

TABLE 3.3: Results of the canal properties from equations

3.6.2 Method 2: Bode plots

The methodology described before were used to obtain the Bode plots for all the three pools and from them calculate the resonance properties. The Bode plot for Pool 2 as an example is shown in Figure 3.18. The location of the first peak can be read from the graph and the magnitude of the peak can be read from the gain axis. The gain in the figure is given in decibels.

The characteristics obtained by the above described Method 2 (by using the numerical solution of the Saint-Venant equations) is shown in Table 3.4.

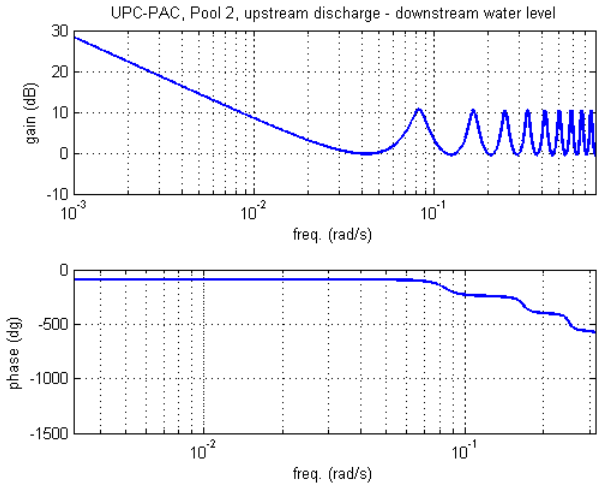

FIGURE 3.18: ATV test on Pool 3, Water level

	Backwater area A_s (m^2)	**Travel time T_R (s)**	**Resonance Frequency ω_R (rad/s)**	**Resonance peak M_R (s/m^2)**
Pool 1	37.5	60	0.105	5.46
Pool 2	37.8	75	0.084	3.39
Pool 3	19.1	38	0.167	7.14

TABLE 3.4: Results of the canal properties from the Bode diagram of a distributed model

3.6.3 Method 3: System identification

Using the delayed ATV tests, a third order model could be identified to represent the canal properties. The data preprocessing and the identification process was carried out as in [van Overloop and Bombois, 2012]. First, as preprocessing, the outliers were removed, the means were subtracted and the data was detrended. Then the data was distributed to identification and validation data (75% identification, 25% validation). The data was re-sampled in order to avoid the identification of higher order behaviour: in this case the information needed is the frequency and the height of the first resonance peak. Since the model contains an integrator, it is difficult to identify. A tamed differentiator is applied to the data: it only differentiates the data at low frequencies where the integrator is present.

After this preprocessing, a 4th order model and a 5th order noise model were identified. The delay is approximated from the cycle time calculated from Equation 3.4. The transfer function of the identified models was multiplied with the inverse of the differentiator and that resulted in a fifth order model.

Table 3.5 shows the characteristics of the models to be identified. The sampling time was chosen in order to avoid higher order resonance peaks. The cutoff frequency of the tamed differentiator was chosen in order to differentiate only the low low frequency data that is relevant for the integrator but not to affect the high frequency peaks. The values were chosen following the recommendations from [van Overloop and Bombois, 2012].

	Cutoff frequency (rad/s)	**Sampling time (s)**	**Delay steps (-)**
Pool 1	0.005	5	2
Pool 2	0.001	5	1
Pool 3	0.001	10	2

TABLE 3.5: The parameters used for the identification of the models from the delayed ATV tests

The resulting models are shown in Figures 3.19, 3.20 and 3.21. For the first two pools at about 70% and for the last pool 90% fit is achieved. Since a fifth order model was used the first two peaks (and the integrator) could be identified. For Pool 3 (Figure 3.21) only one very flat peak could be identified. The lack

of the second harmonic shows that this pool does not exhibit strong resonant behaviour.

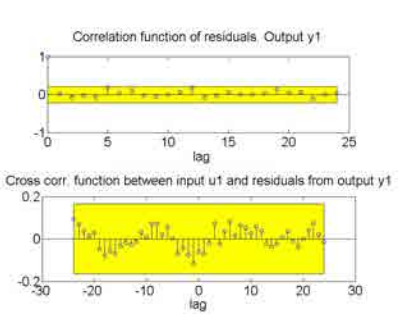

(a) Residuals

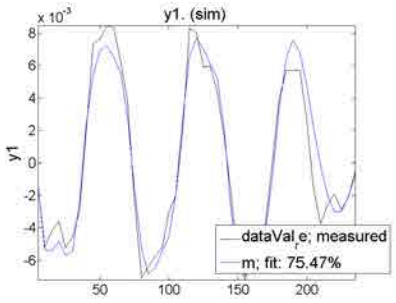

(b) Validation

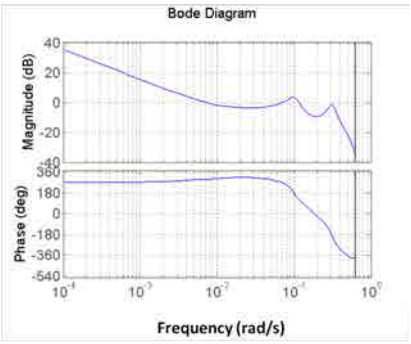

(c) Model

FIGURE 3.19: The identified model for the first pool of the UPC-PAC

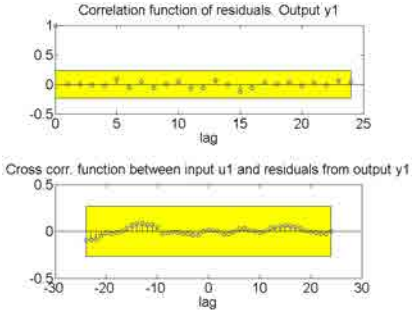

(a) Residuals

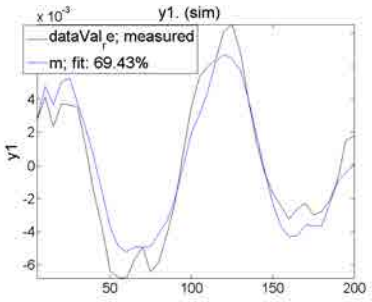

(b) Validation

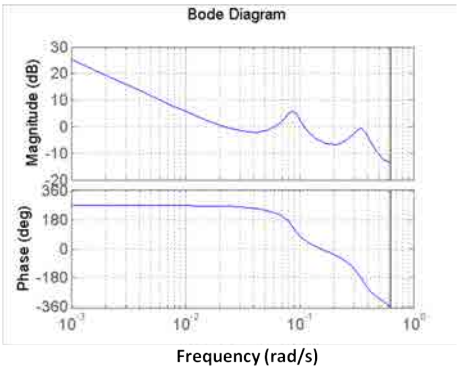

(c) Model

FIGURE 3.20: The identified model for the second pool of the UPC-PAC

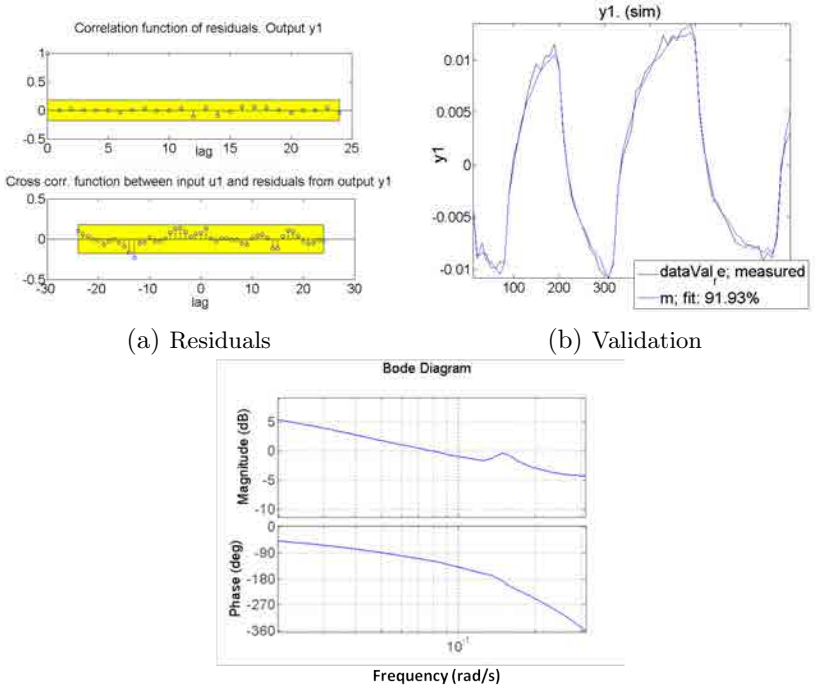

(a) Residuals (b) Validation

(c) Model

FIGURE 3.21: The identified model for the third pool of the UPC-PAC

The numerical results are shown in Table 3.6. The approximation of the backwater areas are bigger for the first two pools (the reaches has similar length) while smaller for the last pool. Pool 3 is half as long as the upstream pools, therefore the backwater area should almost be the half. This difference in this identification experiment might be due to the difficulties of identifying a canal reach with a downstream weir at the downstream end. The resonance frequencies are similar for the first two pools, while it is higher for Pool 3 - as it was expected. The peaks are lower than the ones calculated beforehand. In Pool 3, there is one very small peak showing that that this pool is not so resonant as the others.

	Backwater area A_s (m^2)	**Resonance Frequency ω_R (rad/s)**	**Resonance peak M_R (s/m^2)**
Pool 1	38.5	0.104	1.82
Pool 2	34.6	0.080	1.23
Pool 3	29.7	0.140	0.96

TABLE 3.6: Results of the system identifiction

3.6.4 Method 4: ATV

The results of the ATV test were already described in subsection 3.5.1. Here they are summarized numerically in Table 3.7. The resonance frequency and resonance peak is obtained from the ATV test and the backwater area from the delayed ATV test. The backwater areas are in the same range as expected except the last canal pool. The reasons are already mentioned: due to the downstream weir it shows a different behaviour and the backwater area cannot be determined in the same way.

The resonance frequency is the highest for Pool 1. It was expected to be the highest for Pool 3. However, Pool 3 is affected less by resonance due to the downstream weir, therefore it was more difficult to identify resonance properties (the resonance peak is smaller, the noise-signal ration is higher). Also due to the short lenght of Pool 3 and the constraints with the gate speed the test was complicated to carry out.

The resonance peaks as expected were higher in the first two pools and lower in Pool 3.

	Backwater area A_s (m^2)	**Cycle time T_c (s)**	**Resonance Frequency ω_R (rad/s)**	**Resonance peak M_R (s/m^2)**
Pool 1	35.5	56	0.112	1.21
Pool 2	34.0	88	0.071	1.10
Pool 3	29.3	60	0.105	0.91

TABLE 3.7: Canal properties determinted from the ATV tests

3.6.5 Discussion

The canal properties (backwater area, resonance frequency, resonance peak) of the UPC-PAC were obtained in several ways. First, they were approximated by Equations: 3.3, 3.4 and 3.5. Then a distributed model based on the linearized Saint-Venant equation was calculated [Litrico and Fromion, 2004a] and from the frequency response of this model, the resonance properties of the canal pools were obtained. The same properties were obtained using ATV and delayed ATV tests, and also with system identification methods using the data obtained from the ATV tests. Tables 3.8, 3.9 and 3.10 summarize the results obtained with the four different methods.

	Backwater area A_s (m^2)	**Resonance Frequency ω_R (rad/s)**	**Resonance peak M_R (s/m^2)**
Equation	38.3	0.104	3.17
Bode	37.5	0.105	5.46
ATV	35.5	0.112	1.21
Ident	38.5	0.0958	1.82

TABLE 3.8: Results of the ATV test and the identified models, Pool 1

	Backwater area A_s (m^2)	**Resonance Frequency ω_R (rad/s)**	**Resonance peak M_R (s/m^2)**
Equation	39.7	0.083	2.38
Bode	37.8	0.084	3.39
ATV	34.0	0.071	1.10
Ident	34.6	0.083	1.23

TABLE 3.9: Results of the ATV test and the identified models, Pool 2

	Backwater area A_s (m^2)	**Resonance Frequency ω_R (rad/s)**	**Resonance peak M_R (s/m^2)**
Equation	19.1	0.166	3.55
Bode	19.1	0.167	7.14
ATV	29.3	0.105	0.91
Ident	29.7	0.150	0.96

TABLE 3.10: Results of the ATV test and the identified models, Pool 3

In the majority of the cases all four types of tests have results that are similar in order of magnitude. For the first two pools the results of all four tests are similar, especially for the backwater area and for the resonance frequency. There are differences in the resonance peak between the experimental and theoretical methods. The results for Pool 3 show bigger differences between the different methods.

For the first two pools some general conclusions can be drawn. The resonance frequencies were similar for all type of tests. This shows that the resonance frequency can be approximated very well by calculations.

The experimental values of the resonance peaks are similar, but much lower than the theoretical ones. This can be explained by the fact that in calculations the effect of the upstream and downstream structures were not taken into account. As it was shown before, a weir or a sluice gate causes decreases the resonance peak (compared to the constant discharge case), that is why the experimental resonance peaks are lower. This result also shows the difficulty to obtain values for the resonance peak by calculations and the importance of identification experiments.

The values for the backwater areas were also approximated well with all methods, for the first two pools the areas were approximated within a 15% range of error. The approximation was especially good for Pool 1. As a tendency, the experimentally obtained backwater areas are smaller than the calculated ones.

In the case of Pool 3, the experimentally obtained frequencies (and also the other properties) are more different from the theoretical ones. This can have several explanations. One reason can be the constraint of the gate speed: this pool is the shortest, hence the waves arrive to the downstream end in less time and it was difficult to achieve the appropriate discharge signal needed for the test. The frequency error should be corrected by the identification test. In fact, the identified frequency is closer to the one obtained from the equations.

The difference in backwater area can also be explained with the different configuration of the canal pools. Pool 3 has a weir at the downstream end. The water surface is not completely horizontal, the surface might be bigger as expected. Also due to the presence of the weir this pool shows less resonance therefore the identification experiments might need different design. Finally

as this pool was very short, and the gate speed was limited, the resulting noise-signal ratio was worse for this pool than for the other pools.

The considerable difference between the theoretical and the experimental values for the resonance peak just as in case of the upstream pools is explained by the presence of the structures that are not included in the calculations. Pool 3 has a weir at the downstream end, whose effect of lowering the peak is even bigger than the effect of the gates. That is why the difference between the calculated and the experimental values is bigger than in case of the upstream pools.

In the remaining of this work, the calculated frequencies (that are in almost all cases equal to the experimental ones), the calculated backwater areas and the experimentally obtained resonance peaks are used.

The first two canal pools present significant resonance, while Pool 3 is less affected by resonance.

3.7 Conclusion

Four ways were shown in order to quantify the resonance properties of the UPC-PAC canal: by given equations using the canal geometry, by using Bode plots obtained from the numerical solution of the SV equations, by system identification and by ATV tests.

- The actual identification tests (system identification and ATV) resulted in similar resonance frequencies as the ones calculated from the geometrical data.
- However, for resonance peak heights, the calculation results overestimate the ones obtained by identification. This can be explained by the presence of the structures: their effect was not taken into account in the calculations.
- The results obtained by the ATV test and the system identification are coherent. Both tests are good enough to obtain the resonance properties of the canal.

- The importance of the downstream condition was analyzed: having a sluice gate at the downstream end decreases the resonance peak to some extent while having a weir at the downstream end almost eliminates the resonance.
- In the current configuration it can be said that the first two pools of the UPC-PAC are dominated by resonance while the third pool shows very small resonance.

Chapter 4

Canal modelling and control

4.1 Introduction

In this chapter several models for control purposes are presented and compared in time and frequency domain. Based on these models centralized model predictive controllers are developed. The goal of this chapter is to get more insight about the capacities of each model and their suitability to be inner models for MPC. The chapter is concluded with the choice of the appropriate model for the UPC-PAC. A general categorization of models has already been presented in the introduction, therefore here it is not repeated.

The models are first described for one canal reach, then the whole state space model is constructed for the three reaches. The main variables are Q_{in} (m^3/s) input discharge, Q_{out} (m^3/s) output discharge, H (m) downstream water level, Q_{off} (m^3/s) offtake discharge. In case of some models, an intermediate discharge Q_t is also considered. These discharges and the variables are used to describe a trapezoidal cross section are shown in Figure 4.1.

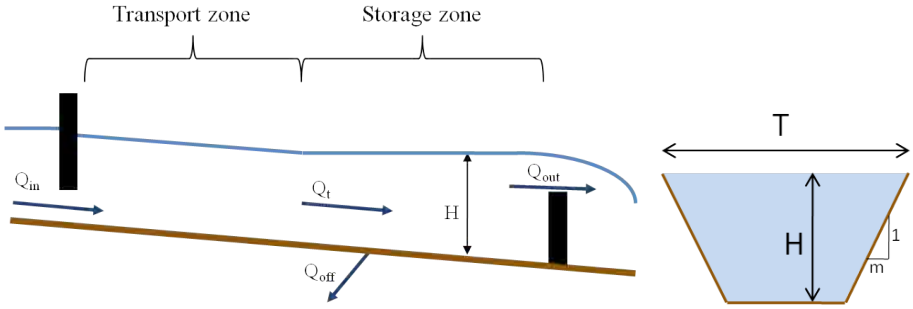

(a) Lateral view (b) Cross section

FIGURE 4.1: The notations used for the model development

The models are linearized around a steady state. In all cases the absolute quantities are noted with capital letters, the steady state values have a zero index, and the values relative to the steady state are noted with small letters. For example, the relative input discharge is

$$q_{in}(t) = Q_{in}(t) - Q_{in0} \tag{4.1}$$

where q_{in} is the relative input discharge, Q_{in} is the absolute input discharge and Q_{in0} is the steady state (reference) input discharge. The objective is to control the downstream water level of a canal pool by manipulating the input discharge.

4.2 Description of the models

4.2.1 Muskingum model (MUS)

The Muskingum model is a frequently used linear model for flood routing [Cunge, 1969]. It has also been used for control purposes [Rodellar et al., 1993], [Gómez et al., 1998] and [Mantecón et al., 2002]. It describes the relationship between the discharge entering and leaving a reach. Since the purpose of this work to develop water level controllers, we need a model describing the relationship between the upstream discharge and the downstream water level. For this reason the canal reach is divided into two zones: a transport zone and a storage zone (Figure 4.1). The Muskingum

model is used to express the relationship between the discharge entering and leaving the transport zone. The model is described with the following storage and continuity equations, respectively:

$$v_{sto}(t) = K\left[\chi q_{in}(t) + (1-\chi)q_t(t)\right] \tag{4.2}$$

$$\frac{dv_{sto}}{dt} = q_{in}(t) - q_t(t) \tag{4.3}$$

where q_{in} is the relative input discharge, q_t is the relative discharge at the end of the transport zone, v_{sto} is the relative storage volume, K is the storage time constant and χ is a dimensionless coefficient. The parameters $K$and χ contain all the information about the reach. The storage time constant (with the dimension of time) can be well approximated as the time it takes for one wave to travel through the reach:

$$K = \frac{X}{C_0 + V_0} \tag{4.4}$$

where X is the length of the canal pool, C_0 is the steady state celerity and V_0 is the steady state velocity. Parameter χ weighs the relative effects of inflow and outflow on the reach storage, which varies in the range [0, 0.5]. It can be approximated from the flow and geometrical properties of the canal [Cunge, 1969]. Applying the Laplace transform from the model above, the following transfer function can be derived:

$$G_{Mq}(s) = \frac{q_t(s)}{q_{in}(s)} = \frac{1 - K\chi s}{1 + K(1-\chi)s}. \tag{4.5}$$

Details about the derivation of this transfer function can be found in [Rodellar et al., 1989]. This transfer function shows the relationship between the upstream discharge and the discharge at the end of the transport zone. Now we need the transfer function between the upstream discharge and the downstream water level. This can be achieved by modelling the storage-zone as a tank:

$$A_e \frac{dh}{dt} = q_t(t) - q_{out}(t) \tag{4.6}$$

where A_e is the surface of the storage area. It can be approximated as:

$$A_e = TX \tag{4.7}$$

where T is the surface width and X is the length of the storage zone. Applying the Laplace transform to Equation 4.6 the following expression is obtained:

$$q_t(s) = A_e h(s)\ s - q_{out}(s). \tag{4.8}$$

By combining Equation 4.5 and Equation 4.8, the transfer function between the upstream discharge and downstream water level can be expressed:

$$G_M(s) = \frac{h(s)}{q_{in}(s)} = \frac{1 - K\chi s}{A_e s + K(1-\chi)A_e s^2}. \tag{4.9}$$

Hence the downstream water level is:

$$h(s) = G_M(s)\, q_{in}(s) - \frac{1}{A_e s} q_{out}(s). \tag{4.10}$$

The final values for Muskingum model are shown in Table 4.1. The parameters for the Muskingum function were calculated as mentioned above: K was approximated by the travel time (See Equation 3.4) while χ was calculated based on the methodology described in [Cunge, 1969]. The surface of the storage zone in case of the UPC-PAC was approximated with the surface of the whole canal pool, since all the canal pool are completely under backwater.

	K(s)	χ (-)	A_e (m^2)
Pool 1	28.29	0.01	28.29
Pool 2	31.67	0.01	31.67
Pool 3	16.65	0.01	16.65

TABLE 4.1: The calculated values of the parameters of the Muskingum model for the UPC-PAC canal

For the discretization of the Muskingum procedure the following inequality should be taken into account [Rodellar et al., 1989]:

$$\Delta t > 2\chi K \tag{4.11}$$

where Δt is the sampling period. In all cases this condition is kept. For the calculation of the step response $\Delta t = 1$ s was used, therefore this condition was kept. For the controller development even bigger sampling time is used, so the condition still holds.

4.2.2 First order model from the Hayami equation (FO)

The Hayami model [Hayami, 1951] is the linearization of the diffusive wave equation with the hypothesis that the celerity and diffusivity are constant:

$$\frac{\partial q}{\partial t} + C_0 \frac{\partial q}{\partial x} - D_0 \frac{\partial^2 q}{\partial x} = 0 \tag{4.12}$$

where q is the relative discharge (deviation from the steady state discharge Q_0), C_0 is the celerity coefficient and D_0 is the diffusion coefficient. For trapezoidal channels (see Figure 4.1) these coefficients are:

$$C_0 = \frac{5Q_0}{3A_{cr0}} - \frac{2Q_0 m}{T_0^2} \tag{4.13}$$

$$D_0 = \frac{Q_0}{2T_0 S_{f0}} \tag{4.14}$$

where T_0 is the top width, m is the side slope, A_cr0 is the cross sectional area, S_{f0} is the friction slope and it can be calculated from the Manning's equation:

$$S_{f0} = \frac{Q_0^2 n^2}{A_{cr0}^2 R_{h0}^{4/3}} \tag{4.15}$$

where n is the Manning's coefficient and R_{h0} is the hydraulic radius.

One of the ways to obtain a simple linear model from the Hayami equation is the momentum matching method, described in [Malaterre, 1994] and [Litrico and Georges, 1999]. The low order moments of the Laplace transforms of the calculated transfer function of the Hayami model are obtained. The concept is to make these moments equal the low order moments of the first or second order function with delay. The low order moments correspond to low frequencies (s close to 0). These frequencies are the most common in natural systems. The following dimensionless coefficient is derived to characterize the canal reach:

$$C_L = \frac{C_0 X}{2D_0} \tag{4.16}$$

where X is the length of the canal reach. Three different categories can be established:

- Category 1: If $C_L > 9/4$, the reach is relatively long, a second order function with delay can be defined.

- Category 2: If $1 < C_L \leq 9/4$, the reach is relatively small, the second order transfer function with delay is unstable, therefore it is possible to define a first order with delay or a second order transfer function. In this case it is possible to equate the first three moments.
- Category 3: When $C_L \leq 1$, the river reach is very short. First order transfer function can be defined by equating the first two moments.

An analysis about canals falling to each category with different length and discharge can be found in [Alvarez Brotons, 2004].

The UPC-PAC falls into Category 3, therefore a first order transfer function without delay can be defined:

$$G_{FOq}(s) = \frac{q_t(s)}{q_{in}(s)} = \frac{1}{1 + K_1 s} \tag{4.17}$$

where

$$K_1 = \frac{X}{C_0}. \tag{4.18}$$

In the remaining of this chapter this model will be referred to as first order (FO) model. Note that this model has no time delay, it is just a simple first order model. Though the original Hayami equation includes more complex wave movement, the first order model lacks all these dynamics.

Just as in the case of the Muskingum model, in order to get a transfer function between the downstream water level and the upstream discharge, Equation 4.8 and Equation 4.17 should be combined, resulting into

$$G_{FO}(s) = \frac{h(s)}{q_{in}(s)} = \frac{1}{A_e K_1 s^2 + A_e s} \tag{4.19}$$

where $G_{FO}(s)$ is the transfer function between the upstream discharge and the downstream water level. Thus the downstream water level can be expressed as:

$$h(s) = G_{FO}(s)\, q_{in}(s) - \frac{1}{A_e s} q_{out}(s). \tag{4.20}$$

The final values for the FO model are shown in Table 4.2 for each reach of the UPC-PAC.

	K_1 (-)	C_0 (m/s)	C_L (-)	A_e (m^2)
Pool 1	278.9	0.31	0	28.29
Pool 2	238.1	0.38	0	31.67
Pool 3	90.23	0.48	0	16.65

TABLE 4.2: The calculated values of the parameters of the first order model for the UPC-PAC canal

4.2.3 The Integrator Delay model (ID)

The ID model was developed in [Schuurmans, 1997] and it is widely used for modelling water systems for control purposes. The model is based on the division of the canal reach into an upstream and a downstream part (see Figure 4.2). The upstream part is characterized by uniform flow, and the downstream part is characterized by backwater. Some canals are completely affected by backwater, like the UPC-PAC used in this study. In the backwater part, the dynamics is complicated, waves are travelling up and down and reflected.

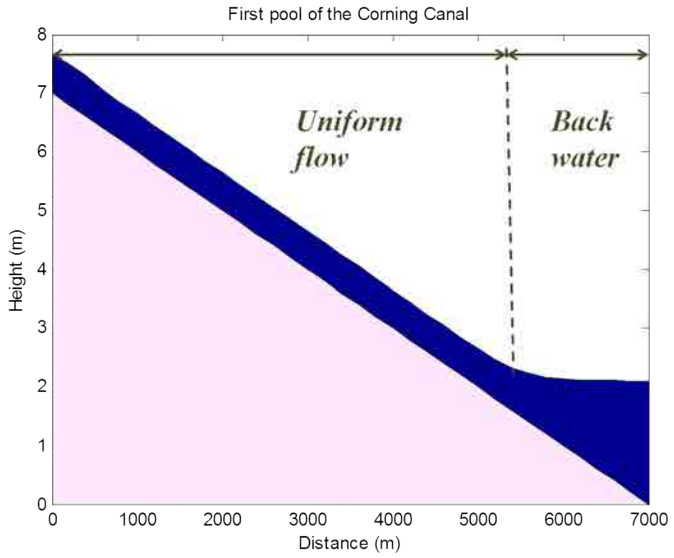

FIGURE 4.2: Profile of the first pool of the Corning canal with 5.5 m^3/s flow

However, in low frequencies it behaves as a tank, the change in water level can be approximated as the integral of the flow change, whose gain is calculated from the backwater surface. The model is illustrated in Figure 4.3. The upper figure shows the discharge step and the lower shows the response of the water level: after a certain time delay the water level starts to increase linearly with a slope of equal to the backwater area, A_{eID}.

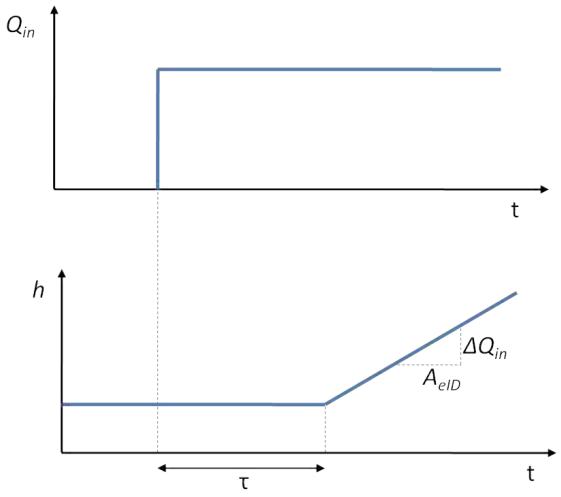

FIGURE 4.3: The ID model

The ID model is very simple, it requires only two parameters that are easy to obtain: the time delay and the backwater area. Both can be calculated from the geometry of the canal or can be obtained using system identification experiments. Since it is a linearized model, it performs well around the point of linearization. These values depend on the operation regime, and in practice can be very different depending on the discharges. An example is shown in [van Overloop, 2006b]: for a steep test reach the difference between the parameters for low flow and high flow resulted to be 63% in time delay and 52% in storage area. First the uniform then the backwater part and finally the by combining the two the whole model is described.

Uniform part

The flow is assumed to be uniform, the waves are assumed to travel only in the downstream direction, the wave deformation is neglected and the water surface

is parallel to the canal bed, having normal depth. A disturbance travels through this part with a speed close to the speed of the kinematic shock wave. This part is only described by one parameter: the time delay (τ_{id}). The output discharge hydrograph is the input discharge hydrograph shifted in time Equation 4.21. The time delay depends on the discharge, however, (that is one of the weakness of this model) it is considered to be constant around the reference discharge. The output discharge can be expressed as:

$$Q_{out}(t) = Q_{in}(t - \tau_{id}) \tag{4.21}$$

and in the Laplace domain:

$$Q_{out}(s) = Q_{in}(s)e^{-s\tau_{id}}. \tag{4.22}$$

The time delay for the ID model (τ_{id}) will be approximated by the following equation:

$$\tau_{ID} = \frac{X}{C_0 + V_0} \tag{4.23}$$

where X is the length of the canal pool, C_0 is the steady state celerity and V_0 is the steady state velocity.

Backwater part

The backwater part is described as a reservoir and the water volume that arrives causes the water level to increase (integrator action). Therefore the only parameter to describe this part is the surface area / backwater area (A_{eID}):

$$A_{eID}\frac{dH}{dt} = Q_{in} - Q_{out}. \tag{4.24}$$

This equation is the following in the Laplace domain:

$$h(s) = \frac{1}{sA_{eID}}(q_{in}(s) - q_{out}(s)). \tag{4.25}$$

The complete ID model

In the uniform part, since the velocity and the celerity are constant, the wave travelling upstream dampens out quickly, therefore it can be assumed that the flow rate downstream is the upstream flow rate plus delay. Altogether the

model is:

$$h(s) = \frac{1}{A_{eID}s} e^{-\tau_{id}s} q_{in}(s) - \frac{1}{A_{eID}s} q_{out}(s) \tag{4.26}$$

where τ_{id} is the time delay, q_{in} is the upstream discharge, q_{out} is the downstream discharge and A_{eID} is the gain of the integrator (backwater area), which can be approximated by the surface of the canal pool:

$$A_{eID} = TX \tag{4.27}$$

where T is the surface width and X is the length of the canal pool. If the water surface is close to the horizontal, this approximation is close to the real backwater surface. In order to develop a controller that is using the downstream water level as controller variable and the upstream discharge as control variable, the transfer function between the upstream discharge and the downstream water level is used:

$$G_{ID}(s) = \frac{h(s)}{q_{in}(s)} = \frac{1}{A_e s} e^{-s\tau_{id}}. \tag{4.28}$$

The final values for the ID model are shown in Table 4.3 for the UPC-PAC canal.

	A_{eID} (m^2)	τ_{ID} (s)
Pool 1	38.28	28.29
Pool 2	39.69	31.67
Pool 3	19.14	16.65

TABLE 4.3: The calculated values of the parameters of the ID model for the UPC-PAC canal

4.2.4 Integrator Delay Zero model (IDZ)

Similar to the ID model, the IDZ model [Litrico and Fromion, 2004b] is an extension of the ID model that includes a zero in the transfer function. It is able to represent the canal behavior in low and high frequencies; the integrator delay accounts for low frequencies, whereas the zero represents the direct influence of the discharge on the water level in high frequencies.

The IDZ model also assumes that the canal pool has two parts: a uniform flow or transport section and a backwater section. For the uniform part, low and

high frequency approximations are taken into account. The transfer function of the IDZ model is similar to Equation 4.28 but extended with a zero:

$$G_{IDZ}(s) = \frac{h(s)}{q_{in}(s)} = \frac{K_{IDZ1}\, s + 1}{A_{eIDZ}\, s} e^{-\tau_{IDZ}\, s} \tag{4.29}$$

where K_{IDZ} is a parameter related to the zero calculated from the canal properties, τ_{IDZ} is the time delay and A_{eIDZ} is the integrator/backwater area approximation. The water level can be expressed as:

$$h(s) = \frac{K_{IDZ1}\, s + 1}{A_{eIDZ}\, s} e^{-\tau_{IDZ}\, s} q_{in}(s) - \frac{K_{IDZ2}\, s + 1}{A_{eIDZ}\, s} q_{out}(s). \tag{4.30}$$

The detailed derivation of these transfer functions can be found in [Litrico and Fromion, 2004b]. The final values for the IDZ model are shown in Table 4.4.

	A_{eIDZ} (m^2)	τ_{IDZ} (s)	K_{IDZ1} (-)	K_{IDZ2} (-)
Pool 1	37.87	28.24	39.46	30.2
Pool 2	38.84	31.56	43.28	34.51
Pool 3	18.68	16.60	24.45	18.97

TABLE 4.4: The calculated values of the parameters of the IDZ model for the UPC-PAC canal

4.2.5 Integrator Resonance model (IR)

The integrator resonance model was developed in [van Overloop et al., 2010b] especially for canals with resonance. The basic idea of the model is to capture the integrator behaviour in low frequencies and the resonance behaviour at high frequencies for short and flat canal pools. These characteristics can be seen from the linearisation of the Saint-Venant equations and are analyzed in Chapter 1 and Chapter 3.

The model is developed by discretising a channel into two elements, neglecting the advection. The equation are presented in the time and in the Laplace domain in [van Overloop et al., 2010b] and summarized in Appendix B. The transfer function from upstream flow q_{in} to the downstream water level h is a third order model without delay consisting of an integrator whose gain is the reciprocal of the storage area (A_s) and a damped oscillator with natural

frequency ω_0 and resonance peak M_r. The following equation presents the Integrator Resonance model as transfer function in the Laplace domain:

$$G_{IR}(s) = \overbrace{\frac{1}{A_s s}}^{\text{Integrator}} \cdot \overbrace{\frac{\omega_0^2}{s^2 + 2\zeta\omega_0 s + \omega_0^2}}^{\text{Resonance}} \tag{4.31}$$

where ω_0 is the natural frequency of the system and ζ is the damping ratio. The natural frequency ω_0 is approximated by the resonance frequency ω_r, that is estimated from the travel time of the waves. The backwater surface and the resonance frequency can be experimentally obtained or can be calculated using equations 3.3 and 3.5 presented in Chapter 3, respectively. The resonance peak and the resonance frequency can be obtained from identification experiments. The damping ratio can be calculated as

$$\zeta = \frac{1}{2\omega A_s M_r}. \tag{4.32}$$

The downstream water level can be expressed as

$$h(s) = \frac{\omega_0^2}{A_s s^3 + \frac{s^2}{M_r} + A_s\omega_0^2 s} q_{in}(s) - \frac{2s^2 + \frac{2}{A_s M_r}s + \omega_0^2}{A_s s^3 + \frac{s^2}{M_r} + A_s\omega_0^2 s} q_{out}(s). \tag{4.33}$$

In order to build the IR models of the UPC-PAC several identification experiments have been carried out. They are described in Chapter 3. The resulting canal properties are presented in Table 4.5: the backwater area obtained by calculation, resonance frequency obtained by calculation (that is equal to the experimentally obtained ones) and calculated and experimentally obtained resonance peak values. For controller development, the experimentally obtained resonance peak values are used. On the other hand, for the time and frequency domain comparisons the theoretical magnitudes are used. The reason is the following: the experimental values contain the effect of the downstream weir. Since none of the other models have the effects of the weir included, for the sake of the comparison for the IR model the theoretical values are used. Based on Chapter 3, the final model for the IR based controller describes the third pool using the ID model since this pool presents few resonance. For the time and frequency domain comparisons all the three pools are modelled with IR model.

	Backwater area A_s (m^2)	**Resonance Frequency ω_R (rad/s)**	**Resonance peak, experimental M_R (s/m^2)**	**Resonance peak, theoretical M_R (s/m^2)**
Pool 1	38.28	0.1037	1.82	5.46
Pool 2	39.69	0.0831	1.23	3.39
Pool 3	19.14	0.1667	0.96	7.14

TABLE 4.5: Canal pool properties of the UPC-PAC used for developing the IR model

4.3 Comparison of the models in the time and frequency domains

In the time domain, the transport part of the models is examined. The response of the downstream discharge to a step input in the upstream discharge is analyzed. In the frequency domain, the relation between the downstream level and the upstream discharge is studied. The use of downstream level in modeling is particularly relevant for the automatic control problem.

4.3.1 Comparison in the time domain

All flow steps are made from the usual operational discharge 60 l/s to 70 l/s. The plots are based on the numerical solution of the equations. The continuous models are first converted to discrete models using zero order hold, then they are solved with a fixed step solver [Shampine and Gahinet, 2006]. This solver is based on an implicit Runge-Kutta method, the Radau IIA. This method belongs to the family of curvature methods, it is a third-order accurate implicit Runge-Kutta algorithm in two stages. The calculated transfer function in the Laplace and Z-domain can be found in Appendix D.

The step response of the Saint-Venant equations was calculated in a way different from all the other five models: with the SIC 1D hydrodynamic model that solves the Saint-Venant equations numerically by using the implicit Preissmann scheme. The Courant number was about 0.5 depending

on the different flow conditions. Therefore in both cases the step response was in fact a response to a ramp as shown in Figure 4.4.

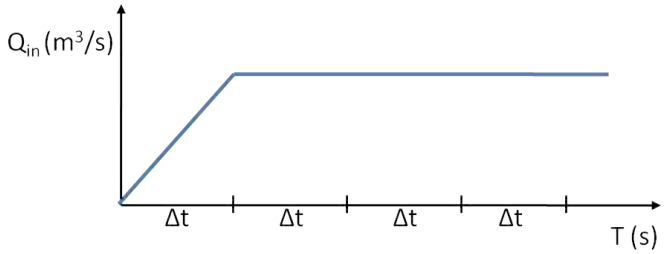

FIGURE 4.4: The ramp function of the step response

The step response of the four models and compared to the step response of the Saint-Venant (SV) equations. Figure 4.5 and Figure 4.6 show the response of the first pool, Figure 4.7 the second and Figure 4.8 the third pool.

With black line (Figure 4.5) the response of the Saint-Venant model is shown. An initial time delay (Figure 4.6) is followed by a fast increase. Then the increase is slowing down, similar to a first order response. Small oscillations can be seen, they are decreasing in magnitude and finally disappearing: this is the effect of the resonance waves.

At a first glance, the first order approximation is close to the Saint-Venant model, especially in the middle terms. However, in the beginning there is an important mismatch: the first order model does not capture the time delay, the response starts at time step zero (Figure 4.6).

The Muskingum model has similar behaviour in the sense that it also lacks the time delay. However, it has a rapid increase in the beginning of the step and approaches the new discharge within 120 seconds.

The ID and IDZ model both approximate correctly the time delay (Figure 4.6). The ID model shows the same step as the input discharge, only delayed in time. This is the most simple approximation. The IDZ model has similar response to a step, but in the beginning it shows an increase, it grows over the final value, then slowly descends. This behaviour is due to the presence of the zero.

The IR model contains no explicit time delay. The step increases fast over the final value, and then approaches it through oscillation. Note that the period of

these oscillations is the same as the period of the response of the Saint-Venant model. The response of the IR model reaches the final value much earlier than the Saint-Venant model.

Comparing the responses of the three pools, there is a difference between the intermediate pools and the last pool: the response of the last pool is faster then the other two. This has two reasons: one is that the third pool is half as long as the others and the other is that it has a weir as downstream boundary condition. The models will be analyzed in the frequency domain, and the final choice will be made by testing numerically the controller developed based on them.

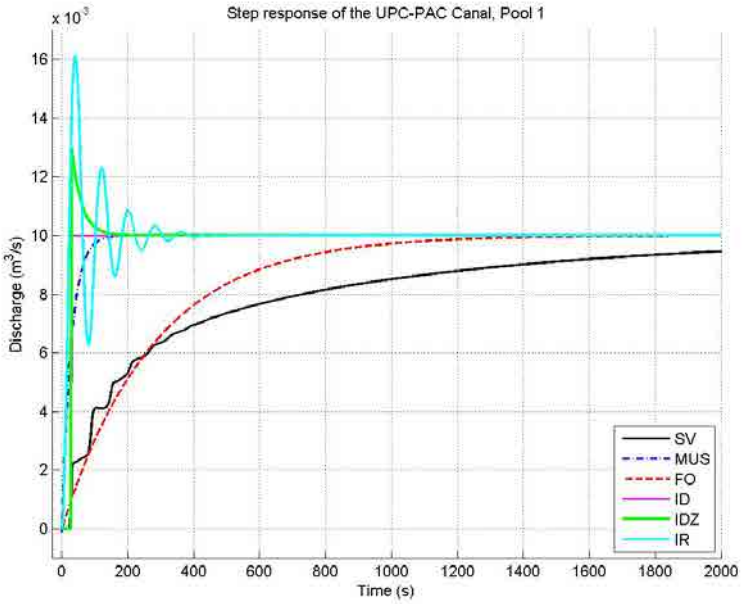

FIGURE 4.5: The simulated step response of the models, Pool 1

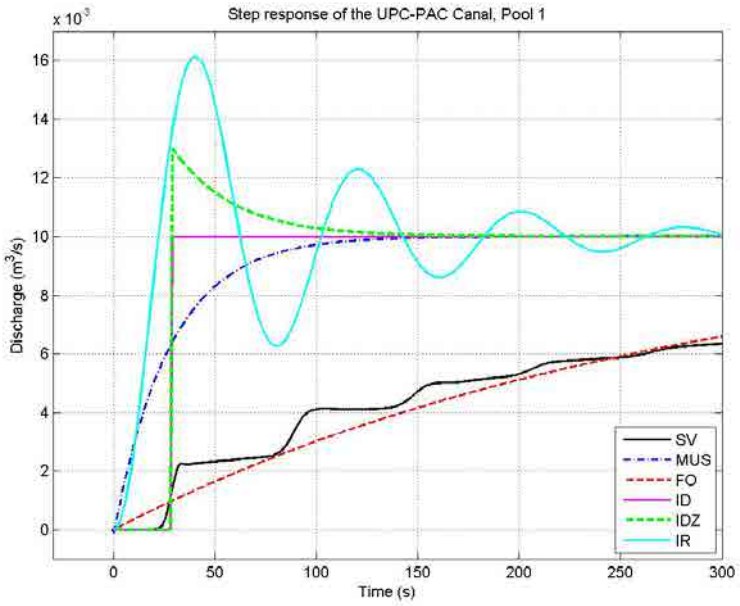

FIGURE 4.6: The step response of the models, Pool 1 - zooming to the beginning to the response

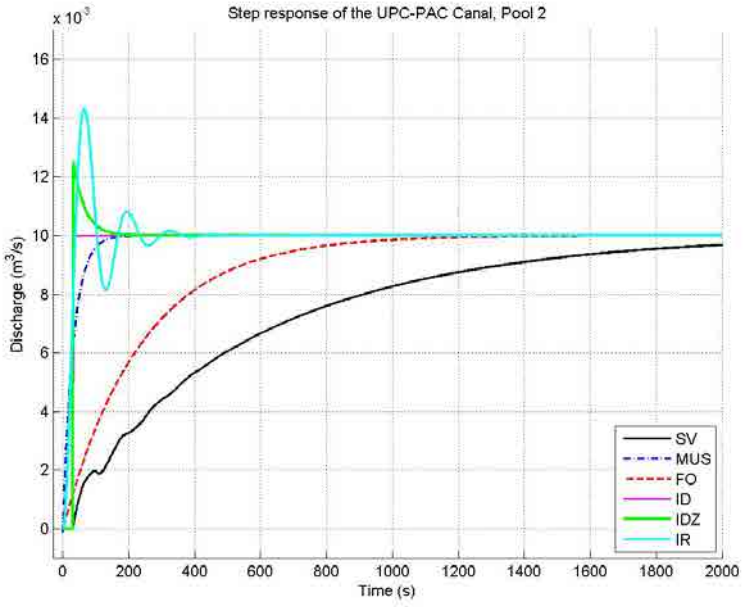

FIGURE 4.7: The simulated step response of the models, Pool 2

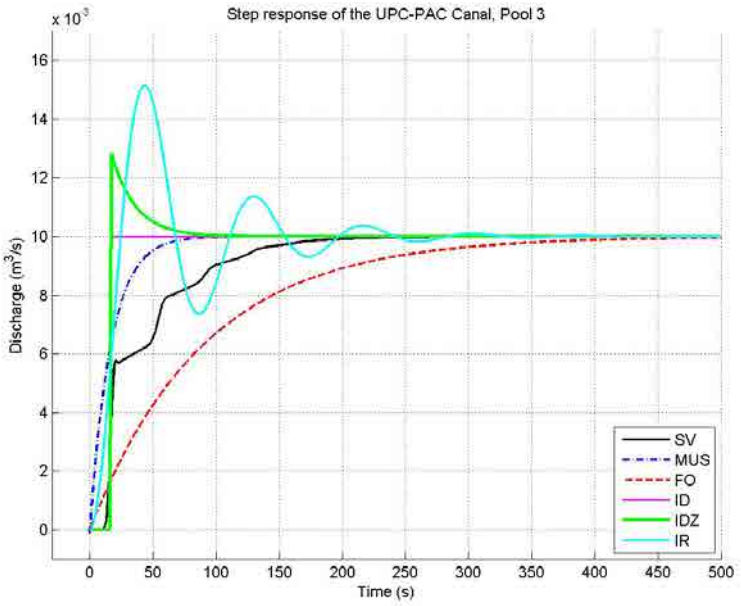

FIGURE 4.8: The simulated step response of the models, Pool 3

4.3.2 Comparison in the frequency domain

The frequency response analysis shows the response of the system when the input is a sinusoidal wave. The phase plot shows the change in the phase of the input wave while the gain plot shows the change in the amplitude of the wave. The frequency responses of the three pools of the UPC-PAC (Figures 4.9, 4.10 and 4.11) were obtained using the approximation method from [Litrico and Fromion, 2004a] to solve numerically the linearized Saint-Venant equations. In this process, just as for the comparison of the step response, the effect of the downstream structures is not taken into account.

For the IR model the theoretical values for the peak and frequencies are used in order not to take into account the effect of the structures. This step is necessary for the comparison of the Bode plots of the models, because all the other models are calculated without taking into account the effect of the structures.

All models are good in low frequencies (Figures 4.9, 4.10 and 4.11): in the gain plot they have the straight line with the same slope and in the phase plot they

start at -90 degrees. This means that all models have an integrator in their structure with appropriate gain (compared to the SV equations).

In higher frequencies the SV model shows clearly the resonance peaks. Only the IR model takes the first peak into account. The IDZ model cuts the resonance peaks, while the other models approximate the gains lower than the SV (See for example Pool 1: Figure 4.9).

The FO model has the lowest gain, the MUS model has higher gain. The gain of the ID model is close that of the SV model, it starts to be lower only close to the frequency of the first peak. The ID model becomes horizontal and crosses the resonance peaks. The IDZ model approximates the high frequency values by averaging the behaviour. This is the reason why it is crossing over the peaks.

In the phase plots (Figures 4.9, 4.10 and 4.11; lower subplots) the phase of the SV model decreases in high frequencies, also showing the resonance waves. The decreasing behaviour is captured by the ID and IDZ model, while the IR is able to overlap with the SV model until the beginning of the second resonance peak. The MUS and FO models remain horizontal. This is the same behaviour that was seen in the step response: the last two models lack the time delay.

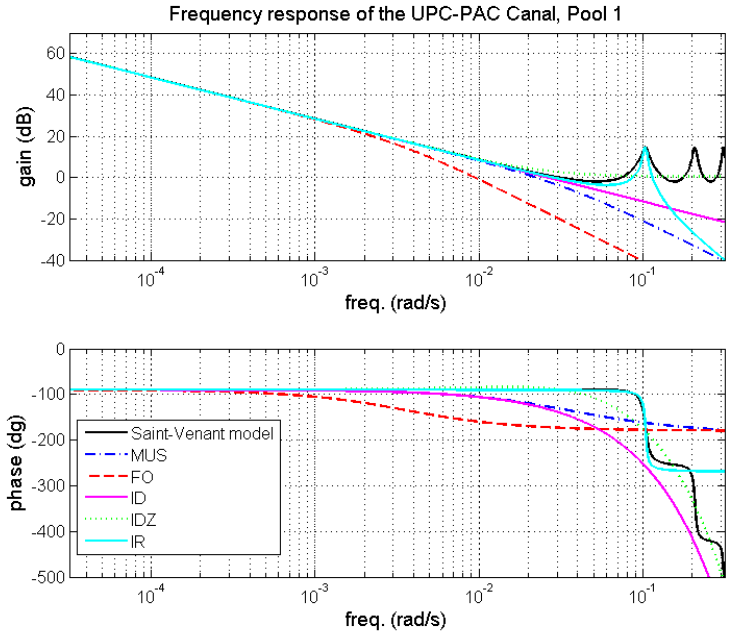

FIGURE 4.9: The frequency response of the models, Pool 1

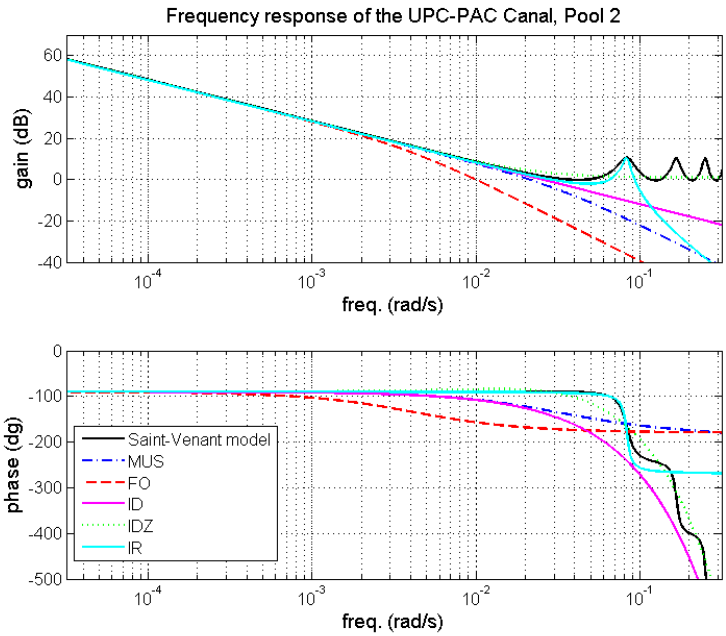

FIGURE 4.10: The frequency response of the models, Pool 2

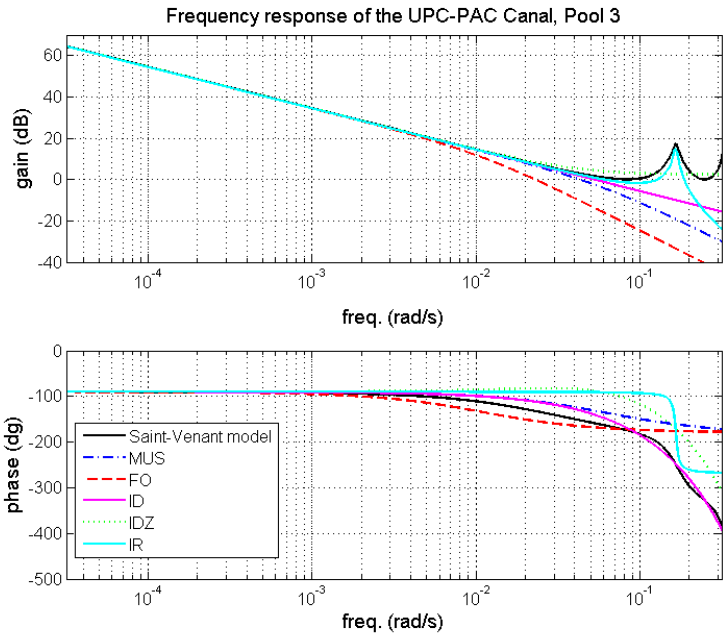

FIGURE 4.11: The frequency response of the models, Pool 3

The behaviour of the three pools are similar. However, a difference can be observed in the location of the peaks: for Pool 3 (Figure 4.11) the first resonance peak is located at higher frequencies. This frequency is higher because the travel time is smaller due to the fact that this pool is the shortest.

As it was seen in the step responses, only the ID and the IDZ approximates the time delay well. All models except the IDZ and the IR are underestimating the high frequency gain.

4.4 State space formulation

In this section a general state space formulation is presented for any of the discharge-water level models presented in this chapter, whose order is less than or equal to three with or without delay. The particular state space equations for the models are shown in the appendix: for the Hayami and Muskingum model in section C.1, for the ID and IDZ model in section C.2 and for the IR model in section C.3.

To build this model we start with a generalized transfer function:

$$h_i = \frac{p_a z^2 + p_b z + p_c}{z^3 + p_d z^2 + p_e z + p_f} z^{-d} q_i - \frac{p_g z^2 + p_h z + p_i}{z^3 + p_d z^2 + p_e z + p_f} q_{i+1} \tag{4.34}$$

where the parameters p_a, p_b, p_c, p_d, p_e, p_f depend on the model, and d is the delay expressed in sampling instants between the relative upstream discharge (q_i) and the relative downstream water level (h_i). The second term is the effect of the discharge (q_{i+1}) leaving the reach (this can be the discharge of the following reach or an offtake), see Figure 4.12.

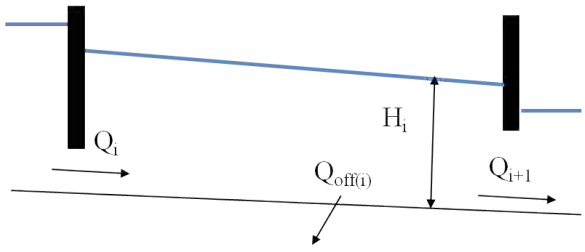

FIGURE 4.12: The frequency response of Pool 3 with downstream weir boundary condition

In the equations the relative quantities (the deviations from the reference quantity) are used, while the notation in Figure 4.12 shows the absolute quantities. (For example as a reminder: $Q_i = Q_{i0} + q_i$.) Equation 4.34 can be written in the time domain as follows:

$$\begin{aligned} h_i(k+1) = \quad & -p_d h_i(k) - p_e h_i(k-1) - p_f h_i(k-2) + p_a q_i(k-d) \\ & + p_b q_i(k-1-d) + p_c q_i(k-2-d)\, q_i - p_g q_{i+1}(k) \\ & + p_h q_{i+1}(k-1) + p_i q_{i+1}(k-2)\, q_i. \end{aligned} \tag{4.35}$$

Consider the water level error defined as:

$$e_i(k) = h_i(k) - h_{spi}(k) \tag{4.36}$$

where h_{spi} is water level setpoint.

Using Equations 4.35 and 4.36, the following equation is obtained:

$$\begin{aligned} e_i(k+1) = \quad & -p_d e_i(k) - p_e e_i(k-1) - p_f e_i(k-2) \\ & + p_a q_i(k-d) + p_b q_i(k-1-d) + p_c q_i(k-2-d)\, q_i \\ & - p_g q_{i+1}(k) + p_h q_{i+1}(k-1) + p_i q_{i+1}(k-2) \\ & - h_{sp}(k+1) - p_d h_{sp}(k) - p_e h_{sp}(k-1) \\ & - p_f h_{sp}(k-2). \end{aligned} \tag{4.37}$$

Consider the discharge is expressed incrementally in the form:

$$\Delta q_i(k) = q_i(k+1) - q_i(k). \tag{4.38}$$

Finally, Equation 4.37 can be converted into the following state space form

$$x_{gen}(k+1) = A_{gen} x_{gen}(k) + B_{gen} u_{gen}(k) + B_{dgen} d_{gen}(k) \tag{4.39}$$

with the state and the control vector respectively, in the form

$$x_{gen}(k) = \begin{bmatrix} q_i(k) \\ \dots \\ q_i(k-d) \\ q_i(k-d-1) \\ q_i(k-d-2) \\ e_i(k) \\ e_i(k-1) \\ e_i(k-2) \end{bmatrix}, \tag{4.40}$$

$$u_{gen}(k) = \Delta q_i(k) \tag{4.41}$$

and the disturbance vector in the form:

$$d_{gen}(k) = \begin{bmatrix} q_{i+1}(k) \\ q_{i+1}(k-1) \\ q_{i+1}(k-2) \\ h_{sp}(k+1) \\ h_{sp}(k) \\ h_{sp}(k-1) \\ h_{sp}(k-2) \end{bmatrix}. \tag{4.42}$$

The state vector contains the upstream discharges in the present and past time steps. The control vector contains only the incremental discharge. The disturbance vector contains information about the output discharges and the setpoints. The matrices are the following:

$$A_{gen} = \begin{bmatrix} 1 & 0 & 0 & 0 & 0 & 0 & 0 & 0 \\ 1 & 0 & 0 & 0 & 0 & 0 & 0 & 0 \\ 0 & 1 & 0 & 0 & 0 & 0 & 0 & 0 \\ 0 & 0 & 1 & 0 & 0 & 0 & 0 & 0 \\ 0 & 0 & 0 & 1 & 0 & 0 & 0 & 0 \\ 0 & 0 & p_a & p_b & p_c & -p_d & -p_e & -p_f \\ 0 & 0 & 0 & 0 & 0 & 1 & 0 & 0 \\ 0 & 0 & 0 & 0 & 0 & 0 & 1 & 0 \end{bmatrix} \tag{4.43}$$

$$B_{gen} = \begin{bmatrix} 1 \\ 0 \\ 0 \\ 0 \\ 0 \\ 0 \\ 0 \\ 0 \end{bmatrix} \tag{4.44}$$

$$B_{dgen} = \begin{bmatrix} 0 & 0 & 0 & 0 & 0 & 0 & 0 \\ 0 & 0 & 0 & 0 & 0 & 0 & 0 \\ 0 & 0 & 0 & 0 & 0 & 0 & 0 \\ 0 & 0 & 0 & 0 & 0 & 0 & 0 \\ 0 & 0 & 0 & 0 & 0 & 0 & 0 \\ -p_g & -p_h & -p_i & -1 & -p_d & -p_e & -p_f \\ 0 & 0 & 0 & 0 & 0 & 0 & 0 \\ 0 & 0 & 0 & 0 & 0 & 0 & 0 \end{bmatrix}. \tag{4.45}$$

4.4.1 Canal reach with a hydraulic structure at the downstream end

If the canal reach has a hydraulic structure downstream, the downstream discharge can be expressed in terms of the water level using the linearized equation of the hydraulic structure:

$$q_{i+1}(k) = k_{hw} h_i(k) \tag{4.46}$$

where k_{hw} is the gain of the structure (in case of the UPC-PAC the gain of the weir). Using this equation in Equation 4.37 the error becomes:

$$\begin{aligned} e_i(k+1) = \; & [-p_d - p_g k_{hw}]\, e_i(k) + [-p_e - p_h k_{hw}]\, e_i(k-1) \\ & [-p_f - p_i k_{hw}]\, e_i(k-2) + p_a q_i(k-d) \\ & + p_b q_i(k-1-d) + p_c q_i(k-2-d) - h_{spi} + (k+1) \\ & + [-p_d - p_g k_{hw}]\, h_{spi}(k) + [-p_e - p_h k_{hw}]\, h_{spi}(k-1) \\ & + [-p_f - p_i k_{hw}]\, h_{spi}(k-2) \end{aligned} \tag{4.47}$$

and the state equation is

$$x_{gen}(k+1) = A_{str} x_{gen}(k) + B_{str} u_{gen}(k) + B_{dstr} d_{str}(k). \tag{4.48}$$

The state, the control and the disturbance vector are the same as in Equation 4.40, Equation 4.41, and Equation 4.42. The matrices are now:

$$A_{str} = \begin{bmatrix} 1 & 0 & 0 & 0 & 0 & 0 & 0 & 0 \\ 1 & 0 & 0 & 0 & 0 & 0 & 0 & 0 \\ 0 & 1 & 0 & 0 & 0 & 0 & 0 & 0 \\ 0 & 0 & 1 & 0 & 0 & 0 & 0 & 0 \\ 0 & 0 & 0 & 1 & 0 & 0 & 0 & 0 \\ 0 & 0 & p_a & p_b & p_c & -p_d - p_g k_{hw} & -p_e - p_h k_{hw} & -p_f - p_i k_{hw} \\ 0 & 0 & 0 & 0 & 0 & 1 & 0 & 0 \\ 0 & 0 & 0 & 0 & 0 & 0 & 1 & 0 \end{bmatrix}, \tag{4.49}$$

$$B_{str} = \begin{bmatrix} 1 \\ 0 \\ 0 \\ 0 \\ 0 \\ 0 \\ 0 \\ 0 \end{bmatrix} \tag{4.50}$$

and

$$B_{dstr} = \begin{bmatrix} 0 & 0 & 0 & 0 & 0 & 0 & 0 \\ 0 & 0 & 0 & 0 & 0 & 0 & 0 \\ 0 & 0 & 0 & 0 & 0 & 0 & 0 \\ 0 & 0 & 0 & 0 & 0 & 0 & 0 \\ 0 & 0 & 0 & 0 & 0 & 0 & 0 \\ -p_g & -p_h & -p_i & -1 & -p_d - p_g k_{hw} & -p_e - p_h k_{hw} & -p_f - p_i k_{hw} \\ 0 & 0 & 0 & 0 & 0 & 0 & 0 \\ 0 & 0 & 0 & 0 & 0 & 0 & 0 \end{bmatrix}. \tag{4.51}$$

4.4.2 State space model for multiple reaches

The general state space model is presented here for two reaches, with offtake flows $q_{off\,i}$ and $q_{off(i+1)}$ at the downstream end of both reaches and a weir

downstream boundary condition for the second reach. The same structure can be generalized for $i = 1, 2, ..., n$ reaches.

The state contains the flow at the present instant k and the previous instants $(k - d - 2)$ and the errors of the water level in the present and the previous instants. This is repeated for the second reach (subscript $i + 1$).

$$x_{gen}(k) = \begin{bmatrix} q_i(k) \\ q_i(k-1) \\ q_i(k-2) \\ ... \\ q_i(k-d) \\ q_i(k-d-1) \\ q_i(k-d-2) \\ e_i(k) \\ e_i(k-1) \\ e_i(k-2) \\ q_{i+1}(k) \\ q_{i+1}(k-1) \\ q_{i+1}(k-2) \\ ... \\ q_{i+1}(k-d) \\ q_{i+1}(k-d-1) \\ q_{i+1}(k-d-2) \\ e_{i+1}(k) \\ e_{i+1}(k-1) \\ e_{i+1}(k-2) \end{bmatrix} \qquad u_{gen}(k) = \begin{bmatrix} \Delta q_i(k) \\ \Delta q_{i+1}(k) \end{bmatrix} \tag{4.53}$$

$$d_{gen}(k) = \begin{bmatrix} q_{offi}(k) \\ q_{offi}(k-1) \\ q_{offi}(k-2) \\ h_{spi}(k+1) \\ h_{spi}(k) \\ h_{spi}(k-1) \\ h_{spi}(k-2) \\ q_{off(i+1)}(k) \\ q_{off(i+1)}(k-1) \\ q_{off(i+1)}(k-2) \\ h_{sp(i+1)}(k+1) \\ h_{sp(i+1)}(k) \\ h_{sp(i+1)}(k-1) \\ h_{sp(i+1)}(k-2) \end{bmatrix} \tag{4.54}$$

Note that, while for a single reach i the control is just incremental flow through the gate i, in the multiple-reach case the control is a vector $u_{gen}(k)$, which contains the incremental flows through all the gates. Note that the disturbance vector contains the offtake flows and the setpoints.

The matrices are the following:

$$
A_{gen} = \left[\begin{array}{ccccccccccccccccccccccccccc}
1 & 0 & 0 & \cdots & 0 & 0 & 0 & 0 & 0 & 0 & 0 & 0 & 0 & 0 & 0 & 0 & 0 & 0 & 0 & 0 & 0 & 0 & 0 & 0 & 0 \\
1 & 0 & 0 & & 0 & 0 & 0 & 0 & 0 & 0 & 0 & 0 & 0 & 0 & 0 & 0 & 0 & 0 & 0 & 0 & 0 & 0 & 0 & 0 & 0 \\
0 & 1 & 0 & & 0 & 0 & 0 & 0 & 0 & 0 & 0 & 0 & 0 & 0 & 0 & 0 & 0 & 0 & 0 & 0 & 0 & 0 & 0 & 0 & 0 \\
\vdots & & & \ddots & \vdots & \vdots & \vdots & \vdots & \vdots & \vdots & \vdots & \vdots & \vdots & \vdots & \vdots & \vdots & \vdots & \vdots & \vdots & \vdots & \vdots & \vdots & \vdots & \vdots & \vdots \\
0 & 0 & 0 & & 0 & 0 & 0 & 0 & 0 & 0 & 0 & 0 & 0 & 0 & 0 & 0 & 0 & 0 & 0 & 0 & 0 & 0 & 0 & 0 & 0 \\
0 & 0 & 0 & & 0 & 1 & 0 & 0 & 0 & 0 & 0 & 0 & 0 & 0 & 0 & 0 & 0 & 0 & 0 & 0 & 0 & 0 & 0 & 0 & 0 \\
0 & 0 & 0 & & 0 & 0 & 1 & 0 & 0 & 0 & 0 & 0 & 0 & 0 & 0 & 0 & 0 & 0 & 0 & 0 & 0 & 0 & 0 & 0 & 0 \\
0 & 0 & 0 & & 0 & 0 & 0 & 0 & 0 & 0 & 0 & 0 & 0 & 0 & 0 & 0 & 0 & 0 & 0 & 0 & 0 & 0 & 0 & 0 & 0 \\
0 & 0 & 0 & & 0 & 0 & 0 & 1 & 0 & 0 & 0 & 0 & 0 & 0 & 0 & 0 & 0 & 0 & 0 & 0 & 0 & 0 & 0 & 0 & 0 \\
0 & 0 & 0 & & 0 & 0 & 0 & 0 & 1 & 0 & 0 & 0 & 0 & 0 & 0 & 0 & 0 & 0 & 0 & 0 & 0 & 0 & 0 & 0 & 0 \\
0 & 0 & 0 & & 0 & 0 & 0 & 0 & 0 & 1 & 0 & 0 & 0 & 0 & 0 & 0 & 0 & 0 & 0 & 0 & 0 & 0 & 0 & 0 & 0 \\
0 & 0 & 0 & & 0 & 0 & 0 & 0 & 0 & 0 & 1 & 0 & 0 & 0 & 0 & 0 & 0 & 0 & 0 & 0 & 0 & 0 & 0 & 0 & 0 \\
0 & 0 & 0 & & 0 & 0 & 0 & 0 & 0 & 0 & 0 & 1 & 0 & 0 & 0 & 0 & 0 & 0 & 0 & 0 & 0 & 0 & 0 & 0 & 0 \\
0 & 0 & 0 & & 0 & 0 & 0 & 0 & 0 & 0 & 0 & 0 & 1 & 0 & 0 & 0 & 0 & 0 & 0 & 0 & 0 & 0 & 0 & 0 & 0 \\
0 & 0 & 0 & & 0 & 0 & 0 & 0 & 0 & 0 & 0 & 0 & 0 & 1 & 0 & 0 & 0 & 0 & 0 & 0 & 0 & 0 & 0 & 0 & 0 \\
0 & 0 & 0 & & 0 & 0 & 0 & 0 & 0 & 0 & 0 & 0 & 0 & 0 & 1 & 0 & 0 & 0 & 0 & 0 & 0 & 0 & 0 & 0 & 0 \\
0 & 0 & 0 & & 0 & 0 & 0 & 0 & 0 & 0 & 0 & 0 & 0 & 0 & 0 & 1 & 0 & 0 & 0 & 0 & 0 & 0 & 0 & 0 & 0 \\
0 & 0 & 0 & & 0 & 0 & 0 & 0 & 0 & 0 & 0 & 0 & 0 & 0 & 0 & 0 & 1 & 0 & 0 & 0 & 0 & 0 & 0 & 0 & 0 \\
0 & 0 & 0 & & 0 & 0 & 0 & 0 & 0 & 0 & 0 & 0 & 0 & 0 & 0 & 0 & 0 & 1 & 0 & 0 & 0 & 0 & 0 & 0 & 0 \\
0 & 0 & 0 & & 0 & 0 & 0 & 0 & 0 & 0 & 0 & 0 & 0 & 0 & 0 & 0 & 0 & 0 & 1 & 0 & 0 & 0 & 0 & 0 & 0 \\
0 & 0 & 0 & & 0 & 0 & 0 & 0 & 0 & 0 & 0 & 0 & 0 & 0 & 0 & 0 & 0 & 0 & 0 & 1 & 0 & 0 & 0 & 0 & 0 \\
0 & 0 & 0 & & 0 & 0 & 0 & 0 & 0 & 0 & 0 & 0 & 0 & 0 & 0 & 0 & 0 & 0 & 0 & 0 & 1 & 0 & 0 & 0 & 0 \\
0 & 0 & 0 & & 0 & 0 & 0 & 0 & 0 & 0 & 0 & 0 & 0 & 0 & 0 & 0 & 0 & 0 & 0 & 0 & 0 & 1 & 0 & 0 & 0 \\
0 & 0 & 0 & & 0 & 0 & 0 & 0 & 0 & 0 & 0 & 0 & 0 & 0 & 0 & 0 & 0 & 0 & 0 & 0 & 0 & 0 & 1 & 0 & 0 \\
0 & 0 & 0 & & 0 & 0 & 0 & 0 & 0 & 0 & 0 & 0 & 0 & 0 & 0 & 0 & 0 & 0 & 0 & 0 & 0 & 0 & 0 & 1 & 0 \\
0 & 0 & 0 & & 0 & 0 & 0 & 0 & 0 & 0 & 0 & 0 & 0 & 0 & 0 & 0 & 0 & 0 & 0 & 0 & 0 & 0 & 0 & 0 & 1
\end{array}\right] \tag{4.55}
$$

$$B_{gen} = \begin{bmatrix} 1 & 0 \\ 0 & 0 \\ 0 & 0 \\ \dots & \\ 0 & 0 \\ 0 & 0 \\ 0 & 0 \\ 0 & 0 \\ 0 & 0 \\ 0 & 0 \\ 0 & 1 \\ 0 & 0 \\ 0 & 0 \\ \dots & \\ 0 & 0 \\ 0 & 0 \\ 0 & 0 \\ 0 & 0 \\ 0 & 0 \\ 0 & 0 \end{bmatrix}, \tag{4.56}$$

and

$$
B_{dgen} = \begin{bmatrix}
0 & 0 & 0 & 0 & 0 & 0 & 0 & 0 & 0 & 0 & 0 & 0 & 0 & 0 & 0 & 0 & 0 & 0 & 0 & 0 \\
0 & 0 & 0 & 0 & 0 & 0 & 0 & 0 & 0 & 0 & 0 & 0 & 0 & 0 & 0 & 0 & 0 & 0 & 0 & 0 \\
0 & 0 & 0 & 0 & 0 & 0 & 0 & 0 & 0 & 0 & 0 & 0 & 0 & 0 & 0 & 0 & 0 & 0 & 0 & 0 \\
\cdots & & & & & & & & & & & & & & & & & & & \\
0 & 0 & 0 & 0 & 0 & 0 & 0 & 0 & 0 & 0 & 0 & 0 & 0 & 0 & 0 & 0 & 0 & 0 & 0 & 0 \\
0 & 0 & 0 & 0 & 0 & 0 & 0 & 0 & 0 & 0 & 0 & 0 & 0 & 0 & 0 & 0 & 0 & 0 & 0 & 0 \\
0 & 0 & 0 & 0 & 0 & 0 & 0 & 0 & 0 & 0 & 0 & 0 & 0 & 0 & 0 & 0 & 0 & 0 & 0 & 0 \\
-p_{gi} & -p_{hi} & -p_{ii} & -1 & -p_{di} & -p_{ei} & -p_{fi} & 0 & 0 & 0 & 0 & 0 & 0 & 0 & 0 & 0 & 0 & 0 & 0 & 0 \\
0 & 0 & 0 & 0 & 0 & 0 & 0 & 0 & 0 & 0 & 0 & 0 & 0 & 0 & 0 & 0 & 0 & 0 & 0 & 0 \\
0 & 0 & 0 & 0 & 0 & 0 & 0 & 0 & 0 & 0 & 0 & 0 & 0 & 0 & 0 & 0 & 0 & 0 & 0 & 0 \\
0 & 0 & 0 & 0 & 0 & 0 & 0 & 0 & 0 & 0 & 0 & 0 & 0 & 0 & 0 & 0 & 0 & 0 & 0 & 0 \\
\cdots & & & & & & & & & & & & & & & & & & & \\
0 & 0 & 0 & 0 & 0 & 0 & 0 & 0 & 0 & 0 & 0 & 0 & 0 & 0 & 0 & 0 & 0 & 0 & 0 & 0 \\
0 & 0 & 0 & 0 & 0 & 0 & 0 & 0 & 0 & 0 & 0 & 0 & 0 & 0 & 0 & 0 & 0 & 0 & 0 & 0 \\
0 & 0 & 0 & 0 & 0 & 0 & 0 & 0 & 0 & 0 & 0 & 0 & 0 & 0 & 0 & 0 & 0 & 0 & 0 & 0 \\
-p_{g(i+1)} & -p_{h(i+1)} & -p_{i(i+1)} & -1 & -p_{d(i+1)} & -p_{e(i+1)} & -p_{f(i+1)} & 0 & 0 & 0 & 0 & 0 & 0 & 0 & 0 & 0 & 0 & 0 & 0 & 0 \\
0 & 0 & 0 & 0 & 0 & 0 & 0 & 0 & 0 & 0 & 0 & 0 & 0 & 0 & 0 & 0 & 0 & 0 & 0 & 0 \\
0 & 0 & 0 & 0 & 0 & 0 & 0 & 0 & 0 & 0 & 0 & 0 & 0 & 0 & 0 & 0 & 0 & 0 & 0 & 0
\end{bmatrix}. \tag{4.57}
$$

4.5 Controller development

In this section a predictive control law is obtained based on the state space models derived in the previous sections. These models can be written in a generic form with a simplified notation as follows:

$$x\left(k+1\right)=Ax\left(k\right)+Bu\left(k\right)+B_{d}d\left(k\right) \tag{4.58}$$

where x is the n-dimensional state vector, u is an m dimensional input vector, A is a $n\times n$ square matrix, B is a $n\times m$ matrix and B_d is a $n_{bd}\times n$ matrix. The disturbance vector d is n_{bd} dimensional. The control formulation is performed in two steps: (1) a prediction of the future state vector over a perdition horizon, and (2) a minimization problem to derive the control.

4.5.1 Prediction

To establish the prediction, we consider a time horizon $[k, k+\lambda]$, where k is the current real time instant and λ is a time horizon to be selected as a parameter. The notation $x(k+j|k)$ indicates the prediction of vector x for a future time instant $k+j$ within this interval. To add more generality in the presentation, time dependent matrices are considered, although they are usually constant in practice. Thus, the prediction starts with the following equation

$$x\left(k+1\left|k\right.\right)=A\left(k\left|k\right.\right)x\left(k\left|k\right.\right)+B\left(k\left|k\right.\right)u\left(k\left|k\right.\right)+B_{d}\left(k\left|k\right.\right)d\left(k\left|k\right.\right) \tag{4.59}$$

where $x(k|k)=x(k)$, $u(k|k)=u(k)$ and $d(k|k)=d(k)$.

Writing the same equation for the future instants:

$$\begin{aligned}x\left(k+2\left|k\right.\right)= \quad & A\left(k+1\left|k\right.\right)x\left(k+1\left|k\right.\right)+B\left(k+1\left|k\right.\right)u\left(k+1\left|k\right.\right)\\ & +B_{d}\left(k+1\left|k\right.\right)d\left(k+1\left|k\right.\right).\end{aligned} \tag{4.60}$$

Substituting Equation 4.59 to Equation 4.60:

$$\begin{aligned}x\left(k+2\left|k\right.\right)= \quad & A\left(k+1\left|k\right.\right)A\left(k\left|k\right.\right)x\left(k\left|k\right.\right)+A\left(k+1\left|k\right.\right)B\left(k\left|k\right.\right)u\left(k\left|k\right.\right)\\ & +B\left(k+1\left|k\right.\right)u\left(k+1\left|k\right.\right)+B_{d}\left(k+1\left|k\right.\right)d\left(k+1\left|k\right.\right)\\ & +A\left(k+1\left|k\right.\right)B_{d}\left(k\left|k\right.\right)d\left(k\left|k\right.\right).\end{aligned} \tag{4.61}$$

The same can be written for $x+3$:

$$\begin{aligned} x\left(k+3\left|k\right.\right) = \quad & = A\left(k+2\left|k\right.\right)A\left(k+1\left|k\right.\right)A\left(k\left|k\right.\right)x\left(k\left|k\right.\right) \\ & +A\left(k+2\left|k\right.\right)A\left(k+1\left|k\right.\right)B\left(k\left|k\right.\right)u\left(k\left|k\right.\right) \\ & +A\left(k+2\left|k\right.\right)A\left(k+1\left|k\right.\right)B_d\left(k\left|k\right.\right)d\left(k\left|k\right.\right) \\ & +A\left(k+2\left|k\right.\right)B\left(k+1\left|k\right.\right)u\left(k+1\left|k\right.\right) \\ & +A\left(k+2\left|k\right.\right)B_d\left(k+1\left|k\right.\right)d\left(k+1\left|k\right.\right) \\ & +B\left(k+2\left|k\right.\right)u\left(k+2\left|k\right.\right) \\ & +B_d\left(k+2\left|k\right.\right)d\left(k+2\left|k\right.\right). \end{aligned} \tag{4.62}$$

Reordering the equation:

$$\begin{aligned} x\left(k+3\left|k\right.\right) = \quad & A\left(k+2\left|k\right.\right)A\left(k+1\left|k\right.\right)A\left(k\left|k\right.\right)x\left(k\left|k\right.\right) \\ & +A\left(k+2\left|k\right.\right)A\left(k+1\left|k\right.\right)B\left(k\left|k\right.\right)u\left(k\left|k\right.\right) \\ & +A\left(k+2\left|k\right.\right)B\left(k+1\left|k\right.\right)u\left(k+1\left|k\right.\right) \\ & +B\left(k+2\left|k\right.\right)u\left(k+2\left|k\right.\right) \\ & A\left(k+2\left|k\right.\right)A\left(k+1\left|k\right.\right)B_d\left(k\left|k\right.\right)d\left(k\left|k\right.\right) \\ & +A\left(k+2\left|k\right.\right)B_d\left(k+1\left|k\right.\right)d\left(k+1\left|k\right.\right) \\ & +B_d\left(k+2\left|k\right.\right)d\left(k+2\left|k\right.\right). \end{aligned} \tag{4.63}$$

In the same way the state can be predicted at the end of the prediction horizon, in the instant k+λ:

$$\begin{aligned} x\left(k+\lambda\left|k\right.\right) = \quad & A\left(k+\lambda\left|k\right.\right)A\left(k+\lambda-1\left|k\right.\right)...A\left(k\left|k\right.\right)x\left(k\left|k\right.\right) \\ & +A\left(k+\lambda-1\left|k\right.\right)...A\left(k+1\left|k\right.\right)B\left(k\left|k\right.\right)u\left(k\left|k\right.\right) \\ & +A\left(k+\lambda-1\left|k\right.\right)...B\left(k+1\left|k\right.\right)u\left(k+1\left|k\right.\right) \\ & ...+B\left(k+\lambda-1\left|k\right.\right)u\left(k+n-1\left|k\right.\right) \\ & +A\left(k+\lambda-1\left|k\right.\right)...A\left(k+1\left|k\right.\right)B_d\left(k\left|k\right.\right)d\left(k\left|k\right.\right) \\ & +A\left(k+\lambda-1\left|k\right.\right)B_d\left(k+1\left|k\right.\right)d\left(k+1\left|k\right.\right) \\ & +B_d\left(k+\lambda-1\left|k\right.\right)d\left(k+\lambda-1\left|k\right.\right). \end{aligned} \tag{4.64}$$

All the single predictions can be lumped together in the following form:

$$\mathbf{X} = \mathbf{A}x_0 + \mathbf{BU} + \mathbf{B_d D} \tag{4.65}$$

where $x_0 = x(k|k)$. The vectors and matrices are detailed above and their size is summarized in Table 4.6.

$$\mathbf{X} = \begin{bmatrix} x\,(k+1\,|k\,) \\ x\,(k+2\,|k\,) \\ x\,(k+3\,|k\,) \\ \dots \\ \dots \\ x\,(k+\lambda\,|k\,) \end{bmatrix} \tag{4.66}$$

$$\mathbf{U} = \begin{bmatrix} u\,(k\,|k\,) \\ u\,(k+1\,|k\,) \\ u\,(k+2\,|k\,) \\ \dots \\ \dots \\ u\,(k+\lambda-1\,|k\,) \end{bmatrix}. \tag{4.67}$$

$$\mathbf{D} = \begin{bmatrix} d\,(k\,|k\,) \\ d\,(k+1\,|k\,) \\ d\,(k+2\,|k\,) \\ \dots \\ \dots \\ d\,(k+\lambda-1\,|k\,) \end{bmatrix} \tag{4.68}$$

$$\mathbf{A} = \begin{bmatrix} A\,(k\,|k\,) \\ A\,(k+1\,|k\,)\,A\,(k\,|k\,) \\ A\,(k+2\,|k\,)\,A\,(k+1\,|k\,)\,A\,(k\,|k\,) \\ \dots \\ \dots \\ A\,(k+\lambda-1\,|k\,)\,A\,(k+\lambda-2\,|k\,)\,...A\,(k\,|k\,) \end{bmatrix} \tag{4.69}$$

$$\mathbf{B} = \begin{bmatrix} B(k\,|k) & 0 & 0 & \\ A(k+1\,|k)\,B(k\,|k) & B(k+1\,|k) & 0 & \\ A(k+2\,|k)\,A(k+1\,|k)\,B(k\,|k) & A(k+2\,|k)\,B(k+1\,|k) & B(k+2\,|k) & \\ \cdots & & & \\ \cdots & & & \\ A(k+\lambda-1\,|k)\ldots A(k+1\,|k)\,B(k\,|k) & A(k+\lambda-1\,|k)\ldots A(k+2\,|k)\,B(k+1\,|k) & \ldots B(k+2\,|k) & B(k+n-1\,|k) \end{bmatrix} \tag{4.70}$$

$$\mathbf{B_d} = \begin{bmatrix} B_d(k\,|k) & 0 & 0 & \\ A(k+1\,|k)\,B_d(k\,|k) & B_d(k+1\,|k) & 0 & \\ A(k+2\,|k)\,A(k+1\,|k)\,B_d(k\,|k) & A(k+2\,|k)\,B_d(k+1\,|k) & B_d(k+2\,|k) & \\ \cdots & & & \\ \cdots & & & \\ A(k+\lambda-1\,|k)\ldots A(k+1\,|k)\,B_d(k\,|k) & A(k+n-1\,|k)\ldots A(k+2\,|k)\,B_d(k+1\,|k) & \ldots B_d(k+2\,|k) & B_d(k+\lambda-1\,|k) \end{bmatrix} \tag{4.71}$$

Matrix	Size
$\boldsymbol{A}$	λn × n
$\boldsymbol{X}$	λn × 1
$\boldsymbol{B}$	λn × mλ
$\boldsymbol{U}$	mλ × 1
$\boldsymbol{B_d}$	λn × n$_d\lambda$
$\boldsymbol{D}$	n$_d\lambda$ × 1
$\boldsymbol{Y}$	n$_q\lambda$ × 1
$\boldsymbol{C}$	n$_q\lambda$ × nλ

TABLE 4.6: Summary of the size of the matrices in MPC

4.5.2 Control

In the previous section (subsection 4.5.1) the prediction was described for all along the prediction horizon, and the state equation for this horizon was expressed in matrix form in Equation 4.65. The control vector $\mathbf{U}$ is the vector 4.67 containing $m\lambda$ unknowns: the values of the control vector u for each reach at every time $k|k, k+1|k, ..., k+\lambda-1|k$. The whole vector $\mathbf{U}$ is obtained though the minimization of the following cost function with constraints:

$$\min_{\mathbf{U}} J = \mathbf{X}^T\mathbf{P}\mathbf{X} + \mathbf{U}^T\mathbf{R}\mathbf{U} \tag{4.72}$$

$$x_{\min} < x < x_{\max}$$

$$u_{\min} < u < u_{\max}$$

where $\mathbf{P}$ $(\lambda n \times \lambda n)$ and $\mathbf{R}$ $(\lambda m \times \lambda m)$ are weighing matrices. More explicitly the cost function can be written in the form:

$$J = \sum_{j=1}^{\lambda} x\,(k+j\,|k)^T\, P_j x\,(k+j\,|k) + \sum_{j=0}^{\lambda-1} u\,(k+j\,|k)^T\, R_j u\,(k+j\,|k) \tag{4.73}$$

where $P_j^{n\times n}$ and $R_j^{m\times m}$ matrices such that:

$$P_j = \begin{bmatrix} p_1 & 0 & 0 & 0 \\ 0 & p_2 & 0 & 0 \\ 0 & 0 & ... & 0 \\ 0 & 0 & 0 & p_n \end{bmatrix}, \tag{4.74}$$

$$R_j = \begin{bmatrix} r_1 & 0 & 0 & 0 \\ 0 & r_2 & 0 & 0 \\ 0 & 0 & ... & 0 \\ 0 & 0 & 0 & r_m \end{bmatrix}. \tag{4.75}$$

In this work all weighing matrices P_j and R_j are chosen to be equal and diagonal, $P_j = P$ for $j = 1, 2, ..., \lambda$ and $R_j = R$ for $j = 0, 1, ..., \lambda - 1$. In other words, the weights of the optimization do not change during the prediction horizon. The matrix R contains the corresponding weights to the input, the matrix P contains the weights on the state. In this case the input is the change in discharge, therefore matrix R penalizes the changes in discharge. Matrix P penalizes the state. We chose to penalize the current water level error ($e_i(k)$), therefore only the diagonal elements of P corresponding to the current water levels in the state are non-zero. The weights on the water level error and change in discharge are normalized: the weights are the reciprocals of the squares of the maximum allowed values [van Overloop, 2006b]. For example: the maximum allowed water level error is chosen to be 3 cm: $eMAVE = 0.03$ m then the corresponding entry of the weighing matrix P can be expressed as:

$$p_1 = \frac{1}{eMAVE^2}. \tag{4.76}$$

The penalties for the change in input discharge (the entries of P) are expressed in the same way.

The general MPC controller was developed without using constraints. In case of the laboratory experiments it was not possible to carry out online optimization and for this reasons the constraints were not implemented. For the numerical simulation the optimization is carried out by quadratic programming, using the function "quadprog" from the computational software Matlab [Mathworks, 2008]. For the laboratory canal the problem is solved (without constraints) analytically [Martín Sánchez and Rodellar, 1996].

4.6 Test for the control algorithms

All tests were carried out by using the 1D hydrodynamic model: Simulation of Irrigation Canals (SIC). The test scenarios are established in order to test the

predictive controllers during this work. There are four test, shown in Table 4.7.

	Setpoint change	**Disturbance**
Known	Test 1	Test 2
Unknown	Test 3	Test 4

TABLE 4.7: Summary of the four tests

Both tests start and finish with the steady state conditions shown in Table 4.8. The discharge is approximately (Q_{appr}) is 60 l/s. The setpoint of the water level in the first pool (Sp1) is 85 cm, the setpoint for the water level in the second pool is 70 cm (Sp2) and in the third pool (Sp3) is 55 cm. The gate openings in order to achieve the given water levels in each pool are shown for Gate 1 (G1), Gate 2 (G2) and Gate 5 (G5). The hight of the final weir (W4) was set to 35 cm .

Q_{appr} (l/s)	**Sp1 (cm)**	**Sp2 (cm)**	**Sp3 (cm)**	**G1 (cm)**	**G3 (cm)**	**G5 (cm)**	**W4 (cm)**
60	85	70	55	7.4	12.6	11.8	35

TABLE 4.8: Steady state

4.6.1 Test 1: Setpoint changes

This test implies three consecutive setpoint changes. First at Pool 1, then after reaching the original situation, a setpoint change in Pool 2 and finally at Pool 3. All setpoint changes are 10 cm – this is more than the 10% change in water level in all the cases. Since the last pool ends with a weir, the last setpoint change implies change in the discharge. Table 4.9 shows the test step by step. The columns Sp show the actual setpoints, and the columns W and Q_w show the properties of the weirs. Q_w gives the weir discharge approximately, while W gives the height of the weir. In this test all offtakes are closed, the weir height is the maximum (90 cm). There is flow only over Weir 4, the flow leaving the canal.

Time (min)	$\mathbf{Q_{appr}}$ (l/s)	**Sp1** (cm)	**Sp2** (cm)	**Sp3** (cm)	**W1** (cm)	$\mathbf{Q_{w1}}$ (cm)	**W3** (cm)	$\mathbf{Q_{w3}}$ (cm)	**W4** (cm)
0	60	85	70	55	90	0	90	0	35
30	84	85	70	60	90	0	90	0	35
60	60	85	70	55	90	0	90	0	35
90	60	85	60	55	90	0	90	0	35
180	60	85	70	55	90	0	90	0	35
210	60	75	70	55	90	0	90	0	35
240	60	85	70	55	90	0	90	0	35
270	End								

TABLE 4.9: Setpoint change test

4.6.2 Test 2: Reaction to disturbances

The disturbance rejection was tested by using the lateral weirs (See Table 4.10). In this test two disturbances occur: after 30 min the weir at the downstream end of Pool 1 is open. At 60 min it is closed, hence the system has 30 min more to recover. After this time, at 90 min the weir at the end of the second reach is open for 30 min. The offtake is closed at 120 min and the test is finished at 150 min. In both cases the offtake discharge is 20 l/s. This is one third of the actual discharge, hence it is a considerable change.

Time (min)	$\mathbf{Q_{appr}}$ (l/s)	**Sp1** (cm)	**Sp2** (cm)	**Sp3** (cm)	**W1** (cm)	$\mathbf{Q_{w1}}$ (cm)	**W3** (cm)	$\mathbf{Q_{w3}}$ (cm)	**W4** (cm)
0	60	85	70	55	90	0	90	0	35
30	60	85	70	55	75	20	90	0	35
60	60	85	70	55	90	0	90	0	35
90	60	85	70	55	90	0	60	20	35
120	60	85	70	55	90	0	90	0	35
150	End								

TABLE 4.10: Disturbance test

4.7 Discussion of the results

4.7.1 Numerical results

For the numerical test the controllers were tuned in the following way: the penalty on the water level error change was set constant (3 cm) while the penalty on the change of the discharge was decreased until some oscillations appeared in the gate movement. The weight (penalty on the change of the discharge) was chosen to be small, but not too small, in order not to produce oscillations. In this way the fastest possible control action was achieved for each controller. The resulting tuning parameters, the Maximum Allowed Value Estimates (MAVE), are shown in Table 4.11.

	eMAVE (m)	**Setpoint duMAVE (m^3/s)**	**Disturbance duMAVE (m^3/s)**
MUS	0.03	0.001	0.001
HAY	0.03	0.001	0.001
ID	0.03	0.011	0.04
IDZ	0.03	0.011	0.02
IR	0.03	0.01	0.03

TABLE 4.11: Tuning parameters

The results of the numerical tests are discussed for the five models separately. The controllers developed based on each model are abbreviated, for example model predictive controller developed based on the MUS model: MPC-MUS.

The Muskingum model was able to control the first two canal pools, although with low performance. For the sepoint changes, the water level goes back slowly through overshoots to the original level after the change. The setpoint change in Pool 1 causes disturbances in Pool 2 and Pool 3 as well. It had problems to control the water level in Pool 3. It was not able to carry out the third setpoint change (Figure 4.13a), just like it was unable to keep the level at setpoint against known disturbances (Figure 4.13b). For the unknown disturbances the performance was even worst. Based on these results this controller is not suggested to be further tested experimentally.

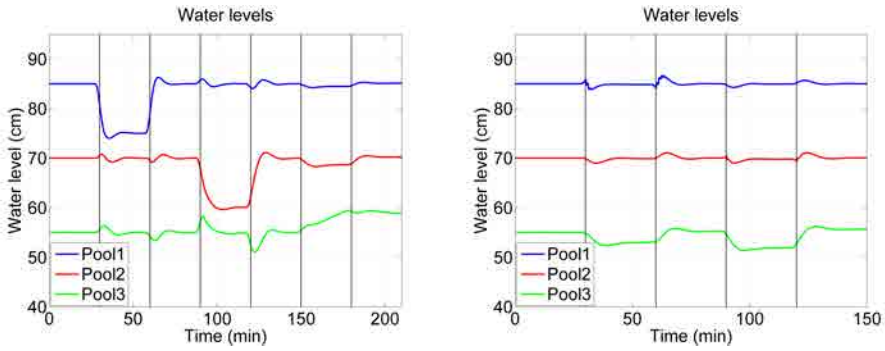

(a) Setpoint changes (b) Disturbances

FIGURE 4.13: MPC-MUS, Known changes

The first order model also had difficulties to control the third pool. In the setpoint change test Figure 4.14a, it was not able to follow the setpoint: the water level in the first pool followed the first change (30 min to 60 min), but it was not able to correct for the disturbances caused by the change of the water level of the third pool (150 min to 180 min). The same occurred in the case of the water level of Pool 2: it did not stay at setpoint when the change in the third pool occurred. The water level in Pool 3 during the first two changes oscillate around setpoint, while in the change of its setpoint it is not able to follow the trajectory.

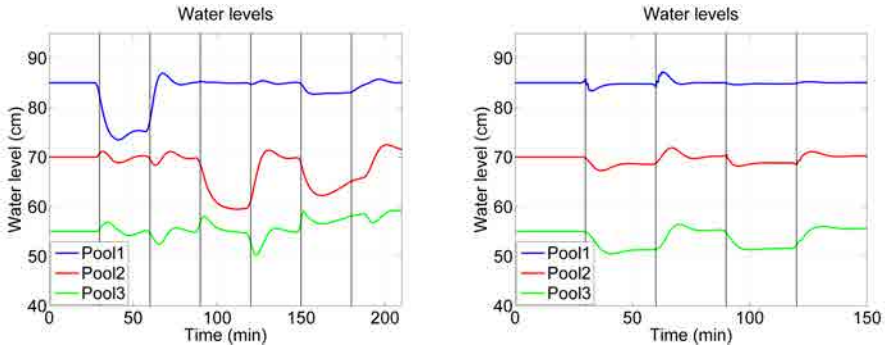

(a) Setpoint changes (b) Disturbances

FIGURE 4.14: MPC-HAY, Known changes

The results of the disturbance test (Figure 4.14b) are slightly better. The control of Pool 1 and Pool 2 is acceptable (Pool 2 shows some steady state

offset, the water levels are 1 cm under setpoint). However, the water level in Pool 3 was not controlled well: in case of both disturbances the water level was kept in a steady state 3 cm lower than the expected one.

For these reasons the performance of the unknown disturbance test is not analyzed here and the controller is not tested experimentally. The MPC-ID showed much better result than the two controllers presented above. The results of Test 1 and Test 2 (known setpoint changes and disturbances) for the MPC-ID are shown in Figure 4.15. The setpoint changes are shown in Figure 4.15a. The time of the setpoint change is marked with black vertical lines. In all three pools, the controller was able to carry out the setpoint change and lead the water level to the new setpoint. When a change occurs in one pool, only a slight perturbation can be observed in the water level of the other pools. The feedforward nature of the MPC can also be observed: the water level starts to change before the required setpoint change in order to minimize the error.

In Figure 4.15b the response to the disturbances is seen. The disturbance caused by the opening of the offtakes can hardly be seen, the controller rapidly answers. Even before the opening of the offtake, the water level is increased. Additional discharge is sent, in order to prepare for the opening of the offtake. This shows the feedforward property of MPC. There are small oscillations seen in the water level. These oscillations are not harmful, since they do not appear in the gate opening.

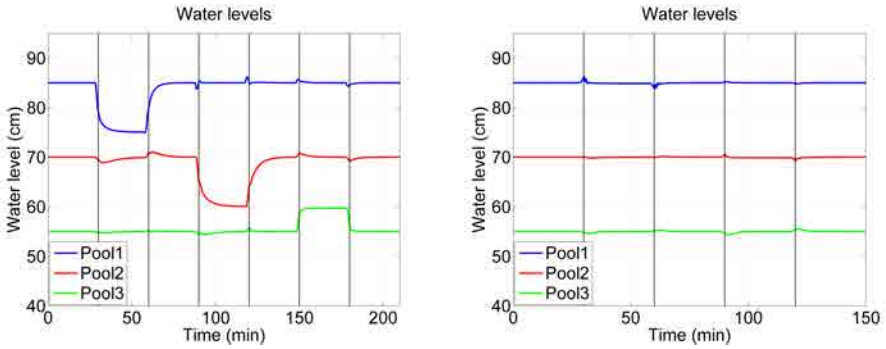

(a) Setpoint changes (b) Disturbances

FIGURE 4.15: MPC-ID, Known changes

The results of the unknown setpoint change and disturbance test are shown in Figure 4.16. In this case there was no feedforward action, the controller started to act when the disturbance was known. It acted just at the moment of the change of the setpoint or the physical arrival of the disturbance. In case of the setpoint change test, there is a small offset in the last pool due to the fact that this is a different discharge regime than the one for which the model was developed. This problem should be solved with a method that is able to eliminate the offset. This problem is addressed in Chapter 5. In case of the disturbance test this problem is clearly seen (Figure 4.16b): the water levels are not kept at setpoint after the disturbance. The water level in the first pool is about 3 cm under setpoint after opening the offtake. Also the water levels in Pool 2 and Pool 3 reach a steady state that is under setpoint. When the offtake is closed (60 min) all water levels return to the setpoint. When the offtake is opened again (90 min) the water levels reach a steady state under setpoint.

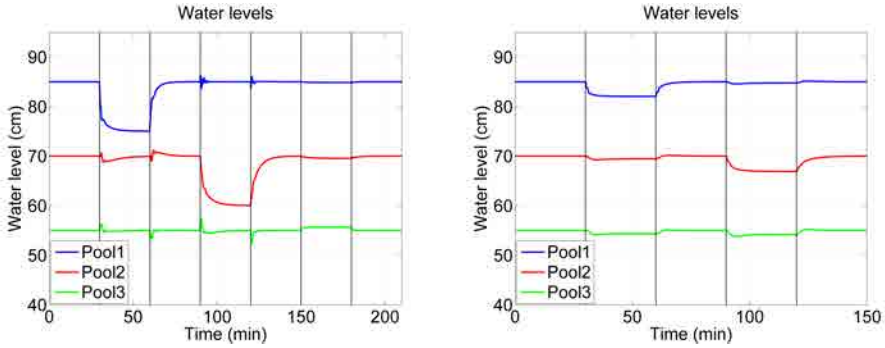

(a) Setpoint changes (b) Disturbances

FIGURE 4.16: MPC-ID, Unknown changes

The IDZ model shows similar results as the ID model. For the setpoint test (Figure 4.17a), the MPC-IDZ shows more strict action: the water levels follow more the shape of the step required by the setpoint signal. However, this fast action leads to a little bit more disturbances in the other water levels (for example some disturbances in the first water level after the setpoint change of the water level in Pool 2, at 90 min). A slight difference can be also seen in case of the disturbance test (Figure 4.17b). Here the IDZ model reacts slower due to the different tuning parameter (for the setpoint change they had the same tuning parameter, see Table 4.11). Since it was not possible to put as small weight as for the ID model to the input change due to the appearing

oscillations, the IDZ model acts slower for disturbance rejection. It is worth mentioning that the IDZ model, having similar structure to the ID model, could accept only a bigger weight on the input change, otherwise it showed oscillatory gate movements.

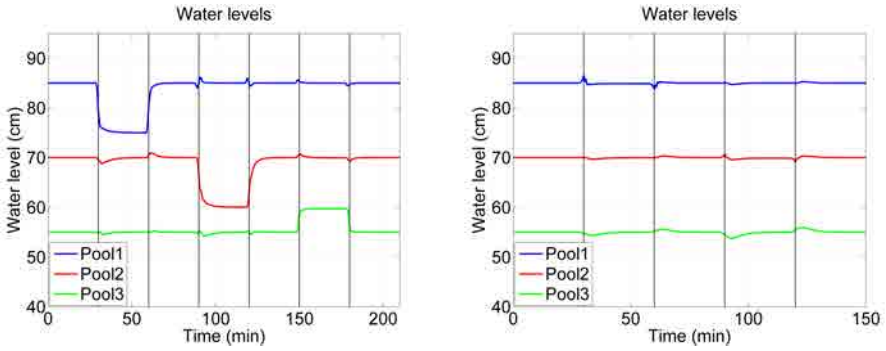

(a) Setpoint changes (b) Disturbances

FIGURE 4.17: MPC-IDZ, Known changes

The response of the MPC-IDZ to unknown changes is shown in Figure 4.18. Similar conclusions can be drawn as above: the response is similar to that of the MPC-ID. For setpoint changes (Figure 4.18a), it acts faster than the MPC-ID, while for disturbance rejection (Figure 4.18b) it acts slower than the MPC-ID. The MPC-IDZ produced steady state error during the setpoint change test of Pool 3 (150 min - 180 min) and during the disturbance test.

With this performance, the MPC-IDZ has similar performance in order of magnitude as the MPC-ID.

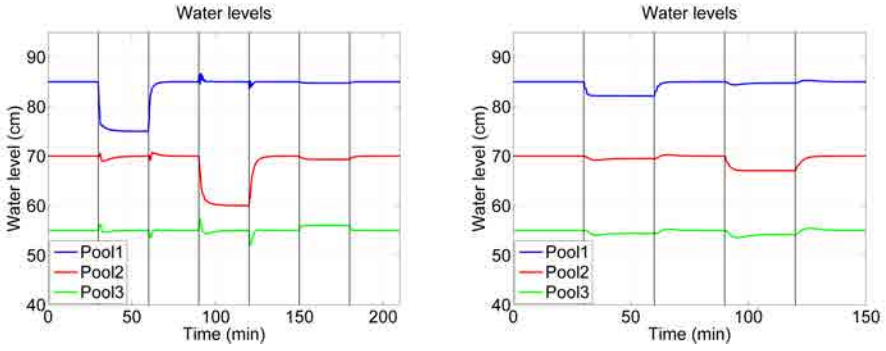

(a) Setpoint changes (b) Disturbances

FIGURE 4.18: MPC-IDZ, Unknown changes

The MPC-IR has similar results as the MPC-ID (Figure 4.19). For the setpoint change test (Figure 5.1b), it reacts slightly faster, it follows the step shape of the trajectory slightly better, while it causes less disturbances in the other levels. It can be seen, for example at 90 min, where the setpoint in Pool 2 changes, and only a small disturbance occurs in Pool 1. For the disturbance rejection test (Figure 4.19b) the results were similar that for the MPC-ID. The MPC-IR showed very good performance for both tests.

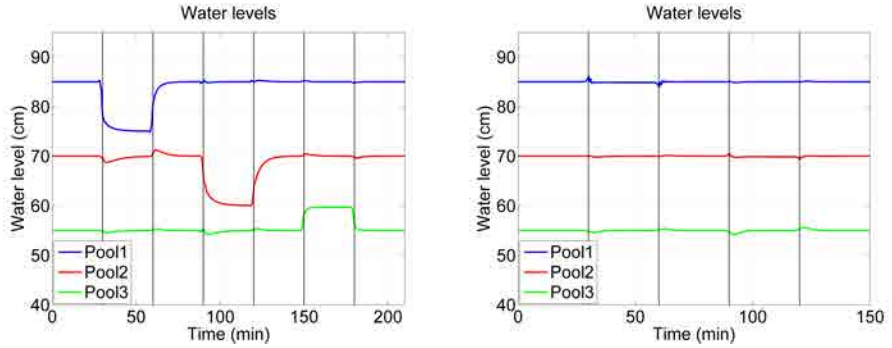

(a) Setpoint changes (b) Disturbances

FIGURE 4.19: MPC-IR, Known changes

The response of the MPC-IR to unknown changes is shown in Figure 4.20. For the unknown setpoint changes (Figure 5.2b), the MPC-IR showed slightly better results than the ID model, the water level produced less over and undershoots. However, still, it was not able to bring the water level of Pool 3 to setpoint (between 150 min and 180 min). The unknown disturbance test (Figure 4.20b) produced similar offsets, the MPC-IR was not able to keep the setpoint constant again unknown disturbances. Generally the MPC-IR model showed good performance, and the controller will be tested experimentally.

As a summary, the MPC-ID, MPC-IDZ and MPC-IR were able to maintain the water level at setpoint while setpoint changes and disturbances occurred. The MPC-ID and MPC-IR are tested experimentally in the following.

The MPC-MUS and MPC-HAY were not able to control the water level during these numerical test, therefore they are not tested further.

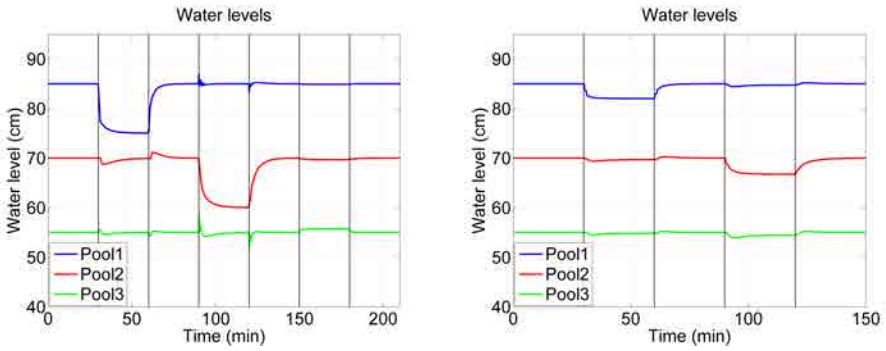

(a) Setpoint changes (b) Disturbances

FIGURE 4.20: MPC-IR, Unknown changes

4.7.2 Experimental analysis of controllers

MPC-ID and MPC-IR were tested experimentally in the laboratory canal UPC-PAC.

The experimental results of the setpoint change are shown in Figure 4.21. Both controllers were able to track the setpoint in the experiment. The IR model shows slower responses, which might be improved with different tuning values. In both cases, an offset can be observed in Pool 2 between 60 min and 90 min. In some cases (for example after the first setpoint change) the water level in the second reach was going slow or not reaching setpoint (Figures 4.21a and 4.21b). Also both models had difficulties with the third setpoint change, which involves about 40% change of discharge.

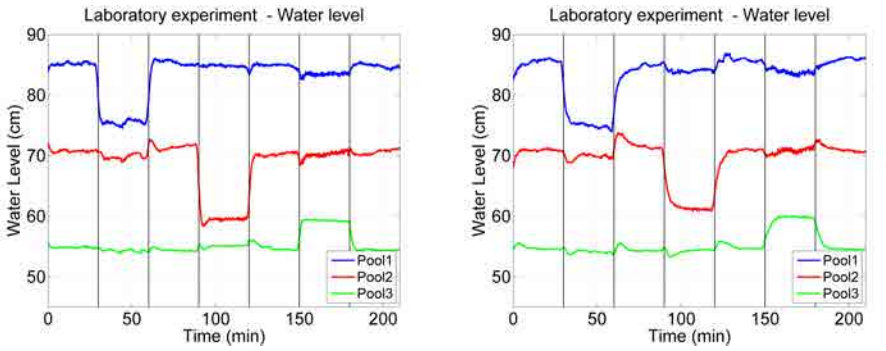

(a) MPC-ID (b) MPC-IR

FIGURE 4.21: Known setpoint changes, experiment

The gate movements belonging to the above experiments are shown in Figure 4.22. In both cases the gates reach a maximum opening: this opening was set in order to avoid free flow conditions. It can be noted when one change requires a gate opening, for example for the first setpoint change test at 30 min the required action is the opening of the gate in Pool 2 (in order to reduce the water level in Pool 1). However, in the beginning of the change also the gate in Pool 1 is acting, in order to facilitate the change. After a short time this gate moves back to its original position. The same behaviour can be seen for the second setpoint change. For the third setpoint change (between 150 min and 180 min), all the three gates are moving because this change involves changing to a new steady state with different discharge. The MPC-ID (Figure 4.22a) showed faster and some slight oscillations. In case of the MPC-IR Figure 4.22b the actions are slower, but also producing the same final gate opening.

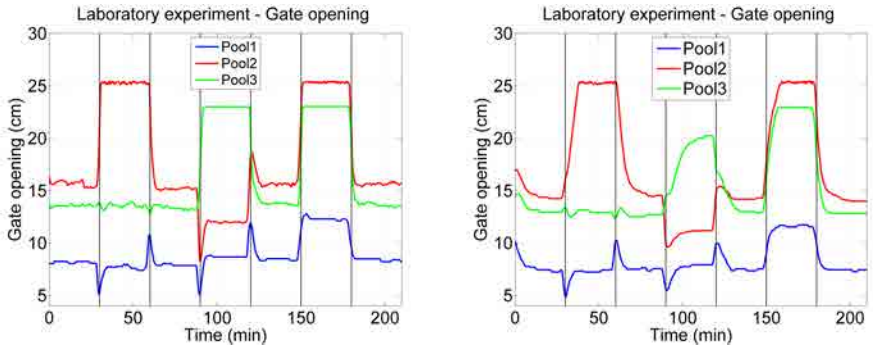

(a) MPC-ID (b) MPC-IR

FIGURE 4.22: Known setpoint changes, experiment, gate openings

In Figure 4.23 the results of the disturbance rejection test is shown. For the MPC-IR the initial values are due to the different steady state where the experiment was started. This initial part is not taken into account in the analysis. Both controllers were able to control the water level, within some offset. In general the MPC-IR produced less offset than the MPC-ID, for example between 90 min and 120 min. In general, the MPC-IR resulted in more smooth water levels, less under- and overshoots.

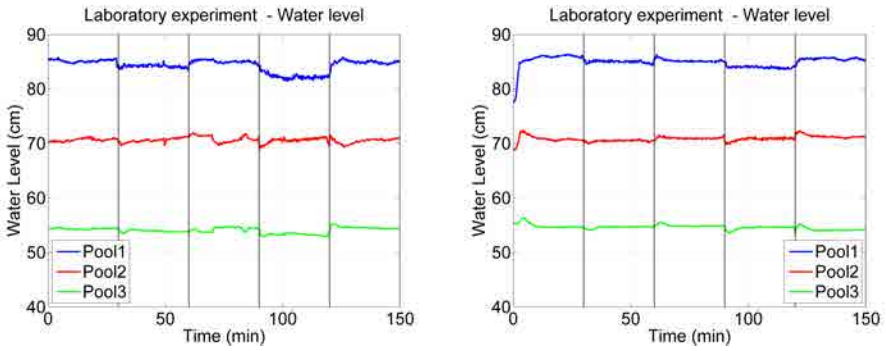

(a) MPC-ID (b) MPC-IR

FIGURE 4.23: MPC-ID, Known disturbances, experiment

The gate openings belonging to the experiment are shown in Figure 4.24. The same phenomena can be seen as before: for the MPC-IR the gate movements are smoother. Also the height of the final opening for the MPC-IR (Figure 4.24b) is different from that of the MPC-ID: the IR model was able to keep the water level closer to setpoint.

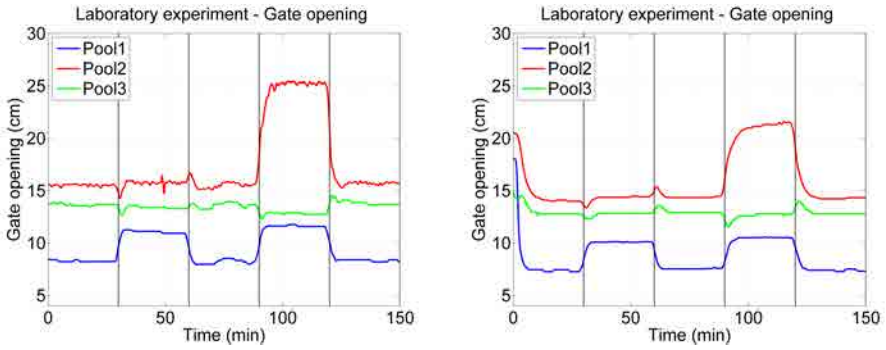

(a) MPC-ID (b) MPC-IR

FIGURE 4.24: MPC-ID, Known disturbances, experiment, gate openings

As a conclusion of the experiments, both MPC-ID and MPC-IR were able to control the UPC-PAC. The MPC-ID showed slightly better performance for the setpoint test, while the MPC-IR showed considerably better performance for the disturbance test.

4.8 Conclusion

In this chapter five simple linear models were compared for control design. They were compared first in the time and then in the frequency domain. Finally predictive controllers were developed based on those models. The controllers giving the best performance numerically were also tested experimentally in the UPC-PAC. From the analysis of the results the following conclusions were drawn:

- The response of the models is very different in time and frequency domain. For example some models that showed good response in the time domain had worse response in the frequency domain; and finally the controller based on those models had low performance. Therefore by examining the response only in the time domain might not be enough for controller development.
- The effect of the downstream structures is very important, they can change the behaviour of the canal pool. For most of the controllers it was more difficult to control Pool 3 that has a weir at the downstream end than the other pools that have sluice gates downstream.
- It was possible to develop controllers with acceptable performance based on any of the 5 white box models, only using the knowledge about the geometry of the canal.
- As general, the models developed for control showed much better performance for the UPC-PAC canal, while the traditional hydrological models had rather poor performance. The Muskingum and the first order model are also discarded due to their poor performance.
- In general the MPC-ID and MPC-IR model have better performance than the MPC-IDZ, and the MPC-MUS and the MPC-FO have much poorer performance, therefore they were discarded as possible models for the UPC-PAC.
- The reason while the IDZ model is not tested is that it is more complicated than the ID model and it did not give any additional benefit compared to the MPC-ID.

- The two controllers MPC-ID and MPC-IR were tested experimentally. Both of them were able to control the canal, both of them gate good performance.
- All models showed steady-state error during the unknown disturbance test. This problem can be solved by different controller development, and it is addressed in the following chapters.

In the remaining of this work the IR model is selected, as it was especially developed for canals prone to resonance, and its performance is in the same order of magnitude as the best performing model, the ID. The controllers are further developed in the following chapters: the development of the offset-free MPC is addressed in Chapter 5 and the possibility of using the gate openings as control action variables is discussed in Chapter 6.

Chapter 5

Offset-free model predictive control

5.1 Introduction

In Chapter 4 MPC was implemented numerically and experimentally with generally good performance, but in the case of some unknown disturbances steady-state offset was present. In this chapter the controller is further developed in order to be able to produce offset-free setpoint tracking. First the steady-state offset problem is described, then a new method is proposed to eliminate steady-state offset. The method is tested numerically and experimentally.

The offset problem appears when the gravity offtakes are open, or in case of the setpoint change in Pool 3. All these cases involve change in discharge over the weirs. In case of the offtakes, the offtake discharge depends on the water level in the pool where the weir is located. In case of the setpoint change in Pool 3, the water level in Pool 3 depends on the discharge (because of the presence of the downstream weir). For the MPC, the controller has to predict the future discharge and the future water levels. Since these two variables in the mentioned cases directly depend on each other, one of them should be estimated. This estimation introduces errors in the prediction and results in steady-state offset.

There are two main ways to eliminate offset: combine an integral action to the MPC controller [Martín Sánchez and Rodellar, 1996] and [Wang, 2009] or model the disturbances [Pannocchia and Rawlings, 2003]. Both methods are common and have successful implementations in the industry.

In the field of canal control, [Begovich et al., 2007c] uses the internal model principle: in order to reject constant disturbance it is necessary that an integrator appear in the closed loop system, that is an internal model of the constant disturbance. Therefore they propose an augmented model that contains a disturbance model based on integrators.

In this work, we propose a method that is based on adding integrator action to the model. The idea is to combine the MPC presented in Chapter 4 and the MPC controller developed in [Martín Sánchez and Rodellar, 1996]. The method is applied to irrigation canals in [Rodellar et al., 1993]. The controller referenced above has integral action, it is able to eliminate steady state offset, however, it does not have the property of treating known disturbances, in other words, acting to a known disturbance before it happens. It uses a constant control action during the whole prediction horizon. Therefore the idea is to combine the advantages of the two controllers: offset-free control and known disturbance handling. There is a certain trade-off between these two actions, in fact.

The new method is introduced in two steps. First the offset-free MPC presented in [Rodellar et al., 1993] is summarized in section 5.2 and then, in section 5.3, the combination of this with the existing controller developed in section 4.5 is shown.

5.2 Controller with integral action

In order to describe the method we assume a system with the following equation:

$$x(k+1) = Ax(k) + Bu(k) + B_{d2}d(k) \tag{5.1}$$

where x is a vector of $n \times 1$, A is a square matrix of $n \times n$, B is a matrix of $n \times m$, u is a vector of $m \times 1$, d is an $n_{bd} \times 1$ disturbance vector and B_{d2} is a matrix of dimension $n \times n_{bd}$; n is the dimension of the system, m is the number

of input variables and n_{bd} is the number of the disturbance states. Then the incremental state and the incremental input can be defined in the following way:

$$x_i(k) = x(k) - x(k-1) \tag{5.2}$$

and

$$u_i(k) = u(k) - u(k-1). \tag{5.3}$$

Using the above expressions for the incremental variables, Equation 5.1 can be expressed in incremental form:

$$x_i(k+1) = Ax_i(k) + Bu_i(k) + B_{d2}d_i(k). \tag{5.4}$$

The control law will be calculated during a given interval, with the length of λ, called the prediction horizon: [k,k+λ]. In this formulation of predictive control constant control input is assumed during all the prediction horizon, therefore the incremental input is zero after the first increment:

$$u_i(n) = 0 \quad \text{for} \quad k+1 < n < k+\lambda. \tag{5.5}$$

Using the incremental model, the state can be calculated for $k+2$:

$$x_i(k+2) = A^2x_i(k) + ABu_i(k) + AB_{d2}d_i(k) + Bu_i(k+1) + B_{d2}d_i(k+1). \tag{5.6}$$

Following the same method during all the prediction horizon, we can arrive to the equation of the state at the end of the prediction horizon:

$$\begin{aligned} x_i(k+\lambda) = \; & A^{\lambda}x_i(k) + A^{\lambda-1}Bu_i(k) + A^{\lambda-2}Bu_i(k+1) + \\ & A^{\lambda-1}B_{d2}d_i(k) + A^{\lambda-2}B_{d2}d_i(k+1) + ... \\ & + B_{d2}d_i(k+\lambda-1). \end{aligned} \tag{5.7}$$

Summing up the state during all the prediction horizon, the following expression can be obtained:

$$\begin{aligned} x(k+\lambda) = \; & (A_{sum}+I)x_0 + B_{sum}u(k) + ([-A_{sum}x(k-1) - B_{sum}u(k-1)]) \\ & + \mathbf{B_{d2m1}D_{2m1}} \end{aligned} \tag{5.8}$$

where A_{sum} is a $n \times n$ matrix, B_{sum} is a $n \times m$ matrix, B_{d2m1} is a $n_{bd2} \times \lambda n$ and D_{2m1} is a vector $n_{bd}\lambda \times 1$. Note that the resulting Equation 5.8 does not contain incremental variables any more. On the left hand side it has the state at the last instant of the prediction horizon, and on the right hand side it contains constant matrices multiplied by the initial state $x_0 = x(k)$, the initial input $u(k)$, and the state and the input one time instant before. The last term $\mathbf{B_{d2m1}D_{2m1}}$ contains the known disturbances during all the prediction horizon.The matrices multiplying the state and the input are the following, respectively:

$$\begin{aligned} A_{sum} = \quad & [A\,(k\,|k\,) + A\,(k+1\,|k\,)\,A\,(k\,|k\,) + ... \\ & +A\,(k+n-1\,|k\,)\,A\,(k+n-2\,|k\,)...A\,(k\,|k\,)] \end{aligned} \tag{5.9}$$

and

$$\begin{aligned} B_{sum} = \quad & [B\,(k\,|k\,)] + [A\,(k+1\,|k\,)\,B\,(k\,|k\,) + B\,(k+1\,|k\,)] + ... \\ & +[A\,(k+n-1\,|k\,)...A\,(k+1\,|k\,)\,B\,(k\,|k\,) + A\,(k+n-1\,|k\,)... \\ & +A\,(k+2\,|k\,)\,B\,(k+1\,|k\,) + ... + B\,(k+n-1\,|k\,)]. \end{aligned} \tag{5.10}$$

The last term contains a matrix multiplied by the the disturbance vector D_{2m1}, which contains the disturbances during all the prediction horizon:

$$\mathbf{D_{2m1}} = \begin{bmatrix} d\,(k) \\ d\,(k+1) \\ ... \\ d\,(k+\lambda-1) \end{bmatrix}. \tag{5.11}$$

The matrix multiplying the disturbances ($\mathbf{B_{d2m1}}$) is a result of the coefficients of $d(k)$, $d(k+1)$,...$d(k+\lambda)$ when equations 5.4, 5.6 ..., 5.7 are added up. The matrix is the following:

$$\mathbf{B_{d2m1}} = \begin{bmatrix} \mathbf{B_{d1m2c1}} & \mathbf{B_{d2m2c2}} & ... & \mathbf{B_{d1m2cn1}} & \mathbf{B_{d1m2cn}} \end{bmatrix} \tag{5.12}$$

where

$$\begin{aligned} \mathbf{B_{d2m1c1}} = \quad & B_d(k|k) + A(k+1|k)B_d(k|k) \\ & +A(k+\lambda-1|k)A(k+\lambda-2|k)...A(k+1|k)B_d(k|k) \end{aligned} \tag{5.13}$$

$$\begin{aligned}\mathbf{B_{d2m1cn2}} = \quad & B_d(k+1|k) + A(k+2|k)B_d(k+1|k) \\ & + A(k+3|k)A(k+2|k)B_d(k+1|k) \\ & + A(k+\lambda-1|k)A(k+\lambda-2|k)...A(k+2|k)B_d(k|k)\end{aligned} \tag{5.14}$$

$$\begin{aligned}\mathbf{B_{d2m1cn1}} = \quad & B_d(k+\lambda-2|k) \\ & + A(k+\lambda-2|k)B_d(k+\lambda-2|k)\end{aligned} \tag{5.15}$$

$$\mathbf{B_{d2m1cn}} = \quad B_d(k+\lambda-1|k). \tag{5.16}$$

The sum of the state equations during the prediction horizon, Equation 5.8, can be expressed in a more compact form:

$$\mathbf{X_{m1}} = \mathbf{A_{m1}}x_0 + \mathbf{B_{m1}}\mathbf{U_{m1}} + \mathbf{B_{dm1}}\mathbf{D_{m1}}. \tag{5.17}$$

The terms of Equation 5.17 are detailed one by one.

The term $\mathbf{X_{m1}}$ is the state at the end of the prediction horizon:

$$\mathbf{X_{m1}} = x\left(k+\lambda\right). \tag{5.18}$$

The input vector U_{m1} is the input vector of the system at the present instant k:

$$\mathbf{U_{m1}} = u(k). \tag{5.19}$$

The matrices multiplying the state and the input are the following, respectively,

$$\mathbf{A_{m1}} = A_{sum} + I \tag{5.20}$$

and

$$\mathbf{B_{m1}} = B_{sum} \tag{5.21}$$

where the matrices A_{sum} and B_{sum} are defined by equations 5.9 and 5.10. The third term accounts for the disturbances (Equation 5.11) and the additional

terms including $u(k-1)$ and $x(k-1)$ of Equation 5.8:

$$\mathbf{D_{m1}} = \begin{bmatrix} \mathbf{D_{1m1}} \\ \mathbf{D_{2m1}} \end{bmatrix}. \tag{5.22}$$

The matrix multiplying this term is composed of two parts, one multiplying the disturbances (Equation 5.12), and the other multiplying the other part of matrix $\mathbf{D_{m1}}$:

$$\mathbf{B_{dm1}} = \begin{bmatrix} \mathbf{B_{d1m1}} & \mathbf{B_{d2m1}} \end{bmatrix}. \tag{5.23}$$

The other parts of matrices $\mathbf{D_{m1}}$ (Equation 5.22) and $\mathbf{B_{dm1}}$ (Equation 5.23) are the following:

$$\mathbf{B_{d1m1}} = [-A_{sum}x\,(k-1) - B_{sum}u\,(k-1)] \tag{5.24}$$

and

$$\mathbf{D_{1m1}} = 1. \tag{5.25}$$

The size of all matrices used in this formulation are summarized in Table 5.1.

Matrix	Size
$\mathbf{A_{m1}}$	n × n
$\mathbf{X_{m1}}$	n × 1
$\mathbf{B_{m1}}$	n × m
$\mathbf{U_{m1}}$	m × 1
$\mathbf{B_{dm1}}$	n × ($n_d\lambda$+1)
$\mathbf{D_{m1}}$	$(\lambda n_d + 1) \times 1$
x_0	n × 1
$\mathbf{D_{1m1}}$	1 × 1
$\mathbf{B_{d1m1}}$	n × 1
$\mathbf{D_{2m1}}$	$\lambda n_d \times 1$
$\mathbf{B_{d2m1}}$	n × λn_d

TABLE 5.1: A summary of the size of the matrices

A predictive control objective associated to Equation 5.17 could be to find the control vector $\mathbf{U_{m1}}$ such that the state vector at $k+\lambda$, $x(k+\lambda|k) = \mathbf{X_{m1}}$ is as close as possible to the setpoint through the minimization of $x(k+\lambda|k)^T Q_\lambda x(k+\lambda|k)$. Our strategy in this chapter consists in combining this objective with the control objective presented in subsection 4.5.2 (Equation 4.73).

5.3 Offset-free predictive control

In this step we combine the controller objective presented above and the one presented in subsection 4.5.2, with the aim of combining the advantages of both strategies.

The basic method has good reaction to known disturbances, but it is not able to respond without offset to unknown disturbances. The simplified method reaches always offset free response, however, its response to known disturbances is not so good.

The control objective aims to find the control vector $\mathbf{U}$ that minimizes the following performance criterion:

$$\begin{aligned} J = \quad & J_1 + J_2 = \sum_{j=1}^{\lambda} x\left(k+j\,|k\right)^T P_j x\left(k+j\,|k\right) \\ & + \sum_{j=0}^{\lambda} \Delta u\left(k+j\,|k_i\right)^T R_j \Delta u\left(k+j\,|k\right) \\ & + x\left(k+\lambda|k\right)^T P_{m1} x\left(k+\lambda\,|k\right). \end{aligned} \tag{5.26}$$

This performance criterion has two parts belonging to each formulation. The first part has two terms and the second part has one term. By assigning appropriate weights to both objectives, it is straightforward to balance between the integral action and the anticipatory action of the MPC.

Now we give the details that allow to express the control objective in a matrix compact form as follows

$$\min_{\mathbf{U}} J = \mathbf{X_{m4}}^T \mathbf{P_{m4}} \mathbf{X_{m4}} + \mathbf{U}^T \mathbf{R} \mathbf{U}. \tag{5.27}$$

and

$$\mathbf{X_{m4}} = \mathbf{A_{m4}} x_0 + \mathbf{B_{m4}} \mathbf{U} + \mathbf{B_{dm4}} \mathbf{D_{m4}} \tag{5.28}$$

where the terms are explained one by one an their size is summarized in Table 5.2. Equation 5.28 comes from the combinations of Equation 4.65 (state equation used in subsection 4.5.1) and Equation 5.17. This, the state

vector X_{m4} is compiled in the form:

$$\mathbf{X_{m4}} = \begin{bmatrix} \mathbf{X} \\ \mathbf{X_{m1}} \end{bmatrix}. \tag{5.29}$$

where x contains the state all the time instants during the prediction horizon and $X_{m1} = x(k+\lambda)$. The vectors x_0 and $\mathbf{U}$ are the same as in Equation 4.65 of the original approach developed in Chapter 4. They are rewritten here for completeness:

$$x_0 = x(k|k) \tag{5.30}$$

and

$$\mathbf{U} = \begin{bmatrix} u\,(k\,|k\,) \\ u\,(k+1\,|k\,) \\ u\,(k+2\,|k\,) \\ \cdots \\ \cdots \\ u\,(k+\lambda-1\,|k\,) \end{bmatrix}. \tag{5.31}$$

The input vector $\mathbf{U}$ contains the input during all the prediction horizon. This is the same input vector used in the previously developed MPC, in subsection 4.5.1. However, the input vector used in this chapter, $\mathbf{U_{m1}}$ contains the input only for the present instant. Therefore the combination of the two state spaces is based on connecting both vectors as follows: the first part (of length m) of the input vector $\mathbf{U}$ (that is $u(k)$) will be made equal to the input vector $\mathbf{U_{m1}}$, as:

$$\mathbf{U_{m1}} = \mathbf{U(1:m)}. \tag{5.32}$$

The matrices are also combined suing the corresponding matrices from the two formulations:

$$\mathbf{A_{m4}} = \begin{bmatrix} \mathbf{A} \\ \mathbf{A_{m1}} \end{bmatrix}. \tag{5.33}$$

Matrix $\mathbf{B_{m4}}$ contains some zeros. The reason for this is the different length of the input vectors: while the input vector of the MPC from Chapter 4 is $m\lambda$ long, the input vector of the method presented here has an input vector $\mathbf{U_{m1}}$

with length of m. Therefore $\mathbf{B_{m4}}$ is the following:

$$\mathbf{B_{m4}} = \begin{bmatrix} \mathbf{B} & \\ \mathbf{B_{m1}} & 0_{n\times m(\lambda-1)} \end{bmatrix}. \tag{5.34}$$

The disturbance vector $\mathbf{D_{m4}}$ is the combination of the disturbance vector of the two methods:

$$\mathbf{D_{m4}} = \begin{bmatrix} \mathbf{D} \\ \mathbf{D_{m1}} \end{bmatrix}. \tag{5.35}$$

Just as the disturbance vector, the matrix multiplying the disturbance vector is the combination of the two matrices from the two methods:

$$\mathbf{B_{dm4}} = \begin{bmatrix} \mathbf{B_d} & \mathbf{B_{dm1}} \end{bmatrix}. \tag{5.36}$$

Matrix	Size
$\mathbf{A_{m4}}$	$(\lambda+1)\,n \times$ n
$\mathbf{X_{m4}}$	$(\lambda+1)n \times 1$
$\mathbf{B_{m4}}$	$(\lambda+1)\,n \times$ mλ
$\mathbf{U}$	m$\lambda \times 1$
$\mathbf{B_{dm4}}$	n $\times$ (n$_d\lambda$+1)
$\mathbf{D_{m4}}$	(n_d+1) $\times$ 1
$\mathbf{Y_{m4}}$	$(\lambda+1)\,n_q \times 1$
$\mathbf{C_{m4}}$	$(\lambda+1)\,n_q \times (\lambda+1)\,n$
x_0	n $\times$ 1

TABLE 5.2: A summary of the size of the matrices for the offset-free method

The weighing matrix $\mathbf{P_{m4}}$ has the following form:

$$\mathbf{P_{m4}} = \begin{bmatrix} \mathbf{P} & 0_{n\lambda\times n} \\ 0_{n\times n\lambda} & P_{m1} \end{bmatrix}. \tag{5.37}$$

This matrix is the combination of the weighing matrix $\mathbf{P}$ presented in subsection 4.5.2 in Equation 4.72 and the matrix P_{m1}.

P_{m1} is a diagonal matrix with size $n \times n$ that has zero entries for the states that we do not want to penalize and non-zero entries for the states that we wish to penalize. In this work these states are the water level errors. The penalty can

also be expressed as before:

$$P_{m1}(i,i) = \frac{1}{eiMAVE^2} \tag{5.38}$$

where $eiMAVE$ is a value to be tuned.

The weighing matrix $\mathbf{R}$ is the same presented in by subsection 4.5.2 Equation 4.75.

Finally, the control vector $\mathbf{U}$ is obtained through the solution of the problem defined by equations 5.27 and 5.28 at each sampling instant k.

5.3.1 Tuning parameters

There are three weights to tune: the penalty on the change of input, the penalty on the state during all the prediction horizon and the penalty on the sum of the states (this is from offset-free approach). This last penalty is the one that should be adjusted in order to influence the strength of the integrating action.

The general tuning parameters (eMAVE, duMAVE, λ) were the same as chosen previously for controller tuning, while the tuning parameter of the presented offset-free method has been chosen in the following way: the weight in the integration procedure was increased until offset-freecontrol was achieved in the given case. As a general guidance this value can be chosen equal to eMAVE and then the effects between the integration and the MPC can be balanced. The final tuning values of the offset free test eMAVE=0.03, duMAVE=0.009 for the disturbance and duMAVE=0.015 for the setpoint test. The eiMAVE=0.03 for both tests.

5.4 Results

5.4.1 Numerical results

The known and unknown setpoint change and disturbance tests defined and used in Chapter 4 have been carried out to assess the extended control approach.

The performance in case of known disturbances is very similar compared to the results without offset free control, while in case of the known setpoint changes the performance is slightly lower. The performances are compared in Figure 5.1.

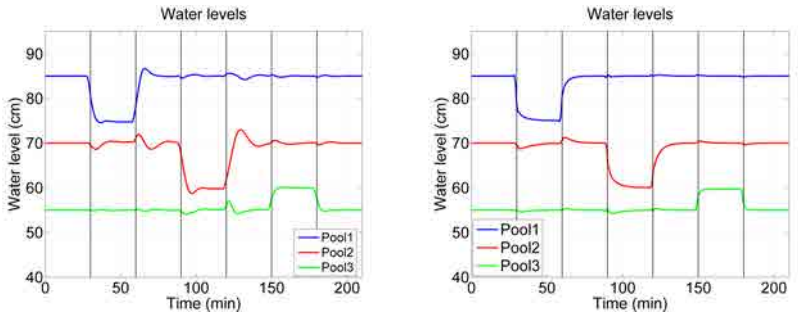

(a) Using offset-free method (b) Without using offset-free method

FIGURE 5.1: MPC-IR, Following the known setpoint changes with and without offser-free method

The over and undershoots of the integrating action can be seen. To some extent, it is a deterioration of the performance. However, it can also be taken into account that this test was designed to be more demanding than the usual changes during canal operation, and the controller was tuned to be able to tackle these changes as unknown disturbances. If the range of the possible unknown disturbances is smaller, more fine tuning is possible, the integration action can be reduced and hence the overshoot. Nevertheless, the controller was able to bring the water levels to the desired setpoint. The controller kept its feedforward property: the setpoint changes are starting before the actual change happened to allow a smoother reaction.

There is almost no performance deterioration in case of the disturbance rejection test. For this reason, this is not discussed here in detail. The reason for this difference of performance between the two types of tests can be the demanding nature of the setpoint test. For the unknown change, the results of the setpoint test are compared in Figure 5.2. Here the difference can clearly be seen between the two approaches. For the third change in the water level of the last pool without using offset-free control, the water level slightly changes, it does not go at all to the required setpoint. In the other pools it reaches the setpoint, however, more slowly. By using the offset-free control

method all setpoints are reached. The setpoints for Pool 1 and Pool 2 are reached faster, though they result in under and overshoot. This phenomenon is present not only in the target pool, but also in the other pools as disturbance propagates. Sometimes small oscillations are seen in the water level of the adjacent pools. These oscillations are not causing any harm, since they are present in the water level, but not in the gate movement. If they were present there, it would lead to wear and tear and they should have been avoided.

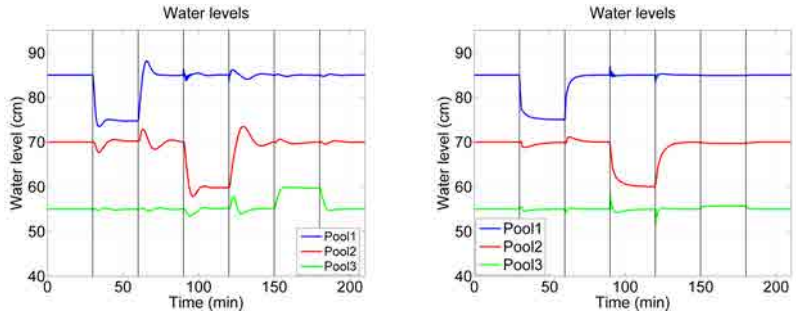

(a) Using offset-free method (b) Without using offset-free method

FIGURE 5.2: MPC-IR, Following the setpoint with and without offset-free method in case of unknown changes

The biggest improvement of the offset-free control can be observed for the disturbance test (Figure 5.3). In this case, without this improvement, the setpoints are not kept in any of the cases, the water level arrives to a steady state sometimes 3 cm off setpoint. This offset is completely eliminated by the proposed method. In less than 5 minutes the water level is back to setpoint. To the other pools only a slight change is propagated and it is corrected fast.

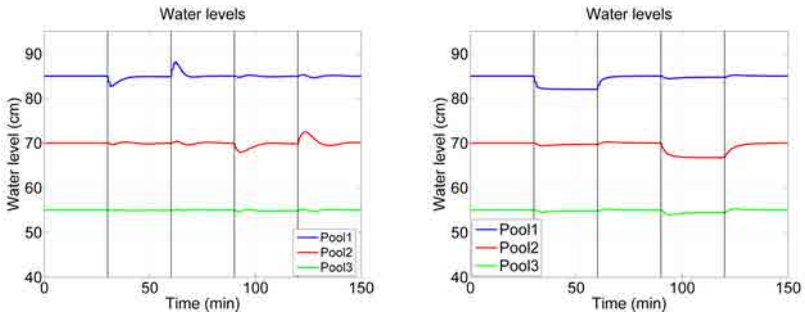

(a) Using offset-free method (b) Without using offset-free method

FIGURE 5.3: MPC-IR, Following the setpoint with and without offser-free method in case of unknown changes

In general, based on the simulation results, it can be said that the proposed offset-free method was able to follow the setpoint or keep it in the presence of unknown disturbances. For the setpoint change test, a trade-off had to be made between the disturbance canceling property and the introduced overshoot.

5.4.2 Experimental results

The controller was implemented and successfully tested on the UPC-PAC. The resulting water levels for known setpoint and disturbance test are shown in Figure 5.4. Just as in case of the numerical simulation, the controller was able to follow the known setpoint changes and disturbances. The feedforward property of MPC is observed: the water level starts to change before the actual change in demand happens.

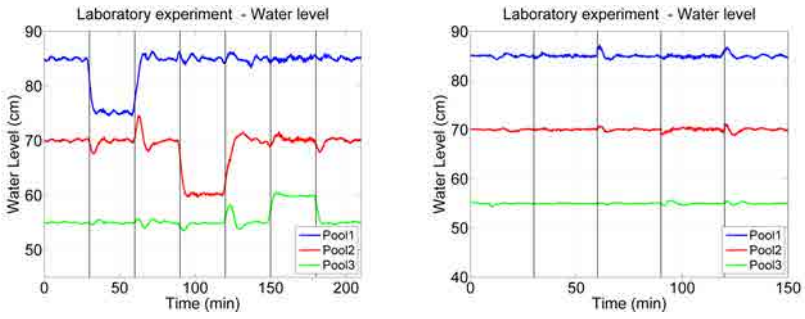

(a) Setpoint change (b) Disturbances

FIGURE 5.4: MPC-IR, Known changes, laboratory experiment

There is a difference compared to the IR test without and with offset free method: using offset free method some large amplitude oscillations in the water level Figure 5.4a. These oscillations are also present in the gate movement. These are caused by the minimum gate movement constraint: the gates cannot move less than 8 mm. Therefore the integral error is accumulating, until a certain point, and then a control action is taken. However this control action makes the water level move to the other side of the setpoint. Then the same phenomenon occurs: the error is accumulated until another action is taken. Hence the water level oscillates around the setpoint. This can be avoided by restricting the control action within a certain vicinity of the setpoint, however, in this case there would always be an offset.

The known disturbance test in Figure 5.4b shows very good results, only small deviations can be observed when the weirs are opened and closed. Note that when the offtake is opened in Pool 1 (30 min), the disturbance is not observed in Pool 2 and Pool 3.

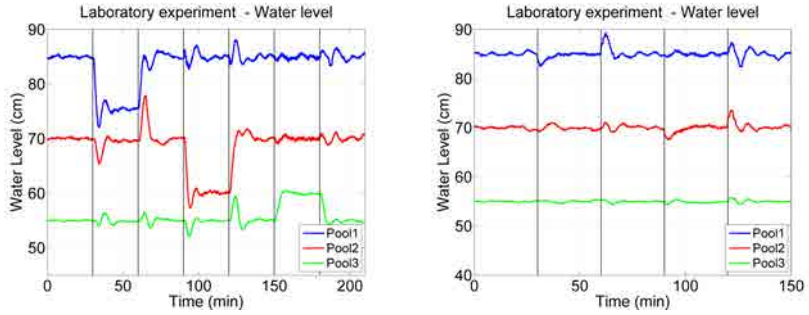

(a) Setpoint change (b) Disturbances

FIGURE 5.5: MPC-IR, Unknown changes, laboratory experiment

The controlled water levels in case of the unknown changes are shown in Figure 5.5. The same oscillations in the water level can be seen as commented above. In all cases the offset-free control is reached. As it was expected, the overshoot is bigger than for the known changes. The changes only start after the disturbance happens, as the controller knows it only from measurements. Especially for the disturbance test case in Figure 5.5b (as it is less demanding as commented before), the controller shows very good performance: the water levels are kept at setpoint, and they return to setpoint after the changes in about 5 minutes.

In general it was possible to implement the presented offset-free method and it was able to achieve offset free control in the laboratory canal.

5.4.3 Conclusion

- A new offset-free centralized model predictive controller has been proposed and tested numerically and experimentally on the UPC-PAC.
- The offset free control showed very good results with numerical simulations, the controller was able to react to unknown disturbances without steady-state offset.

  Similar results were obtained experimentally.
- Both in case on numerical and experimental results, there is significant under and overshoot. The reason for this might be the too small weight on the integral action. While this weight proved to be adequate for the numerical model, it might be too small for the experimental plant and lead to excessive gate movements.
- In case of experimental implementation, if there is a constraint on minimal gate movement, the implementation of the offset-free method will result in small oscillations in the gate movement around the desired position. This can be avoided by tuning or implementing restrictions on the gate movement.
- It can be concluded that, after some tuning and tests, this method can be used as a simple way to implement offset-free predictive controllers for irrigation canals.

Chapter 6

Gate opening as control action variable

6.1 Introduction

In Chapter 4 model predictive controllers were developed and in general they showed good performance, but in certain cases they produced steady state offset. An offset free method was introduced in Chapter 5 in order to solve this problem. In this chapter the improvement of the controllers is further investigated: the question of using gate opening as control action variable is addressed. First a short introduction about the use of different control action variables is presented. Then a model is introduced that combines the gate equation into the state space. This model was already published in [Horváth et al., 2013a] and tested using LQG controllers. Here, model predictive controllers based on this model are developed and tested numerically and experimentally.

6.2 The use of different control action variables

In this section the use of different control action variables in control of irrigation canals is discussed. An irrigation canal with several reaches is a complex system

where each reach can be considered as a subsystem. These subsystems are coupled through the discharge under the gates. A change in the opening of one gate affects the gate discharge of the gates upstream and downstream of the given gate and also the water levels upstream and downstream. This new change in the discharge can be considered as a perturbation that travels upstream and downstream. This effect is stronger in flat canals, with low friction, but it is present in any canal under subcritical flow.

In order to develop a distant downstream controller (either water level or discharge is controlled) the choice of the control action variables can be the upstream discharge or the upstream gate opening. Both of these approaches are commonly used in canal control [Malaterre, 2008]. The difference between the two approaches is discussed below, first in the case of decentralized control and second in the case of centralized control.

In case of decentralized control, several controllers are trying to control individual systems that are in fact heavily coupled. For two canal reaches connected by a gate, the gate opening can be the control action variable for the downstream reach, while it is an unknown perturbation for the upstream reach. Not taking this effects into account can lead to disturbance amplification and unacceptable controller performance [Schuurmans, 1997]. One way to decouple these variables is using discharge as control action variable instead of gate opening. In this case the gate opening is set by a slave controller, taking into account the water level upstream of the gate that belongs to the other canal pool. The slave controller can have several configurations, the most simple is the inverted gate equation. A better approximation is to take into account the change in water levels by using the method of characteristics [Malaterre and Baume, 1999] or the integrator delay zero model [Litrico et al., 2008]. In [Malaterre and Baume, 1999] different possible configurations with different canal geometries are compared by using PI controllers. The best results were achieved by using discharge as control action variable and a slave controller that takes into account the water level changes.

For centralized systems no such tests have been carried out. In case of using discharge as control variable the internal model has no direct information about the effect of the change of the water levels caused by the change of the opening. Moreover, the controller has no information about the change of discharge

further propagated upstream. This information enters the controller when they occur in nature (after a certain delay) and then the controller is able to react to that. Hence, these type of controllers as first action can only act on the gates that are the neighbours of the gate where the opening occurred. In order to develop a controller that is aware of this dynamics and can act faster, the dynamics of the gates should be considered and implemented [Malaterre, 2008]. The gates in this case need to be modelled. It is possible to be carried out by identification experiments or by linearizing the gate equation. In both cases the problem is if the model is used in a regime far from the one where it was linearized. This problem can be overcome by using multiple models [van Overloop et al., 2008].

6.3 Gate modelling

In order to combine the model of gates into the state space model of the system the classical gate equation is linearized. The equation is the following:

$$Q = C_d L B \sqrt{2g(H_1 - H_2)} \tag{6.1}$$

where Q is the discharge under the gate, C_d is the discharge coefficient, L is the gate opening, B is the width of the gate, g is the acceleration of gravity, H_1 is the water level upstream and H_2 is the water level downstream. The variables used for the gate modelling can be seen in Figure 6.1.

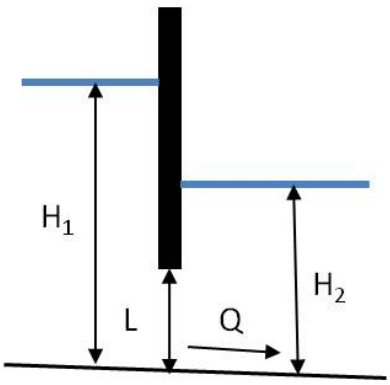

FIGURE 6.1: The variables for one sluice gate

Equation 6.1 can be linearized around the steady state Q_0, L_0, H_{10}, H_{20}. The deviations from this steady state are noted by q, l, h_1, h_2, and the relative discharge is:

$$q = k_l l + k_{h1} h_1 + k_{h2} h_2. \tag{6.2}$$

The gains of the linearized equation are calculated as the following:

$$k_{h1} = \frac{\partial Q}{\partial H_1} = \frac{1}{2} C_d L_0 B \sqrt{2g} \frac{1}{\sqrt{H_1 - H_2}} \tag{6.3}$$

$$k_{h2} = \frac{\partial Q}{\partial H_2} = -\frac{1}{2} C_d L_0 B \sqrt{2g} \frac{1}{\sqrt{H_1 - H_2}} \tag{6.4}$$

$$k_l = \frac{\partial Q}{\partial L} = C_d \sqrt{2g(H_1 - H2)}. \tag{6.5}$$

6.4 General state space equations

We are going to develop the state space model using a general model structure for a third order system. The state space can be constructed in the same manner to models with different order. First the expression of the downstream water level, then the expression of the upstream water level is described, then expressions for introducing a structure at the downstream end of the canal are given. Finally, combining the equations derived before for the gate discharge Equation 6.2 with the equations for the downstream and upstream water level, the state space is constructed.

The general model is expressed in the z-domain. Any model described in this domain can be used to follow this methodology. In our case, we used the IR model, whose discrete transfer functions (the parameters for p_{ia},..,p_{iu} for $i = 1, ..3$) are given in Appendix D.

Expression of the downstream water level

The water level at the downstream end of each canal pool is influenced by the discharge entering the reach (upstream discharge) and the discharge leaving

the reach: the downstream discharge and the discharge through the offtakes. An expression in the z-domain can be written as:

$$\begin{aligned} h_i = \quad & \frac{p_{ai}z^3 + p_{bi}z^2 + p_{ci}z + p_{di}}{z^3 + p_{ei}z^2 + p_{fi}z + p_{gi}} q_i z^{-1} \\ & - \frac{p_{hi}z^3 + p_{ii}^2 z + p_{ji}z + p_{ki}}{z^3 + p_{ei}z^2 + p_{fi}z + p_{gi}} q_{i+1} z^{-1} \\ & - \frac{p_{hi}z^3 + p_{ii}^2 z + p_{ji}z + p_{ki}}{z^3 + p_{ei}z^2 + p_{fi}z + p_g} q_{offi} z^{-1} \\ & + \frac{p_{li}}{z^3 + p_{ei}z^2 + p_{fi}z + p_{gi}} \end{aligned} \tag{6.6}$$

where q_i is the input discharge, q_{i+1} is the output discharge (input discharge of the next reach), q_{offi} is the offtake discharge, and the coefficients p_a, p_b, ..., p_l are specific of the chosen model. Equation 6.6 has four terms: the first term accounts for the influence of the upstream discharge (q_i) to the downstream water level (h_i), the second is the influence of the downstream discharge (q_{i+1}) to the downstream water level, the third term accounts for the influence of the offtake discharge (q_{offi}) to the downstream water level, and the last term contains constants depending on the model. The i subscript refers to the i$^{\text{th}}$ reach. Equation 6.6 can be expressed in the time domain:

$$\begin{aligned} h_i(k+3) = \quad & -p_{ei}h(k+2) - p_{fi}h_i(k+1) - p_{gi}h_i(k) \\ & + p_{ai}q_i(k+2) + p_{bi}q_i(k+1) + p_{ci}q_i(k) + p_{di}q_i(k-1) \\ & - p_{hi}q_{i+1}(k+2) - p_{ii}q_{i+1}(k+1) - p_{ji}q_{i+1}(k) - p_{ki}q_{i+1}(k-1) \\ & - p_{hi}q_{offi}(k+2) - p_{ii}q_{offi}(k+1) - p_{ji}q_{offi}(k) - p_{ki}q_{offi}(k-1) \\ & + p_{li}. \end{aligned} \tag{6.7}$$

The water level error is introduced as the difference between the actual value and the setpoint h_{isp}:

$$e_i(k) = h_i(k) - h_{isp}(k). \tag{6.8}$$

The water level error (Equation 6.8) can be combined to Equation 6.7:

$$\begin{aligned} e_i(k+1) = \quad & -p_{ei}e(k) - p_{fi}e_i(k-1) - p_{gi}e_i(k-2) \\ & -h_{isp}(k+1) - p_{ei}h_{spi}(k) - p_{fi}h_{spi}(k-1) - p_{gi}h_{spi}(k-2) \\ & +p_{ai}q_i(k) + p_{bi}q_i(k-1) + p_{ci}q_i(k-2) + p_{di}q_i(k-3) \\ & -p_{hi}q_{i+1}(k) - p_{ii}q_{i+1}(k-1) - p_{ji}q_{i+1}(k-2) - p_{ki}q_{i+1}(k-3) \\ & -p_{hi}q_{offi}(k) - p_{ii}q_{offi}(k-1) - p_{ji}q_{offi}(k-2) - p_{ki}q_{offi}(k-3) \\ & +p_{li}. \end{aligned} \tag{6.9}$$

Expressing the upstream water level

Assuming the same structure of model, the same denominator the following model can be written for the water level in the upstream end of the reach h_u:

$$\begin{aligned} h_{ui} = \quad & \frac{p_{mi}z^3 + p_{ni}z^2 + p_{oi}z + p_{pi}}{z^3 + p_{ei}z^2 + p_{fi}z + p_{gi}} q_i z^{-1} \\ & - \frac{p_{qi}z^3 + p_{ri}^2 z + p_{si}z + p_{ti}}{z^3 + p_{ei}z^2 + p_{fi}z + p_{gi}} q_{i+1} z^{-1} \\ & - \frac{p_{qi}z^3 + p_{ri}^2 z + p_{si}z + p_{ti}}{z^3 + p_{ei}z^2 + p_{fi}z + p_{g}} q_{offi} z^{-1} \\ & + \frac{p_{ui}}{z^3 + p_{ei}z^2 + p_{fi}z + p_{gi}} \end{aligned} \tag{6.10}$$

where h_{ui} is the upstream water level in the i$^{\text{th}}$ reach and p_m, p_n,...,p_u are model specific coefficients. This equation has also four terms just as the one expressing the downstream water level. The first term is the transfer function between the upstream discharge (q_i) and the upstream water level, the second term is the transfer function between the downstream discharge (q_{i+1}) and the upstream water level, the third one is the transfer function between the offtake discharge (q_{offi}) and the upstream water level and the fourth term is a model specific constant. Note that the denominator of the terms is the same as for the equation of the downstream water level (Equation 6.6). This equation can

be expressed in the time domain as well:

$$\begin{aligned} h_{ui}(k+1) = \quad & -p_{ei}h_{ui}(k) - p_{fi}h_{ui}(k-1) - p_{gi}h_{ui}(k-2) \\ & +p_{mi}q_i(k) + p_{ni}q_i(k-1) + p_{oi}q_i(k-2) + p_{pi}q_i(k-3) \\ & -p_{qi}q_{i+1}(k) - p_{ri}q_{i+1}(k-1) - p_{si}q_{i+1}(k-2) - p_{ti}q_{i+1}(k-3) \\ & -p_{qi}q_{offi}(k) - p_{ri}q_{offi}(k-1) - p_{si}q_{offi}(k-2) - p_{ti}q_{offi}(k-3) \\ & +p_{ui}. \end{aligned} \tag{6.11}$$

The gate discharge equation

The equation of is derived to a specific gate (Equation 6.2) can be generalized to any gate in the canal system. For example the discharge under the i$^{\text{th}}$ gate is:

$$q_i(k) = k_{li}l_i(k) + k_{h1i}h_{ui}(k) + k_{h2i}h_{i-1}(k). \tag{6.12}$$

Instead of the water level, the water level error (Equation 6.8) can be substituted into Equation 6.12:

$$q_i(k) = k_{li}l_i(k) + k_{h1i}h_{ui}(k) + k_{h2i}h_{spi-1}(k) + k_{h2i}e_{i-1}(k). \tag{6.13}$$

Gate opening

For the construction of the state space the incremental gate opening is used:

$$l_i(k+1) = l_i(k) + \Delta l_i(k). \tag{6.14}$$

Including the weir at the downstream end of the third reach

In order to construct a state space for a canal of multiple reaches, we have to pay special attention to the last reach. In case this reach, the outflow can be known (for example there is a pump) or there can be a hydraulic structure, as in case of the UPC-PAC. Then the linearized equation of the structure can be combined into the model. Now the UPC-PAC is taken as an example, and its third reach is modelled with a weir at the end. The inflow to this reach is q_3 and the outflow is q_4. The outflow depends on the weir, and it can be approximated using the linearized equation of the weir.

The linearized weir discharge equation is the following:

$$q_4(k) = k_{hw} h_3(k). \tag{6.15}$$

Just as before, Equation 6.15 can be combined with the expression of the water level error (Equation 6.8):

$$q_4(k) = k_{hw} e_3(k) + k_{hw} h_{3sp}(k). \tag{6.16}$$

Using the experssion of the output discharge Equation 6.16 and the general equation of the downstream water level error (Equation 6.9), the water level error in the third reach can be expressed as:

$$\begin{aligned} e_3(k+1) = \quad & -p_{e3}e(k) - p_{f3}e_i(k-1) - p_{g3}e_3(k-2) - h_{3sp}(k+1) \\ & -p_{e3}h_{sp3}(k) - p_{f3}h_{sp3}(k-1) - p_{g3}h_{sp3}(k-2) + p_{a3}q_3(k) \\ & +p_{b3}q_3(k-1) + p_{c3}q_3(k-2) + p_{d3}q_3(k-3) - p_{h3}k_{hw}e_3(k) \\ & -p_{h3}k_{hw}h_{3sp}(k) - p_{i3}k_{hw}e_3(k-1) - p_{i3}k_{hw}h_{3sp}(k-1) \\ & -p_{j3}k_{hw}e_3(k-2) - p_{j3}k_{hw}h_{3sp}(k-2) - p_{k3}k_{hw}e_3(k-3) \\ & -p_{k3}k_{hw}h_{3sp}(k-3) - p_{h3}q_{off3}(k) - p_{i3}q_{off3}(k-1) \\ & -p_{j3}q_{off3}(k-2) - p_{k3}q_{off3}(k-3) + p_{l3}. \end{aligned} \tag{6.17}$$

Combining the equation of the outflow of the last reach (Equation 6.16) with the general expression for the upstream water level in any reach (Equation 6.11), the upstream water level in the third reach can be written as:

$$\begin{aligned} h_{u3}(k+1) = \quad & -p_{e3}h(k) - p_{f3}h_i(k-1) - p_{g3}h_3(k-2) + p_{m3}q_3(k) \\ & +p_{n3}q_3(k-1) + p_{o3}q_3(k-2) + p_{p3}q_3(k-3) - p_{q3}k_{hw}e_3(k) \\ & -p_{q3}k_{hw}h_{3sp}(k) - p_{r3}k_{hw}e_3(k-1) - p_{r3}k_{hw}h_{3sp}(k-1) \\ & -p_{s3}k_{hw}e_3(k-2) - p_{s3}k_{hw}h_{3sp}(k-2) - p_{t3}k_{hw}e_3(k-3) \\ & -p_{t3}k_{hw}h_{3sp}(k-3) - p_{q3}q_{off3}(k) - p_{r3}q_{off3}(k-1) \\ & -p_{s3}q_{off3}(k-2) - p_{t3}q_{off3}(k-3) + p_{u3}. \end{aligned} \tag{6.18}$$

The whole state space model

The state space model is constructed using the equation for downstream water level error (Equation 6.9), the upstream water level (Equation 6.11), the gate

discharge (Equation 6.13) and the gate opening (Equation 6.14). For the last reach, the specific equations are used for the downstream water level error (Equation 6.17) and the upstream water level (Equation 6.18). A final state space model can be developed in the form of

$$x(k+1) = Ax(k) + Bu(k) + B_d d(k). \tag{6.19}$$

The state ($x(k)$) contains the upstream water levels in the present and past instants, the dowsntream water levels in the present and past instants, the gate discharges in the present and past instants and the gate openings. The final matrices for the state space are shown in Appendix E.

6.5 State space model including gate opening as control action variable

In order to show the difference between the two approaches (1) discharge as control action variable (2) gate equation is combined to the state space, some step tests are carried out. To emphasize the differences, and 8-pool test canal is chosen.

The capability of state space model containing the gate equations can be seen if the model with gate openings as control action variables (Figure 6.2) is compared to the model where the control action variable is the discharge (Figure 6.3). These figures show the step responses of the ID models built for a canal with 8 reaches in order to see the disturbance propagation.

Using model with discharge as control action variable, a change in the discharge in a canal pool causes a change only in the water level of the same pool and in the water level of the canal pool upstream to it. It does not cause any change in the discharges in the state, since all the discharges are influenced only by the control variable (that is the change in discharge). A simple test is carried out using a canal of 8 canal pools, with constant water level in the reservoir upstream and constant downstream discharge. The canal pools are connected by sluice gates. In Figure 6.2, the discharge under Gate 5 is increased and the response of the water levels can be seen. The water level in the Pool 4 (directly upstream of Gate 5) decreases and the water level in Pool 5 (directly

downstream of the Gate 5) increases. The disturbance does not travel upstream or downstream in the canal according to this model, while in reality it does as it can be seen from the numerical solution of the Saint-Venant equations.

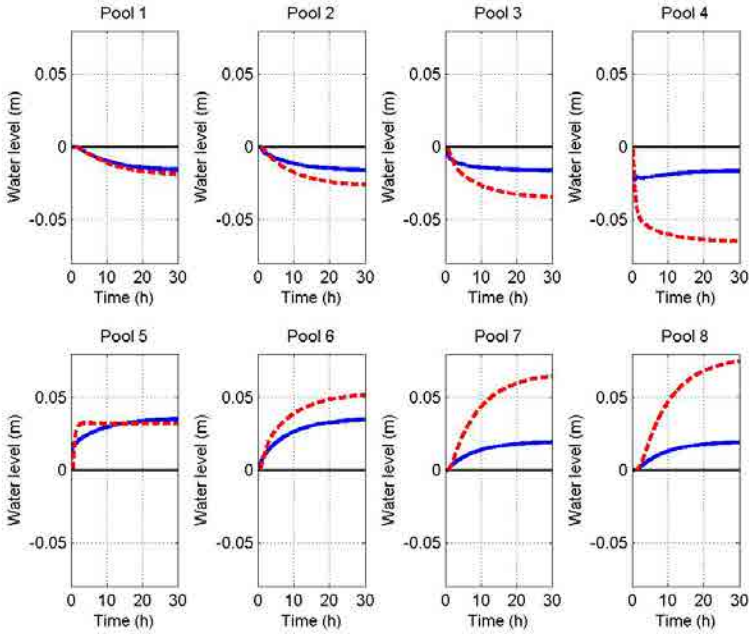

FIGURE 6.2: Model including gate openings

In case of the model with gate opening as control action variable, the linearized gate equation is used. The water levels (h_{ui}) upstream in the pool are not measured variables. Instead, they are related to discharges by using models as the one in Equation 6.11. The result of this combined model is that the effects of water level changes can propagate downstream and upstream as well. This can be seen in Figure 6.2. The advantage of this model is twofold: (1) it is able to reproduce the disturbances travelling in both directions, and (2) it does not need measured data about the water levels at the upstream end of the canal pools.

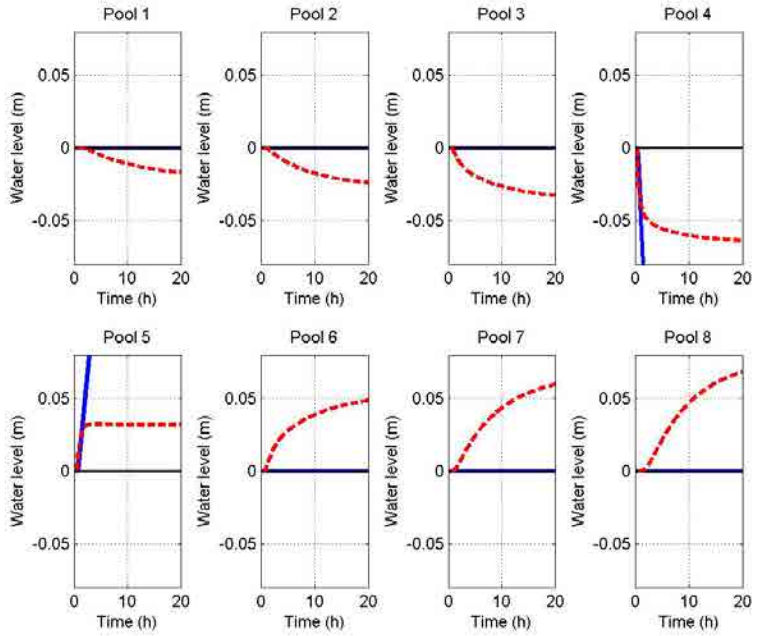

FIGURE 6.3: Model with discharge as control action variable

6.6 Control implementation

Using the general state space development, the parameters of any third or less order model in the z domain can be fit. The expressions to be discretized for the IR model are derived in Appendix B. These equations were discretized by zero order hold using the Matlab software, the numerical results are presented in Appendix D. The state space was build as it was explained above, and the controller was developed in the same way as explained in section 4.5.

This controller was tuned in the same manner as the ones presented before: as a first estimate the normalized errors are used and then the penalty is decreased on the control action in order to make the controller faster until its limits. The controllers are separately tuned for the setpoint change and the disturbance rejection given that both tests are very demanding but of different nature. After the controller was tuned for the simple MPC case, the offset-free part is connected and it is tuned in the same manner: the penalty on the integral

error is increased until offset-free control is achieved (for the unknown changes tests). The resulting tuning parameters are shown in Table 6.1.

	eMAVE	**duMAVE**	**eiMAVE**
Setpoint change	0.03	0.015	-
Disturbances	0.03	0.009	-
Offset free setpoint	0.03	0.015	0.4
Offset free disturbances	0.03	0.009	0.09

TABLE 6.1: The tuning parameters for the MPC with gate openig as control action variables

6.7 Results of the controller using gate opening as control action variable

6.7.1 Numerical results

The results of the known and unknown setpoint change test are shown in Figure 6.4. For the known setpoint change test (Figure 6.4a) the results using gate opening as control action variable are not as good as the ones using discharge. While the water levels in each pool follow the setpoint very well, there is considerable disturbance present in the other pools. This effect might be balanced by different tuning: by using less sharp control action less disturbance would be propagated.

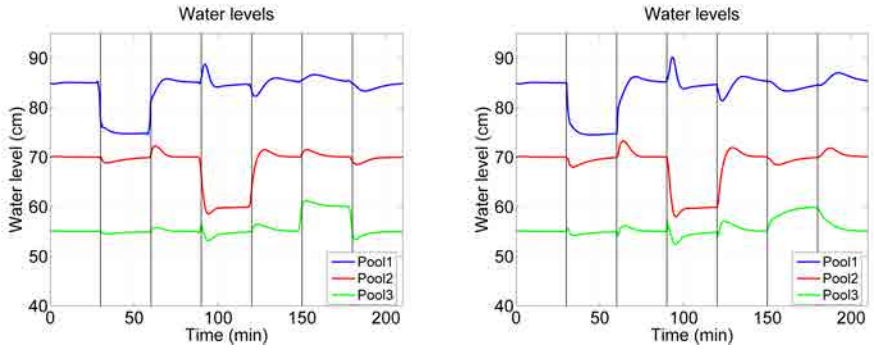

(a) Known setpoint change (b) Unknown setpoint change

FIGURE 6.4: Setpoint test, known and unknown changes, gate opening as control action variable

For the unknown setpoint change test (Figure 6.4b) the main difference is that even the last setpoint is reached (in case of using discharge as control action variable this setpoint was not reached). The water level arrives to this setpoint slowly, this might be improved.

For the disturbances case the result (Figure 6.5) for the known disturbances (Figure 6.5a) is similar to the case with discharge as control variable. However, for the unknown disturbance case the results are considerably better (Figure 6.5b): there is no steady state offset, the controller slowly brings back to water levels to the setpoint. This is due to the better modeling of the system. This is a big advantage compared to the case when the discharge is the control variable.

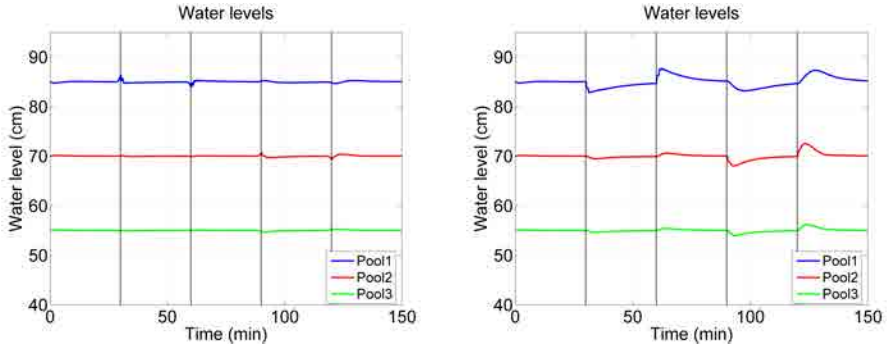

(a) Known disturbances (b) Unknown disturbances

FIGURE 6.5: Known and unknown disturbances, gate opening as control action variable

Though this method did not produce steady state offset, in case of unknown disturbances it acted slow. This action can be improved by combining it with the offset-free method introduced in Chapter 5. The results of the combination of the gate opening as control action variable and the offset free method is shown in Figure 6.6.

For the setpoint change test (Figure 6.6a) all the water levels followed the setpoint without offset. Some over- and undershoot is produced by the integration e.g. after 90 min at Pool 1. All the changes are very fast and sharp, the new setpoints are reached within 8 mintues. For the unknown disturbances (Figure 6.6b) the controller kept the water levels at setpoint without excessive over- and undershoots. All levels are returned to setpoint in

5 minutes. Only few disturbance is propagated, e.g. at 30 min when Weir 1 is open in the first pool almost no disturbance is noticed in the water levels of Pool 2 and Pool 3.

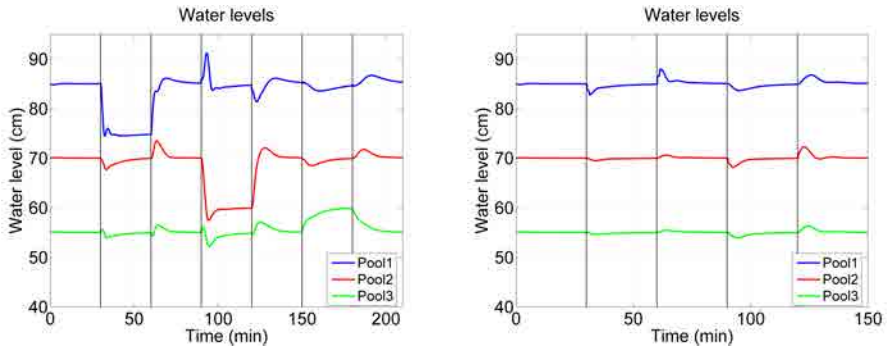

(a) Setpoint change test (b) Disturbance test

FIGURE 6.6: Unknown setpoint change and disturbance test, gate opening as control action variable with offset-free method, simulation

6.7.2 Experimental results

The results of the known setpoint change and disturbance test using gate opening as control action variable are shown in Figure 6.7.

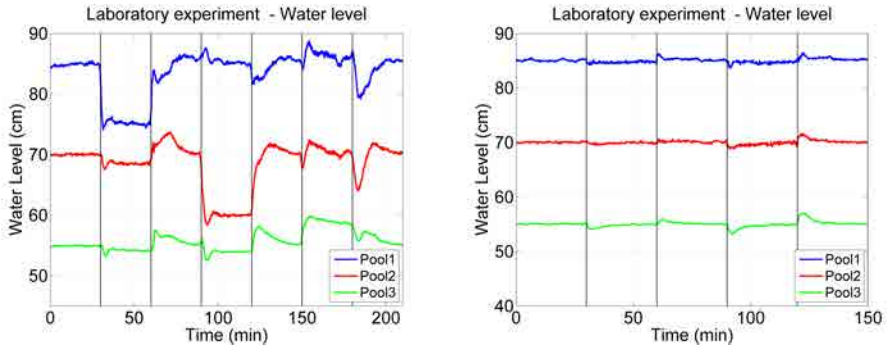

(a) Setpoint change test (b) Disturbance test

FIGURE 6.7: Known setpoint change and disturbance test, gate opening as control action variable, laboratory experiment

The setpoint change (Figure 6.7a) test shows that the controller was able to keep the water levels at setpoint. However, the perturbations introduced to the

other levels are much more significant compared to the case when discharge is used as control action variable. On the other hand, the known disturbance test (Figure 6.7b) shows very good results, better than the test when discharge is the control action variable.

The results of the unknown setpoint change and disturbance test using gate opening as control action variable are shown in Figure 6.8. Both test resulted in zero steady-state offset that is a big advantage compared to the case when discharge was used as control action variable. For the setpoint change test several oscillations and overshoots can be seen (Figure 6.8a). On the other hand, the last setpoint change is almost reached, unlike in the case when the discharge was used as control action variable. The unknown disturbance test (Figure 6.8b) shows no unnecessary oscillations. The water levels go smoothly to the setpoint. This is a considerable improvement compared to having the discharge as control action variable. The lowest performance of the setpoint change test might be possible to improve with better tuning.

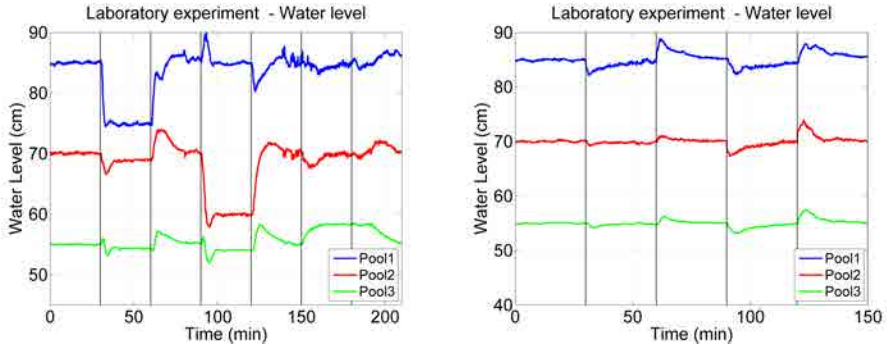

(a) Setpoint change test (b) Disturbance test

FIGURE 6.8: Unknown setpoint change and disturbance test, gate opening as control action variable, laboratory experiment

The results of the known setpoint change and disturbance test using gate opening as control action variable combined with the offset-free method are shown in Figure 6.9. For the setpoint change test (Figure 6.9a) the offset free method eliminated the big oscillations. For the disturbance test (Figure 6.9b), the offset-free method made the action faster, the water levels go back faster to setpoint. In general terms the offset-fee method improved slightly the response for known disturbances.

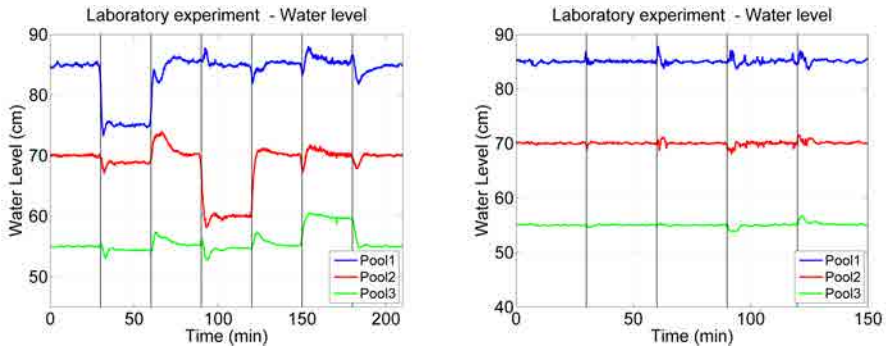

(a) Setpoint change test (b) Disturbance test

FIGURE 6.9: Known setpoint change and disturbance test, gate opening as control action variable with offset-free method, laboratory experiment

The results of the unknown setpoint change and disturbance test using gate opening as control action variable combined with the offset-free method are shown in Figure 6.10.

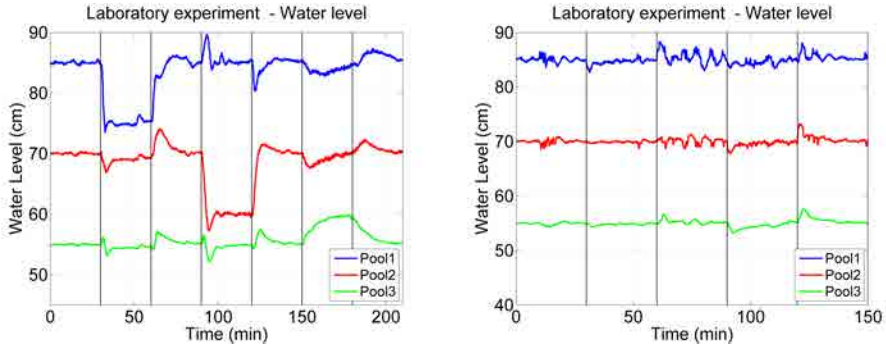

(a) Setpoint change test (b) Disturbance test

FIGURE 6.10: Unknown setpoint change and disturbance test, gate opening as control action variable with offset-free method, laboratory experiment

In this case the setpoint change test (Figure 6.10a) slightly improved compared to the case without the use of the offset-free method: especially the oscillation in the level of Pool 1 at 150 min - this time is the change of the water level in Pool 3, that is equal to the change in discharge. For the unknown disturbance test (Figure 6.10a) the water levels were kept at setpoint or oscillation around setpoint. This might be the result of the too strong integral action and the minimum gate movement restriction: due to this restriction the gate cannot

move exactly to the position that would maintain the desired water level, there is always a small steady-state error. The integral action tries to eliminate this error, therefore it makes the gate move. However, as the minimal movement is restricted, the gate moves to a new position that also generates a steady-state error, but in the other direction. Then the process starts again. This phenomena is seen as oscillations in the water level around the setpoint.

6.8 Conclusion

- The choice of the control action variables has been investigated for centralized MPC: discharge or gate opening both by numerical and laboratory tests. In case of known disturbances, the use of gate opening as control variable performed slightly worst (it acted slower) than the discharge as control action variable, however, for the unknown disturbance case using the gate opening and a more complex model seemed to achieve offset-free control.
- The simulation results showed that it is possible to design and implement controllers using the gate opening as control action variable and the linearized gate equations.
- In case of using the gate opening as control action variable a model of the system of canal reaches can be built without using the measurement of the water level at the upstream end of the canal pools (directly downstream of the gate). While for a slave controller both water levels upstream and downstream of the gate should be known, by using this more complex model the water level directly downstream of the gate is approximated, the controller does not use the information of that water level measurement.
- By using the gate opening as control action variable, constraints can be added to the gate opening or to its change. This can be useful to maintain submerged conditions or in case of gate speed restrictions.
- An additional advantage of using the gate opening as control action variable is that the controller produced no steady state offset even in cases when unknown changes occurred in the discharge without offset-free methods.

- If the gate equation is combined to the state space, the water level measured downstream of the gate is not used for the calculations. This makes this control method more robust for sensor failures.
- Having the gate opening as control action variable in MPC, it is easier to apply constraints to the gate opening itself (maximum gate opening) and to the change of gate opening (gate speed).
- All these conclusions about the choice of control action variables are valid for the studied canal type: short and flat canals.

Chapter 7

Conclusion

7.1 Conclusions on the flow measurement

The weirs and the gates of the UPC-PAC are used for discharge measurement in the same way as in real irrigation canals. These structures had to be calibrated and tested. Both the weirs and the gates are possible to be used for discharge measurement. In the UPC-PAC the error of the measurement is less than 4%. These structures proved to be a simple and trustful way of discharge measurement.

7.2 Conclusions of the hydraulic behaviour of the UPC-PAC

The UPC-PAC belongs to the category of short and flat canals that are prone to resonance. This is a common canal type and the knowledge of its behaviour is crucial for control purposes. These pools exhibit resonance behaviour that should be taken into account for controller design. In order to model or filter out the resonance waves, the most important characteristics of them should be known: the resonance frequency and the resonance peak. These parameters can be obtained by calculation or by identification using direct measurements on the canal. The difference between the calculated and the identified values is

not so considerable for the resonance frequency, however, it is remarkable for the resonance peak, especially in presence of hydraulic structures. Always it is advisable to do some simple identification experiments like ATV.

Pool 1 and Pool 2 showed considerable resonance phenomenon, while Pool 3 due to the presence of the downstream weir showed very slight resonance.

7.3 Conclusion on modelling and control of resonant canal pools

Different internal models for model predictive control have been compared in the time and frequency domain, and finally MPC controllers were developed using these models and their performance were compared and analyzed. From the compared models two were hydrological models (Muskingum and Hayami) and three were developed especially for controller design: Integrator Delay, Integrator Delay Zero and Integrator Resonance. The best performing controllers (MPC-ID and MPC-IR) were also tested experimentally on the UPC-PAC. Both controllers showed very good performance for known changes, however for unknown disturbances in some cases (for example an offtake is opened) they produced steady state offset.

Using the canal properties obtained in Chapter 3, a simple model especially developed for resonant canal pools, Integrator Resonance has been applied to the laboratory canal. This was the first time that this model has been applied experimentally for control purposes. The result is that this model in some aspects showed better performance than the ID model. It was shown in the introduction that in extreme resonant situations there is a clear need to use the IR model. In this work the capacities of this model were tested. In all tests the IR model performed well.

After all test, the IR model was chosen to model the first two canal pools of the UPC-PAC, while Pool 3 (since it shows few resonance) was modelled with the ID model.

7.4 Conclusions on offset free control in irrigation canals

The modelling of weir-type offtakes raises a difficulty when using MPC. As the weir determines the relationship between the offtake discharge and the water level, it is complicated to predict the offake discharge in the future instants (as it depends on the water level, that is also predicted). If the offtake discharge is not well approximated during the prediction horizon, it will cause a model mismatch and this can result in a steady-state offset.

A new method to eliminate steady-state offset is introduced. This method is based on the combination of an integrating method to the original. The basic idea is to extend the objective function of MPC with the objective function of an other method, that has no steady state offset, but it is not able to take into account known changes. The method shows satisfactory results. Although in introduces small overshoots, it completely eliminates the offset while keeping the feedforward property of MPC.

Another way was shown to reduce or almost eliminate steady-state offset: combining the gate equation into the state space model (Chapter 6). For short and flat canal pools, if the gate equation is combined into the state space of the internal model, the use of offset-free methods might be possible to be avoided.

7.5 Conclusion on the choice of control variables

The use of different control action variables has been investigated: discharge or gate opening. For both approaches a general state space formulation is given. The methods are compared numerically and experimentally. The use of gate opening as control action variable provided several advantages.

First, as it was seen in the experimental results, an MPC based on the model with gate openings shows no steady state offset, even against unknown discharge changes in case of the UPC-PAC even with no offset-free method.

While the model containing the discharge as control action variable resulted in steady state offset, the model containing the gate openings was able to eliminate it. The reason is that this model is more complex, it also includes the relation between the downstream discharge and the upstream water level - this processes that are not included in the simple model.

It should be mentioned that this method combined with the offset-free method (presented in Chapter 5) produced some unnecessary over- and undershoots that might be avoided with better tuning at each canal.

Another advantage as that the controller does not use the information about the water levels directly downstream of the gates, they are calculated internally by the model. This can result in less measurement error is introduced and it is more robust for sensor failures.

Finally, by using the gate openings as control action variable, it is straightforward to put constraints to the gate opening or to the change of the gate opening (e.g. due to the speed of the motors).

These observations are valid for the type of canal pools investigated: short and flat pools.

7.6 General conclusion

In this work the model predictive control of resonance sensitive canals has been analyzed. A recently proposed model, the Integrator Resonance model [van Overloop et al., 2010b] is implemented and successfully tested on the experimental laboratory facility, the UPC-PAC. Tests with scheduled and unscheduled changes have been carried out. The performance for the unscheduled changes were not satisfactory, due to the steady-state offset. A new type of integrator method in order to achieve offset-free control was proposed. The question of the choice of the control action variables was also investigated. It resulted that using the gate opening as control action variable has several advantages, including the decrease of the steady state offset.

7.7 Future work

The integrator resonance model showed good performance in the experimental canal UPC-PAC. It should be further tested on the field. The proposed offset-free method should also be tested, it can be compared to the existing methods in terms of stability and robustness. The choice of control action variables can also be further investigated, different methods of including the gates to the controller can be implemented. Including the gate modelling into the centralized controller can considerably improve the control system. As to the UPC-PAC, the experimental platform proved to be a good means of testing control algorithms. Several challenges have been faced that are not always present in simulation, for example uncertainties in the measurements. An experimental irrigation canal is an important step of testing control algorithms between the numerical test and the real implementation.

Bibliography

[Afzalimehr and Bagheri, 2009] Afzalimehr, H. and Bagheri, S. (2009). Discharge coefficient of sharp-crested weirs using potential flow. *Journal of Hydraulic Research*, 47(6):820–823.

[Aguilar et al., 2011] Aguilar, J., Langarita, P., Linares, L., Galvis, E., Horváth, K., Rodellar, J., and Gómez, M. (2011). Control automático de niveles en un canal experimental dividido en tres tramos. In *JIA 2011. II Jornadas del Ingeniería del agua, Modelos numéricos en dinámica fluvial*.

[Aguilar et al., 2009] Aguilar, J., Langarita, P., Linares, L., and Rodellar, J. (2009). Automatic control of flows and levels in an irrigation canal. *IEEE Transactions on Industry Applications*, 45(6):2198 –2208.

[Aguilar et al., 2012] Aguilar, J. V., Langarita, P., Linares, L., Rodellar, J., and Soler, J. (2012). Adaptive predictive expert control of levels in large canals for irrigation water distribution. *International Journal of Adaptive Control and Signal Processing*, 10(26):945–960.

[Akouz et al., 1998] Akouz, K., Malaterre, P.-O., Dahhou, B., and Roux, G. (1998). Predictive control applied to ASCE canal 2. In *Systems, Man, and Cybernetics, 1998. 1998 IEEE International Conference on*, pages 3920–3924.

[Alvarez Brotons, 2004] Alvarez Brotons, X. (2004). Control predictivo de canales de riego utilizando modelos de prediccin de tipo Muskingum (primer orden) y de tipo Hayami (segundo orden). Master's thesis, Technical University of Catalonia, Spain.

[Bagheri and Heidarpour, 2010] Bagheri, S. and Heidarpour, M. (2010). Application of free vortex theory to estimating discharge coefficient for sharp-crested weirs. *Biosystems Engineering*, 105(3):423–427.

[Bagheri and Heidarpour, 2012] Bagheri, S. and Heidarpour, M. (2012). Characteristics of Flow over Rectangular Sharp-Crested Side Weirs. *Journal of Irrigation and Drainage Engineering*, 138(6):541–547.

[Bastin et al., 2009] Bastin, G., Bayen, A., D'Apice, C., Litrico, X., and Piccoli, B. (2009). Open problems and research perspectives for irrigation channels. *Networks and heterogeneous media*, 4(2):I–V.

[Bautista and Clemmens, 2005] Bautista, E. and Clemmens, A. (2005). Volume compensation method for routing irrigation canal demand changes. *Journal of Irrigation and Drainage Engineering*, 131(6):494–503.

[Begovich et al., 2007a] Begovich, O., Felipe, J. C., and Ruiz, V. M. (2007a). Real-time implementation of a decentralized control for an open irrigation canal prototype. *Asian Journal of Control*, 9(2):170–179.

[Begovich et al., 2007b] Begovich, O., Martinez, E., and Ruiz, V. M. (2007b). Decentralized fuzzy gain scheduling control for an open irrigation canal prototype. In *ICEEE 4th International Conference on Electrical & Electronics Engineering*, pages 14–17.

[Begovich et al., 2007c] Begovich, O., Ruiz, V. M., Besançon, G., Aldana, C., and Georges, D. (2007c). Predictive control with constraints of a multi-pool irrigation canal prototype. *Latin American applied research*, 37(3):177–185.

[Begovich et al., 2005] Begovich, O., Ruiz, V. M., Georges, D., and Besançon, G. (2005). Real-time application of a fuzzy gain scheduling control scheme to a multi-pool open irrigation canal prototype. *Journal of intelligent fuzzy systems*, 16(3):189–199.

[Benayache et al., 2008] Benayache, Z., Besançon, G., and Georges, D. (2008). A new nonlinear control methodology for irrigation canals based on a delayed input model. In *Preprints of the 17th IFAC World Congress*, pages 2544–2549, Seoul, Korea.

[Bolea et al., 2009] Bolea, Y., Martinez-Gonzalez, R., Grau, A., and Martinez-Garcia, H. (2009). An LPV fractional model for canal control. In *System Identification*, volume 15, pages 1786–1791.

[Brunner, 1995] Brunner, G. W. (1995). *HEC-RAS River Analysis System: User's Manual*. US Army Corps of Engineers, Hydrologic Engineering Center.

[Buyalski et al., 1991] Buyalski, C., Ehler, D. G., Falvey, H. T., and Rogersand D. C.and Serfozo, E. A. (1991). Canal systems automation manual. Technical Report Volume 1, U.S. Department of the Interior. Bureau of Reclamation.

[Cardona et al., 1997] Cardona, J., Gómez, M., and Rodellar, J. (1997). A decentralized adaptive predictive controller for irrigation canals. In *Proceedings of the International Workshop on the Regulation of Irrigation Canals: State of the Art of Research and Applications, RIC97*, volume 1, pages 215–219, Marrakech, Morocco.

[Charbonnaud et al., 2011] Charbonnaud, P., Carrillo, F., and Duviella, E. (2011). A supervised robust predictive multi-controller for large operating conditions of an open-channel system. In *World Congress*, volume 18, pages 4620–4625.

[Chentouf, 2001] Chentouf, B. (2001). Robust regulation of a river reach governed by Hayami model. In *Proceedings of the 40th IEEE conference on decision and control*, pages 4962–4967.

[Chevereau and Schwartz-Benezeth, 1987] Chevereau, G. and Schwartz-Benezeth, S. (1987). Bival system for downstream control. In *Planning, operation, rehabilitation, and automation of irrigation water delivery systems: proceedings of a symposium*, volume 1-5, pages 155–163, New York, N.Y. (USA). American Society of Civil Engineers.

[Chow, 1959] Chow, V. T. (1959). *Open-channel hydraulics*. McGraw-Hill Book Co. Inc, New York.

[Chung and Kang, 2006] Chung, W. and Kang, Y. (2006). Classifying river waves by the Saint Venant equations decoupled in the laplacian frequency domain. *Journal of Hydraulic Engineering*, 132(7):666–680.

[Clemmens, 2003] Clemmens, A. (2003). Calibration of submerged radial gates. *Journal of Hydraulic Engineering*, 129(9):680–687.

[Clemmens et al., 1998] Clemmens, A., Kacerek, T., Grawitz, B., and Schuurmans, W. (1998). Test cases for canal control algorithms. *Journal of Irrigation and Drainage Engineering*, 124(1):23–30.

[Clemmens et al., 2012] Clemmens, A., Litrico, X., van Overloop, P.-J., and Strand, R. (2012). Estimating canal pool resonance with auto tune variation. *Journal of Irrigation and Drainage Engineering*, 138(1):9–15.

[Compas et al., 1997] Compas, J. M., Pages, J., and Sau, J. (1997). Predictive control based coordinated operation of a series of river developments. In *Proceedings of the International Workshop on the Regulation of Irrigation Canals: State of the Art of Research and Applications, RIC97*, pages 239–248, Marrakech, Morocco.

[Cunge, 1969] Cunge, J. A. (1969). On the subject of a flood propagation computation method (Muskingum method). *Journal of Hydraulic Research*, 7(2):205–230.

[Cunge et al., 1980] Cunge, J. A., Holly, F. M., and Verwey, A. (1980). *Practical aspects of computational river hydraulics*. Pitman Publishing Limited, London.

[Damas et al., 2000] Damas, M., Salmeron, M., and Ortega, J. (2000). ANNs and GAs for predictive control of water supply networks. In *Neural Networks, 2000. IJCNN 2000, Proceedings of the IEEE-INNS-ENNS International Joint Conference on*, volume 4, pages 365 –370 vol.4.

[Dias et al., 1988] Dias, F., Keller, J. B., and Vanden-Broeck, J.-M. (1988). Flows over rectangular weirs. *Physics of Fluids*, 31(8):2071–2076.

[Doan et al., 2009] Doan, D., Keviczky, T., Negenborn, R. R., and De Schutter, B. (2009). An iterative approach for distributed model predictive control of irrigation canals. In *Book of abstracts of the 14th Belgian-French-German Conference on Optimization*, pages 70–70. Citeseer.

[Dodge, 2001] Dodge, R. (2001). *Water Measurement Manual: A Guide to Effective Water Measurement Practices for Better Water Management*. U.S. Government Printing Office.

[Durdu, 2004] Durdu, O. F. (2004). Optimal control of irrigation canals using recurrent dynamic neural network (RDNN). In *Critical Transitions in Water and Environmental Resources Management*, pages 1–12.

[Duviella et al., 2010] Duviella, E., Puig, V., Charbonnaud, P., Escobet, T., Carrillo, F., and Quevedo, J. (2010). Supervised gain-scheduling multimodel

versus linear parameter varying internal model control of open-channel systems for large operating conditions. *Journal of Irrigation and Drainage Engineering*, 136(8):543–552.

[Ferro, 2000] Ferro, V. (2000). Simultaneous flow over and under a gate. *Journal of Irrigation and Drainage Engineering*, 126(3):190–193.

[Foss et al., 1989] Foss, B., Haug, J., Alne, J., and Aam, S. (1989). User experience with on-line predictive river flow regulation. *IEEE Transactions on Power Systems*, 4(3):1089 –1094.

[Galvis et al., 2011] Galvis, E., Horváth, K., Rodellar, J., and Gómez, M. (2011). Control automático en canales de riego experiencias en el canal de laboratorio UPC-PAC. In *Proceedings of the IV Seminar for advanced industrial control applications*, pages 83–88., Barcelona.

[Georges, 2009] Georges, D. (2009). Infinite-dimensional nonlinear predictive control design for open-channel hydraulic systems. *Networks and heterogeneous media*, 4(2):267–285.

[Gómez et al., 2002] Gómez, M., Rodellar, J., and Mantecón, J. (2002). Predictive control method for decentralized operation of irrigation canals. *Applied Mathematical Modelling*, 26(11):1039–1056.

[Gómez et al., 1998] Gómez, M., Rodellar, J., Vea, F., Mantecón, J., and Cardona, J. (1998). Decentralized predictive control of multi-reach canals. *1998 IEEE International Conference on Systems, Man, and Cybernetics*, pages 3885–3890.

[Goussard, 1993] Goussard, J.-J. (1993). *Automation of canal irrigation systems*. International Commission on Irrigation and Drainage.

[Hashemy Shahdany et al., 2012] Hashemy Shahdany, S. M., Maestre, J. M., van Overloop, P.-J., and Monem, M. J. (2012). An application of a dynamical set point policy to main irrigation canals using in-line storage. In *Proceedings of the European Geosciences Union General Assembly*, page 12185, Vienna, Austria.

[Hayami, 1951] Hayami, S. (1951). On the propagation of flood waves. *Bulletins-Disaster Prevention Research Institute, Kyoto University*, 1:1–16.

[Henderson, 1966] Henderson, F. M. (1966). *Open Channel Flow*. Macmillan, New York.

[Herschy, 1995] Herschy, R. (1995). General purpose flow measurement equations for flumes and thin plate weirs. *Flow Measurement and Instrumentation*, 6(4):283–293.

[Horváth et al., 2011a] Horváth, K., Galvis, E., Gómez, M., and Rodellar, J. (2011a). Control automático en canales de riego experiencias en el canal de laboratorio UPC-PAC. In *RLHE 2011, IV Seminario sobre las Líneas Prioritarias de Investigación de la Red de Laboratorios de Hidráulica de España*, pages 20–21., Madrid.

[Horváth et al., 2011b] Horváth, K., Galvis, E., Gómez, M., and Rodellar, J. (2011b). Pruebas de algoritmos de control automático en un canal de laboratorio y un canal simulado. In *JIA 2011. II Jornadas del Ingeniería del agua, Modelos numéricos en dinámica fluvial*, Barcelona.

[Horváth et al., 2012] Horváth, K., Galvis, E., Gómez, M., and Rodellar, J. (2012). Comparison of two control algorithms based on different canal models using numerical simulation and experiments on a laboratory canal. In *HIC 2012, 10th International Conference on Hydroinformatics*, Hamburg.

[Horváth et al., 2013a] Horváth, K., Gómez, M., and Rodellar, J. (2013a). The effect of the choice of the control variables of the water level control of open channels. In *The 10th IEEE International Conference on Networking, Sensing and Control*, Paris, France.

[Horváth et al., 2013b] Horváth, K., van Overloop, P.-J., Galvis, E., Gómez, M., and Rodellar, J. (2013b). Multivariable model predictive control of water levels on a laboratory canal. In Gourbesville, P., Cunge, J., and Caignaert, G., editors, *Advances in Hydroinformatics*. Springer Verlag, Singapore.

[Igreja et al., 2011] Igreja, J., Cadete, F., and Lemos, J. (2011). Application of distributed model predictive control to a water delivery canal. In *19th Mediterranean Conference on Control Automation (MED)*, pages 682 –687.

[Igreja and Lemos, 2009] Igreja, J. and Lemos, J. M. (2009). Nonlinear model predictive control of a water distribution canal pool. In *International Workshop on Assessment and Future Directions of Nonlinear Model Predictive Control*, volume 384, pages 521–529, Pavia, Italy. Springer.

[Ines et al., 2006] Ines, A., Honda, K., Das Gupta, A., Droogers, P., and Clemente, R. (2006). Combining remote sensing-simulation modeling and genetic algorithm optimization to explore water management options in irrigated agriculture. *Agricultural Water Management*, 83(3):221–232.

[Kulin and Compton, 1975] Kulin, G. and Compton, P. R. (1975). *A guide to methods and standards for the measurement of water flow*. US Dept. of Commerce, National Bureau of Standards, Washington.

[Lemos et al., 2012a] Lemos, J., Pinto, L., Rato, L., and Rijo, M. (2012a). Distributed LQG control of a water delivery canal with feedforward from measured consumptions. In *20th Mediterranean Conference on Control & Automation (MED)*, pages 722–727. IEEE.

[Lemos et al., 2012b] Lemos, J. M., Igreja, J., Cadete, F., Rijo, M., and Rato, L. M. (2012b). Experimental application to a water delivery canal of a distributed MPC with stability constraints. In *10th International Conference on Hydroinformatics HIC 2012*, Hamburg, Germany.

[Lemos et al., 2009] Lemos, J. M., Machado, F., Nogueira, N., Rato, L. M., and Rijo, M. (2009). Adaptive and non-adaptive model predictive control of an irrigation channel. *Networks and heterogeneous media*, 4(2):303–324.

[Lemos et al., 2007] Lemos, J. M., Rato, L. M., Machado, F., Nogueira, N., Salgueiro, P., and Neves-Silva, R. (2007). Predictive adaptive control of water level in canal pools. In *Proceedings of the 16th International Conference on Systems Science*.

[Li et al., 2004] Li, Y., Cantoni, M., and Weyer, E. (2004). Design of a centralized controller for an irrigation channel using H∞ loop-shaping. In *Proc UKACC Control conference*, UK. University of Bath.

[Lin et al., 2002] Lin, C., Yen, J. F., and Tsai, C. T. (2002). Influence of sluice gate contraction coefficient on distinguishing condition. *Journal of Irrigation and Drainage Engineering*, 128(4):249–252.

[Litrico and Fromion, 2004a] Litrico, X. and Fromion, V. (2004a). Frequency modeling of open-channel flow. *Journal of hydraulic engineering*, 130(8):806–815.

[Litrico and Fromion, 2004b] Litrico, X. and Fromion, V. (2004b). Simplified modeling of irrigation canals for controller design. *Journal of Irrigation and Drainage Engineering*, 130(5):373–383.

[Litrico and Fromion, 2006a] Litrico, X. and Fromion, V. (2006a). H-infinity control of an irrigation canal pool with a mixed control politics. *Control Systems Technology, IEEE Transactions on*, 14(1):99 – 111.

[Litrico and Fromion, 2006b] Litrico, X. and Fromion, V. (2006b). Tuning of robust distant downstream pi controllers for an irrigation canal pool. i: Theory. *Journal of irrigation and drainage engineering*, 132(4):359–368.

[Litrico and Georges, 1999] Litrico, X. and Georges, D. (1999). Robust continuous-time and discrete-time flow control of a dam-river system. (i) modelling. *Applied Mathematical Modelling*, 23(11):809–827.

[Litrico et al., 2008] Litrico, X., Malaterre, P.-O., Baume, J., and Ribot-Bruno, J. (2008). Conversion from discharge to gate opening for the control of irrigation canals. *Journal of Irrigation and Drainage Engineering*, 134(3):305–314.

[Litrico et al., 2007] Litrico, X., Malaterre, P.-O., Baume, J.-P., Vion, P., and Ribot-Bruno, J. (2007). Automatic tuning of PI controllers for an irrigation canal pool. *Journal of irrigation and drainage engineering*, 133(1):27–37.

[Lopez-Antens et al., 2007] Lopez-Antens, G., Ruiz-Carmona, V., Arteaga-Tovar, E., and Ostos-Santos, J. (2007). Orientations of the control theory in the automation of canals. *Ingenieria hidráulica en México*, 22(1):117–123.

[Lozano, 2009] Lozano, D. (2009). Field calibration of submerged sluice gates in irrigation canals. *Journal of Irrigation and Drainage Engineering*, 135(6):763–772.

[Maestre Torreblanca, 2010] Maestre Torreblanca, J. M. (2010). *Distributed model predictive control based on game theory.* PhD thesis, University of Seville, Sevilla, Spain.

[Malaterre, 1994] Malaterre, P.-O. (1994). *Modelisation, Analysis and LQR Optimal Control of an Irrigation Canal.* PhD thesis, LAAS-CNRS-ENGREF-Cemagref, France.

[Malaterre, 1998a] Malaterre, P.-O. (1998a). Classification of canal control algorithms. *Journal of Irrigation and Drainage Engineering*, 124(1):3–10.

[Malaterre, 1998b] Malaterre, P.-O. (1998b). PILOTE: Linear quadratic optimal controller for irrigation canals. *Journal of Irrigation and Drainage Engineering*, 124(4):187–194.

[Malaterre, 2008] Malaterre, P.-O. (2008). Control of irrigation canals: Why and how? In *Proceedings of the International Workshop on Numerical Modelling of Hydrodynamics for Water Resources*, pages 271–292, Zaragoza, Spain.

[Malaterre, 2011] Malaterre, P.-O. (2011). Canari - www database on irrigation canals. http://www.canari.free.fr/classtxt.htm. Accessed: 06/05/2011.

[Malaterre, 2012] Malaterre, P.-O. (2012). Sic 5.26, Simulation of Irrigation Canals. http://sic.g-eau.net/?lang=fr. Accessed: 20/07/2021.

[Malaterre and Baume, 1997] Malaterre, P.-O. and Baume, J. P. (1997). Sic 3.0, a simulation model for canal automation design. In Mokhlisse, A., editor, *International Workshop on Regulation of Irrigation Canals: State of art of research and applications*, volume I, pages 68–75. L.A.A.A.-C.N.R.S.

[Malaterre and Baume, 1999] Malaterre, P.-O. and Baume, J. P. (1999). Optimum choice of control action variables and linked algorithms: Comparison of different alternatives. In *Proceedings of USCID Workshop on Modernization of irrigation water delivery systems*, pages 387–405, Phoenix, Arizona, USA.

[Malaterre and Rodellar, 1997] Malaterre, P.-O. and Rodellar, J. (1997). Multivariable predictive control of irrigation canals. design and evaluation on a 2-pool model. In Mokhlisse, A., editor, *International Workshop on Regulation of Irrigation Canals: State of art of research and applications*, volume 1, pages 230–238, Toulouse. L.A.A.A.-C.N.R.S.

[Mantecón et al., 2002] Mantecón, J., Gómez, M., and Rodellar, J. (2002). A simulink-based scheme for simulation of irrigation canal control systems. *Simulation*, 78(8):485–493.

[Mareels et al., 2005] Mareels, I., Weyer, E., Ooi, S., Cantoni, M., Li, Y., and Nair, G. (2005). Systems engineering for irrigation systems: Successes and challenges. *Annual reviews in control*, 29(2):191–204.

[Martín Sánchez, 1974] Martín Sánchez, J. M. (1974). *Contribución a los sistemas adaptativos con modelo de referencia a partir de la teoría de hiperestabilidad*. PhD thesis, Technical University of Catalonia, Barcelona, Spain.

[Martín Sánchez and Rodellar, 1996] Martín Sánchez, J. M. and Rodellar, J. (1996). *Adaptive predictive control: from the concepts to plant optimization*. Prentice-hall, London.

[Mathworks, 2008] Mathworks (2008). Matlab. http://www.mathworks.com/products/matlab/.

[Miltenburg, 2008] Miltenburg, I. J. (2008). Determination of canal characteristics with experimental and modeling. Master's thesis, Delft University of Technology, Delft, The Netherlands.

[Montazar et al., 2005] Montazar, A., van Overloop, P.-J., and Brouwer, R. (2005). Centralized controller for the narmada main canal. *Irrigation and drainage*, 54(1):79–89.

[Munier et al., 2010] Munier, S., Belaud, G., and Litrico, X. (2010). Closed-form expression of the response time of an open channel. *Journal of Irrigation and Drainage Engineering*, 136(10):677–684.

[Negenborn et al., 2009a] Negenborn, R., Sahin, A., Lukszo, Z., De Schutter, B., and Morari, M. (2009a). A non-iterative cascaded predictive control approach for control of irrigation canals. In *Proceedings of the 2009 IEEE International Conference on Systems, Man, and Cybernetics*, pages 3552–3557.

[Negenborn et al., 2009b] Negenborn, R., van Overloop, P.-J., Keviczky, T., and De Schutter, B. (2009b). Distributed model predictive control of irrigation canals. *Networks and heterogeneous media*, 4(2):359–380.

[Negenborn et al., 2009c] Negenborn, R. R., van Overloop, P.-J., and De Schutter, B. (2009c). Coordinated model predictive reach control for irrigation canals. In *Proceedings of the European Control Conference 2009*, pages 1420–1425.

[Nixon et al., 2001] Nixon, J., Dandy, G., and Simpson, A. (2001). A genetic algorithm for optimizing off-farm irrigation scheduling. *Journal of Hydroinformatics*, 3:11–22.

[Ooi and Weyer, 2011] Ooi, S. and Weyer, E. (2011). Detection of oscillations in control loops in irrigation channels. *Control Engineering Practice*, 19(3):311–319.

[Pages et al., 1998] Pages, J., Compas, J., and San, J. (1998). Mimo predictive control with constraints by using an embedded knowledge based model [hydraulic structures]. In *Systems, Man, and Cybernetics, 1998. 1998 IEEE International Conference on*, volume 4, pages 3902 –3907 vol.4.

[Pannocchia and Rawlings, 2003] Pannocchia, G. and Rawlings, J. B. (2003). Disturbance models for offset-free model-predictive control. *AIChE Journal*, 49(2).

[Puig et al., 2005] Puig, V., Quevedo, J., Escobet, T., Charbonnaud, P., and Duviella, E. (2005). Identification and control of an open-flow canal using lpv models. In *Decision and Control, 2005 and 2005 European Control Conference. CDC-ECC '05. 44th IEEE Conference on*, pages 1893–1898. ID: 1.

[Puig et al., 2009] Puig, V., Romera, J., Quevedo, J., Cardona, C. M., Salterain, A., Ayesa, E., Irizar, I., Castro, A., Lujan, M., Charbonnaud, P., Chiron, P., and Trouvat, J.-L. (2009). Optimal predictive control of water transport systems: Arret-Darre/Arros case study. *Water science and technology*, 60(8):2125–2133.

[Raso et al., 2012] Raso, L., van Overloop, P.-J., and Schwanenberg, D. (2012). Optimal control of water systems under uncertainty using stochastic approximation algorithm. In *10th International Conference on Hydroinformatics, HIC 2012*.

[Ratinho et al., 2002] Ratinho, T., Figueiredo, J., and Rijo, M. (2002). Modelling, control and field tests on an experimental irrigation canal. In *Proceedings of the 10th Mediterranean Conference on Control and Automation*, pages 53–62.

[Rijo, 2003] Rijo, M. (2003). Local automatic control modes in an experimental irrigation canal. *Irrigation and Drainage Systems*, 17(3):179–193.

[Rodellar et al., 1993] Rodellar, J., Gómez, M., and Bonet, L. (1993). Control method for on-demand operation of open channel flow. *Journal of Irrigation and Drainage Engineering*, 119(2):225–241.

[Rodellar et al., 1989] Rodellar, J., Gómez, M., and Martín Vide, J. P. (1989). Stable predictive control of open-channel flow. *Journal of Irrigation and Drainage Engineering*, 115(4):701–713.

[Rogers and Goussard, 1998] Rogers, D. and Goussard, J. (1998). Canal control algorithms currently in use. *Journal of Irrigation and Drainage Engineering*, 124(1):11–15.

[Ruiz and Ramirez, 1998] Ruiz, V. and Ramirez, J. (1998). Predictive control in irrigation canal operation. In *International conference on systems, man, and cybernetics, Conference Proceeding*, volume 1-5, pages 3897–3901, New York, NY. IEEE.

[Sánchez-Juny et al., 2005] Sánchez-Juny, M., Castellet, E. B., and Agudo, J. P. (2005). *Hidráulica*, volume 1. EDICIONES UPC, Barcelona, Spain.

[Sawadogo et al., 2000] Sawadogo, S., Faye, R., Benhammou, A., and Akouz, K. (2000). Decentralized adaptive predictive control of multi-reach irrigation canal. *SMC 2000 IEEE IEEE International Conference on Systems, Man, and Cybernetics, VOL 1-5*, pages 3437–3442.

[Sawadogo et al., 1998] Sawadogo, S., Faye, R., Malaterre, P.-O., and Mora-Camino, F. (1998). Decentralized predictive controller for delivery canals. *1998 IEEE International Conference on Systems, Man, and Cybernetics*, pages 3880–3884.

[Sawadogo et al., 1995] Sawadogo, S., Malaterre, P.-O., and Kosuth, P. (1995). Multivariable optimal control for on-demand operation of irrigation canals. *International Journal of Systems Science*, 26(1):161–178.

[Schuurmans, 1995] Schuurmans, J. (1995). Open-channel flow model approximation for controller design. *Applied Mathematical Modelling*, 19(9):525–530.

[Schuurmans, 1997] Schuurmans, J. (1997). *Control of water levels in open channels*. PhD thesis, Delft University of Technology, Delft, The Netherlands.

[Schuurmans et al., 1995] Schuurmans, J., Bosgra, O., and Brouwer, R. (1995). Open-channel flow model approximation for controller design. *Applied Mathematical Modelling*, 19(9):525 – 530.

[Schuurmans et al., 1999] Schuurmans, J., Clemmens, A. J., Dijkstra, S., Hof, A., and Brouwer, R. (1999). Modeling of irrigation and drainage canals for controller design. *Journal of irrigation and drainage engineering*, 125(6):338–344.

[Schwanenberg et al., 2010] Schwanenberg, D., Verhoeven, G., and Raso, L. (2010). Nonlinear model predictive control of water resources systems in operational flood forecasting. In *Operational Flood Forecasting, 55th Internationales Wissenschaftliches Kolloqium, Ilmenau, Germany, 13-17 Sep 2010*.

[Sepúlveda, 2008] Sepúlveda, C. (2008). *Instrumentation, model identification and control of an experimental irrigation canal*. PhD thesis, Technical University of Catalonia, Barcelona, Spain.

[Sepúlveda et al., 2009] Sepúlveda, C., Gómez, M., and Rodellar, J. (2009). Benchmark of discharge calibration methods for submerged sluice gates. *Journal of Irrigation and Drainage Engineering*, 135(5):676–682.

[Setz et al., 2008] Setz, C., Heinrich, A., Rostalski, P., Papafotiou, G., and Morari, M. (2008). Application of model predictive control to a cascade of river power plants. In *IFAC World Congress*, pages 11978–11983.

[Shampine and Gahinet, 2006] Shampine, L. and Gahinet, P. (2006). Delay-differential-algebraic equations in control theory. *Applied Numerical Mathematics*, 56(3):574 – 588.

[Silva et al., 2007] Silva, P., Botto, M., Figueiredo, J., and Rijo, M. (2007). Model predictive control of an experimental water canal. In *Proceedings of the European Control Conference*, pages 2977–2984, Greece.

[Soler et al., 2008] Soler, J., Gómez, M., and Rodellar, J. (2008). A control tool for irrigation canals with scheduled demands. *Journal of Hydraulic Research*, 46(sup1):152–167.

[Stringam, 1998] Stringam, B. L. (1998). *A fuzzy logic controller for downstream water-level control in canals*. PhD thesis, Logan, UT, USA.

[Swamee, 1988] Swamee, P. K. (1988). Generalized rectangular weir equations. *Journal of Hydraulic Engineering*, 114(8):945–949.

[Swamee, 1992] Swamee, P. K. (1992). Sluice gate discharge equations. *Journal of Irrigation and Drainage Engineering*, 118(1):56–60.

[U.S. Department of the Interior, Bureau of Reclamation, 2013] U.S. Department of the Interior, Bureau of Reclamation (2013). Laboratory model canal. http://www.usbr.gov/pmts/hydraulics_lab/facilities/canalmodeldetails.pdf. Accessed: 20/01/2013.

[van Overloop, 2006a] van Overloop, P.-J. (2006a). Drainage control in water management of polders in the netherlands. *Irrigation and Drainage Systems*, 20(1):99–109.

[van Overloop, 2006b] van Overloop, P.-J. (2006b). *Model predictive control on open water systems*. PhD thesis, Delft University of Technology, Delft, The Netherlands.

[van Overloop and Bombois, 2012] van Overloop, P.-J. and Bombois, X. (2012). Identification of properties of open water channels for controller design. In *IFAC Symposium on System Identification*, volume 16, pages 1019–1024.

[van Overloop et al., 2010a] van Overloop, P.-J., Clemmens, A., Strand, R., Wagemaker, R., and Bautista, E. (2010a). Real-time implementation of model predictive control on Maricopa-Stanfield irrigation and drainage district's WM canal. *Journal of Irrigation and Drainage Engineering*, 136(11):747–756.

[van Overloop et al., 2010b] van Overloop, P.-J., Miltenburg, I. J., Bombois, X., Clemmens, A. J., Strand, R., and van de Giesen, N. (2010b). Identification of resonance waves in open water channels. *Control Engineering Practice*, 18(8):863–872.

[van Overloop et al., 2010c] van Overloop, P.-J., Negenborn, R., De Schutter, B., and van de Giesen, N. (2010c). Predictive control for national water flow optimization in The Netherlands. In Negenborn, R., Lukszo, Z., and Hellendoorn, H., editors, *Intelligent Infrastructures*, volume 42 of *Intelligent Systems, Control and Automation: Science and Engineering*, chapter 17, pages 439–461. Springer, Dordrecht, The Netherlands.

[van Overloop et al., 2005] van Overloop, P.-J., Schuurmans, J., Brouwer, R., and Burt, C. (2005). Multiple-model optimization of proportional integral controllers on canals. *Journal of Irrigation and Drainage Engineering*, 131(2):190–196.

[van Overloop et al., 2008] van Overloop, P.-J., Weijs, S., and Dijkstra, S. (2008). Multiple model predictive control on a drainage canal system. *Control Engineering Practice*, 16(5):531–540.

[Villemonte, 1947] Villemonte, J. R. (1947). Submerged weir discharge studies. *Engineering News-Record*, 139(26):886–869.

[Wahlin, 2004] Wahlin, B. T. (2004). Performance of model predictive control on asce test canal 1. *Journal of Irrigation and Drainage Engineering*, 130(3):227–238.

[Wahlin and Clemmens, 2006] Wahlin, B. T. and Clemmens, A. (2006). Automatic downstream water-level feedback control of branching canal networks: Theory. *Journal of Irrigation and Drainage Engineering*, 132(3):198–207.

[Wang, 2009] Wang, L. (2009). *Model predictive control system design and implementation using MATLAB*. Springer, New York.

[Weyer, 2001] Weyer, E. (2001). System identification of an open water channel. *Control Engineering Practice*, 9(12):1289 – 1299.

[White, 1999] White, F. M. (1999). *Fluid Mechanics*. McGraw-Hill, New York.

[World Water Assessment Programme and Unesco, 2009] World Water Assessment Programme, U. N. and Unesco (2009). *Water in a Changing World*. Number v. 2 in United Nations world water development report. Earthscan.

[World Water Assessment Programme and Unesco, 2012] World Water Assessment Programme, U. N. and Unesco (2012.). *The United Nations World Water Development report 4:*. UNESCO, Paris :. Available online.

[Xu et al., 2010a] Xu, M., van Overloop, P.-J., van de Giesen, N., and Stelling, G. (2010a). Real-time control of combined surface water quantity and quality: polder flushing. *Water science and technology*, 61(4):869–878.

[Xu et al., 2010b] Xu, M., van Overloop, P.-J., and van de Giesen, N. C. (2010b). On the study of control effectiveness and computational efficiency of reduced Saint-Venant model in model predictive control of open channel flow. *Advances in Water Resources*, 2(34):282–290.

[Zafra-Cabeza et al., 2011] Zafra-Cabeza, A., Maestre, J., Ridao, M., Camacho, E., and Sánchez, L. (2011). Hierarchical distributed model predictive control for risk mitigation: An irrigation canal case study. In *American Control Conference (ACC), 2011*, pages 3172 –3177.

Appendix A

Measured data for weir calibration

Discharge (m^3/s)	**Weir height (m)**	**Water level (m)**
0.0397	0.493	0.645
0.0333	0.493	0.637
0.0435	0.493	0.654
0.0308	0.493	0.626
0.0464	0.443	0.617
0.0330	0.443	0.587
0.0379	0.443	0.595
0.0252	0.443	0.561
0.0267	0.493	0.615
0.0217	0.493	0.6
0.0579	0.443	0.644
0.0545	0.443	0.635

TABLE A.1: Measured data, Weir 1

Discharge (m^3/s)	**Weir height (m)**	**Water level (m)**
0.0625	0.443	0.653
0.0480	0.443	0.622
0.0400	0.543	0.699
0.0268	0.543	0.65
0.0265	0.443	0.565
0.0663	0.543	0.76
0.0595	0.543	0.747
0.0512	0.543	0.727
0.0425	0.443	0.607

TABLE A.2: Measured data, Weir 2

Discharge (m^3/s)	**Weir height (m)**	**Water level (m)**
0.0318	0.543	0.686
0.0415	0.543	0.714
0.0375	0.543	0.702
0.0764	0.543	0.780
0.0535	0.543	0.729
0.0645	0.493	0.705
0.0641	0.543	0.752
0.0708	0.493	0.722
0.0564	0.493	0.694
0.0416	0.493	0.661
0.0845	0.493	0.750
0.0295	0.493	0.630

TABLE A.3: Measured data, Weir 3

Discharge (m^3/s)	**Weir height (m)**	**Water level (m)**
0.0508	0.193	0.365
0.0508	0.193	0.365
0.0494	0.193	0.362
0.0366	0.193	0.336
0.0195	0.193	0.289
0.0307	0.193	0.3215
0.0280	0.193	0.314
0.0470	0.193	0.36
0.0519	0.193	0.368
0.0508	0.193	0.366
0.0523	0.193	0.369
0.0215	0.193	0.296
0.0794	0.293	0.523
0.0532	0.293	0.477
0.0563	0.343	0.532
0.0527	0.343	0.52
0.0237	0.343	0.453
0.0648	0.343	0.549
0.0518	0.343	0.522
0.0518	0.343	0.523
0.0394	0.343	0.495
0.0394	0.343	0.4945
0.0226	0.343	0.449
0.0570	0.343	0.531
0.0545	0.343	0.528
0.0627	0.343	0.548
0.0301	0.343	0.47

TABLE A.4: Measured data, Weir 4 (Part 1)

Discharge (m^3/s)	**Weir height (m)**	**Water level (m)**
0.0590	0.343	0.538
0.0590	0.343	0.54
0.0988	0.393	0.664
0.0371	0.393	0.541
0.0242	0.393	0.509
0.0536	0.393	0.576
0.0197	0.393	0.491
0.0533	0.393	0.578
0.0843	0.443	0.689
0.0727	0.443	0.669
0.0605	0.443	0.643
0.0286	0.443	0.571
0.0371	0.443	0.587
0.0269	0.443	0.564
0.0627	0.443	0.649
0.0704	0.443	0.662
0.0268	0.543	0.661
0.0269	0.543	0.662
0.0516	0.543	0.723
0.0471	0.193	0.359
0.0345	0.193	0.331
0.0845	0.293	0.529
0.0309	0.343	0.474
0.0570	0.343	0.5315
0.0290	0.343	0.467
0.0676	0.393	0.605
0.0458	0.443	0.61
0.0442	0.543	0.709

Table A.5: Measured data, Weir 4 (Part 2)

Appendix B

The Integrator Resonance model

The development of the IR model from [van Overloop et al., 2010b]. A channel is discretized in two elements and the following assumptions are used: (1) the advection can be neglected because the water level changes are small compared to the depth of the channel and (2) the cross sectional area, the wetted perimeter and the hydraulic radius can be considered constant. A constant mean flow Q_0 is present (Figure B.1). In this development no lateral in or outflow is considered.

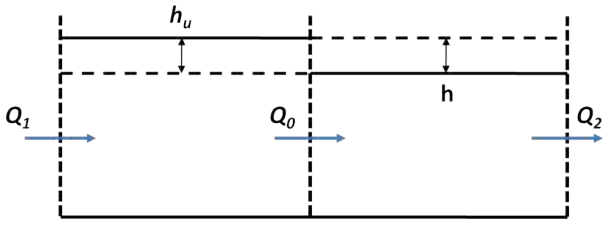

FIGURE B.1: (Channel discretization to develop the IR model, from [van Overloop et al., 2010b]

After the linearisation of the Saint-Venant equations and transformation to the Laplace domain the following equations can be written. The upstream and the

downstream water level is expressed as:

$$h_u = \frac{q_1 - q}{0.5XT_0s} \tag{B.1}$$

and

$$h = \frac{q - q_2}{0.5XT_0s} \tag{B.2}$$

where h_u is the upstream and h is the downstream water level, q is the intermediate discharge in the section, q_1 is the upstream and q_2 is the downstream discharge, X is the length of the section, T_0 is the top width and s is the Laplace variable. The intermediate discharge is expressed as:

$$q = \frac{\frac{4gH_0}{X^2}}{s^2 + \frac{2gQ_0}{C_{z0}^2 R_{h0} T_0 H_0}s + \frac{8gH_0}{X^2}}(q_1 + q_2) + \frac{\frac{gQ_0^2}{C_{z0}^2 R_{h0} T_0 H_0}s}{s^2 + \frac{2gQ_0}{C_{z0}^2 R_{h0} T_0 H_0}s + \frac{8gH_0}{X^2}} \tag{B.3}$$

where H_0 is the reference water depth, Q_0 is the reference discharge, C_{z0} is the Chézy coefficient, R_h is the hydraulic radius. From the combination of these three equations (Equations B.1, B.2 and B.3), different transfer functions can be expressed.

The downstream water level can be expressed as

$$\begin{aligned} h = \; & \frac{\frac{4gH_0}{X^2}\frac{1}{0.5XT_0s}}{s^2 + \frac{2gQ_0}{C_{z0}^2 R_{h0} T_0 H_0}s + \frac{8gH_0}{X^2}} q_1 \\ & - \frac{1}{0.5XT_0s}\left(1 - \frac{\frac{4gH_0}{X^2}}{s^2 + \frac{2gQ_0}{C_{z0}^2 R_{h0} T_0 H_0}s + \frac{8gH_0}{X^2}}\right) q_2 \\ & \frac{\frac{1}{0.5XT_0s}\frac{gQ_0^2}{C_{z0}^2 R_{h0} T_0 H_0}s}{s^2 + \frac{2gQ_0}{C_{z0}^2 R_{h0} T_0 H_0}s + \frac{8gH_0}{X^2}}. \end{aligned} \tag{B.4}$$

The first term is the transfer function between the input discharge and the downstream water level and the second term is the transfer function between the output (downstream) discharge and the downstream water level and the

third term is constant. The upstream water level can be expressed as:

$$\begin{aligned} h_u = \quad & \frac{1}{0.5XT_0s}\left(1 - \frac{\frac{4gH_0}{X^2}}{s^2 + \frac{2gQ_0}{C_{z0}^2 R_{h0} T_0 H_0}s + \frac{8gH_0}{X^2}}\right)q_1 \\ & - \frac{\frac{4gH_0}{X^2}\frac{1}{0.5XT_0s}}{s^2 + \frac{2gQ_0}{C_{z0}^2 R_{h0} T_0 H_0}s + \frac{8gH_0}{X^2}}q_2 \\ & - \frac{\frac{1}{0.5XT_0s}\frac{gQ_0^2}{C_{z0}^2 R_{h0} T_0 H_0}s}{s^2 + \frac{2gQ_0}{C_{z0}^2 R_{h0} T_0 H_0}s + \frac{8gH_0}{X^2}}. \end{aligned} \tag{B.5}$$

This equation has also three terms, the first term is the transfer function between the input discharge and the upstream water level, the second term is the transfer function between the output discharge and the upstream water level and the third term is constant.

The offtake discharges can be expressed using the same terms as the ones used for the downstream discharge.

The basic idea of the model, that the transfer function between the downstream water level (first term of Equation B.11) is a third order system: a second order function with resonance (underdamped) and an integrator:

$$H_{IR}(s) = \overbrace{\frac{1}{A_s \cdot s}}^{\text{Integrator}} \cdot \overbrace{\frac{\omega_0^2}{s^2 + 2 \cdot \zeta \cdot \omega_0 s + \omega_0^2}}^{\text{Resonance}}. \tag{B.6}$$

From this, the parameters of the transfer function: the frequency (ω_0) and the damping (ζ) and the resonance peak can be expressed as:

$$\omega_0 = \sqrt{\frac{8gH_0}{X^2}} \tag{B.7}$$

$$\zeta = \frac{\sqrt{2g}Q_0X}{4C_{z0}^2R_0T_0H_0^{\frac{2}{3}}} \tag{B.8}$$

$$M\left(\omega_0\right) = \left|\frac{\frac{8gH_0}{T_0L^3}}{-j\omega_0^3 - \frac{2gQ_0}{C_{z0}^2R_{h0}H_0}\omega_0^2 + \frac{8gH}{X^2}j\omega_0}\right| = \frac{C_{z0}^2R_{h0}H_0}{2gQ_0X} \tag{B.9}$$

$$\zeta = \frac{1}{2\omega A_s M_r}. \tag{B.10}$$

Using these equations (B.7, B.8 and B.9), the whole expression for the downstream water level (Equation B.11) and for the upstream water level (Equation B.12):

$$\begin{aligned} h = \quad & \frac{1}{A_s s}\frac{\omega_0^2}{s^2+2\zeta\omega_0 s+\omega_0^2}q_1 \\ & -\frac{1}{0.5A_s s}(1-\frac{\omega_0^2/2}{s^2+2\zeta\omega_0 s+\omega_0^2})q_2 + \\ & \frac{Q_0^2}{A_s^2 M_r}s^2+2\zeta\omega_0 s+\omega_0^2. \end{aligned} \tag{B.11}$$

and

$$\begin{aligned} h_u = \quad & \frac{1}{0.5A_s s}(1-\frac{\omega_0^2/2}{s^2+2\zeta\omega_0 s+\omega_0^2})q_1 + \\ & \frac{1}{A_s s}\frac{\omega_0^2}{s^2+2\zeta\omega_0 s+\omega_0^2}q_2 + \\ & \frac{Q_0^2}{A_s^2 M_r}s^2+2\zeta\omega_0 s+\omega_0^2. \end{aligned} \tag{B.12}$$

The parameters in these equations can be calculated or obtained by identification experiments (like in Chapter 3). After discretising the equations the discrete state space model can be written, detalied in Appendix C or using the gate openigs as control action variable Appendix E.

Appendix C

State space representation of the models

C.1 State space representation of the models Hayami, Muskingum - second order models without delay

A general form of a model of second order without delay can be written as:

$$h_i = \frac{p_{ai}z + p_{bi}}{z^2 + p_{ci}z + p_{di}} q_i + \frac{p_{gi}}{z-1} q_{i+1} \tag{C.1}$$

where h_i is the downstream water level in the i^{th} reach, q_i is the upstream and q_{i+1} is the downstream discharge and the coefficients p_{ai}, p_{bi}, p_{ci}, p_{di} and p_{gi} are model specific. Equation C.1 has two terms: the first term is a second order discrete function, the transfer function between the upstream discharge and the downstream water level. The second term is just a first order transfer function with a one pole (an integrator); it is the transfer function between the downstream discharge and the downstream water level.

The equation can be rewritten as where p_{fi} and p_{gi} are roots of the equation $z^2 + p_{ci}z + p_{di}$:

$$h_i = \frac{p_{ai}z + p_{bi}}{(z - p_{ei})(z - p_{fi})}q_i + \frac{p_{gi}}{z-1}q_{i+1}. \tag{C.2}$$

In this case, since the system has an integrator $p_{fi} = 1$ always. Hence:

$$h_i = \frac{p_{ai}z + p_{bi}}{(z - p_{ei})(z-1)}q_i + \frac{p_{gi}}{z-1}q_{i+1}. \tag{C.3}$$

Rearranging the above equation the following can be written:

$$\begin{aligned} h_i(k+1) = \quad & -p_{ci}h_i(k) - p_{di}h_i(k-1) + p_{ai}q_i(k) + p_{bi}q_i(k-1) + \\ & p_{gi}q_{i+1}(k) - p_{ei}p_{gi}q_{i+1}(k-1). \end{aligned} \tag{C.4}$$

The water level error can be included in the formulation by using Equation 4.36:

$$\begin{aligned} e_i(k+1) = \quad & -p_{ci}e_i(k) - p_{di}e_i(k-1) \\ & +p_{ai}q_i(k) + p_{bi}q_i(k-1) \\ & +p_{gi}q_{i+1}(k) - p_{ei}p_{gi}q_{i+1}(k-1) \\ & -h_{spi}(k+1) - p_{ci}h_{spi}(k) - p_{di}h_{spi}(k-1) \end{aligned} \tag{C.5}$$

So far the model was presented for one reach. In order to formulate it for the three reaches of the UPC-PAC, first the model of the last reach is developed, because it is different from the models of the intermediate reaches. In order to model the last reach with a weir at the downstream end, the outflow should be expressed with the help of the weir equation. The linearized weir discharge equation is the following:

$$q_4(k) = k_{hw}h_3(k) \tag{C.6}$$

where q_4 is the outflow from Pool 3, k_{hw} is the gain of the linearized weir discharge equation and h_3 is the water level in Pool 3. Hence the water level error for the last reach can be written as:

$$\begin{aligned} e_3(k+1) = \quad & e_3(k)(-p_{c3} + p_{g3}k_{hw}) + e_3(k-1)(-p_{d3} - p_{e3}p_{g3}k_{hw}) \\ & +p_{a3}q_3(k) + p_{b3}q_3(k-1) - h_{sp3}(k+1) \\ & +h_{sp3}(k)(-p_{c3} + p_{g3}k_{hw}) + \\ & +h_{sp3}(k-1)(-p_{d3} - p_{e3}p_{g3}k_{hw}). \end{aligned} \tag{C.7}$$

With this formulation the state (x_{gen}), input (u_{gen}) and disturbance (d_{gen}) vectors are presented in the following:

$$x_{gen}(k) = \begin{bmatrix} q_1(k) \\ q_1(k-1) \\ q_1(k-2) \\ e_1(k) \\ e_1(k-1) \\ e_1(k-2) \\ q_2(k) \\ q_2(k-1) \\ q_2(k-2) \\ e_2(k) \\ e_2(k-1) \\ e_2(k-2) \\ q_3(k) \\ q_3(k-1) \\ q_3(k-2) \\ e_3(k) \\ e_3(k-1) \\ e_3(k-2) \end{bmatrix}, \tag{C.8}$$

$$u_{gen}(k) = \begin{bmatrix} \Delta q_1(k) \\ \Delta q_2(k) \\ \Delta q_3(k) \end{bmatrix} \tag{C.9}$$

and

$$d_{gen}(k) = \begin{bmatrix} q_{off1}(k+1) \\ q_{off1}(k) \\ q_{off1}(k-1) \\ q_{off1}(k-2) \\ h_{sp1}(k+1) \\ h_{sp1}(k) \\ h_{sp1}(k-1) \\ h_{sp1}(k-2) \\ q_{off2}(k) \\ q_{off2}(k+1) \\ q_{off2}(k-1) \\ q_{off2}(k-2) \\ h_{sp2}(k+1) \\ h_{sp2}(k) \\ h_{sp2}(k-1) \\ h_{sp2}(k-2) \\ q_{off3}(k+1) \\ q_{off3}(k) \\ q_{off3}(k-1) \\ q_{off3}(k-2) \\ h_{sp3}(k+1) \\ h_{sp3}(k) \\ h_{sp3}(k-1) \\ h_{sp3}(k-2) \end{bmatrix}. \tag{C.10}$$

The disturbance vector consists of the different setpoints and offtake discharges in the present, past and future instants. The matrices in the state equation are the following:

$$A_{gen} = \begin{bmatrix}
1 & 0 & 0 & 0 & 0 & 0 & 0 & 0 & 0 & 0 & 0 & 0 & 0 & 0 & 0 & 0 & 0 & 0 \\
1 & 0 & 0 & 0 & 0 & 0 & 0 & 0 & 0 & 0 & 0 & 0 & 0 & 0 & 0 & 0 & 0 & 0 \\
0 & 1 & 0 & 0 & 0 & 0 & 0 & 0 & 0 & 0 & 0 & 0 & 0 & 0 & 0 & 0 & 0 & 0 \\
p_{a1} & p_{b1} & 0 & -p_{c1} & -p_{d1} & 0 & p_{g1} & p_{e1}p_{g1} & 0 & 0 & 0 & 0 & 0 & 0 & 0 & 0 & 0 & 0 \\
0 & 0 & 0 & 1 & 0 & 0 & 0 & 0 & 0 & 0 & 0 & 0 & 0 & 0 & 0 & 0 & 0 & 0 \\
0 & 0 & 0 & 0 & 1 & 0 & 0 & 0 & 0 & 0 & 0 & 0 & 0 & 0 & 0 & 0 & 0 & 0 \\
0 & 0 & 0 & 0 & 0 & 0 & 1 & 0 & 0 & 0 & 0 & 0 & 0 & 0 & 0 & 0 & 0 & 0 \\
0 & 0 & 0 & 0 & 0 & 0 & 1 & 0 & 0 & 0 & 0 & 0 & 0 & 0 & 0 & 0 & 0 & 0 \\
0 & 0 & 0 & 0 & 0 & 0 & 0 & 1 & 0 & 0 & 0 & 0 & 0 & 0 & 0 & 0 & 0 & 0 \\
0 & 0 & 0 & 0 & 0 & 0 & p_{a2} & p_{b2} & 0 & -p_{c2} & -p_{d2} & 0 & p_{g2} & -p_{e2}p_{g2} & 0 & 0 & 0 & 0 \\
0 & 0 & 0 & 0 & 0 & 0 & 0 & 0 & 0 & 1 & 0 & 0 & 0 & 0 & 0 & 0 & 0 & 0 \\
0 & 0 & 0 & 0 & 0 & 0 & 0 & 0 & 0 & 0 & 1 & 0 & 0 & 0 & 0 & 0 & 0 & 0 \\
0 & 0 & 0 & 0 & 0 & 0 & 0 & 0 & 0 & 0 & 0 & 0 & 1 & 0 & 0 & 0 & 0 & 0 \\
0 & 0 & 0 & 0 & 0 & 0 & 0 & 0 & 0 & 0 & 0 & 0 & 1 & 0 & 0 & 0 & 0 & 0 \\
0 & 0 & 0 & 0 & 0 & 0 & 0 & 0 & 0 & 0 & 0 & 0 & 0 & 1 & 0 & 0 & 0 & 0 \\
0 & 0 & 0 & 0 & 0 & 0 & 0 & 0 & 0 & 0 & 0 & 0 & p_{a3} & p_{b3} & 0 & -p_{c3} + p_{g3}k_{hw} & -p_{d3} + p_{e3}p_{g3}k_{hw} & 0 \\
0 & 0 & 0 & 0 & 0 & 0 & 0 & 0 & 0 & 0 & 0 & 0 & 0 & 0 & 0 & 1 & 0 & 0 \\
0 & 0 & 0 & 0 & 0 & 0 & 0 & 0 & 0 & 0 & 0 & 0 & 0 & 0 & 0 & 0 & 1 & 0
\end{bmatrix} \tag{C.11}$$

and

$$B_{gen} = \begin{bmatrix} 1 & 0 & 0 \\ 0 & 0 & 0 \\ 0 & 0 & 0 \\ 0 & 0 & 0 \\ 0 & 0 & 0 \\ 0 & 0 & 0 \\ 0 & 1 & 0 \\ 0 & 0 & 0 \\ 0 & 0 & 0 \\ 0 & 0 & 0 \\ 0 & 0 & 0 \\ 0 & 0 & 0 \\ 0 & 0 & 1 \\ 0 & 0 & 0 \\ 0 & 0 & 0 \\ 0 & 0 & 0 \\ 0 & 0 & 0 \\ 0 & 0 & 0 \end{bmatrix}. \tag{C.12}$$

The matrix B_{dgen} has few non-zero entries, these are the following:

$B_{dgen}(4,2) = p_{g1}$
$B_{dgen}(4,3) = -p_{g1}p_{e1}$
$B_{dgen}(4,5) = -1$
$B_{dgen}(4,6) = -p_{c1}$
$B_{dgen}(4,7) = -p_{d1}$
$B_{dgen}(8,9) = p_{g2}$
$B_{dgen}(8,10) = -p_{g2}p_{e2}$
$B_{dgen}(8,12) = -1$
$B_{dgen}(8,13) = -p_{c2}$
$B_{dgen}(8,14) = -p_{d2}$
$B_{dgen}(12,16) = p_{g3}$
$B_{dgen}(12,17) = -p_{g3}p_{e3}$

$B_{dgen}(12,19) = -1$
$B_{dgen}(12,20) = -p_{c3} + p_{g3}k_{hw}$
$B_{dgen}(12,21) = -p_{d3} - p_{e3}p_{g3}k_{hw}$.

C.2 State space representation of the models ID, IDZ - first order models with a zero with delay

Similar to the models above, first the general equation of the water level is given:

$$h_i = \frac{p_{ai}z + p_{bi}}{z-1} z^{-p_{ci}} q_i + \frac{p_{di}z + p_{ei}}{z-1} q_{i+1} \tag{C.13}$$

where h_i is the downstream water level, q_i is the input discharge, q_{i+1} is the output discharge and p_{ai}, p_{bi}, p_{ci}, p_{di}, p_{ei} are model specific parameters. The i subscript refers to the i^{th} reach. The first term of the equation is the transfer function between the upstream discharge and the downstream water level, the second term is the transfer function between the output discharge and the downstream water level. Both terms have a pole at the origin (integrator) and zeros in the numerator. Since the ID model does not contain zeros, the coefficients p_{ai} and p_{di} are zero. The first term has a delay. The time delay expressed in sampling instants is denoted with p_{ci}. The following expression for the water level can be derived:

$$h_i(k+1) = h_i(k) + p_{ai}q_i(k+1-p_{ci}) + p_{bi}q_i(k-p_{ci}) + p_{di}q_{i+1}(k+1) + p_{ei}q_{i+1}(k). \tag{C.14}$$

By using Equation 4.36 the water level error can be expressed as:

$$\begin{aligned} e_i(k+1) = \quad & e_i(k) + p_{ai}q_i(k+1-p_{ci}) + p_{bi}q_i(k-p_{ci}) \\ & + p_{di}q_{i+1}(k+1) + p_{ei}q_{i+1}(k) \\ & - h_{spi}(k+1) + h_{spi}(k). \end{aligned} \tag{C.15}$$

After having developed the general equation for an intermediate pool, we are going to develop the equation of the downstream pool with a weir at the end. As addition to the linearized weir discharge equation Equation C.6 we will use

the following approximation for the weir discharge in the future instant $(k+1)$:

$$q_4(k+1) \approx k_{hw} h_3(k). \tag{C.16}$$

Note that this equation using the water level at instant k instead of $k+1$. This is a simplification that is used in order to simplify the formulation. Using equations C.6 and C.16 the water level error in Pool 3 is expressed as:

$$\begin{aligned} e_3(k+1) = \quad & e_3(k)(1 + p_{d3}k_{hw} + p_{e3}k_{hw}) \\ & + p_{a3}q_3(k-1) + p_{b3}q_3(k-2) \\ & - h_{sp3}(k+1) + h_{sp3}(k)(1 + p_{d3}k_{hw} + p_{e3}k_{hw}). \end{aligned} \tag{C.17}$$

So far general equations were presented with delay p_{ci}. From this point we specify the equations for the UPC-PAC and use the following delays in the pools: $p_{c1} = 3$, $p_{c2} = 3$ and $p_{c3} = 2$. The state, the input and the disturbance vector is the following:

$$x_{gen}(k) = \begin{bmatrix} q_1(k) \\ q_1(k-1) \\ q_1(k-2) \\ q_1(k-3) \\ e_1(k) \\ e_1(k-1) \\ e_1(k-2) \\ q_2(k) \\ q_2(k-1) \\ q_2(k-2) \\ q_2(k-3) \\ e_2(k) \\ e_2(k-1) \\ e_2(k-2) \\ q_3(k) \\ q_3(k-1) \\ q_3(k-2) \\ e_3(k) \\ e_3(k-1) \\ e_3(k-2) \end{bmatrix}, \tag{C.18}$$

$$u_{gen}(k) = \begin{bmatrix} \Delta q_1(k) \\ \Delta q_2(k) \\ \Delta q_3(k) \end{bmatrix} \tag{C.19}$$

and

$$d_{gen}(k) = \begin{bmatrix} q_{off1}(k+1) \\ q_{off1}(k) \\ q_{off1}(k-1) \\ q_{off1}(k-2) \\ h_{sp1}(k+1) \\ h_{sp1}(k) \\ h_{sp1}(k-1) \\ h_{sp1}(k-2) \\ q_{off2}(k) \\ q_{off2}(k+1) \\ q_{off2}(k-1) \\ q_{off2}(k-2) \\ h_{sp2}(k+1) \\ h_{sp2}(k) \\ h_{sp2}(k-1) \\ h_{sp2}(k-2) \\ q_{off3}(k+1) \\ q_{off3}(k) \\ q_{off3}(k-1) \\ q_{off3}(k-2) \\ h_{sp3}(k+1) \\ h_{sp3}(k) \\ h_{sp3}(k-1) \\ h_{sp3}(k-2) \end{bmatrix}. \tag{C.20}$$

The matrices of the state space equation are the following:

$$A_{gen} = \begin{bmatrix}
1 & 0 & 0 & 0 & 0 & 0 & 0 & 0 & 0 & 0 & 0 & 0 & 0 & 0 & 0 & 0 & 0 & 0 & 0 & 0 & 0 & 0 \\
 & 1 & 0 & 0 & 0 & 0 & 0 & 0 & 0 & 0 & 0 & 0 & 0 & 0 & 0 & 0 & 0 & 0 & 0 & 0 & 0 & 0 \\
 & & 0 & 1 & 0 & 0 & 0 & 0 & 0 & 0 & 0 & 0 & 0 & 0 & 0 & 0 & 0 & 0 & 0 & 0 & 0 & 0 \\
 & & & 0 & 0 & 1 & 0 & 0 & 0 & 0 & 0 & 0 & 0 & 0 & 0 & 0 & 0 & 0 & 0 & 0 & 0 & 0 \\
 & & & & 0 & 0 & p_{a1} & 0 & 0 & 0 & 0 & 0 & 0 & 0 & 0 & 0 & 0 & 0 & 0 & 0 & 0 & 0 \\
 & & & & & 0 & 0 & p_{b1} & 0 & 0 & 0 & 0 & 0 & 0 & 0 & 0 & 0 & 0 & 0 & 0 & 0 & 0 \\
 & & & & & & 0 & 0 & 1 & 0 & 0 & 0 & 0 & 0 & 0 & 0 & 0 & 0 & 0 & 0 & 0 & 0 \\
 & & & & & & & 0 & 0 & 1 & 0 & 0 & 0 & 0 & 0 & 0 & 0 & 0 & 0 & 0 & 0 & 0 \\
 & & & & & & & & $p_{d1}+p_{e1}$ & 0 & 0 & 0 & 0 & 0 & 0 & 0 & 0 & 0 & 0 & 0 & 0 \\
 & & & & & & & & & 0 & 0 & 1 & 0 & 0 & 0 & 0 & 0 & 0 & 0 & 0 & 0 & 0 \\
 & & & & & & & & & & 0 & 0 & 1 & 0 & 0 & 0 & 0 & 0 & 0 & 0 & 0 & 0 \\
 & & & & & & & & & & & 0 & 0 & 1 & 0 & 0 & 0 & 0 & 0 & 0 & 0 & 0 \\
 & & & & & & & & & & & & 0 & 0 & 1 & 0 & 0 & 0 & 0 & 0 & 0 & 0 \\
 & & & & & & & & & & & & & 0 & 0 & 1 & 0 & 0 & 0 & 0 & 0 & 0 \\
 & & & & & & & & & & & & & & 0 & 0 & 1 & 0 & 0 & 0 & 0 & 0 \\
 & & & & & & & & & & & & & & & 0 & 0 & 1 & 0 & 0 & 0 & 0 \\
 & & & & & & & & & & & & & & & & 0 & 0 & 1 & 0 & 0 & 0 \\
 & & & & & & & & & & & & & & & & & 0 & 0 & 1 & 0 & 0 \\
 & & & & & & & & & & & & & & & & & & 0 & 0 & 1 & 0 \\
 & & & & & & & & & & & & & & & & & & & 0 & 0 & 1 \\
 & & & & & & & & & & & & & & & & & & & & 0 & 0 \\
 & & & & & & & & & & & & & & & & & & & & & 0
\end{bmatrix}, \tag{C.21}$$

$$B_{gen} = \begin{bmatrix} 1 & 0 & 0 \\ 0 & 0 & 0 \\ 0 & 0 & 0 \\ 0 & 0 & 0 \\ 0 & p_{d1} & 0 \\ 0 & 0 & 0 \\ 0 & 0 & 0 \\ 0 & 1 & 0 \\ 0 & 0 & 0 \\ 0 & 0 & 0 \\ 0 & 0 & 0 \\ 0 & 0 & p_{d2} \\ 0 & 0 & 0 \\ 0 & 0 & 0 \\ 0 & 0 & 1 \\ 0 & 0 & 0 \\ 0 & 0 & 0 \\ 0 & 0 & 0 \\ 0 & 0 & 0 \\ 0 & 0 & 0 \end{bmatrix} \tag{C.22}$$

and

$$B_{dgen} = \begin{bmatrix}
0 & 0 & 0 & 0 & 0 & 0 & 0 & 0 & 0 & 0 & 0 & 0 & 0 & 0 & 0 & 0 & 0 & 0 & 0 & 0 & 0 \\
0 & 0 & 0 & 0 & 0 & 0 & 0 & 0 & 0 & 0 & 0 & 0 & 0 & 0 & 0 & 0 & 0 & 0 & 0 & 0 & 0 \\
0 & 0 & 0 & 0 & 0 & 0 & 0 & 0 & 0 & 0 & 0 & 0 & 0 & 0 & 0 & 0 & 0 & 0 & 0 & 0 & 0 \\
0 & 0 & 0 & 0 & 0 & 0 & 0 & 0 & 0 & 0 & 0 & 0 & 0 & 0 & 0 & 0 & 0 & 0 & 0 & 0 & 0 \\
p_{d1} & p_{e1} & 0 & 0 & -1 & 1 & 0 & 0 & 0 & 0 & 0 & 0 & 0 & 0 & 0 & 0 & 0 & 0 & 0 & 0 & 0 \\
0 & 0 & 0 & 0 & 0 & 0 & 0 & 0 & 0 & 0 & 0 & 0 & 0 & 0 & 0 & 0 & 0 & 0 & 0 & 0 & 0 \\
0 & 0 & 0 & 0 & 0 & 0 & 0 & 0 & 0 & 0 & 0 & 0 & 0 & 0 & 0 & 0 & 0 & 0 & 0 & 0 & 0 \\
0 & 0 & 0 & 0 & 0 & 0 & 0 & 0 & 0 & 0 & 0 & 0 & 0 & 0 & 0 & 0 & 0 & 0 & 0 & 0 & 0 \\
0 & 0 & 0 & 0 & 0 & 0 & 0 & 0 & 0 & 0 & 0 & 0 & 0 & 0 & 0 & 0 & 0 & 0 & 0 & 0 & 0 \\
0 & 0 & 0 & 0 & 0 & 0 & 0 & p_{d2} & p_{e2} & 0 & 0 & -1 & 1 & 0 & 0 & 0 & 0 & 0 & 0 & 0 & 0 \\
0 & 0 & 0 & 0 & 0 & 0 & 0 & 0 & 0 & 0 & 0 & 0 & 0 & 0 & 0 & 0 & 0 & 0 & 0 & 0 & 0 \\
0 & 0 & 0 & 0 & 0 & 0 & 0 & 0 & 0 & 0 & 0 & 0 & 0 & 0 & 0 & 0 & 0 & 0 & 0 & 0 & 0 \\
0 & 0 & 0 & 0 & 0 & 0 & 0 & 0 & 0 & 0 & 0 & 0 & 0 & 0 & 0 & 0 & 0 & 0 & 0 & 0 & 0 \\
0 & 0 & 0 & 0 & 0 & 0 & 0 & 0 & 0 & 0 & 0 & 0 & 0 & 0 & p_{d3} & p_{e3} & 0 & 0 & -1 & 1+(p_{d3}+p_{e3})k_{hw} & 0
\end{bmatrix}. \tag{C.23}$$

C.3 State space representation of the models IR - third order model without delay

The general form of the IR model is a third order model without delay.

$$h_i = \frac{p_{ai}z^2 + p_{bi}z + p_{ci}}{z^3 + p_{di}z^2 + p_{ei}z + p_{fi}}q_i + \frac{p_{gi}z^2 + p_{hi}z + p_{ii}}{z^3 + p_{di}z^2 + p_{ei}z + p_{fi}}q_{i+1} \tag{C.24}$$

where h_i is the downstream water level, q_i is the input discharge, q_{i+1} is the output discharge and p_{ai}, p_{bi}, p_{ci}, p_{di}, p_{ei}, p_{fi}, p_{gi}, p_{hi}, p_{ii} are model specific parameters. The first term of the equation is the transfer function between the upstream discharge and the downstream water level, the second term is the transfer function between the output discharge and the downstream water level. Both transfer functions have the same denominator, with other words the transfer functions have the same poles. Equation C.24 can be written in the time domain:

$$\begin{aligned} h_i(k+1) = \quad & -p_{di}h(k) - p_{ei}h(k-1) - p_{fi}h(k-2) + p_{ai}q_1(k-d) \\ & +p_{bi}q_1(k-1-d) + p_{ci}q_1(k-2-d)\,q_1 + p_{gi}q_2(k) \\ & +p_{hi}q_2(k-1) + p_iq_2(k-2)\,q_2 \end{aligned} \tag{C.25}$$

Combining the above equation with Equation 4.36 the water level error can be expressed:

$$\begin{aligned} e_i(k+1) = \quad & -p_de_i(k) - p_ee_i(k-1) - p_fe_i(k-2) \\ & +p_aq_i(k) + p_bq_i(k-1-d) + p_cq_i(k-2)\,q_i \\ & +p_gq_{i+1}(k) + p_hq_{i+1}(k-1) + p_iq_{i+1}(k-2) \\ & -h_{sp}(k+1) - p_dh_{sp}(k) - p_eh_{sp}(k-1) \\ & -p_fh_{sp}(k-2) \end{aligned} \tag{C.26}$$

where e_i is the water level error and h_{spi} is the setpoint. With the same procedure described above in section C.2 and section C.1 combining the linearized weir equation to the water level error equation Equation C.26 the water level error can be expressed for the last reach. Then the state space equation can be built, where the state, input and disturbance vector are the

following:

$$x_{gen}(k) = \begin{bmatrix} q_1(k) \\ q_1(k-1) \\ q_1(k-2) \\ e_1(k) \\ e_1(k-1) \\ e_1(k-2) \\ q_2(k) \\ q_2(k-1) \\ q_2(k-2) \\ e_2(k) \\ e_2(k-1) \\ e_2(k-2) \\ q_3(k) \\ q_3(k-1) \\ q_3(k-2) \\ e_3(k) \\ e_3(k-1) \\ e_3(k-2) \end{bmatrix}, \tag{C.27}$$

$$u_{gen}(k) = \begin{bmatrix} \Delta q_1(k) \\ \Delta q_2(k) \\ \Delta q_3(k) \end{bmatrix} \tag{C.28}$$

and

$$d_{gen}(k) = \begin{bmatrix} q_{off1}(k+1) \\ q_{off1}(k) \\ q_{off1}(k-1) \\ q_{off1}(k-2) \\ h_{sp1}(k+1) \\ h_{sp1}(k) \\ h_{sp1}(k-1) \\ h_{sp1}(k-2) \\ q_{off2}(k) \\ q_{off2}(k+1) \\ q_{off2}(k-1) \\ q_{off2}(k-2) \\ h_{sp2}(k+1) \\ h_{sp2}(k) \\ h_{sp2}(k-1) \\ h_{sp2}(k-2) \\ q_{off3}(k+1) \\ q_{off3}(k) \\ q_{off3}(k-1) \\ q_{off3}(k-2) \\ h_{sp3}(k+1) \\ h_{sp3}(k) \\ h_{sp3}(k-1) \\ h_{sp3}(k-2) \end{bmatrix}. \tag{C.29}$$

The matrices for the state space equation are described in the the following. Matrix A is a 18×18 matrix, here the non-zero entries are given:

$A_{gen}(1,1) = 1$
$A_{gen}(2,1) = 1$
$A_{gen}(3,2) = 1$
$A_{gen}(4,1) = p_{a1}$
$A_{gen}(4,2) = p_{b1}$
$A_{gen}(4,3) = p_{c1}$
$A_{gen}(4,4) = -p_{d1}$
$A_{gen}(4,5) = -p_{e1}$
$A_{gen}(4,6) = -p_{f1}$
$A_{gen}(4,7) = p_{g1}$
$A_{gen}(4,8) = p_{h1}$
$A_{gen}(4,9) = p_{i1}$
$A_{gen}(5,4) = 1$
$A_{gen}(6,5) = 1$

$A_{gen}(7,7) = 1$
$A_{gen}(8,7) = 1$
$A_{gen}(9,8) = 1$
$A_{gen}(10,7) = p_{a2}$
$A_{gen}(10,8) = p_{b2}$
$A_{gen}(10,9) = p_{c2}$
$A_{gen}(10,10) = -p_{d2}$
$A_{gen}(10,11) = -p_{e2}$
$A_{gen}(10,12) = -p_{f2}$
$A_{gen}(10,13) = p_{g2}$
$A_{gen}(10,14) = p_{h2}$
$A_{gen}(10,15) = p_{i2}$
$A_{gen}(11,10) = 1.$
$A_{gen}(12,11) = 1$
$A_{gen}(13,13) = 1$
$A_{gen}(14,13) = 1$
$A_{gen}(15,14) = 1$
$A_{gen}(16,13) = p_{a2}$
$A_{gen}(16,8) = p_{b2}$
$A_{gen}(16,9) = p_{c2}$
$A_{gen}(16,10) = -p_{d3} - p_{g3}k_{hw}$
$A_{gen}(16,11) = -p_{e3} - p_{h3}k_{hw}$
$A_{gen}(16,12) = -p_{f3} - p_{i3}k_{hw}$
$A_{gen}(17,16) = 1$
$A_{gen}(18,17) = 1$

Matrix B_{gen} is a 18×3 matrix, here the non-zero entries are given:

$B_{gen}(1,1) = 1$
$B_{gen}(7,2) = 1$
$B_{gen}(13,3) = 1.$

Matrix B_{dgen} is a 18×24 matrix, here the non-zero entries are given:

$B_{dgen}(4,2) = -p_{g1}$
$B_{dgen}(4,3) = -p_{h1}$
$B_{dgen}(4,4) = -p_{i1}$
$B_{dgen}(4,5) = -1$
$B_{dgen}(4,6) = -p_{d1}$
$B_{dgen}(4,7) = -p_{e1}$
$B_{dgen}(4,8) = -p_{f1}$
$B_{dgen}(8,10) = -p_{g2}$
$B_{dgen}(8,11) = -p_{h2}$
$B_{dgen}(8,12) = -p_{i2}$
$B_{dgen}(8,13) = -1.$
$B_{dgen}(8,14) = -p_{d2}$
$B_{dgen}(8,15) = -p_{e2}$
$B_{dgen}(8,16) = -p_{f2}$
$B_{dgen}(12,18) = -p_{g3}$
$B_{dgen}(12,19) = -p_{h3}$
$B_{dgen}(12,20) = -p_{i3}$
$B_{dgen}(12,21) = -1$
$B_{dgen}(12,22) = -p_{d3} - p_{g3}k_{hw}$
$B_{dgen}(12,23) = -p_{e3} - p_{h3}k_{hw}$
$B_{dgen}(12,24) = -p_{f3} - p_{i3}k_{hw}$

Appendix D

Calculated transfer functions of the models

D.1 Laplace domain

Pool 1

$$G_{ID1}(s) = \frac{1}{38.28s} e^{-28.29s} \tag{D.1}$$

$$G_{MUS1}(s) = \frac{-0.28s + 1}{1072.28s^2 + 38.28s} \tag{D.2}$$

$$G_{HAY1}(s) = \frac{1}{10676.18s^2 + 38.28s} \tag{D.3}$$

$$G_{IDZ1}(s) = \frac{39.46s + 1}{37.87s} e^{-28.24s} \tag{D.4}$$

$$G_{IR1}(s) = \frac{0.000281}{s^3 + 0.02106s^2 + 0.010816s} \tag{D.5}$$

$$G_{IRD1}(s) = \frac{-0.05195s^s - 0.001094s - 0.0000281}{s^3 + 0.02106s^2 + 0.010816s} \tag{D.6}$$

$$G_{IDZD1}(s) = \frac{-30.20s - 1}{37.87s} \tag{D.7}$$

Pool 2

$$G_{ID2}(s) = \frac{1}{39.69s} e^{-31.67s} \tag{D.8}$$

$$G_{MUS2}(s) = \frac{-0.3167s + 1}{1244.50s^2 + 39.69s} \tag{D.9}$$

$$G_{HAY2}(s) = \frac{1}{9450.82s^2 + 39.69s} \tag{D.10}$$

$$G_{IDZ2}(s) = \frac{43.28s + 1}{38.84s} e^{-31.56s} \tag{D.11}$$

$$G_{IR2}(s) = \frac{0.000185}{s^3 + 0.02509s^2 + 0.0064s} \tag{D.12}$$

$$G_{IRD2}(s) = \frac{-0.05780s^s - 0.001450s - 0.000185}{s^3 + 0.02509s^2 + 0.0064s} \tag{D.13}$$

$$G_{IDZD2}(s) = \frac{-34.51s - 1}{38.84s} \tag{D.14}$$

Pool 3

$$G_{ID3}(s) = \frac{1}{19.14s} e^{-16.65s} \tag{D.15}$$

$$G_{MUS3}(s) = \frac{-0.3167s + 1}{1244.50s^2 + 39.69s} \tag{D.16}$$

$$G_{HAY3}(s) = \frac{1}{1727.03s^2 + 19.14s} \tag{D.17}$$

$$G_{IDZ3}(s) = \frac{24.45s + 1}{18.68s} e^{-16.60s} \tag{D.18}$$

$$G_{IR3}(s) = \frac{0.000660}{s^3 + 0.03015s^2 + 0.0196s} \tag{D.19}$$

$$G_{IRD3}(s) = \frac{-0.06734s^s - 0.00203s - 0.00066}{s^3 + 0.03015s^2 + 0.0196s} \tag{D.20}$$

$$G_{IDZD3}(s) = \frac{-18.97s - 1}{18.68s} \tag{D.21}$$

D.2 Z domain

Pool 1

$$G_{ID1}(z) = \frac{0.2612}{z - 1}z^{-3} \tag{D.22}$$

$$G_{MUS1}(z) = \frac{0.03932z + 0.03910}{z^2 - 1.6998z + 0.6997} \tag{D.23}$$

$$G_{HAY1}(z) = \frac{0.004628z + 0.004573}{z^2 - 1.965z + 0.9648} \tag{D.24}$$

$$G_{IDZ1}(z) = \frac{1.0418z - 0.7778}{z - 1}z^{-3} \tag{D.25}$$

$$G_{IR1}(z) = \frac{0.04215z^2 + 0.1513z + 0.03787}{z^3 - 1.9195z^2 + 1.7296z - 0.8102} \tag{D.26}$$

$$G_{IRD1}(z) = \frac{-0.4773z^2 + 0.6290z - 0.3829}{z^3 - 1.9195z^2 + 1.7296z - 0.8102} \tag{D.27}$$

$$G_{IDZD1}(z) = \frac{-0.7974z + 0.5334}{z - 1} \tag{D.28}$$

Pool 2

$$G_{ID2}(z) = \frac{0.2520}{z-1} z^{-3} \tag{D.29}$$

$$G_{MUS2}(z) = \frac{0.03405z + 0.03475}{z^2 - 1.727z + 0.7269} \tag{D.30}$$

$$G_{HAY2}(z) = \frac{0.005217z + 0.005145}{z^2 - 1.959z + 0.9589} \tag{D.31}$$

$$G_{IDZ2}(z) = \frac{1.114z - 0.8566}{z-1} z^{-3} \tag{D.32}$$

$$G_{IR2}(z) = \frac{0.02809z^2 + 0.1022z + 0.02475}{z^3 - 2.242z^2 + 2.020z - 0.7781} \tag{D.33}$$

$$G_{IRD2}(z) = \frac{-0.5500z^2 + 0.8200z - 0.4250}{z^3 - 2.242z^2 + 2.020z - 0.7781} \tag{D.34}$$

$$G_{IDZD2}(z) = \frac{-0.8889z + 0.6311}{z-1} \tag{D.35}$$

Pool 3

$$G_{ID3}(z) = \frac{0.5225}{z-1} z^{-2} \tag{D.36}$$

$$G_{MUS3}(z) = \frac{0.1268z + 0.1108}{z^2 - 1.545z + 0.5452} \tag{D.37}$$

$$G_{HAY3}(z) = \frac{0.02791z + 0.02690}{z^2 - 1.895z + 0.8951} \tag{D.38}$$

$$G_{IDZ3}(z) = \frac{1.308z - 0.7733}{z-1} z^{-2} \tag{D.39}$$

$$G_{IR3}(z) = \frac{0.09285z^2 + 0.3104z + 0.07946}{z^3 - 1.306z^2 + 1.046z - 0.7397} \tag{D.40}$$

$$G_{IRD3}(z) = \frac{-0.5805z^2 + 0.5165z - 0.4186}{z^3 - 1.306z^2 + 1.046z - 0.7397} \tag{D.41}$$

$$G_{IDZD3}(z) = \frac{-1.015z + 0.4802}{z - 1} \tag{D.42}$$

Appendix E

State space model containing gate openings

The state matrix A is a 34 $\times$ 34 matrix, and it is described by its entries. The input matrix, B, is 34 $\times$ 3 and the disturbance matrix B_d is 34 $\times$ 27. The dimension of the state vector x is 34 $\times$ 1, and of the input vector u is 3 $\times$ 1 and the disturbance vector is 27 $\times$ 1.

The input vector, the state vector, and the disturbance vector are the following, respectively:

$$u(k) = \begin{bmatrix} \Delta l_1(k) \\ \Delta l_2(k) \\ \Delta l_3(k) \end{bmatrix}, \tag{E.1}$$

$$x(k) = \begin{bmatrix} q_1(k) \\ q_1(k-1) \\ q_1(k-2) \\ q_1(k-3) \\ e_1(k) \\ e_1(k-1) \\ e_1(k-2) \\ h_{u1}(k) \\ l_1(k) \\ q_2(k) \\ q_2(k-1) \\ q_2(k-2) \\ q_2(k-3) \\ e_2(k) \\ e_2(k-1) \\ e_2(k-2) \\ h_{u2}(k) \\ l_2(k) \\ q_3(k) \\ q_3(k-1) \\ q_3(k-2) \\ q_3(k-3) \\ e_3(k) \\ e_3(k-1) \\ e_3(k-2) \\ h_{u3}(k) \\ l_3(k) \end{bmatrix} \tag{E.2}$$

and

$$d(k) = \begin{bmatrix} q_{off1}(k+1) \\ q_{off1}(k) \\ q_{off1}(k-1) \\ q_{off1}(k-2) \\ h_{sp1}(k+1) \\ h_{sp1}(k) \\ h_{sp1}(k-1) \\ h_{sp1}(k-2) \\ 1 \\ q_{off2}(k) \\ q_{off2}(k+1) \\ q_{off2}(k-1) \\ q_{off2}(k-2) \\ h_{sp2}(k+1) \\ h_{sp2}(k) \\ h_{sp2}(k-1) \\ h_{sp2}(k-2) \\ 1 \\ q_{off3}(k+1) \\ q_{off3}(k) \\ q_{off3}(k-1) \\ q_{off3}(k-2) \\ h_{sp3}(k+1) \\ h_{sp3}(k) \\ h_{sp3}(k-1) \\ h_{sp3}(k-2) \\ 1. \end{bmatrix} \tag{E.3}$$

Matrix A is a 34×34 matrix. Only the non-zero entries are given as:

$A(1,8) = kh_{21}$
$A(1,11) = k_{l1}$
$A(2,1) = 1$
$A(3,2) = 1$
$A(4,3) = 1$
$A(5,1) = p_{a1}$
$A(5,2) = p_{b1}$
$A(5,3) = p_{c1}$
$A(5,4) = p_{d1}$
$A(5,5) = -p_{e1}$
$A(5,6) = -p_{f1}$
$A(5,7) = -p_{g1}$
$A(5,12) = -p_{h1}$
$A(5,13) = -p_{i1}$
$A(5,14) = -p_{j1}$
$A(5,15) = -p_{k1}$
$A(6,5) = 1$
$A(7,6) = 1$
$A(8,1) = p_{m1}$
$A(8,2) = p_{n1}$
$A(8,3) = p_{o1}$
$A(8,4) = p_{p1}$
$A(8,8) = -p_{e1}$
$A(8,9) = -p_{f1}$
$A(8,10) = -p_{g1}$
$A(8,12) = -p_{q1}$
$A(8,13) = -p_{r1}$
$A(8,14) = -p_{s1}$
$A(8,15) = -p_{t1}$
$A(9,8) = 1$
$A(10,9) = 1$
$A(11,11) = 1$
$A(12,5) = k_{h12}$
$A(12,19) = k_{h22}$
$A(12,22) = k_{l2}$
$A(13,12) = 1$
$A(14,13) = 1$
$A(15,14) = 1$
$A(16,12) = p_{a2}$
$A(16,13) = p_{b2}$
$A(16,14) = p_{c2}$
$A(16,15) = p_{d2}$
$A(16,16) = -p_{e2}$
$A(16,17) = -p_{f2}$
$A(16,18) = -p_{g2}$
$A(16,23) = -p_{h2}$
$A(16,24) = -p_{i2}$
$A(16,25) = -p_{j2}$
$A(16,26) = -p_{k2}$
$A(17,16) = 1$
$A(18,17) = 1$
$A(19,12) = p_{m2}$
$A(19,13) = p_{n2}$
$A(19,14) = p_{o2}$
$A(19,15) = p_{p2}$
$A(19,19) = -p_{e2}$
$A(19,20) = -p_{f2}$
$A(19,21) = -p_{g2}$
$A(19,23) = -p_{q2}$
$A(19,24) = -p_{r2}$
$A(19,25) = -p_{s2}$
$A(19,26) = -p_{t2}$
$A(20,19) = 1$
$A(21,20) = 1$
$A(22,22) = 1$
$A(23,16) = k_{h13}$
$A(23,30) = k_{h23}$
$A(23,33) = k_{l3}$

$A(24,23) = 1$
$A(25,24) = 1$
$A(26,25) = 1$
$A(27,23) = p_{a3}$
$A(27,24) = p_{b3}$
$A(27,25) = p_{c3}$
$A(27,26) = p_{d3}$
$A(27,27) = -p_{e3} - p_{h3}k_w$
$A(27,28) = -p_{f2} - p_{i3}k_w$
$A(27,29) = -p_{g2} - p_{j3}k_w$
$A(27,34) = -p_{k3}k_w$
$A(28,27) = 1$
$A(29,28) = 1$
$A(30,23) = p_{m3}$
$A(30,24) = p_{n3}$
$A(30,25) = p_{o3}$
$A(30,26) = p_{p3}$
$A(30,30) = -p_{e3}$
$A(30,31) = -p_{f3}$
$A(30,32) = -p_{g3}$
$A(30,34) = -p_{t3}k_w$
$A(30,27) = -p_{q3}k_w$
$A(30,28) = -p_{r3}k_w$
$A(30,29) = -p_{s3}k_w$
$A(31,30) = 1$
$A(32,31) = 1$
$A(33,33) = 1$
$A(34,29) = 1.$

Matrix B is a 34×3 matrix, and the non-zero entries are the following:

$B(1,1) = k_{l1}$
$B(11,1) = 1$
$B(12,2) = k_{l2}$
$B(22,2) = 1$
$B(23,3) = k_{l3}$
$B(33,3) = 1$
.

The matrix B_d is 34×27, and the non-zero entries are given as:

$B_d(5,1) = -p_{h1}$
$B_d(5,2) = -p_{i1}$
$B_d(5,3) = -p_{j1}$
$B_d(5,4) = -p_{k1}$
$B_d(5,5) = -1$
$B_d(5,6) = -p_{e1}$
$B_d(5,7) = -p_{f1}$
$B_d(5,8) = -p_{g1}$
$B_d(5,9) = -p_{l1}$
$B_d(8,1) = -p_{q1}$
$B_d(8,2) = -p_{r1}$
$B_d(8,3) = -p_{s1}$
$B_d(8,4) = -p_{t1}$
$B_d(8,9) = p_{u1}$
$B_d(12,5) = k_{h12}$
$B_d(16,10) = -p_{h2}$
$B_d(16,11) = -p_{i2}$
$B_d(16,12) = -p_{j2}$
$B_d(16,13) = -p_{k2}$
$B_d(16,14) = -1$

$B_d(16,15) = -p_{e2}$
$B_d(16,16) = -p_{f2}$
$B_d(16,17) = -p_{g2}$
$B_d(16,18) = -p_{l2}$
$B_d(19,10) = -p_{q2}$
$B_d(19,11) = -p_{r2}$
$B_d(19,12) = -p_{s2}$
$B_d(19,13) = -p_{t2}$
$B_d(19,18) = p_{u2}$
$B_d(23,14) = k_{h13}$
$B_d(27,19) = -p_{h3}$
$B_d(27,20) = -p_{i3}$
$B_d(27,21) = -p_{j3}$
$B_d(27,22) = -p_{k3}$
$B_d(27,23) = -1$
$B_d(27,24) = -p_{e3} - p_{h3}k_w$
$B_d(27,25) = -p_{f3} - p_{i3}k_w$
$B_d(27,26) = -p_{g3} - p_{j3}k_w$
$B_d(27,27) = -p_{l3}$
$B_d(30,19) = -p_{q3}$
$B_d(30,20) = -p_{r3}$
$B_d(30,21) = -p_{s3}$
$B_d(30,22) = -p_{t3}$
$B_d(30,27) = p_{u3}$
$B_d(30,23) = -k_w p_{q3}$
$B_d(30,24) = -k_w p_{r3}$
$B_d(30,25) = -k_w p_{s3}$
$B_d(30,26) = -k_w p_{t3}$.

Appendix F

Publications

Aguilar, J., Langarita, P., Linares, L., Galvis, E., Horváth, K., Rodellar, J., and Gómez, M. (2011). Control automático de niveles en un canal experimental dividido en tres tramos. In *JIA 2011. II Jornadas del Ingeniería del agua, Modelos numéricos en dinámica fluvial*

Horváth, K., Galvis, E., Gómez, M., and Rodellar, J. (2011a). Control automático en canales de riego experiencias en el canal de laboratorio UPC-PAC. In *RLHE 2011, IV Seminario sobre las Líneas Prioritarias de Investigación de la Red de Laboratorios de Hidráulica de España*, pages 20–21., Madrid

Horváth, K., Galvis, E., Gómez, M., and Rodellar, J. (2011b). Pruebas de algoritmos de control automático en un canal de laboratorio y un canal simulado. In *JIA 2011. II Jornadas del Ingeniería del agua, Modelos numéricos en dinámica fluvial*, Barcelona

Galvis, E., Horváth, K., Rodellar, J., and Gómez, M. (2011). Control automático en canales de riego experiencias en el canal de laboratorio UPC-PAC. In *Proceedings of the IV Seminar for advanced industrial control applications*, pages 83–88., Barcelona

Horváth, K., Galvis, E., Gómez, M., and Rodellar, J. (2012). Comparison of two control algorithms based on different canal models using numerical

simulation and experiments on a laboratory canal. In *HIC 2012, 10th International Conference on Hydroinformatics*, Hamburg

Horváth, K., Gómez, M., and Rodellar, J. (2013a). The effect of the choice of the control variables of the water level control of open channels. In *The 10th IEEE International Conference on Networking, Sensing and Control*, Paris, France

Horváth, K., van Overloop, P.-J., Galvis, E., Gómez, M., and Rodellar, J. (2013b). Multivariable model predictive control of water levels on a laboratory canal. In Gourbesville, P., Cunge, J., and Caignaert, G., editors, *Advances in Hydroinformatics*. Springer Verlag, Singapore

Index